Evolutionary Structural Optimisation as a Robust and Reliable Design Tool

Kaarel Proos, BE (Hons)

School of Aeronautical, Mechatronic and Mechanical Engineering

The University of Sydney, Australia

Thesis submitted in fulfillment of the requirements for the degree of Doctor of Philosophy

March 2002

Abstract

Evolutionary Structural Optimisation (ESO) is a relatively new design tool used to improve and optimise the design of structures. It is a heuristic method where a few elements of an initial design domain of finite elements are iteratively removed. Such a process is carried out repeatedly until an optimum design is achieved, or until a desired given area or volume is reached.

There have been many contributions to the ESO procedure since its conception back in 1992. For example, a provision known as Bi-Directional ESO (BESO) has now been incorporated where elements may not only be removed, but added. Also, rather than deal with elements where they are either present or not, the designer now has the option to change the element's properties in a progressive fashion. This includes the modulus of elasticity, the density of the material and the thickness of plate elements, and is known as Morphing ESO. In addition to the algorithmic aspects of ESO, a large preference exists to optimise a structure based on a selection of criteria for various physical processes. Such examples include stress minimisation, buckling and electromagnetic problems.

In a changing world that demands the enhancement of design tools and methods that incorporate optimisation, the development of methods like ESO to accommodate this demand is called for. It is this demand that this thesis seeks to satisfy. This thesis develops and examines the concept of multicriteria optimisation in the ESO process. Taking into account the optimisation of numerous criteria simultaneously, Multicriteria ESO allows a more realistic and accurate approach to optimising a model in any given environment.

Two traditional methods – the Weighting method and the Global Criterion (Min-max) method have been used, as has two unconventional methods – the Logical AND method and the Logical OR method. These four methods have been examined for different combinations of Finite Element Analysis (FEA) solver types. This has included linear static FEA solver, the natural frequency FEA solver and a recently developed inertia FE solver. Mean compliance minimisation (stiffness maximisation), frequency maximisation and moment of inertia maximisation are an assortment of the specific objectives incorporated. Such a study has provided a platform to use many other criteria and multiple combinations of criteria.

In extending the features of ESO, and hence its practical capabilities as a design tool, the creation of another optimisation method based on ESO has been ushered in. This method concerns the betterment of the bending and rotational performance of cross-sectional areas and is known as Evolutionary Moment of Inertia Optimisation (EMIO). Again founded upon a domain of finite elements, the EMIO method seeks to either minimise or maximise the rectangular, product and polar moments of inertia. This dissertation then goes one step further to include the EMIO method as one of the objectives considered in Multicriteria ESO as mentioned above.

Most structures, (if not all) in reality are not homogenous as assumed by many structural optimisation methods. In fact, many structures (particularly biological ones) are composed of different materials or the same material with continually varying properties. In this thesis, a new feature called Constant Width Layer (CWL) ESO is developed, in which a distinct layer of material evolves with the developing boundary. During the optimisation process, the width of the outer surrounding material remains constant and is defined by the user.

Finally, in verifying its usefulness to the practical aspect of design, the work presented herein applies the CWL ESO and the ESO methods to two dental case studies. They concern the optimisation of an anterior (front of the mouth) ceramic dental bridge and the optimisation of a posterior (back of the mouth) ceramic dental bridge. Comparisons of these optimised models are then made to those developed by other methods.

Declaration

Candidate's Certificate

This is to certify that the work presented in this thesis was carried out by the candidate in the Discipline of Structural Optimisation, The School of Aerospace, Mechanical and Mechatronic Engineering, The University of Sydney, and has not been submitted to any other university of institution for a higher degree.

……..

Kaarel Proos, 2002

Acknowledgments

This thesis has come about from the contributions, support and friendship of the many acknowledged below;

Thanks Grant for your time, supervision and encouragement. You're a supervisor who has excelled in what was called for and even what was not. You know your stuff and have done well to share it with me. Thanks also for being a mate. Ozzie, your help and recommendations have been invaluable. It was great to do stuff with you outside the academic world and sad having you leave. Wishing you both the best for your future.

Mike and Jim – thanks for helping me with an area that I didn't have much idea about. It was great interacting with you guys. You did well to reach out and interact the areas of dentistry and engineering.

Douglass – you've been a great help in terms of the technical and computer support. Thank you. Yvonne for your prompt and effective administration – thank you.

To my mates Algis, Bartox, Eugene, Quan, Qing, Wei, Alicia, Yi, Ping, and anyone else – thanks for your friendship, encouragement and enjoyable times. Lencs – thank you greatly for your tech support and general willingness to lend a hand, and Qing and Bartox – for your help also. Especially thank you Qing for proof-reading the thesis.

Thanks to the Australian Research Council for financially supporting me for the last three years.

Particular mention must be made concerning my beautiful sister Laine, and lovely Grandma – Asta. They have provided wonderful support in the past four years – support that has made things much easier for me.

Final mention goes to my Lord and Saviour Jesus Christ who has given us all the privilege and ability to think and apply the things we learn about His wonderful creation and saving grace. Thank You.

Table of Contents

Nomenclature

A, A_0	cross-section area and original cross-section area
C	mean compliance
C_{all}	mean compliance prescribed limit
$crit$	criterion
d	distance
d_j^+	measure of under-achievement
d_j^-	measure of over-achievement
$\boldsymbol{d}$	global nodal displacement
e	subscript of element
E	Young's modulus
$f(\boldsymbol{x})$	vector of objective functions
$f(\boldsymbol{x}^*)$	utopia point
$f_j(\boldsymbol{x}_j^{min})$	vector of minimum objective functions
$F_{multicrit}^i$	weighted criterion sensitivity number
$G_{multicrit}^i$	global criterion sensitivity number
i	element number
I_x, I_y, I_z	moment of inertia about x, y and z-axis
I_{xy}	product of inertia
j	criterion number
k_x, k_y, k_z	radius of gyration about x, y, and z-axis
k_{xy}	product radius of gyration
K	stiffness
$\boldsymbol{K}$	global stiffness matrix
m_n	modal mass
M	applied moment or number of elements
$\boldsymbol{M}$	global mass matrix
n	natural frequency subscript
N	number of criteria
OC_e^{crit}	element criterion sensitivity number

$OC_{\max}^{crit}$	maximum value of criterion sensitivity number
p	constant of global criterion method
$\boldsymbol{P}$	nodal load vector
r	tooth notch radius
t	thickness
u^i	element displacement vector
$\boldsymbol{u}_n^{\,i}$	element eigenvector
$U(f(\boldsymbol{x}))$	utility function
$\boldsymbol{u}_n$	eigenvector
V	volume
w	pontic connector width
w_j	weighting preference
$\boldsymbol{x}$	design variable vector
$\boldsymbol{x}^*$	optimum design variable vector
X_c, Y_c	centroid coordinates

Greek Symbols

α^i	strain energy sensitivity number
α_e^{crit}	element sensitivity number of *crit* criterion
$\alpha_{\max}^{crit}$	maximum value of element sensitivity number of *crit* criterion
$\alpha_{average}^{crit}$	average value of element sensitivity number of *crit* criterion
α_{MOI}	moment of inertia sensitivity number
$\left\{\alpha_n^i\right\}^{new}$	linearly adjusted frequency sensitivity number
$\left\{\alpha_n^i\right\}^{old}$	original frequency sensitivity number
$\left\{\alpha_n^*\right\}^{old}$	original maximum value frequency sensitivity number
ε_j	criterion constraint
ν	Poisson's ratio
σ_e^{vm}	von Mises stress of element
$\sigma_{\max}^{vm}$	maximum value of von Mises stress

ω_n	natural frequency
ρ	density

Abbreviations

2-D	two dimensional
3-D	three dimensional
BESO	bi-directional evolutionary structural optimisation
CWL	constant width layer
EMIO	evolutionary moment of inertia optimisation
ESO	evolutionary structural optimisation
FE	finite element
FEA	finite element analysis
FG	fixed grid
GA	genetic algorithm
ICC	intelligent cavity creation
MOI	moment of inertia
RoG	radius of gyration
RR	ESO rejection ratio
SS	ESO steady state

List of Publications

Journal Papers

Proos, K., A., Steven, G., P., Querin, O., M., Xie, Y., M. (1999), "Multicriteria Evolutionary Structural Optimisation", submitted to *Design Optimisation – International Journal for Product and Process Improvement*, December.

Proos, K., A., Steven, G., P., Swain, M., Ironside, J. (2001), "Preliminary Studies on the Optimum Shape of Dental Bridges", *Computer Methods in Biomechanics and Biomedical Engineering*, Vol. 4, No. 1, pp. 77-92.

Proos, K., A., Steven, G., P., Swain, M., Ironside, J. (2001), "Optimisation of Ceramic Dental Bridges", *Journal of the Australian Ceramic Society*, Vol. 36, pp. 65-75.

Proos, K., A., Steven, G., P., Querin, O., M., Xie, Y., M. (2001), "Multicriterion Evolutionary Structural Optimisation Using the Weighting and the Global Criterion Methods", *AIAA Journal*, Vol. 39, No. 10, pp. 2006-2012.

Proos, K., A., Steven, G., P., Querin, O., M., Xie, Y., M. (2001), "Stiffness and Inertia Multicriteria Evolutionary Structural Optimisation", *Engineering Computations – International Journal of Computer Aided Engineering and Software*, Vol. 18, No. 7, pp. 1031-1054.

Proos, K., A., Steven, G., P., Querin, O., M., Xie, Y., M. (2001), "Stiffness, Frequency and Inertia Multicriteria Evolutionary Structural Optimisation", *Structural and Multidisciplinary Optimization*, In Press.

Proos, K., Swain, M., Ironside, J., Steven G. (2001). “Design of All Ceramic Bridges with the Aid of a Finite Element Optimisation Algorithm”, submitted to *The Australian Dental Journal*, August.

Conference Papers

Proos, K., A., Steven, G., P., Swain, M., Ironside, J. (2000), “Optimisation of Ceramic Dental Bridges”, *Transactions of the AUSTCERAM2000 – International Ceramics Conference*, Sydney Australia, 25th-28th June, pp. 139.

Proos, K., A., Steven, G., P., Querin, O., M., Xie, Y., M. (2000), “Multicriteria Evolutionary Structural Optimisation using the Weighting and the Global Criterion Methods”, *AIAA/NASA/USAF/ISSMO Symposium on MDO,* Long Beach, California, 6-8th September.

Steven, G., P., Proos, K., A., Xie, Y., M. (2001), “Multi-criteria Evolutionary Structural Optimization involving Inertia”, *The First MIT Conference on Computational Fluid and Solid Mechanics*, Massachusetts, USA, 12th-14th June.

Proos, K., Swain, M., Ironside, J., Steven G. (2001). “Two Dimensional Finite Element Analyses of Dental Crowns and Bridges”, *Proceedings of the 5th Symposium on Computer Methods in Biomechanics & Biomedical Engineering*, Rome, Italy, 31st October – 3rd November.

Proos, K., A., Steven, G., P., Querin, O., M., Xie, Y., M. (2002), “Evolutionary Moment of Inertia Optimisation”, submitted to *Fifth World Congress on Computational Mechanics*, Vienna, Austria, 7-12th July.

Chapter 1

Introduction

1.1 Optimisation

> ***Optimisation.*** *[f. optimise v. + -ation.] the making the best (of anything); the action or process of rendering optimal; the state or condition of being optimal (Oxford University Press, 1989).*

Optimisation is an action, form of thinking or process that is and has been used since the beginning of time – in its existence in nature and by man. It is to find the best solution to a problem (Beale, 1988). Mathematically, it means to maximise or minimise a function $f(x_1,\ldots,x_n)$ of n variables, where n may be any integer greater than zero. That is,

$$min\ f(x_1,\ldots,x_n) \tag{1.1}$$

where $\boldsymbol{x} \in R^n$ denotes the vector of design variables. This function may be unconstrained, or it may have certain constraints $g_i(\boldsymbol{x})$ on the variables of the function:

$$g_i(x_1,\ldots,x_n) \geq b_i \tag{1.2}$$

where $i = 1,\ldots,m$. An arena such as optimisation has and continues to be applicable to any field of study, and has set its mark in the engineering field (Ashley, 1982). This has come about because ingrained in the whole ethos of engineering is the search for the best solution to any given engineering problem. Of the wide range of optimisation studies existing in the engineering field, one of these, structural optimisation, lays the foundation or cornerstone for this thesis.

1.2 Structural Optimisation

The desire and drive towards the improvement in the performance of any given object, set in a structural environment of loads, constraints and restraints is known as structural optimisation. This improvement may be in anything related to the structure ranging from the need to reduce the structural weight without compromising structural integrity (Schmidt, 1981) to the need to reduce the combined manufacturing cost of the structure and its operational cost throughout its expected lifetime (Sheu and Prager, 1968).

Over the past four centuries, as the areas of engineering, mathematics, science and technology have become better established, the implementation of structural optimisation has become more profound. Much of the structural optimisation work carried out at the beginning of this period largely consisted of trials and unintentional experiments. This included the works of Leonardo da Vinci, Galileo and Euler (Wasiutynski and Brandt, 1963).

At the end of the 19th century and the turn of the 20th Century, came the capability of engineers to combine optimisation principles and analytical prowess. This saw the likes of Maxwell's proved theorems (1872) paving the way for Michell (1904) to determine theories encompassing the form of frames of minimum weight, known as Optimal Layout Theory.

The next sixty years continued to contribute to the ever-growing database of structural optimisation knowledge – specifically in the area of truss structures. It seemed to take on three directions: the minimisation of the truss's weight, the minimisation of the strain energy design for a given material volume and the optimisation of statically indeterminate structures of uniform strength. Significant contributors to these ideas were: Rabinovich (1933), Wasiutynski (1939) and Prager (1956).

Many of these techniques were addressed by classical optimisation i.e. calculus based optimisation (Haftka *et al.*, 1985). This work mainly concerned simple discrete or continuous structures that were optimised using classical techniques of ordinary differential calculus. Such work laid the foundation for certifying the validity of other more recent optimisation methods.

In the past fifty years, progress has seen the transition from this initial method to include a class of optimisation where variables in the optimisation equation are of a discrete nature. Mathematical programming has played a key role in this as seen by the contribution of methods such as linear and non-linear mathematical programming (Haftka *et al.*, 1985). Common to linear programming is the Simplex method (Van Der Veen, 1967). Constrained and non-constrained techniques have also been utilised in conjunction with mathematical programming. Such techniques have been presented in the form of the Lagrange Multiplier method and the Penalty Function method (Vanderplaats, 1984; Haftka *et al.*, 1985).

Many structural optimisation methods have emerged in recent decades with the development of computer technology. A large proportion of these methods uses discrete finite elements. They can be broadly arranged into three main areas of optimisation: topology optimisation, shape optimisation and size optimisation. A description of these areas and a sample of some of the methods that encapsulate these areas are as follows.

1.2.1 Topology Optimisation

Topology optimisation describes the process that defines the topology relationship in a structure. The resulting optimised structure can be vastly different from the initial starting design and so is independent of it. The implication of this is that there is no restriction on the final form of the structure relative to the initial form.

1.2.1.1 Optimality Criteria

The Optimality Criteria method is one example implementing topology optimisation (Prager and Rozvany, 1977; Rozvany *et al.*, 1995). It is an alternative method to mathematical programming whereby it attempts to satisfy a set of criteria such as a fully stressed design or a set of Kuhn-Tucker conditions. The alteration or removal of elements in a finite element mesh achieves this. Such a method is capable of treating a large number of design variables with ease, but requires significant intuitive input from the user (Rozvany *et al.*, 1995).

1.2.1.2 Homogenisation Method

Topology optimisation has greatly been impacted by the Homogenisation method (Bendsøe, 1995) in the past decade. This method simultaneously envelops the optimisation of a structure's topology, shape and size. It does so by assigning finite elements (with numerous local variables) to the whole domain of the structure. For each element, parameters of size and orientation of internal rectangular holes are varied, having the effect of a varying porous material over the whole structure. The basis with which this optimal material distribution is found, is by the use of mathematical programming techniques with sequential quadratic programming. Many publications and contributions have been made to progress this method – see Bendsøe and Kikuchi (1988), Allaire and Kohn (1993) and Maute and Ramm (1995).

1.2.1.3 Evolutionary Structural Optimisation

The Evolutionary Structural Optimisation method (ESO) (Xie and Steven, 1997) is also an effective tool that is capable of handling topology optimisation. It is a heuristic process that uses discrete finite elements as its foundation. It uses the Finite Element method as its analysis engine. Its approach to optimising a structure is to remove elements iteratively, which has been set up in a particular environment of loads, constraints and/or restraints. It is based on the simple concept that by slowly removing inefficient material from a structure, the topology of the structure evolves towards an optimum. Here "inefficiency" is a very general term, meaning the sensitivity of the alteration of an element in a FEA mesh to the optimality criterion. This sensitivity can be a composite of several performance measures and the optimality criterion can be a composite of several individual physical criteria. Much work has been done on ESO where many detailed studies have established systematic rules that make the method work for a full range of structural situations (Xie and Steven, 1997).

1.2.1.4 Genetic Algorithms

Topology optimisation of structures can also be achieved using Genetic Algorithms (Goldberg, 1989). This involves the optimisation of a population of chromosomes, where each chromosome represents a possible optimal solution. This is done by defining each chromosome with a character string of binary digits i.e. 0's and 1's. An artificial gene-transformation mechanism is applied where these chromosomes are ranked, with the more

favourable ones being selected and reproduced. Some of the poorly ranked members are selected and mutated with the more favourable ones. This occurs until the GA principle, over its successive generations, produces an optimum topology (Woon *et al.*, 2002).

1.2.2 Shape Optimisation

Shape Optimisation is a restricted form of topology optimisation. It determines the optimal boundaries of a structure for the given fixed topology. In this form of optimisation, the object is to find the best shape that will have the best objective outcome as defined by designer.

1.2.2.1 Evolutionary Structural Optimisation

Shape optimisation may be added to the ESO algorithm by adding a constraint to the method, which allows elements that exist only at the surface to be removed. This is known as the Nibbling constraint. In many design assignments, internal cavities are not allowed to be created, as only material is allowed to be nibbled away from the boundaries. Querin (1997) gives such an example, where shape optimisation is applied to an object hanging under its own weight. There are also several benchmark types and illustrative examples in Xie and Steven (1997).

1.2.2.2 Mathematical Programming Approach

Mathematical programming is the most typical approach to shape optimisation used in the 1970s and 1980s. In mathematical programming, the problem is defined mathematically by an objective function that is described in terms of a series of design variables. Differentials of the objective function are obtained directly or by computation with a finite difference form of the differential. Second differentials are obtained for the Hessian matrix. The design variables that fit the design criteria are then found using the Conjugate gradient, steepest decent or quadratic programming search engines (Kristensen *et al.*, 1976; Pederson *et al.*, 1992). Several categories of mathematical programming exist such as linear and non-linear, integer linear, sequential and stochastic programming (Haftka *et al.*, 1985).

1.2.2.3 Computer Aided Optimisation

The Computer Aided Optimisation method or alternatively, Simulated Biological Growth deals with the optimisation of structures specifically in the context of shape (Mattheck and Moldenhauer, 1990). It uses a discretised model of finite elements, and volumetrically 'swells' these structural elements using a swelling operation. This is done iteratively by thermally loading the structure proportional to the stresses created in the domain by normal loading. In addition to shape optimising a structure, it removes notch stresses and promotes a stress-state at the surface of the structure.

1.2.3 Size Optimisation

Size optimisation defines the approach to change the sizes and dimensions of a structure to achieve the optimum design. This is obtained by finding the best possible combination of these sizes and dimensions. Two major categories exist.

1.2.3.1 Discrete Structures

This is an area that has received significant attention over the past forty years, particularly with pin and rigid jointed structures. Here a structure is defined by its loads and supports, and its members are adjusted according to the optimisation goal. Mathematical programming (described above) has been a traditional method to solve the optimisation problem of discrete structures. Recently, the Optimality Criteria (Rozvany *et al.*, 1995) and ESO techniques (Xie and Steven, 1997) have been successfully used in this area. The optimisation of discrete structures involves the modification of plate thicknesses and beam cross sectional areas, making it quite a simplistic method (Bendsøe and Kikuchi, 1988).

1.2.3.2 Continuum Structures

This form of optimisation involves the modification of parameters that generally define the size of complex structures. Usually it is many parameters for each constituent making up the structure. Various examples include varying the stiffener pitch, skin thickness or ply angle of such structures as carbon fibre laminates, stiffened panels, wing layouts, spars and ribs. The

combination of these design variables that give the best result are found using optimisation techniques such as mathematical programming and genetic algorithms (see above).

As has been briefly reviewed, there are many structural optimisation methods available. Each has their own advantages and disadvantages, and each is appropriate for specific optimisation problems. In spite of this extensive array of methods in use, the studies conducted in this thesis shall all be based on Evolutionary Structural Optimisation. The primary reason for this is that this project was proposed and funded with the intention to develop the method further. This focus does not intend to undermine any of the other methods. Rather, it seeks to promote the capability and robustness of ESO amongst these other methods.

1.3 Evolutionary Structural Optimisation

Amongst the many structural optimisation methods that have been developed, one remains continually attractive due to its simplicity and continues to grow in its development in recent years. It is the Evolutionary Structural Optimisation (ESO) method. Since its inception back in 1992 by Xie and Steven (1997), ESO has grown to be a robust, yet simple design tool growing in its capabilities to serve the designer in a complex range of environments and objectives. In its original form, it had as its removal technique a condition to remove elements based on the von Mises stress level of each element. A general description of the original stress based ESO process is briefly outlined as follows.

The determination of elements to be removed was originally made by comparing the von Mises stress of each element σ_e^{vm} to the maximum von Mises stress that exists in the whole structure $\sigma_{\max}^{vm}$. At the end of each finite element analysis, all the elements that satisfy the following condition were deleted from the model:

$$\sigma_e^{vm} < RR.\sigma_{\max}^{vm} \tag{1.3}$$

Here, *RR* is the current Rejection Ratio. It is used to dampen or delay the element removal process and is confined to the condition ($0.0 \leq RR \leq 1.0$). The same cycle of removing

elements using the inequality of Equation (1.3) is repeated until no more elements are able to be removed (with the given *RR*). When this situation occurs, a Steady State has been reached. The *RR* is then updated with a counter function using a Steady State (*SS*) number:

$$RR = a_0 + a_1 \times SS + a_2 \times SS^2 + \ldots \tag{1.4}$$

The *SS* number is an integer counter that varies by increments of one, and is confined to the condition ($0 \leq SS < \infty$). The variables a_0, a_1, a_2 etc are coefficients that determine the nature of the variation in the *RR* number. Usually, they are set as $a_0 = a_2 = 0.0$ and $a_1 = 0.001$. Thus the increase of the *RR* is linear. Having updated the *RR* number, another comparison is made amongst the elements using Equation (1.3) to determine element removal. The *RR* is increased until elements are removed. When elements satisfy this inequality and are removed, another FEA is carried out on the now modified structure. This process is repeated until a desired volume fraction is obtained – for example, 50 % of the initial design domain. This process is illustrated in the flow chart given by Figure 1.1.

Today, ESO is still heavily based on the FEA computational engine, although, there now exists the alternative to use another approximate, yet faster computational engine known as the Fixed Grid (FG) method (García, 1999). Also, the basis with which to remove elements has progressed from that of the objective to create a uniform stress throughout the structure. It now includes the option of sensitivity numbers (based on many individual criteria) for the element removal process. Thus, Equation (1.3) has been converted to include the sensitivity numbers of one of many different optimality criteria. It may be presented as:

$$\alpha_e^{crit} < RR_i \alpha_{\max}^{crit} \tag{1.5}$$

The term α_e^{crit} is the sensitivity number of the e^{th} element for the *crit* criterion in question, and the term $\alpha_{\max}^{crit}$ is the maximum sensitivity value that exists for that criterion.

The sensitivity number calculated for each element represents the influence of that element on the overall magnitude of the structure's criterion. The optimality criterion used by ESO has included stiffness (Chu *et al.*, 1996), stress minimisation (Li *et al.*, 1999a), strain (Xie and Steven, 1997), buckling (Manickarajah *et al.*, 1998), torsional stiffness (Li *et al.*, 1999b),

heat transfer and conduction (Li *et al.*, 1997), incompressible fluid flow problems (Li, 2000), electrostatic (Li, 2000) and magnetostatic (Li, 2000) problems.

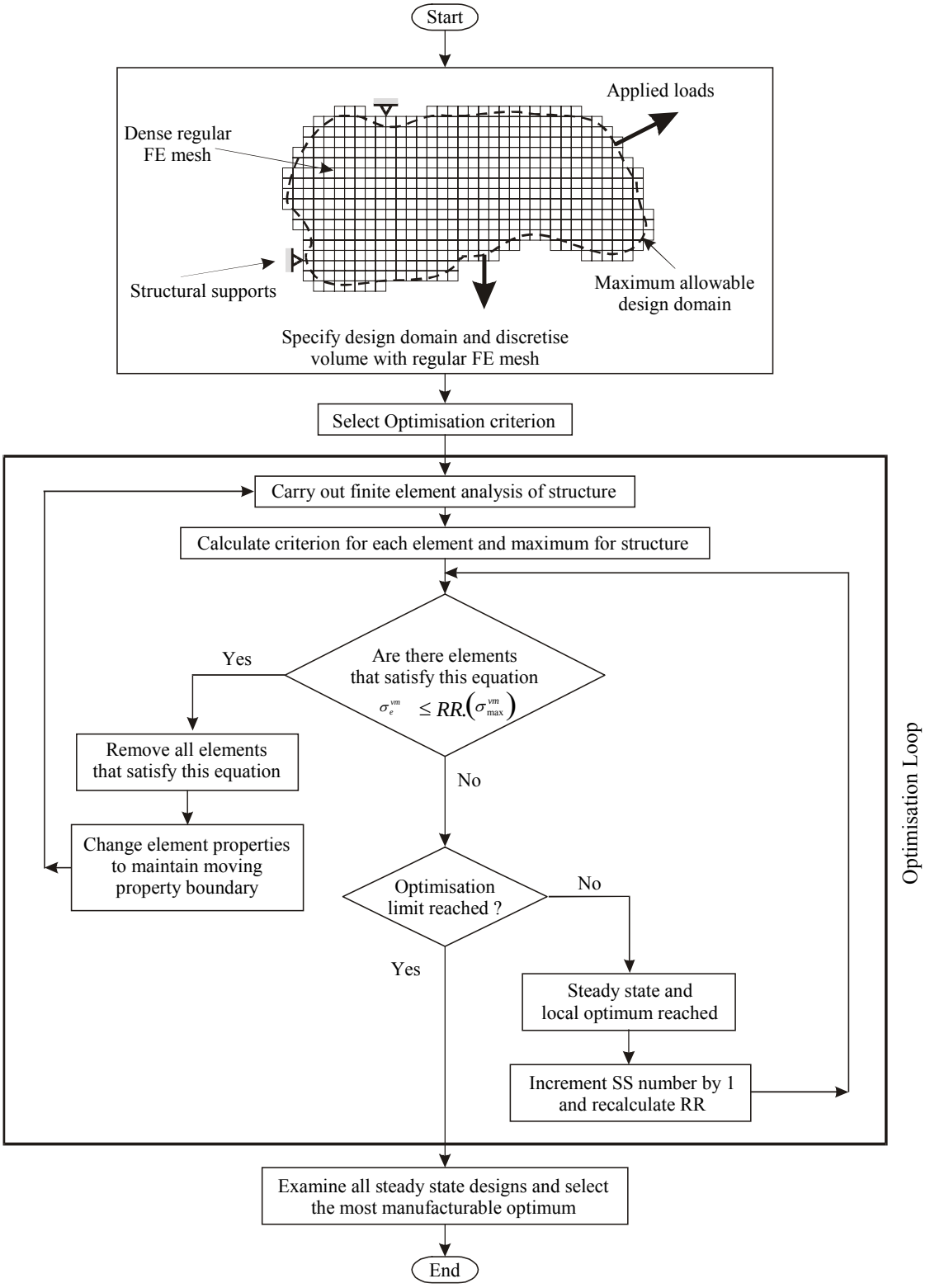

Figure 1.1 Flow chart depicting the logical steps of the ESO process.

Many other features have been integrated into the ESO process. Multiple load cases and multiple support environments were first reported by Xie and Steven (1994) and Steven *et al*. (1995). This allowed for the optimisation of structures that were subject to different load cases at different times, and structures that were held or supported in different ways and at different times.

Similar to shape optimisation, another innovation has been ESO Morphing (Querin, 1997). This is where, rather than completely remove elements as in classical ESO, the elements are removed gradually. For the case of beams this graduation could be applied to a variation in cross-sectional area: for plates – to a set of varying thickness', modulus of elasticity or density; and for bricks – to a range of modulus of elasticity or density.

To overcome any doubts about the question of material being inappropriately removed in ESO, a Bi-directional Evolutionary Structural Optimisation (BESO) has been formulated (Querin, 1997; Young *et al.*, 1999). This method allows the addition of material as well as the removal of material to take place simultaneously. Those regions of high stress for example, are attended to by the addition of material to those areas in need. Thus the evolutionary process can start from the smallest possible structural kernel and grow towards an optimum. Such a final optimum design is the same as that obtained by removal evolution.

One of the latest innovations to ESO has been the introduction of Configurational Optimisation - alternatively known as Group ESO (Lencus *et al.*, 1999a). This is where rather than considering each element as a design variable, groups or configurations of elements are put under scrutiny for removal, Morphing (Lencus *et al.*, 1999b) or Nibbling. This allows for layout optimisation and can be used at an early stage of the design process where the configuration of the structural entities, holes, stiffeners and skin thickness values are not fixed.

Many other optimisation characteristics have been created to exist inside the ESO regime to extend its capabilities. Some of these are ESO applied to composite panels (Falzon *et al.*, 1996), topology optimisation with material and geometric non-linearities (Querin *et al.*, 1996), Intelligent Cavity Creation (ICC) (Kim *et al.*, 1998), Post processing of 2-D topologies (Kim *et al.*, 2000) and shape design for elastic contact problems (Li *et al.*, 1998a).

The repertoire of ESO has been extensive in its practical applications as well. A sample of these applications include the optimisation of wheels (Guan *et al.*, 1997), spanners (Steven *et al.*, 1997), bikes (Steven *et al.*, 1997), milk crates (Barton *et al.*, 1998), generic aircraft spoilers (Lencus *et al*, 1999b) and aircraft airframes (Lencus *et al.*, 2000).

As can be seen, ESO has been developed to be used in many different contexts and for many purposes. This section has sought to identify some of these developments. It is hoped that the reader will not only become aware of the wide variety of applications that ESO may be used for, but also that there are further areas of research that ESO may be adapted into. One of these is Multicriteria Optimisation.

1.4 Multicriteria Optimisation

Having established the structural optimisation problem, situations may arise where a number of different objectives need to be satisfied. Many different factors or criteria need to be considered when a solution to a problem is sought. The more each problem takes into account different criteria, the more complex and the process of solving that problem become. In many cases, these criteria are in conflict with one another in what they set out to achieve. And so a number of solutions, rather than one solution may be available. Such a dilemma in conflicting objectives exists in numerous fields of study: engineering design, agriculture, economics, urban planning etc. In engineering design for example, a load-carrying beam in an aircraft fuselage has the ultimate objective of minimum weight, that is, material volume reduction. On the one hand, the design objective may be to increase the structures' stiffness – and on the other hand, the objective may be to reduce the frequency – requiring a stiffness reduction or a mass increase. Here, these multiple objective criteria of stiffness and frequency are somewhat in conflict with one another.

In the case of structural optimisation, no doubt, designers have always been faced with the dilemma of numerous conflicting objectives. It is only in recent times that there has been an intense concentration of research dedicated to structural multicriteria optimisation. Many publications have been continually produced since the last half of the 1970's up until the present. Some of these are noted by Sawaragi *et al.* (1985). Koski (1993) has compiled a detailed review of multicriteria structural optimisation papers developed in the past fifteen

years. A survey providing a broad perspective of the possible applications for multicriteria optimisation has been put together by Stadler and Dauer (1993).

1.4.1 Problem Definition

The problem of conflicting objectives may be defined as a multicriteria optimisation dilemma. Multicriteria (multicriterion, multi-objective, multi-goal or Pareto) optimisation in the structural optimisation context is the process of forming a solution that satisfies all these conflicting objectives in the best way possible. That is, multicriteria optimisation provides information about the optimum performance of the structure taking into account different criteria (Carmichael, 1980; Adali, 1983).

Consider N different criteria (objective functions) f_j for $j = 1, 2, \ldots, N$, each based on a vector of design variables $\boldsymbol{x} = [x_1\ x_2\ \ldots\ x_m]^T$. Multicriteria optimisation may then be defined in terms of the equation:

$$\min f(\boldsymbol{x}) = \min_{x \in \Omega} [f_1(\boldsymbol{x}), f_2(\boldsymbol{x}), \ldots, f_j(\boldsymbol{x}), \ldots, f_N(\boldsymbol{x})]^T \tag{1.6}$$

Here, Ω is the feasible set in the design space (or design domain) R^n defined by equality and inequality constraints:

$$\begin{aligned} g(\boldsymbol{x}) &\leq 0 \\ h(\boldsymbol{x}) &= 0 \end{aligned} \tag{1.7}$$

For the case of two criteria (Figure 1.2), the vector of design variables is given as $\boldsymbol{x} = [x_1\ x_2]^T$ where the constraints that define the design domain are:

$$\begin{aligned} &\text{Min } x_1 \leq g_1(x) \leq \text{Max } x_1 \\ &\text{Min } x_2 \leq g_2(x) \end{aligned} \tag{1.8}$$

The solution to the multicriteria problem is known as a Pareto optimum (or a non-inferior solution, non-dominated solution or efficient solution) (Carmichael, 1980; Das and Dennis, 1997). V. Pareto formulated this concept in 1896 (Lógó and Vásárhelyi, 1988).

Usually, it is not one Pareto solution that exists for a multicriteria problem, but a range of such solutions that make up the optimum (Pietrzak, 1999). Once this optimum has been achieved, any further improvement in one criterion requires a clear tradeoff with at least one other criterion (Grandhi *et al.*, 1993). Koski defines the Pareto optimum as follows:

> *A vector* $\mathbf{x}^* \in \Omega$ *is Pareto optimal for Equation (1.6) if and only if there exists no* $\mathbf{x} \in \Omega$ *such that* $f_j(\mathbf{x}) \leq f_j(\mathbf{x}^*)$ *for* $j = 1, 2, \ldots, N$ *with* $f_k(\mathbf{x}) < f_k(\mathbf{x}^*)$ *for at least one* k.

In words, he defined the Pareto optimum as $\boldsymbol{x}^*$ is a Pareto optimal solution if there exists no feasible solution $\boldsymbol{x}$ which can decrease some objective functions without causing at least one objective function to increase (Koski, 1994). This is provided all objectives concern minimisation (which is equivalent to the negative of maximisation).

Thus on the solution space (or criterion space) the Pareto optimum solution is sought and may be usually found in the feasible domain (Hajela, 1990; Koski, 1993). The Pareto optimum solution for two criteria is a set of optimal points on a plane. Generally, these points may be connected to form a 'string' on a 2-D plot (Figure 1.3). For three criteria, the optimal solution is a 'blanket' of optimal points in a 3-D space. When displayed graphically, a Pareto surface is interpolated and formed from these points.

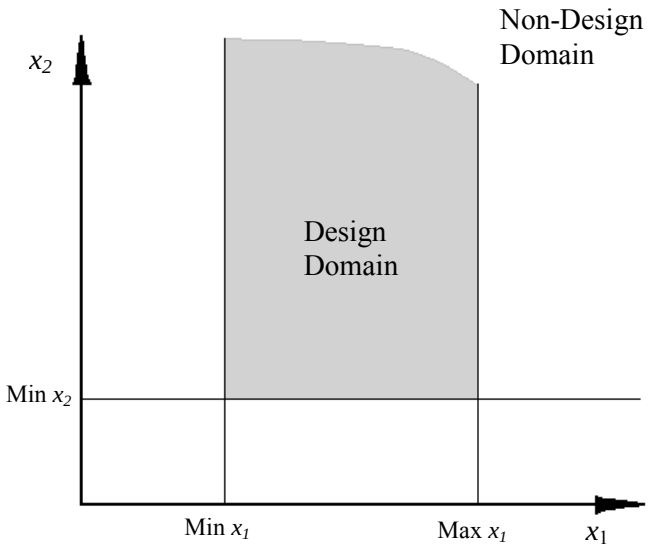

Figure 1.2 Design (or decision) space with two design variables x_1 and x_2.

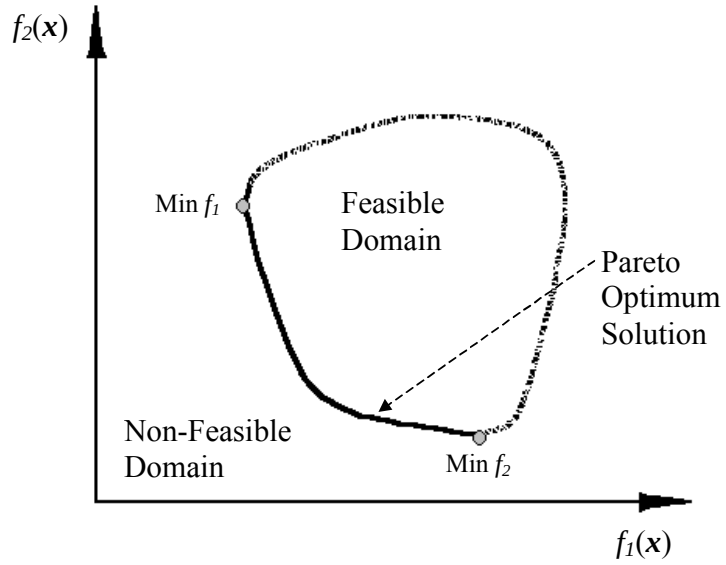

Figure 1.3 Solution (or criteria) space where two objectives $f_1(\boldsymbol{x})$ and $f_2(\boldsymbol{x})$ are minimised.

1.4.2 Solution Method

To obtain the Pareto optimum solution, many different methods can be used. These include, but are not restricted to the distance method, the linear weighting method, the constraint method, the utility function method, the goal programming method, the trade-off method, the surrogate-worth trade off method, the compromise programming method, the noninferior set estimation method, game theory approach and so on (Chen and Wu, 1998, Koski, 1993). As can be seen, the list demonstrates the significant amount of thought that has been put into the study of multicriteria structural optimisation. Having such numerous multicriteria methods stems from the vast array of different optimisation methods that exist.

This section attempts to categorise some the various methods traditionally used to solve the multicriteria problem. Different researchers may use small variations in these methods. The same multicriteria method too may be used by structural optimisation methods that are quite different (some of which were outlined in Section 1.2). Thus this chapter seeks to capture the essence of a few of these multicriteria methods, rather than explain specifically how they were used. The omission of other multicriteria methods also does not necessarily imply that they are not commonly used or invalid for multicriteria structural optimisation.

1.4.2.1 Distance Method

The distance method was introduced by J. Koski (Lógó and Vásárhelyi, 1988), and may alternatively be known as the Min-max, norm, global criterion or the metric method. It is a method that is based on minimising a distance function d, which calculates the distance between some attainable set $f(\boldsymbol{x})$ and some chosen reference point in the criterion space $f(\boldsymbol{x}_{ref})$ (Koski, 1993; Shih *et al.*, 1989). Usually, this metric function d is elected to represent the distance between the Pareto optimum solution and the ideal solution or utopia point $f(\boldsymbol{x}^*)$. This is so when the ideal solution is not feasible. For the case of two criteria, the ideal solution $f(\boldsymbol{x}^*)$ consists of the union of the minimum value of both functions $f_1(\boldsymbol{x})$ and $f_2(\boldsymbol{x})$ (Figure 1.4):

$$f(\boldsymbol{x}^*) = [\min f_1(\boldsymbol{x}), \min f_2(\boldsymbol{x})] = [f_1(\boldsymbol{x}^*), f_2(\boldsymbol{x}^*)] \tag{1.9}$$

The objective to minimise the distance d between the attainable set and the ideal solution may thus be given as:

$$f(\boldsymbol{x}) = \min d \tag{1.10}$$

where:

$$d = \left[\sum_{j=1}^{N} \left[f_j(\boldsymbol{x}) - f_j(\boldsymbol{x}_j^*) \right]^p \right]^{\frac{1}{p}} \tag{1.11}$$

Here, N is the number of criteria, p is a constant that is usually fixed and is defined by the constraint $1 \leq p \leq \infty$. Typically, $p = 2$ is used, although $p = 1$ or ∞ have been used frequently in structural design applications (Rao *et al.*, 1990; Koski, 1994). The extreme case $p = 1$ is known as the linear weighting method if the origin is used at a reference point ie $f(\boldsymbol{x}_{ref}) = 0$ (which is examined next). The case $p = 2$ is called the weighted quadratic method. The extreme case $p = \infty$ corresponds to the weighted minimax problem (Koski, 1994).

In practical applications, where the numerical values used may have huge variations with respect to each other, it is useful to normalise all the criteria before optimisation. One

possibility is to normalise the distance function d by dividing it by the respective minimum value of each criteria ie that which corresponds to the utopia point $f(\boldsymbol{x}^*)$ as has been done by numerous authors (Shih and Hajela, 1989; Rao *et al.*, 1990):

$$d = \left[\sum_{j=1}^{N} \left[\frac{f_j(\boldsymbol{x}) - f_j(\boldsymbol{x}_j^*)}{f_j(\boldsymbol{x}_j^*)} \right]^p \right]^{\frac{1}{p}} \tag{1.12}$$

In this case, all the criteria are limited to having the same non-existent dimensions. Other literature (Lógó and Vásárhelyi, 1988; Hajela and Shih, 1990; Koski, 1994), have used the relative distance between the maximum and minimum value of each criteria to normalise the distance function:

$$d = \left[\sum_{j=1}^{N} \left[\frac{f_j(\boldsymbol{x}) - f_j(\boldsymbol{x}_j^{\min})}{f_j(\boldsymbol{x}_j^*) - f_j(\boldsymbol{x}_j^{\min})} \right]^p \right]^{\frac{1}{p}} \tag{1.13}$$

where $f_j(\boldsymbol{x}_j^{min})$ is the minimum value of each criteria j. Note here, the numerator has been modified to calculate the relative distance between the solution and the minimum ideal for that criterion. Hence, the non-dimensional criteria also become limited to an equal range ie $d \in [0,1]$.

The mathematical programming used to optimise discrete structures (Rao, 1984; Tseng and Lu, 1990; Osyczka and Montusiewicz, 1993; Grandhi *et al.*, 1993) and continuum structures (Chen and Wu, 1998) as well as the area of genetic algorithms (Osyczka and Kunda, 1995) are a few optimisation methods that use the global criterion technique.

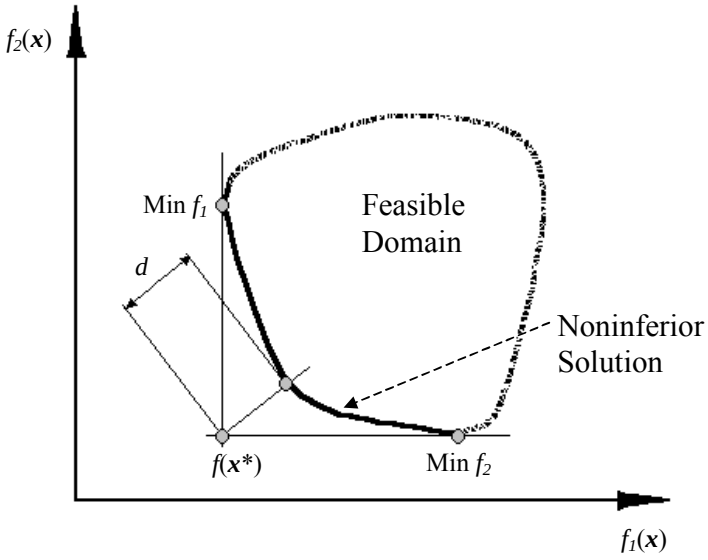

Figure 1.4 2-D plot of distance function d to be minimised, where two objectives $f_1(\boldsymbol{x})$ and $f_2(\boldsymbol{x})$ are to be minimised.

1.4.2.2 Linear Weighting Method

This method is extremely common in solving multicriteria optimisation problems and is the easiest one to be implemented (Chen and Wu, 1998). It is sometimes referred to as the Utility method. Basically, it involves optimising a utility function created by multiplying each criterion function with a preferred weight and adding the criterion together. So it becomes a single criterion optimisation problem which can be solved with traditional optimisation methods.

The weighting method is an extension of the global criterion method, where the constants $p = 1$ and $f_j(\boldsymbol{x}_j^*) = 0$ for $j = 1, \ldots, N$ are chosen, and the weighting preference of each criterion w_j is introduced:

$$\min f(\boldsymbol{x}) = \min\left[\sum_{j=1}^{N} w_j f_j(\boldsymbol{x})\right] \tag{1.14}$$

The weights $0.0 \le w_j \le 1.0$, for $j = 1, \ldots, N$, are usually normalised by:

$$\sum_{j=1}^{N} w_j = 1 \tag{1.15}$$

The weights represent the relative importance of each criterion and are selected by the designer or the decision-maker. In terms of practical applications, it is difficult to know or fix in advance the weights for a design process. Thus it seems appropriate to select the right weights during the process. In so doing, the whole set of Pareto optima is produced using the weighting method, provided that the problem $f(\boldsymbol{x})$ is convex. For the case of two criteria, the gradient of the convex curve generally approximates the negative ratio between the two weights selected - Figure 1.5 (Balachandran and Gero, 1984; Koski, 1985).

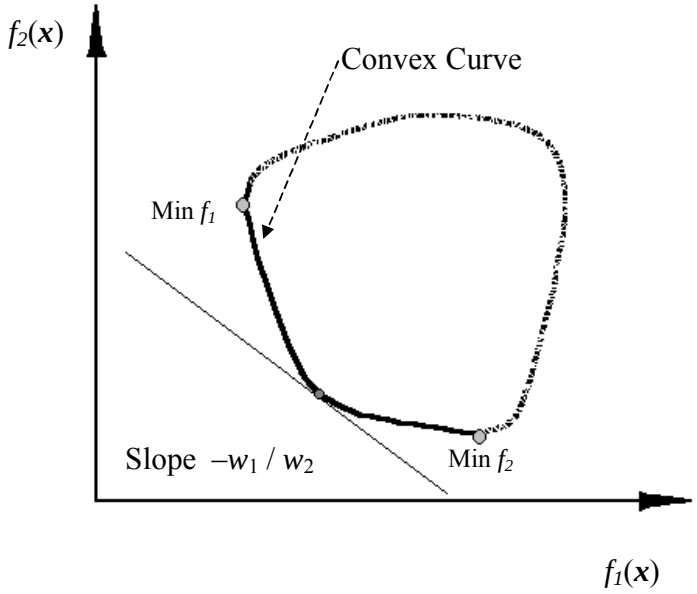

Figure 1.5 Geometric representation of weighting method, where two objectives $f_1(\boldsymbol{x})$ and $f_2(\boldsymbol{x})$ are to be minimised.

As mentioned above, one of the disadvantages to the weighting method is that it may fail to generate the Pareto optimal set of a multicriteria problem in non-convex cases. Koski (1985) used two simple truss examples to show how this situation may easily occur. However, such cases are not typical in structural optimisation (Koski, 1994). Another possible disadvantage of the method occurs when the Pareto set generated is too large for a decision-maker to analyse in order to arrive at a preferred solution. Also, it may be that it is not possible to

retain all the Pareto optimal solutions as restricted by computational cost (Rosenman and Gero, 1985). This occurs when a large number of criteria are optimised.

Some structural optimisation methods that use the linear weighting method are shape optimisation of discrete structures (Adali, 1983; Koski, 1985; Koski, 1988; Tappeta and Renaud, 2001; Zhang, 2001) and continuum structures (Saravanos and Chamis, 1992; Krog and Olhoff, 1999).

1.4.2.3 Constraint Method

This method involves the selection of one of the criterion as the objective function, and the remaining criteria are handled by formulating appropriate design constraints. The constraints may be thought of as reducing the feasible region (Carmichael, 1980). Thus the constraint method can be seen to optimise the single criterion:

$$\min f(\boldsymbol{x}) = \min f_k(\boldsymbol{x}) \tag{1.16}$$

subject to the constraints:

$$f_j(\boldsymbol{x}) \leq \varepsilon_j \tag{1.17}$$

for $j = 1,\ldots, k\text{-}1, k\text{+}1,\ldots, N$, where the kth objective was chosen and ε_j are parametrically varied target levels of the N objective functions.

This formulation is a single objective problem so it can be solved by conventional optimisation methods (Balachandran and Gero, 1984). Each optimisation combination relative to each constraint set usually corresponds to one Pareto optimum. Put together, this method can thus generate the whole Pareto optimal set, provided that the problem is a convex case only. The constraint method has been applied to various structural optimisation problems (Koski, 1994). It has been reported that the constraint method provides direct control of generating members of the Pareto set and is generally an efficient method for defining the shape of the Pareto set (Grandhi *et al.*, 1993).

1.4.2.4 Utility Function Method

The Utility function method is one that can take on many forms (Rao, 1990). Generally, the decision-maker defines a utility function $U_j(f_j(\boldsymbol{x}))$ for each objective $f_j(\boldsymbol{x})$, depending on the importance of $f_j(\boldsymbol{x})$ compared to the other objective functions For example, the utility function could be the mass squared. The thinking behind this is that the decision-maker has some utility associated with each of the jth objective functions. Then, the problem is converted to the minimisation of the utility function:

$$\min U(\boldsymbol{f}(\boldsymbol{x})) = \min U_j(f_j(\boldsymbol{x})) \tag{1.18}$$

subject to the constraints:

$$g(\boldsymbol{x}) \leq 0 \tag{1.19}$$

for $j = 1,\ldots, N$. The most common form of utility function assumes that it is additively separable with respect to all the objective functions. Thus, it may be presented as:

$$\min U(\boldsymbol{f}(\boldsymbol{x})) = \min\left[\sum_{j=1}^{N} U_j(f_j(\boldsymbol{x}))\right] \tag{1.20}$$

A special form of the Utility function that has been used extensively in structural optimisation problems incorporates the scalar weighting factor w_j:

$$\min U(\boldsymbol{f}(\boldsymbol{x})) = \min\left[\sum_{j=1}^{N} w_j U_j(f_j(\boldsymbol{x}))\right] \tag{1.21}$$

w_j of course indicates the relative importance. This is the equivalent to the linear weighting method and may be used to calculate the solution of Pareto optima, provided that it is of convex nature.

Some of the pros given for the utility function method are that it is a simple method, where it is easier to assess N different utility functions than to assess $U(\boldsymbol{f}(\boldsymbol{x}))$ directly. Similarly, it is

easy to work with the scalar weighting factor w_j. On the downside, there are only a few cases where the utility function is additively separable, or convex (Rao *et al.*, 1990).

1.4.2.5 Goal Programming

In goal programming, the decision-maker is required to specify goals for each criterion ie goals are 'programmed'. The optimum solution is thus defined as the one that minimises the deviations from these set goals. In its simplest form, this can be defined as:

$$\min\left[\sum_{j=1}^{N}\left(d_j^+ + d_j^-\right)^p\right]^{\frac{1}{p}} \tag{1.22}$$

subject to:

$$g(\boldsymbol{x}) \leq 0 \qquad j = 1, 2, \ldots, m \tag{1.23}$$

$$f_j(\boldsymbol{x}) - d_j^+ + d_j^- = b_j \qquad j = 1, 2, \ldots, N \tag{1.24}$$

$$d_j^+ \geq 0 \qquad j = 1, 2, \ldots, N \tag{1.25}$$

$$d_j^- \geq 0 \qquad j = 1, 2, \ldots, N \tag{1.26}$$

$$d_j^+ d_j^- = 0 \qquad j = 1, 2, \ldots, N \tag{1.27}$$

where the goals set by the decision-maker are b_j, the under-achievement and over achievement of the jth goal are d_j^+ and d_j^- respectively, and the value p is a fixed constant chosen by the decision-maker with $p \geq 1$.

If the goals of the decision-maker are defined to be equivalent of the individual minima of each objective $f(\boldsymbol{x}^*)$, then no over-achievement is possible and the problem becomes:

$$\min\left[\sum_{j=1}^{N}\left(d_j^+\right)^p\right]^{\frac{1}{p}} \tag{1.28}$$

subject to:

$$g_j(\boldsymbol{x}) \leq 0 \qquad j = 1, 2, \ldots, m \tag{1.29}$$

$$f_j(\boldsymbol{x}) - f_j(\boldsymbol{x}^*) = d_j^+ \qquad j = 1, 2, \ldots, N \tag{1.30}$$

$$d_j^+ \geq 0 \qquad j = 1, 2, \ldots, N \tag{1.31}$$

A system of relative weighting may be incorporated into the minimisation of each deviation, as has been suggested by Rao *et al.* (1990). A disadvantage of the goal programming method in general, is that the determination of the pre-specified goal requires some knowledge of the individual minima of the objective function, which may not be easy to achieve with non-convex problems, or be able to be obtained at all (Grandhi *et al.*, 1993). Tseng and Lu (1990) use goal programming to structurally optimise discrete structures.

1.4.3 Decision Making

Given an array of Pareto optima produced (possibly using one of the multicriteria methods mentioned above), it is usually the preference of the designer to have one solution selected for the desired task. The dilemma that designers thus face, given this array of solutions (most probably conflicting), is to discern which one is the more important.

Different approaches (Koski, 1994) have been taken in selecting the Pareto optimum. The designer may proceed from each Pareto optimum to a better one until the satisfactory solution is achieved. Another approach is to compute a large collection of Pareto optima and choose the best one by direct comparisons. Factors such as the designer's personal preferences, possibly based on experience, can be thus incorporated into the process. In other approaches such as the so-called a priori approach, all the decisions of selection may have already been made, as is the case for the utility function method. If all the parameters are fixed where all decisions have been made, then a scalar optimisation problem is obtained. Another approach, like the one just mentioned, also does not utilise the full capacity of the multicriteria formulation, because some crucial parameters are fixed in advance. As has been seen above, goal programming incorporates this approach, where the decision-maker is required to specify the goals for each criterion.

1.4.4 Multicriteria Evolutionary Structural Optimisation

Part of the work of this thesis attempts to establish and understand in detail, multicriteria optimisation applied to Evolutionary Structural Optimisation. It does so by examining some of the multicriteria solution methods proposed above. It does not attempt to establish an approach that finalises the design process by making a decision as to the most preferred designs. Rather, it provides a platform to assist the designer in obtaining the preferred design, which at the same time incorporates some form of optimality for the various conflicting criteria considered.

Multicriteria optimisation applied to ESO was first proposed by Querin (1997). He suggested that elements could be discretely removed by taking into account all of the criteria in question. His thinking was that keeping in mind that for all the uses of ESO, there had only been one criterion used at any one time. There would be instances when the designer may wish to apply more than one criterion and optimise the structure such that it satisfied all of the selected criteria. The use of a logical AND operator removal method was thus recommended, where elements were removed only if they satisfied the inequality equation for ALL criteria (modified from Equation (1.5)):

$$OC_e^{crit} \le RR.OC_{\max}^{crit} \tag{1.32}$$

where:

OC_e^{crit} is the value of the criterion *crit* for the element *e*;

$OC_{\max}^{crit}$ is the maximum value of the *crit* criterion.

Thus a proposal to incorporate multiple criteria into ESO was made, however, no investigation or verification was pursued. He also put forward a similar proposal with respect to ESO to accommodate structures that were subject to multiple load cases and moving supports. In fact, the study of moving supports was incorporated into ESO using the AND operator (Querin, 1997). Li (2000) continued this line of thinking by proposing the logical AND operator scheme and a new simple weighting scheme be applied to ESO for multiple heat load cases.

In the Logical AND scheme, an element was eliminated from the design domain only if ALL its relative usage efficiencies were lower than the threshold:

$$\alpha_j^e \le RR_{SS} \qquad (j = 1, 2, \ldots, LCN) \tag{1.33}$$

where α_j^e is the sensitivity number for element e, corresponding to the jth heat load case for LCN number of heat load cases. For the weighting scheme, the overall contribution of an element was considered as the reference of determining the presence and absence of an element. To calculate this efficiency, the weighted average sum of all relative efficiency factors under different load cases was used:

$$\alpha^e = \sum_{j=1}^{LCN} w_j \times \alpha_j^e \qquad (\sum_{j=1}^{LCN} w_j = 1) \tag{1.34}$$

where w_j represents the weighting factor and is employed to reflect the importance or operation 'frequency' of each load case. These schemes were also extended to the simultaneous optimisation of structures based on both thermal strength and heat performance, and also to minimising the maximum von Mises stress together with maximising the stiffness of a structure. In these studies comparisons between topologies were made, giving the reader a sense of the trade-offs made in the simultaneous optimisation cases. A relationship between the logical AND scheme and the weighting scheme was established.

It is at this stage of the ESO development that this thesis continues to investigate the multicriteria ESO arena. It extends the above investigated schemes to other criteria not yet studied in a multicriteria context, and clarifies more clearly how these schemes work and are linked – if they are linked at all! This clarification is also needed for ESO applied to three criteria as well. One may argue that the extension of these schemes to other criteria is just applications of the same process. But there is no verification or proof that these schemes could be applied to other criteria or produce solutions in the Pareto sense. And so, this thesis seeks to do that.

The question also arises as to the application of other multicriteria methods or schemes into the ESO algorithm. Even though many multicriteria methods exist and have been applied to a vast amount of structural optimisation problems, this does not mean that every method can

be applied to ESO. This is because, as has been seen, some of the methods require the designer or decision-maker to have considerable knowledge of the final solution for individual optimised criterion ie goal programming or knowledge of the constraints ie constraint method. ESO is a heuristic method where the optimised solution, and the process to obtain it, is not known until the solution has been arrived at. And so, this iterative nature of ESO makes it difficult for the goal programming method and the constraint method to be used. Concerning the constraint method, it is very complex to run the ESO iteration process driven by one criterion, which at the same time is 'guarded' by physical constraints to which topologies are not allowed to violate.

It is worth noting that although the literature has much to say about multi-criteria optimisation, it generally applies to deterministic analysis, where gradients can be calculated and mathematical searches undertaken. The general case where one has a totally arbitrary design space with a large array of topological outcomes, together with multi-criteria optimality conditions has not been previously fully investigated. The way forward in such circumstances is not clear.

This thesis introduces and adapts the traditional global criterion method as well as introduces another new method of multicriteria optimisation to ESO. It is the Logical OR operator method, similar to the logical AND operator method. To the author's knowledge, there is no known work produced on the implementation of the logical OR operator to ESO nor the global criterion method. However, the author does not claim to have proposed the logical OR operator method, but rather, has sought to investigate and apply it to numerous multicriteria conditions. Hence, this introduction sees four multicriteria methods that will be applied to ESO in order to be compared and analysed. Other multicriteria methods mentioned above (Section 1.4.2) have not been included in this dissertation because of time constraints to the project. Furthermore, for the analysis of this project, parameters that affect such things as the shape and distribution of points along the Pareto curve shall be investigated.

One point of interest concerning the multicriteria method applied to ESO is the number of criteria actually being optimised for. Because ESO generally involves starting off with an over designed domain and the removal of elements from this domain (unless BESO is being used), the consequence is that weight (or alternatively volume) is being reduced during the

evolutionary process. This in itself becomes an implicit criterion. And so when ESO addresses the optimisation of numerous criteria, say N criteria, then in fact, the total criteria being optimised for becomes $N + 1$ criteria. This includes the additional preference to reduce weight. Such a point could be graphically examined by displaying the $N + 1$ criteria on a graph – with each criterion being represented on a separate axis. One axis would represent the weight objective. Of course this graphical representation is limited to a 3-D space to be visible.

Other structural optimisation methods – particularly classical continuous type problems (Osyczka, 1981, Pietrzak, 1994) or discrete variable problems (Hajela *et al.*, 1990; Koski and Silvennoinen, 1990; Grandhi *et al.*, 1993) or both (Shih and Hajela, 1989) do include weight or volume reduction as a specific criterion. For simplicity, the weight reduction component is excluded in this thesis as being identified as a formal criterion. Unless stated otherwise, only those mentioned will be considered as the formal objectives or criteria.

1.5 Scope of Research

The way that structures operate is extremely complex. This is true for all things such as the inter-atomic forces between molecules making up structures varying to things like the bulk forces having an impact on the overall structure. Structural analysis is a tool used to model and analyse these complex structures. But in order to analyse, simple models that imitate the actual one can only be constructed. Engineering analysis is at this stage of development. However, things are now changing such that the computational power of processing tools is becoming more powerful, the analytical methods are becoming more flexible, the modelling techniques are becoming more robust, and thus analysis is becoming more accurate. The models created nowadays replicate more precisely what actually exists.

This thesis contributes to the arenas of analytical and modelling flexibility. Features are developed within the ESO framework, so that the optimisation designs created are more so appropriate for the tasks required.

The objective of this research is to extend the capabilities and features of ESO, as well as to highlight at present its usefulness with some practical case examples. The aim is not to

mathematically verify the ESO technique as a valid structural optimisation process. Rather it is to validate the ESO technique combined with other methods that make it more practical to the designer and engineer. In the development of this extension of work, many examples have been presented. The first example in each new concept (outlined in each chapter) is benchmarked with those results produced by other methods. Furthermore, this thesis aims to substantiate the usefulness of the technique by way of various practical case studies.

The approach to satisfying the above objectives takes the form of four main topics. The first is Multiple Criteria ESO. Today, the enhancement and optimisation of structures more so necessitates rather than accommodates the need for the inclusion of numerous coexisting objectives. The optimisation of any given structure using ESO has solely been founded upon a single criterion, although as mentioned above, implementation has been made for more than one. This work implements the proposal of optimising numerous criteria simultaneously in the ESO process. It gives a foretaste of the bi and tri-criteria that can be used in ESO, and concerns various two criteria combinations and a three criteria combination. Numerous multicriteria methods have been implemented and tested in the process.

The second topic is greatly interconnected to the first. It is the optimisation of cross-sectional areas of structures based on enhancing the moment of inertia properties. Similar to ESO, this new method is introduced as Evolutionary Moment of Inertia Optimisation (EMIO). Whether it is the bending performance (associated with the rectangular and product moment of inertia) or the rotational performance (likewise associated with the polar moment of inertia), the betterment of such quantities is also a necessity in optimisation. EMIO addresses the shape and topologies of any given cross-section based on the designer's moment of inertia preference. The concept is then integrated into the multicriteria process as an additional criterion to be simultaneously optimised.

The third area of investigation that continues to advance the ESO method is Constant Width Layer (CWL) ESO. Most real structures, especially biological ones, are not composed of isotropic material throughout. In fact, many structures are composed of a material with continually varying properties. Many too are constructed with discrete layers of different materials. This thesis seeks to include an aspect of that reality by optimising structures made of two distinct materials. The first is a material of one property type that is located along the

perimeter of the structure – where shape optimisation takes place. The second type of material fills the remainder of the structure. During the optimisation process, the width of that outer surrounding material remains constant with the overall shape being evolved. The methodology could be extended to many layers.

There are many different applications where Constant Width Layer ESO may be used. This work seeks to apply the CWL ESO method to the area of dentistry – or more specifically – to the restoration of dental bridges. This is a technique where a prosthetic tooth is created and is attached to the two surrounding teeth. Hence, this section focuses on two case studies, which have not previously been examined in the ESO arena. They constitute the fourth topic, and are the optimisation of anterior (front of the mouth) ceramic dental bridges, and the optimisation of posterior (back of the mouth) ceramic dental bridges. In these studies, various models simulating the in-vivo environment are optimised and are rigorously compared to other models produced by other means. These studies have paved the way for ESO being of primary significance in many other case studies to come.

1.6 Layout of Thesis

Presenting such topics has been done by way of organising this manuscript into nine chapters. The composition and structure of this dissertation into these chapters derives from a series of papers published or prepared for publication in journals and conference proceedings. A compendium of these papers is listed at the beginning of this thesis (see List of Publications).

This first chapter has established the basic concepts and workings of different structural optimisation methods, the development of the ESO method over recent years, and the latest advances associated with ESO. Also, it establishes the multicriteria structural optimisation problem, highlighting various methods used to solve the problem. It then has put forward the thesis proposal to demonstrate how multicriteria optimisation, Evolutionary Moment of Inertia Optimisation and Constant Thickness Layer ESO has been incorporated into ESO and the factors that affect it.

The second chapter formally incorporates multiple criteria optimisation into the ESO process. This is done using the traditional weighting and logical AND operator method, as well as introducing the two new methods – the logical OR operator method, and the global criterion method. The two criteria that are optimised simultaneously are the maximisation of the first mode of natural frequency and the minimisation of the mean compliance of the structure (which is inversely proportional to stiffness).

There is a clear requirement nowadays to improve the design of structures such as to increase the bending rigidity of a beam about a defined axis, or to increase or decrease the tendency of a rotational object to accelerate or de-accelerate, for a given cross-sectional area. Chapter three examines the new design method - Evolutionary Moment of Inertia Optimisation, where the objective is to optimise the Moment of Inertia (MOI). This concerns the cross-section of objects, restricted to 2-D geometries of finite element meshes. The specific components studied herein are the rectangular, product and polar moment of inertia.

In continuation of the recent development of ESO applied to the simultaneous objective to maximise the natural frequency and to minimise the mean compliance, Chapter 4 presents the multicriteria ESO optimisation of two new criteria – the minimisation of mean compliance and the maximisation of the specific inertia. This has been done with the four different multicriteria methods mentioned above.

Chapter 5 examines the multicriteria optimisation of three criteria applied to the ESO design algorithm. These objectives are the maximisation of specific stiffness, the maximisation of the fundamental frequency and the maximisation of the radius of gyration. Again, four different multicriteria methods are incorporated into the multicriteria ESO technique. Two examples have been used to validate these methods in the multicriteria ESO process.

Chapter 6 introduces and examines the concept of shape optimisation with the presence of a constant layer of material around the perimeter of the structure in question (CWL ESO). Two different examples are presented and variables affecting the algorithm are examined.

An anterior and posterior dental bridge made of a new ceramic material In-Ceram (Vita Zahnfabrik H. Rauter GmbH & Co. KG, 1998) is the focus of Chapter 7 and 8 respectively. The CWL ESO algorithm is the basis for the optimisation of these bridges. The mechanical

behaviour of pre-existing models has been compared with the optimised profiles obtained from the CWL ESO algorithm. Such comparisons were made using Finite Element Analysis (FEA).

The final chapter brings together all the ideas presented in this manuscript, highlighting the significance and implications of the work presented. It makes recommendations to further advance the ESO cause in its contribution to structural optimisation.

1.7 References

Adali, S.(1983), "Pareto Optimal Design of Beams Subjected to Support Motions", *Computers and Structures*, Vol. 16, pp. 297-303.

Allaire, G., Kohn, R., V. (1993), "Topology Optimization and Optimal Shape Design Using Homogenisation", Bendsøe, M., P., Mota Soares, C., A., (Eds.) *Topology Design of Structures*, Kluwer Academic Publishers, Dordrecht, Netherlands, pp. 207-218.

Ashley, H. (1982), "On Making Things the Best – Aeronautical Uses of Optimization", *Journal of Aircraft*, Vol. 19, No. 1.

Balachandran, M., Gero, J., S. (1984), "A Comparison of the Three Methods for Generating the Pareto Optimal Set", *Engineering Optimization*, Vol. 7, pp. 319-336.

Barton, A., C., Steven, G., P., Querin, O., M., Xie, Y., M. (1998), "Minimising Material Usage in a Plastic Milk Crate through Structural Optimisation", Schäfer, A., I., Basson, L., Richards, B., S., (Eds.) *Environmental Engineering Research Event, Environmental Engineering in Australia: Opportunities and Challenges*, Avoca Beach, Australia, 7th-9th December, pp. 135-140.

Beale, E., M., L., (1988), *Introduction to Optimization*, John-Wiley and Sons, Great Britain.

Bendsøe, M., P., Kikuchi, N. (1988), "Generating Optimal Topologies in Structural Design Using a Homogenisation Method", *Computer Methods in Applied Mechanics and Engineering*, Vol. 71, pp. 197-224.

Bendsøe, M., P. (1995), *Optimisation of Structural Topology, Shape, and Material*, Springer, Berlin, Germany.

Carmichael, D., G. (1980), "Computation of Pareto Optima in Structural Design", *Numerical Methods in Engineering*, Vol. 15, pp. 925-952.

Chen, T., Wu, S. (1998), "Multiobjective Optimal Topology Design of Structures", *Computational Mechanics*, Vol. 21, 483-492.

Chu, D., N., Xie, Y., M., Hira, A., Steven, G., P. (1996), "Evolutionary Structural Optimisation for Problems with Stiffness Constraints", *Finite Elements in Analysis and Design*, Vol. 21, pp. 239-251.

Falzon, B., G., Steven, G., P., Xie, Y., M. (1996), "Shape Optimisation of Interior Cutouts in Composite Panels", *Structural Optimization*, Vol. 11, pp. 43-49.

García, M., J. (1999), *Fixed Grid Finite Elements Analysis in Structural Design and Optimisation*, Doctorate Thesis, School of Aeronautical, Mechatronic and Mechanical Engineering, University of Sydney, Australia.

Goldberg, D., E. (1989), *Genetic Algorithms in Search, Optimization and Machine Learning*, Addison-Wesley, USA.

Grandhi, R., V., Bharatram, G., Venkayya, V. (1993), "Multiobjective Optimization of Large-Scale Structures", *AIAA Journal*, Vol. 31, No. 7, pp. 1329-1337.

Guan, H., Steven, G., P., Querin, O., M., Xie, Y., M. (1997), "Design of Wheels by the Evolutionary Structural Optimisation Method", *Proceedings of EPMESC VI – the Sixth International Conference on Education and Practice of Computational Methods in Engineering and Science*, Guangzhou, China, 4th-7th August, Vol. 1, pp. 203-208.

Haftka, R., T., Kamat, M., P. (1985), *Elements of Structural Optimization*, Martinus Nijhoff Publishers, The Netherlands.

Hajela, P., Shih, C., -J. (1990), "Multiobjective Optimum Design in Mixed Integer and Discrete Design Variable Problems", *AIAA Journal*, Vol. 28, No. 4, pp. 670–675.

Kim, H., Querin, O., M., Steven, G., P., Xie, Y., M. (1998), "Development of an Intelligent Cavity Creation (ICC) Algorithm for Evolutionary Structural Optimisation", *Proceedings of the Australasian Conference on Structural Optimisation*, Sydney, Australia, pp. 241-250.

Kim, H., Querin, O., M., Steven, G., P. (2000), "Post-Processing of the Two-Dimensional Evolutionary Structural Optimisation Topologies", Parmee, I., C., (Ed.) *Evolutionary Design and Manufacture: Selected Papers from Adaptive Computing in Design and Manufacture '00*, Springer, UK.

Koski, J. (1985), "Defectiveness of Weighting Method in Multicriterion Optimization of Structures", *Communications in Applied Numerical Methods*, Vol. 1, pp. 333-337.

Koski, J. (1988), "Multicriteria Truss Optimization", Stadler, W. (Ed.), *Multicriteria Optimization in Engineering and the Sciences*, Plenum Press, New York, United States of America, pp. 263-307.

Koski, J., Silvennoinen, R. (1990), "Multicriteria Design of Ceramic Piston Crown", *Engineering Costs and Production Economics*, Vol. 20, pp. 175-189.

Koski, J. (1993), "Multicriteria Optimization in Structural Design: State of the Art", *Advances in Design Automation*, Vol. 1, pp. 621-629.

Koski, J. (1994), "Multicriterion Structural Optimization", Adeli, H., (Ed.), *Advances in Design Optimization*, Chapman and Hall, London, United Kingdom.

Krog, L., Olhoff, N. (1998), "Optimum Topology and Reinforcement Design of Disk and Plate Structures with Multiple Stiffness and Eigenfrequency Objectives", *Computers and Structures*, Vol. 72, pp. 535-563.

Kristensen, E., Madsen, N. (1972), "On the Optimum Shape of Fillets in Plates Subject to Multiple In-Plane Loading Cases", *International Journal of Numerical Methods in Engineering*, Vol. 10, pp. 1007-1019.

Lencus, A., Querin, O., M., Steven, G., P., Xie, Y., M. (1999a), "Modifications to the Evolutionary Structural Optimisation (ESO) Method to Support Configurational Optimisation", *CD-Rom Proceedings of the 3rd World Congress of Structural and Multidisciplinary Optimization*, New York, USA.

Lencus, A., Querin, O., M., Steven, G., P., Xie, Y., M. (1999b), "Group ESO with Morphing", *First ASMO UK / ISSMO Conference on Engineering Design Optimization*, Ilkley, UK, pp. 241-248.

Lencus, A., Querin, O., M., Steven, G., P., Xie, Y., M. (2000), "Aircraft Wing Design Automation with ESO and GESO", *Proceedings of OptiCON2000 conference on Optimization Software, Methods and Applications*, Newport Beach, California, USA, 26th-27th October.

Li, Q., Steven, G., P., Querin, O., M., Xie, Y., M. (1997), "Optimal Shape Design for Steady Heat Conduction by the Evolutionary Procedure, Inverse Problems in Heat Transfer and Fluid Flow", Dulikravich, G., S., Woodbury, K., A., (Eds.) *ASME Proceedings of the 32nd National Heat Transfer Conference*, ASME HTD, Vol. 340, pp.159-164.

Li, Q., Steven, G., P., Xie, Y., M. (1999a), "Evolutionary Shape Optimization A Stress Based Sensitivity Analysis Method", *Proceedings of the Second Australian Congress on Applied Mechanics ACAM '99*, Canberra, Australia, 9th-12th February.

Li, Q., Steven, G., P., Querin, O., M., Xie, Y., M. (1999b), "Evolutionary Optimization for Cross Sectional Shape of Torsional Shafts", *Proceedings of the 3rd World Congress on Structural and Multidisciplinary Optimization (WCSMO-3)*, CD Volume, New York, USA.

Li, Q. (2000), *Evolutionary Structural Optimization for Thermal and Mechanical Problems*, Doctorate Thesis, School of Aeronautical, Mechatronic and Mechanical Engineering, University of Sydney, Australia.

Li, W., Steven, G., P., Xie, Y., M. (1998a), "Shape Design for Elastic Contact Problems by Evolutionary Structural Optimisation", *Seventh AIAA/NASA/USAF/ISSMO Symposium on Multidisciplinary Analysis and Optimization,* St Louis, Missouri, USA, 2-4th September, pp. 1108-1114.

Lógó, J., Vásárhelyi, A. (1988), "Pareto Optima of Reinforced Concrete Frames", *Periodica Polytechnica, Civil Engineering*, Vol. 32, pp. 87-96.

Manickarajah, D., Xie, Y., M., Steven, G., P. (1998), "An Evolutionary Method for Optimization of Plate Buckling Resistance", *Finite Elements in Analysis and Design*, Vol. 29, pp. 205-230.

Mattheck, C., Moldenhauer, H. (1990), "An Intelligent CAD-Method Based on Biological Growth", *Fatigue and Fracture of Engineering Material and Structures*, Vol. 13, pp. 41-51.

Maute, K., Ramm, E. (1995), "Adaptive Topology Optimization", *Structural and Multidisciplinary Optimization*, Vol. 10, pp. 100-112.

Maxwell, J., C. (1872), "On Reciprocal Figures, Frames and Diagrams of Force", *Trans. Roy. Soc. Edinb.*, Vol. 26, No. 1.

Michell, A., G., M. (1904), "The Limits of Economy of Material in Frame-Structures", *Philosophical Magazine*, Vol. 8, pp. 589-597.

Osyczka, A. (1981), "An Approach to Multicriterion Optimization for Structural Design", *International Symposium on Optimum Structural Design*, Arizona, 19th-22nd October, pp. 1037-1040.

Osyczka, A., Montusiewicz, J. (1993), "A Random-Search Approach to Multicriterion Discrete Optimization", Gutkowski, W., Bauer, J. (Eds.), *Discrete Structural Optimization*, Springer-Verlag, Berlin, Germany, pp. 71-79.

Osyczka, A. (1995), "A New Method to Solve Generalized Multicriteria Optimization Problems Using the Simple Genetic Algorithm", *Structural Optimization*, Vol. 10, pp. 94-99.

Oxford University Press (1989), *Oxford English Dictionary (2nd Edition)*, Oxford University Press, London, UK.

Pedersen, P., Tobiesen, L., Jensen, S. (1992), "Shapes of Orthotropic Plates for Minimum Energy Concentration", *Mechanical Structures and Machinery*, Vol 20, pp. 499-514.

Pietrzak, J. (1994), "Bi-criteria optimisation of structures liable to instability", *Structural and Multidisciplinary Optimization*, Vol. 7, pp. 61-65.

Prager, W. (1956), "Minimum Weight Design of Plates", *Applied Mechanics Review*, Vol. 9.

Prager, W., Rozvany, G., I., N. (1977), "Optimization of Structural Geometry", Bednarek, A., R., Cesarj, L., (Eds.) *Dynamical Systems*, Academic Press, New York, pp. 265-293.

Querin, O., M., Steven, G., P., Xie, Y., M. (1996), "Topology Optimisation of Structures with Material and Geometric Non-Linearities", *Sixth AIAA/NASA/USAF/ISSMO Symposium on Multidisciplinary Analysis and Optimization,* Bellevue, Washington, USA, 4-6th September, pp. 1812-1818.

Querin, O., M. (1997), *Evolutionary Structural Optimisation: Stress Based Formulation and Implementation*, Doctorate Thesis, School of Aeronautical, Mechatronic and Mechanical Engineering, University of Sydney, Australia.

Rabinovich, I., M. (1933), "On The Theory of Statically Indeterminate Lattices", *Centr. Inst. Transp. Stroit.*.

Rao, S. (1984), "Multiobjective Optimization in Structural Design with Uncertain Parameters and Stochastic Processes", *AIAA Journal*, Vol. 22, pp. 1670-1678.

Rao, S., S. (1987), “Game Theory Approach for Multiobjective Structural Optimization”, *Computers and Structures*, Vol. 25, pp. 119-127.

Rao, S., S., Dhingra, A., K., Miura, H. (1990), “Pareto-Optimal Solutions in Helicopter Design Problems”, *Engineering Optimisation*, Vol. 15, pp. 211-231.

Rosenman, M., A., Gero, J., S. (1985), “Reducing the Pareto Optimal Set in Multicriteria Optimization (With Applications to Pareto Optimal Dynamic Programming)”, *Engineering Optimization*, Vol. 8, pp. 189-206.

Rozvany, G., I., N., Bendsøe, M., P., Kirsch, U. (1995), “Layout Optimization of Structures”, *Applied Mechanics Review*, Vol. 48, No. 2, pp. 41-119.

Saravanos, D., Chamis, C. (1992), "Multiobjective Shape and Material Optimization of Composite Structures Including Damping", *AIAA Journal*, Vol. 30, pp 805-813.

Sawaragi, Y., Nakayama, H., Tanino, T. (1985), *Theory of Multiobjective Optimization*, Academic Press Inc., Orlando, USA.

Schmidt, L., A. (1989), “Structural Synthesis – Its Genesis and Development”, *AIAA Journal*, Vol. 19, No. 10.

Sheu, C., Y., Prager, W. (1968), “Recent Developments in Optimal Structural Design”, *Applied Mechanics Reviews*, Vol. 21, No. 10.

Shih, C., -J., Hajela, P. (1989), “Multicriterion Optimum Design of Belleville Spring Stacks with Discrete and Integer Decision Variables”, *Engineering Optimization*, Vol. 15, pp. 43-55.

Stadler, W., Dauer, J. (1993), “Multicriteria Optimization in Engineering: A Tutorial and Survey”, Kamat, M., (Ed.) Structural Optimization: Status and Promise, AIAA Inc., Washington, USA.

Steven, G., P., Querin, O., M., Xie, Y., M. (1995), "Multiple Constraint Environments for Evolutionary Structural Optimization", Olhoff, N., Rozvany, G., I., N., (Eds.) *Proceedings of the First World Congress on Structural and Multidisciplinary Optimization*, Goslar, Germany, 28th May – 2nd June, pp. 213-218.

Steven, G., P., Querin, O., M., Xie, Y., M. (1997), "Structural Perfection: Real or Imaginary (or the Place of FEA)", *Proceedings of NAFEMS World Congress '97*, Stuttgart, Germany, 9th–11th April, Vol. 1, pp. 37-48.

Tappeta, R., Renaud, J. (2001), "Interactive Multiobjective Optimization Design Strategy for Decision Based Design", *Journal of Mechanical Design*, Vol. 123, pp. 205-215.

Tseng, C., Lu, T. (1990), "Minimax Multiobjective Optimization in Structural Design", *International Journal for Numerical Methods in Engineering*, Vol. 30, pp. 1213-1228.

Van Der Veen, B. (1967), *Introduction to the Theory of Operational Research*, N.V. Philips' Gloeilampenfabrieken, The Netherlands.

Vanderplaats, G., N. (1984), *Numerical Optimization Techniques for Engineering Design with Applications*, McGraw-Hill, USA.

Vita Zahnfabrik H. Rauter GmbH & Co. KG (1998), *Vita Full Ceramics, Vita In-Ceram® Alumina, Brochure B/IC-AL*.

Wasiutynski, Z. (1939), "The Strength Design (In Polish)", *Acad. Tech. Sci.*, Warsaw, Poland.

Wasiutynski, Z., Brandt, A. (1963), "The Present State of Knowledge in the Field of Optimum Design of Structures", *Applied mechanics Review*, Vol. 16, No. 5.

Woon, S., Querin, O., Steven, G., Tong, L. (2002), "Optimisation of Continuum Structures Through a Multi-GA Hybrid", submitted to *9th AIAA/ISSMO Symposium on Multidisciplinary Analysis and Optimisation*, Atlanta, Georgia, 4-6th September.

Xie, Y., M., Steven, G., P. (1994), "Optimal Design of Multiple Load Case Structures Using an Evolutionary Procedure", *Engineering Computations*, Vol. 11, pp. 295-302.

Xie, Y., M., Steven, G., P. (1997), *Evolutionary Structural Optimisation*, Springer-Verlag, London, UK.

Young, V., Querin, O., M., Steven, G., P., Xie, Y., M. (1999), "3D and Multiple Load Case Bi-directional Evolutionary Structural Optimisation (BESO)", *Structural and Multidisciplinary Optimization*, Vol. 18, pp. 183-192.

Zhang, W., Domaszewski, M., Fleury, C. (2001), "An Improved Weighting Method with Multibounds Formulation and Convex Programming for Multicriteria Structural Optimization", *International Journal for Numerical Methods in Engineering*, Vol. 52, pp. 889-902.

Chapter 2

Stiffness and Frequency Multicriteria ESO

2.1 Introduction

Previous research for dual-criteria ESO has been presented for minimising the maximum von Mises stress together with maximising the stiffness of a structure (Li, 2000). Here, Li used the linear weighting method to produce an appropriate trade-off between the 'stiffest design' and the 'strongest design'. It was found that the optimised designs with the stiffness maximisation criterion differed from those with the stress minimisation one. From a programming perspective, this multicriteria problem involved the simultaneous optimisation of two linear static analyses (stiffness and stress). With this establishment comes the question – what about the simultaneous optimisation of other combinations of criteria – or alternatively other combinations of FEA solver analyses? Does a Pareto distribution of solutions exist? For example, how does Multicriteria ESO handle the objective to optimise a linear static analysis criteria in conflict with the objective to optimise a natural frequency analysis criteria?

Many papers have examined multicriteria optimisation involving linear static analyses (ie stiffness maximisation). The majority of these have examined the corresponding criteria of weight (or alternatively volume or area) reduction combined with stiffness maximisation (or alternatively displacement minimisation): Osyczka (1981), Grandhi *et al.* (1993), Otswald (1996), Koski (1998), Jensen (1998), Pietrzak (1999a), Tappeta *et al.* (2000), Zhang (2001), Tappeta and Renaud (2001). As mentioned previously, the minimisation of weight is not herein considered as a formal objective in light of the ESO process, where it is implicit with the removal of material.

There are relative few papers that examine the simultaneous optimisation of both linear static and natural frequency objectives. This alludes to the fact that it is a new topic in multicriteria optimisation. A number of these papers also include a third additional objective, which are covered in detail in Chapter 5. The bi-criteria topics of stress (linear-static problem) and frequency (natural frequency problem) has been indirectly addressed by Dems and Gutkowski (1998). They used a method that is based upon simultaneous solutions of equations and inequalities from the Kuhn-Tucker conditions necessary for an optimum problem. By seeking to minimise the volume of a 2-D Finite Element body made with a constant thickness, they applied constraints imposed on the stress and eigenfrequency. They were able to give a practical method of the shape optimisation of machine parts and structural members subjected to multiple static and dynamic loading conditions.

The closest approach of multicriteria optimisation applied to the use of 2-D Finite Elements for linear static and natural frequency problems has been accomplished by Chen and Wu (1998). They defined their problem as the minimisation of the objective function based on the global criterion function (see Equation (1.13)). The global criterion function combined the objectives to maximise the stiffness and maximise the fundamental eigenvalues of 2-D FE plates with orthogonal loading. Using a structural optimisation method that was based on changing the design variables of normalised densities of the finite elements (similar to the homogenisation method – Bendsøe and Kikuchi, N. (1988)), they were able to demonstrate the variations of the compliances and eigenvalues according to their weights in the cost function. The larger the weight, the better the result for the corresponding objective.

This chapter investigates the multicriteria optimisation problem incorporated into ESO for two different solver types – linear static analysis and natural frequency analysis. More specifically, it has the objectives to maximise the stiffness and to maximise the first mode of natural frequency. Under investigation will be whether the four multicriteria methods presented in Section 2.4 of this chapter, produce solutions of Pareto nature. The relationship between the four methods as well as the factors affecting the distribution of points making up the Pareto solution will be identified. In contrast to the work of Chen and Wu (1998), the examples covered in this chapter are all two dimensional plane stress problems, where the applied loads are in-plane.

2.2 Determination of Sensitivity Numbers for Element Removal

The procedure for the weighted method and global criterion method of multicriteria optimisation begins with the evaluation of the two criteria on the model in question. This is proceeded by the options for combining these two criteria into one, which shall later be adopted by the evolutionary algorithm for element removal. A similar procedure is used for the multicriteria optimisation based on the logical operators. Again the two criteria are analysed, followed by element removal based on the logical AND operator and another procedure of element removal based on the logical OR operator.

The evaluation of the element stiffness and frequency sensitivity numbers is described in this section. A description of the multicriteria method of weighting and the global criterion method by combining the two different criteria into one new criterion is presented in Section 2.3. The AND and OR logical Multicriteria ESO use the sensitivity numbers to evaluate whether elements are to be removed. The removal of the elements based on these Multicriteria ESO methods will be explained in Section 2.4.

2.2.1 Stiffness Contribution

In the finite element method, the static behavior of a structure is given by:

$$[\boldsymbol{K}]\{\boldsymbol{d}\} = \{\boldsymbol{P}\} \tag{2.1}$$

where $[\boldsymbol{K}]$ is the global stiffness matrix, $\{\boldsymbol{d}\}$ and $\{\boldsymbol{P}\}$ are the global nodal displacement and nodal load vectors respectively. For a constant load, an inverse measure of the overall stiffness of a structure is known as the mean compliance, C, and is defined as:

$$C = \tfrac{1}{2}\{\boldsymbol{P}\}^T\{\boldsymbol{d}\} \tag{2.2}$$

Therefore, the single criterion objective to minimise the mean compliance C is mathematically given as:

$$\text{minimise } (C) \tag{2.3}$$

Minimising the mean compliance maximises the overall stiffness of a structure. Hence the stiffness constraint is given in the form $C \le C_{all}$, where C_{all} is the prescribed limit for C (Xie and Steven, 1997; Manickarajah and Xie, 1997).

From this comes the stiffness sensitivity number for problems with an overall stiffness constraint (Xie and Steven, 1997):

$$\alpha^i = \tfrac{1}{2}\{u^i\}^T [K^i]\{u^i\} \tag{2.4}$$

where $\{u^i\}$ is the displacement vector of the i^{th} element and $[K^i]$ is the stiffness matrix of the i^{th} element. The quantity α^i indicates the change in the strain energy as a result of removing the i^{th} element. To achieve the optimisation objective through element removal, the element that has the lowest value of α^i is removed so that the increase in C is minimal.

Note that although C inevitably goes up with element removal, the optimisation process is such that the product of the compliance and the structures' volume (V): ($C \times V$) goes down. In other words, the 'specific stiffness' (K / V) is increased optimally.

2.2.2 Frequency Contribution

The dynamic behavior of the structure is represented by the following general eigenvalue problem:

$$([\boldsymbol{K}] - \omega_n^2 [\boldsymbol{M}])\{\boldsymbol{u}_n\} = \{0\} \tag{2.5}$$

where $[\boldsymbol{M}]$ is the global mass matrix, ω_n is the n^{th} natural frequency and $\{\boldsymbol{u}_n\}$ is the eigenvector corresponding to ω_n. The mathematical representation for the single criterion maximisation of the fundamental frequency may, therefore, be given as:

$$\text{maximise } (\omega_n) \tag{2.6}$$

The frequency sensitivity number α_n^i for the n^{th} mode, which is an indicator of the frequency change (or to be more precise, the change of the square of the frequency) due to the removal of the i^{th} element is given by Equation (2.7) (Xie and Steven, 1996):

$$\alpha_n^i = \frac{1}{m_n} \{\boldsymbol{u}_n{}^i\}^T (\omega_n^2 [\boldsymbol{M}^i] - [\boldsymbol{K}^i]) \{\boldsymbol{u}_n{}^i\} \tag{2.7}$$

in which m_n is the modal mass, $\boldsymbol{u}_n{}^i$ is the element eigenvector, $[\boldsymbol{K}^i]$ and $[\boldsymbol{M}^i]$ are the stiffness and mass matrices of the removed element. The removal of elements whose frequency sensitivity number is the highest, results in a maximum increase in the chosen frequency. The removal of elements whose frequency sensitivity number is the lowest results in a maximum decrease in the chosen frequency. Removal of those elements whose α is close to zero, results in very little change, that is, keeping the frequency constant (Xie and Steven, 1996). Note that due to Equation (2.5), the sum of α_i over all the elements must be zero.

For Multicriteria ESO, using linear static sensitivity numbers in collaboration with the frequency sensitivity numbers necessitates a linear scaling in the frequency sensitivity numbers.

For the case of weighting and the global criterion method of Multicriteria ESO, this is done to alleviate the problem of combining the stiffness sensitivity number (with element removal based on the lowest sensitivity values) and the frequency sensitivity number (with element removal based on the highest sensitivity values). The shift allows the criteria to be combined into the single weighted criterion $F_{multicrit}^i$ or a balanced global criterion $G_{multicrit}^i$ (see Equations 2.9 and 2.11) with the removal of elements based on their lowest sensitivity values.

For the cases of the logical Multicriteria ESO, a linear shift in the frequency sensitivity number is made to alleviate the problem of relatively contrasting the stiffness sensitivity numbers (with element removal based on the lowest sensitivity values), and the frequency sensitivity numbers (with element removal based on the highest sensitivity values).

The frequency sensitivity number linear shift is attained using the formula:

$$\left\{\alpha_n^i\right\}^{new} = -\left(\left\{\alpha_n^i\right\}^{old}\right) + \left\{\alpha_n^*\right\}^{old} \tag{2.8}$$

where:

$\left\{\alpha_n^i\right\}^{new}$ is the new frequency sensitivity number for the i^{th} element and the n^{th} natural frequency;

$\left\{\alpha_n^i\right\}^{old}$ is the old frequency sensitivity number for the i^{th} element and the n^{th} natural frequency;

$\left\{\alpha_n^*\right\}^{old}$ is the old maximum frequency sensitivity number for the n^{th} natural frequency.

Figure 2.1 illustrates the linear shift in the natural frequency sensitivity number.

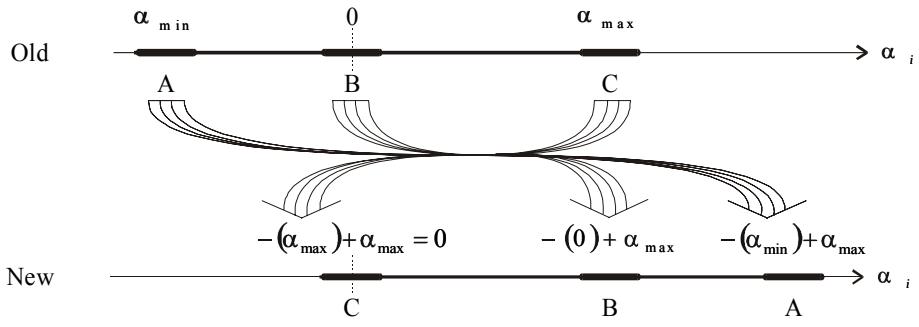

Figure 2.1 Change in natural frequency sensitivity number.

In the formulation of this linear shift of the natural frequency sensitivity number to make it comparable to the same process of element removal for the stiffness sensitivity number, it was decided that normalisation of the sensitivity numbers of any of the criteria was not necessary. This was because, as shall be seen in Sections 2.4.3 and 2.4.4 (for the logical operators only), the decision to remove elements for each criterion is made by a comparison of each criterions' sensitivity numbers to the rejection ratio multiplied by the maximum sensitivity value of that criterion (see Equation (1.5)). Thus the deletion condition is relative to each criterion. Only then can the criterion be compared to each other as determined by either the logical AND operation method or the logical OR operation method.

2.3 Multicriteria Optimisation Techniques

2.3.1 Weighting Method Formulation

The Weighting method is similar to those mentioned by Grandhi *et al.* (1993) and Pietrzak (1994 and 1999b). It is used because of its simplicity to produce the whole set of Pareto optima for Equation (1.6), by varying the weighting on each criterion. This is only true for the case where problem (1.6) is convex (Koski, 1985). These weights indicate the relative importance of the criteria. Such a method can also take the designer's preference into account.

Having obtained the sensitivity numbers of the two criteria (described in the previous section), each of these numbers is normalised, and is then assigned their weighting factor. This formulation is based on the linear weighting method outlined in Section 1.4.2.2, in particular, Equation (1.14). These sensitivity numbers are finally added together to form a new single number:

$$F^{i}_{multicrit} = w_1 R^{i}_1 + w_2 R^{i}_2 + \ldots + w_N R^{i}_N = \sum_{j=1}^{N} w_j R^{i}_j \tag{2.9}$$

where:

$F^{i}_{multicrit}$	is the multiple criteria function that determines element removal;
w_j	is the j^{th} criteria weighting factor with $0.0 \le w_j \le 1.0$ and $j = 1,\ldots,N$;
$R^{i}_j = \dfrac{\alpha^{i}_j}{\alpha^{*}_j}$	is the ratio of the j^{th} criteria sensitivity number (α^{i}_j) for each element i, to the maximum value of the j^{th} criteria sensitivity number (α^{*}_j);
N	is the total number of criteria.

The criteria weighting is subject to the normalisation:

$$\sum_{j=1}^{N} w_j = 1 \tag{2.10}$$

2.3.2 Global Criterion Method Formulation

The global criterion method is used because it does not (unlike the weighting method) allow the designer to select a proportion of weighting allocated to each criterion. Rather, it implicitly allocates equal weighting to all criteria. It is based on the formulation of a metric function that represents the distance between the ideal solution (the minimum value of each criterion) and the optimum solution. The minimisation of this function according to Hajela and Shih (1990) results in the true optimum. This basis of this method was outlined in Section 1.4.2.1.

The metric function, obtained from the normalised Equation (1.13), is calculated by:

$$G^i_{multicrit} = \left[\left(R^i_1 - S^i_1\right)^p + \left(R^i_2 - S^i_2\right)^p + \ldots + \left(R^i_N - S^i_N\right)^p\right]^{\frac{1}{p}}$$
$$= \left[\sum_{j=1}^{N}\left(R^i_j - S^i_j\right)^p\right]^{\frac{1}{p}} \tag{2.11}$$

where:

$G^i_{multicrit}$ is the metric multiple criteria objective function that determines element removal for each element *i;*

$S^i_j = \frac{\alpha^{\min}_j}{\alpha^*_j}$ is the ratio of the minimum value of the j^{th} criteria sensitivity number ($\alpha^{\min}_j$), to the maximum value of the j^{th} criteria sensitivity number (α^*_j).

p is a constant constrained by the condition $1 \leq p \leq \infty$. Typically $p = 1$ or 2. In this chapter, p is elected to be equivalent to the number of criteria analysed ie $p = N = 2$. The reasoning behind this was that the norm of vectors is kept in the $p = 2$ space. The best example of this is the "least squares" method. This shall be the case for the other chapter based on the multicriteria optimisation of two criteria ie Chapter 4.

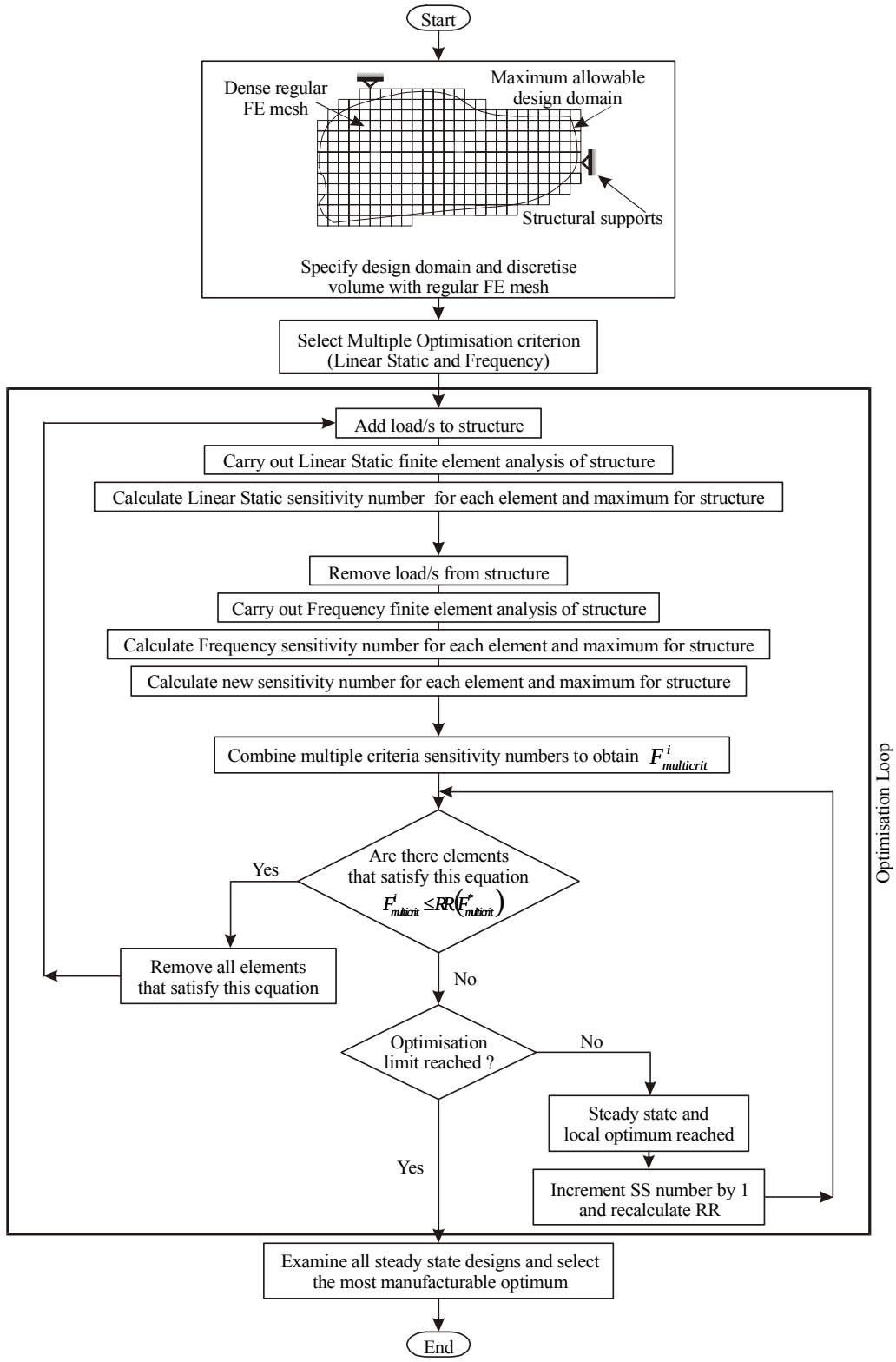

Figure 2.2 Flow chart depicting the logical steps of the Weighting method Multicriteria ESO.

2.4 Evolutionary Optimisation Procedure

2.4.1 Weighting Method Multicriteria ESO

The ESO algorithm for multi-criteria optimisation has a similar structure to that for single criterion ESO. However, it needs to use the natural frequency FEA solver in addition to that of the linear static FEA solver at each iteration. The evolutionary procedure for weighted Multicriteria optimisation based on ESO for stiffness and natural frequency is thus given as:

Step 1: Discretise the structure using a fine mesh of finite elements;

Step 2: Add load/s to structure;

Step 3: Solve the linear static problem - Equation (2.1);

Step 4: Calculate the linear static sensitivity number α_i using Equation (2.4);

Step 5: Remove load/s from structure;

Step 6: Solve the eigenvalue problem - Equation (2.5);

Step 7: Calculate the natural frequency sensitivity number α_n^i using Equation (2.7);

Step 8: Calculate the new natural frequency sensitivity number $\left\{\alpha_n^i\right\}^{new}$ using Equation (2.8);

Step 9: Combine the two criteria sensitivity numbers using Equation (2.9) to obtain $F_{multicrit}^i$;

Step 10: Remove a number of elements that have the lowest values of $F_{multicrit}^i$;

Step 11: Repeat Steps 2 to 10 until an optimum is reached.

Figure 2.2 illustrates the set of logical steps mentioned above. As can be seen, included in this flow chart is the natural frequency FEA solver in addition to the linear static FEA solver. The analysis time in the following examples is thus expected to take considerably longer compared to that of a single criterion optimisation problem, as both solvers are utilised for the combining of criteria per iteration. The evolution time will approximately double that than if one criterion is optimised for.

2.4.2 Global Criterion Method Multicriteria ESO

The solution procedure for achieving Multicriteria ESO using the global criterion method is similar to that in Sub-section 2.4.1. The only difference is in Steps 9 and 10 which should be replaced by:

Step 9: Combine the two criteria sensitivity numbers using Equation (2.11) to obtain $G^i_{multicrit}$;

Step 10: Remove a number of elements that have the lowest values of $G^i_{multicrit}$;

2.4.3 Logical AND Multicriteria ESO

Also for the logical AND operator, the solution to be obtained for achieving Multicriteria ESO uses a procedure similar to that of the linear weighting ESO method. Variations are in Steps 9, 10 and 11, which should be replaced by:

Step 9: Remove a number of elements that satisfy both the deletion criteria of the stiffness sensitivity number AND the deletion criteria of the frequency sensitivity number;

Step 10: Repeat Steps 2 to 9 until an optimum is reached.

2.4.4 Logical OR Multicriteria ESO

The solution procedure for achieving Multicriteria ESO using the OR logical operator is similar to that in the sub-section titled "Weighting method Multicriteria ESO". Again, Steps 9, 10 and 11, should be shortened down to two steps:

Step 9: Remove the number of elements that satisfy either the deletion criteria of the stiffness sensitivity number OR the deletion criteria of the frequency sensitivity number;

Step 10: Repeat Steps 2 to 9 until an optimum is reached.

2.5 Examples and Discussion

The examples presented in this section are all two-dimensional plane stress problems, with only in-plane vibration considered. The elements used here are of the four noded linear quadrilateral type. The two driving criteria are the maximisation of the stiffness and the maximisation of the first mode of natural frequency.

Concerning the pictorial topologies presented in this section, the areas displaying dark elements represent the remaining solid elements, where as the areas displaying small dots represent the nodes where elements have been removed. This shall be the case for all examples in the remaining chapters, unless indicated otherwise.

2.5.1 A Rectangular Plate with Fixed Supports

A rectangular aluminium plate of dimension 0.15 m × 0.1 m is fixed at two diagonal corners, with two horizontal loads (each 100 N) applied on the other two diagonal corners as seen in Figure 2.3. These are included for the linear static stress analysis, but are removed for the frequency analysis.

This example is based on a rectangular plate model that was used by Xie and Steven in their investigation of ESO for dynamic problems (Xie and Steven, 1996). The physical data is as follows: Young's modulus E = 70 GPa, Poisson's ratio ν = 0.3, thickness t = 0.01 m and density ρ = 2700 kg/m^3. The domain is divided into 45 × 30 square elements.

Figure 2.4 shows for a 30 % volume reduction, the comparison between the first mode natural frequency and the mean compliance of the structure for a range of different weighting of the criteria. The corresponding topologies for these weighting are seen in Figure 2.5.

For the extreme case of pure stiffness optimisation (w_{stiff} : w_{freq} = 1.0 : 0.0), the mean compliance is at the lowest possible value of 0.1837 Nm (see point 5.a), Figure 2.4). This verifies that this configuration is the stiffest possible structure. The natural frequency for this topology is 2666.6 Hz - the lowest frequency possible with 30 % of the material removed from the initial structure. Thus the optimisation based purely on each single criterion is optimum for its own objective.

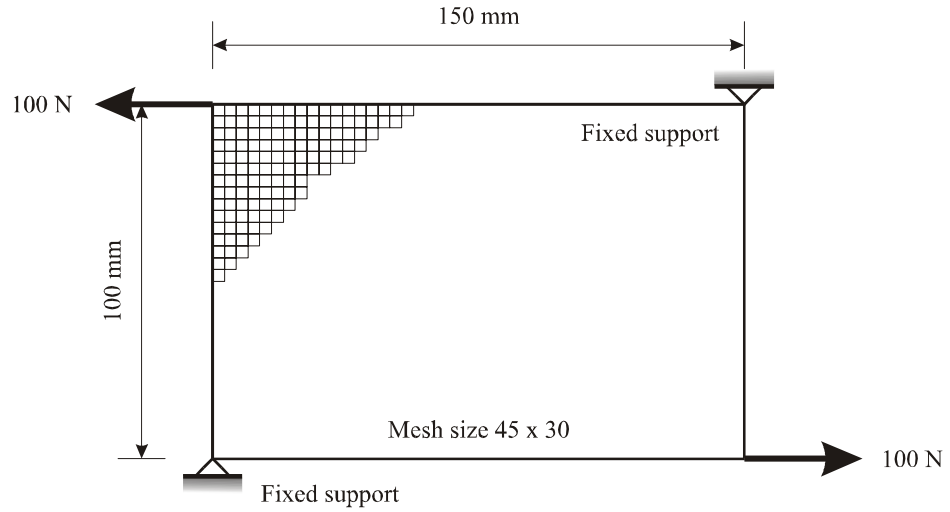

Figure 2.3 Initial design domain of a rectangular plate under loading with fixed supports. First mode natural frequency: 2498.9 Hz, mean compliance: 0.1751 Nm.

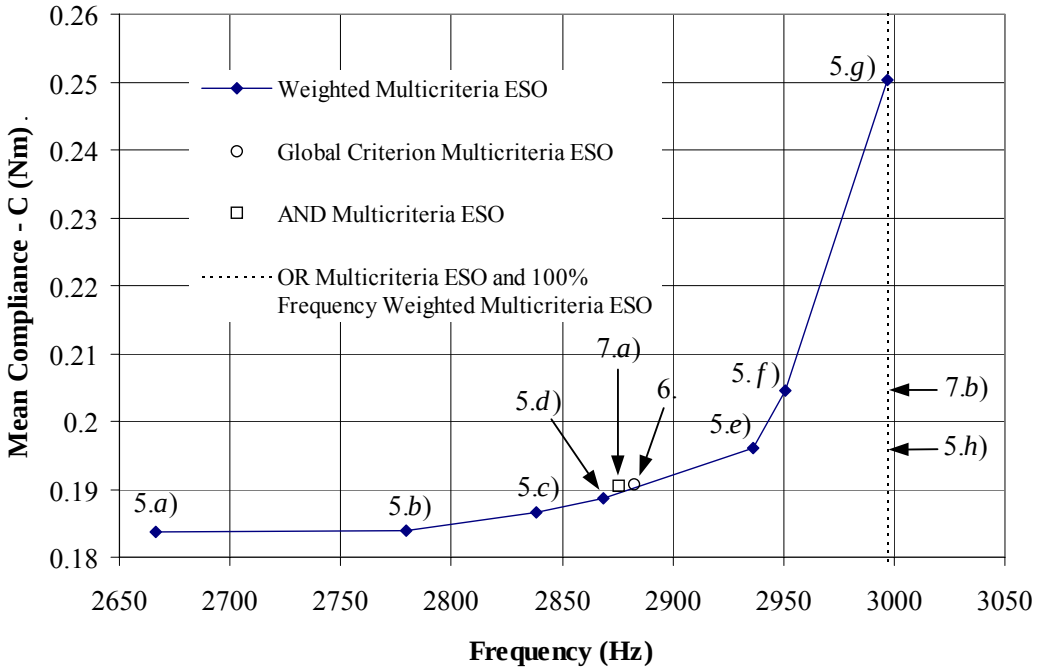

Figure 2.4 Plot of first mode natural frequency versus mean compliance with 30 % of the material removed. Points marked by the letters 5.a) through to 5.h), 6. and 7.a) to 7.b) correspond to the topologies (and criteria weighting) shown in Figures 2.5, 2.6 and 2.7 respectively.

The mean compliance of the initial design domain is 0.1751 Nm, showing that the mean compliance of the fully stiff optimised design (0.1837 Nm) has increased by 4.9 %. In other words, the stiffness of the structure has decreased due to the removal of 30 % of the material from the initial design domain. However, this volume reduction is greater than the reduction in stiffness, meaning that the specific stiffness of the optimised topology is greater than the initial design domain. This is indicated by a decrease in the C multiplied by the volume term (V): ($C \times V$) for the initial structure of 3.502×10^{-4} Nm^4 (0.1751×0.002) to 2.572×10^{-4} Nm^4 ($0.1837 \times (0.7 \times 0.002)$) for the fully stiff topology. Increased specific stiffness is one of the integrated objectives that occur for stiffness optimisation as the design evolves.

Looking now at point 5.b), it shows the mean compliance and frequency for a topology weighted 90 % of stiffness criteria. By introducing a component of frequency optimisation of 10 %, the natural frequency of the structure has increased by 4.3 % to 2779.8 Hz, although, this has resulted at the expense of stiffness. The mean compliance has now risen to 0.1829 Nm – an increase of 1 % from the fully stiff design.

For the case of 10 % stiffness criteria and 90 % frequency criteria (see point 5.g) in Figure 2.4), the first mode natural frequency has increased up to 2996.7 Hz, which is just below a 12.4 % increase from the frequency of the fully stiff optimised design. The mean compliance has increased by 36.2 % to 0.2503 Nm.

The dotted line on the right hand side represents the frequency that has resulted for the full frequency optimised design ($w_{stiff} : w_{freq} = 0.0 : 1.0$). No compliance value can be calculated for this topology (30 % of the material removed), as the elements that attach the applied loads to the structure have been removed (see Figure 2.5 h)). Here, the frequency is 2997.1 Hz - a 12.4 % increase from the fully stiff design. The natural frequency of the initial design domain is 2498.9 Hz. For 30 % of material removed, the topology based on 100 % frequency optimisation has a higher frequency by 19.9 %. Note that this topology, seen in Figure 2.5 h), is identical to the one obtained by Xie and Steven (1996) in their investigation.

By changing the criteria weighting ie increasing the frequency weighting and decreasing the stiffness weighting, it can be observed that the natural frequency of the structure increases, and the mean compliance increases – meaning the overall stiffness of the structure decreases.

Any improvement of one criterion requires a clear trade-off with the other. These solutions are all optimal for their own criteria weight allocation, verifying that they all form the Pareto solution. As can be seen, the points are generally equidistant, and together form a shape that is exponential. This would suggest that the non-dimensionalising factors in Equation (2.9) (ie each sensitivity number being divided by the maximum value of each respective criteria sensitivity number), is effective in making the two criteria comparable.

Such a weighting preference with its respective optimum combination of stiffness and frequency cannot be chosen adequately until after such a Pareto solution is formed. Tappeta and Renaud (1999) described this shortcoming concerning their Interactive Multi-Objective Optimisation Procedure: it had no formal means to capture the decision-maker's preliminary preferences. The computational cost to produce such a Pareto set is large, as each point on the optimum solution involves a full ESO analysis. This drawback is insignificant compared to benefit of the designer's preference being able to obtain an optimal design.

The configuration of the topology driven by the global criterion method is presented in Figure 2.6. Its mean compliance is 0.1907 Nm and its natural frequency is 2882.6 Hz. These values can been observed in Figure 2.4 – represented by point 6. It has a topology very much like the 50 % stiffness: 50 % frequency weighted configuration. This is not surprising considering that in the global criterion formulation between criteria (see Section 2.3.2) equal weighting is implied.

A similar topology to the 50 % stiffness: 50 % frequency weighted configuration is made by the AND operator method. It is presented in Figure 2.7 a). Its mean compliance is 0.1905 Nm, and its natural frequency is 2875.7 Hz (indicated in Figure 2.4 – represented by point 7.a)). These values are very close to the 50 % : 50 % configuration values. A similar observation between the 50 % : 50 % weighting method and the logical AND method was made by Li (2000) in his analysis of the Logical AND scheme applied to the simultaneous optimisation of thermal stress and heat flux criteria. He found that when comparing the weighting scheme, the solution of the equal weighting factor scheme most closely resembled that of the logical AND scheme.

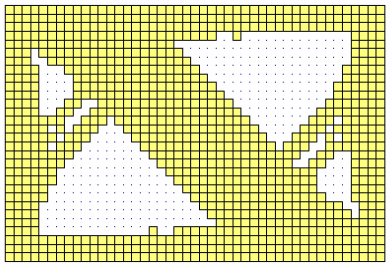

a) $w_{stiff} : w_{freq} = 1.0 : 0.0$

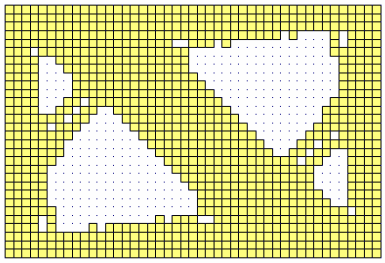

b) $w_{stiff} : w_{freq} = 0.9 : 0.1$

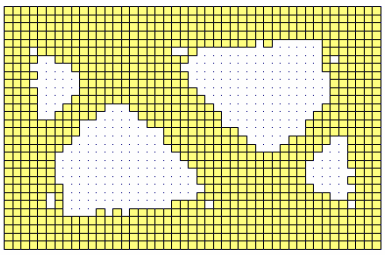

c) $w_{stiff} : w_{freq} = 0.7 : 0.3$

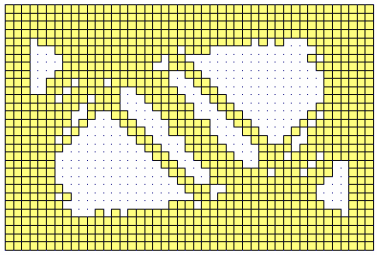

d) $w_{stiff} : w_{freq} = 0.5 : 0.5$

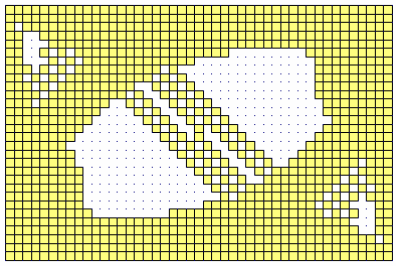

e) $w_{stiff} : w_{freq} = 0.3 : 0.7$

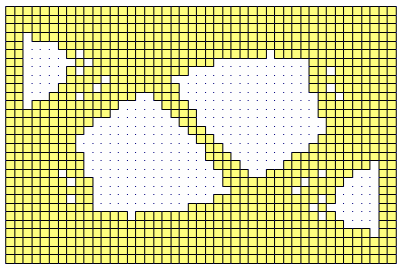

f) $w_{stiff} : w_{freq} = 0.2 : 0.8$

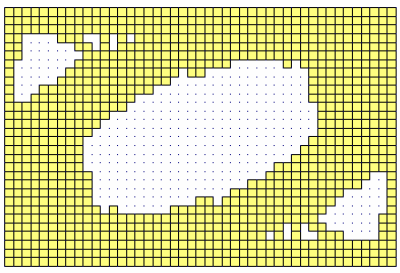

g) $w_{stiff} : w_{freq} = 0.1 : 0.9$

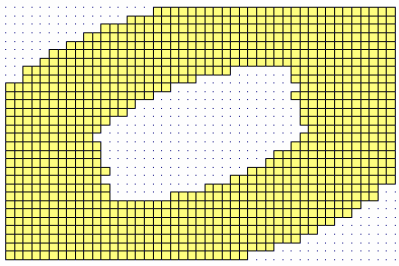

h) $w_{stiff} : w_{freq} = 0.0 : 1.0$

Figure 2.5 Optimal designs of the rectangular plate for different weighting criteria of stiffness and natural frequency. Material removed: 30 %. Refer to Figure 2.4 for the corresponding frequencies and mean compliance numbers.

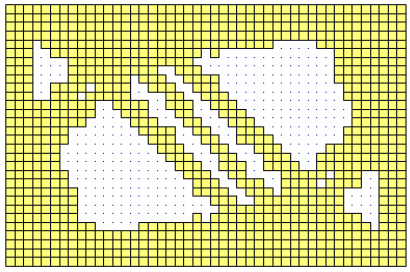

Figure 2.6 Optimum design of the rectangular plate for the global criterion method of Multicriteria ESO of stiffness and natural frequency. Material removed: 30 %.

From the above observations and taking into account the theory behind the logical AND operation method, it is suggested that for any given volume fraction during the evolution (or alternatively any given iteration), the elements remaining are required by at least one criterion, maybe both. Also, for this specific case, the combined effect of optimising both criteria with equal weighting, is equivalent to individual effects of optimising either criterion over the different sections of the design domain. It is of interest to see if this remains consistent for the other examples and criteria combinations (see Chapters 4 and 5).

The logical OR configuration for this plate problem is exactly the same as the 100 % frequency criteria design (see Figure 2.7 b)). Hence, it too does not have a compliance number, but a first mode natural frequency of 2997.1 Hz. The reasoning behind this exactness is that during the evolution, the compliance sensitivity numbers (α^i) are always greater than "0" (ie $\alpha^i \neq 0$) whereas the frequency sensitivity numbers (α_n^i) can be "0" when they are 'shifted' using Equation (2.8). When element removal happens, only elements with $\alpha_n^i = 0$ are removed. In other words, the logical OR operation always picks the frequency criterion. This is the reason that the logical OR would lead to a frequency optimised topology. In addition, based on the theory behind the element removal for the logical OR operator, at any given iteration during the evolution, the elements remaining are conclusively required by both criteria. Again the question remains if this shall be consistent for the succeeding examples.

Similar Pareto curves of frequency versus mean compliance have been constructed for other volume fractions i.e. 10 % of material removed etc. They too generally have curves where the mean compliance increases at an increasing rate and the natural frequency increases at a

decreasing rate for an increase in the frequency component of criteria (or a decrease in the stiffness component of criteria). Again, trends similar to the exponential trend have been formed.

Any deviation of points from this trend is attributed to the evolution history of the criteria weighting not having the topology that exactly matches the specified volume fraction. For example, an evolution history of a specified percentage of stiffness criteria may not exactly have a topology with 30 % of the material removed, but rather, 28 % or 31%. The closest volume fraction to the specified one is selected ie 31 %.

It has also been observed that for different volume fractions, as the amount of material is removed, the magnitude of the first mode natural frequency increases, the $C \times V$ term of the structure decreases (specific stiffness therefore increases), and the deviation of the points from the exponential trend increases. The deviation of points occurs because the exact volume fractions are not available for each criteria ratio. Also, a coarse mesh has been used.

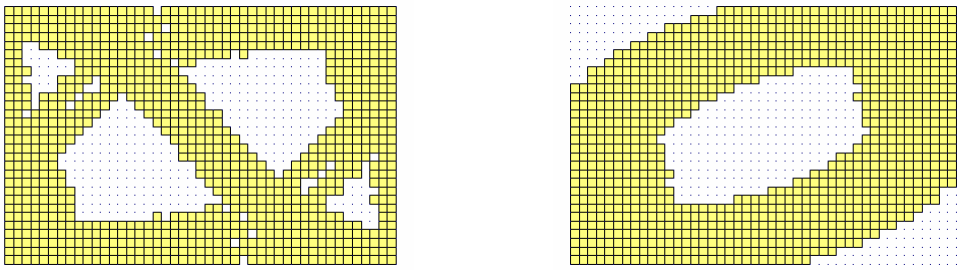

a) AND Multicriteria ESO **b)** OR Multicriteria ESO

Figure 2.7 Optimal designs of the rectangular plate for the AND and OR method of multicriteria optimisation of stiffness and natural frequency. Material removed 30 %.

2.5.2 A Short Beam

This second example is based on a short beam model that has been used by Xie and Steven (1996) in their investigation of ESO for dynamic problems.

Figure 2.8 shows a short beam of dimension 5.0 m × 1.0 m. The beam is clamped on both sides. Only in-plane vibration is considered. Young's modulus E = 200 GPa, Poisson's ratio ν = 0.3, thickness t = 0.01 m and density ρ = 7000 kg/m^3 are assumed.

Figure 2.9 illustrates how the natural frequency and mean compliance varies for a range of criteria ratios for the short beam with 20 % of the material having been removed. The corresponding topologies are displayed in Figures 2.10 and 2.11.

The fully stiff design (w_{stiff} : w_{freq} = 1.0 : 0.0) has a natural frequency of 36.07 Hz, which is an increase of 1.8 % from the initial design domain. The corresponding mean compliance number is 0.0391 Nm. The structure completely optimised for frequency (w_{stiff} : w_{freq} = 0.0 : 1.0) has a first mode frequency of 43.78 Hz (an increase of 23.5 % from the initial design domain). Its mean compliance is 0.1855 Nm. Note that this topology, seen in Figure 2.10 g), is identical to the one obtained by Xie and Steven (1996) in their investigation.

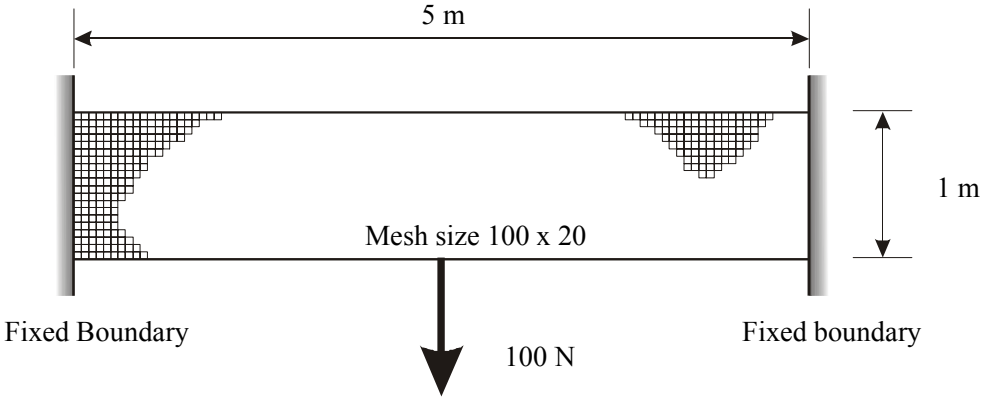

Figure 2.8 Initial design domain of a short beam under loading. First mode natural frequency: 35.44 Hz, mean compliance: 0.0335 Nm.

The comparison of these two extremes in multicriteria optimisation shows that the short beam optimised completely for frequency has a frequency that is 21.4 % greater than the short beam optimised completely for stiffness. On the other hand, the beam optimised 100 % for stiffness has a mean compliance that is 78.9 % less than the beam designed for 100 % frequency. These points then are purely optimal for each given criterion. There exists no other topology for that given volume fraction that better these topologies based on each 'pure' criterion.

As in the first example, all of the points between these 'pure' criterion ideal points (Figure 2.9) form the Pareto solution. Any improvement of one criterion requires a clear trade-off of the other. Each point represents an optimum topology for the given ratio of frequency and mean compliance weights. Beginning with the fully stiff design (see point 10.a) in Figure 2.9), as the component of frequency criteria is increased, the first mode natural frequency increases at a decreasing rate and the mean compliance increases at an increasing rate. This occurs up to the full frequency optimised design (see point 10.g) in Figure 2.10).

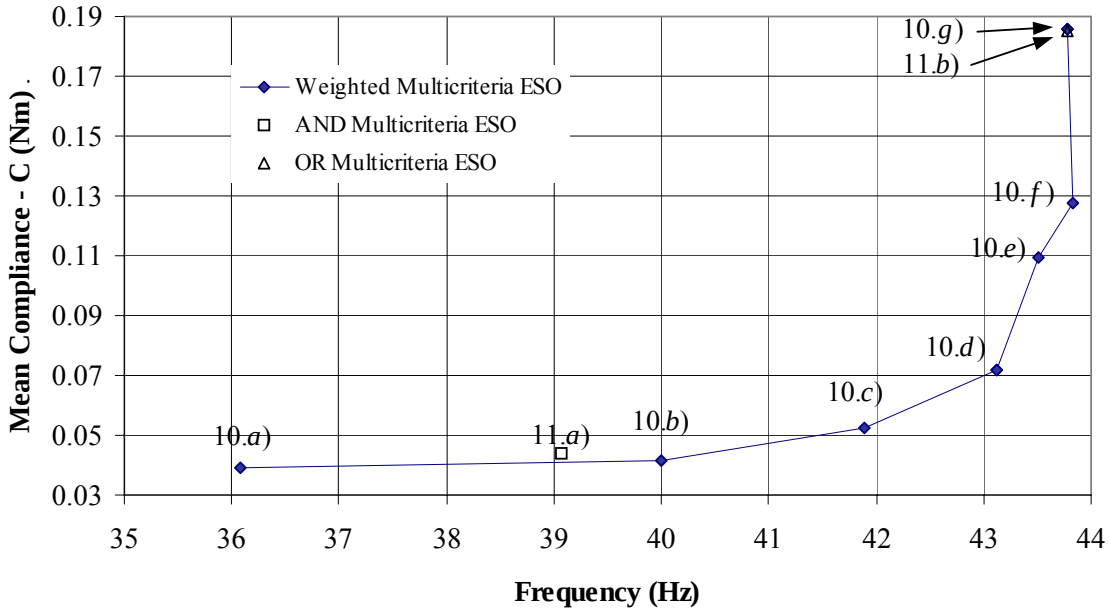

Figure 2.9 Plot of first mode natural frequency versus mean compliance with 20 % of the material removed. Points marked by the letters 10.a) through to 10.g) and 11.a) to 11.b) correspond to the topologies (and criteria weighting) shown in Figures 2.10 and 2.11 respectively.

The trend of these points significantly imitates that of an exponential trend, however, the points along the Pareto solution are similarly spaced. The slight deviation of points from the exponential trend or from being equidistant is attributed to the mismatch in the solutions' available volume fraction as mentioned in the first example.

Figure 2.11 a) shows the resulting design driven by the AND Multicriteria ESO technique. As can be seen with the aid of Figure 2.9, it has a topology very similar to that produced by the $w_{stiff} : w_{freq} = 0.9 : 0.1$ weighting Multicriteria ESO. The mean compliance number and natural frequency of the AND design are 0.0437 Nm and 39.07 Hz, with respective increases from the initial design domain of 30.6 % and 10.2 %. This observation is unlike the one made in the previous example with the logical AND solution being similar to equal criteria weighting. Nevertheless, because its numerical solution exists on the Pareto solution formed by the weighting method, the combined effect of optimising both criteria is still equivalent to the individual effect of optimising either criterion. However for this example, the combined effect is not equal, rather, it is skewed (90 % stiffness and 10 % frequency).

The resulting design driven by the OR Multicriteria ESO technique is seen in Figure 2.11 b). Its shape and topology is almost identical to the full frequency optimised design, as is its mean compliance and frequency. This is reflected in its compliance and frequency characteristics (point 11.b), Figure 2.9) being similar to the characteristics of the full frequency design (point 10.g), Figure 2.9). Again this solution lies on the Pareto curve produced by the linear weighting method. The reasoning for this is given in the previous example.

For other volume fractions, it has been found that as more elements are removed, the natural frequency of the structure increases, as does the mean compliance. The C term decreases, denoting an increase in the stiffness of the structure. But for all volume fractions, the same Pareto trend exists. It must be noted that the global criterion method was not utilised in this example because during the time of implementation of this example for the specific study in mind (Proos *et al.*, 1999), the global criterion multicriteria ESO method had not been developed. However the other examples in this chapter and the remaining chapters do incorporate the method, which is sufficient to investigate its properties and relationship to the other Multicriteria ESO methods.

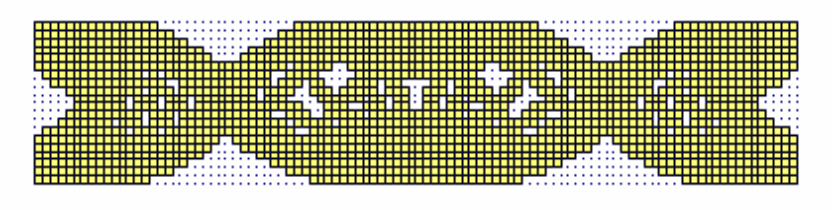

a) $w_{stiff} : w_{freq} = 1.0 : 0.0$

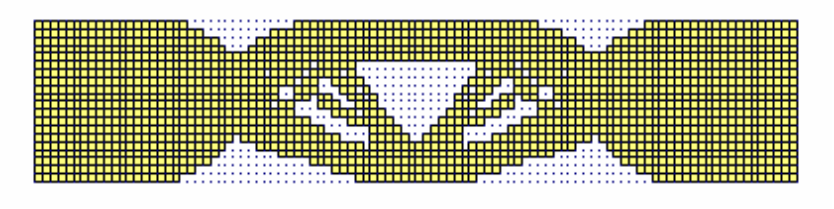

b) $w_{stiff} : w_{freq} = 0.9 : 0.1$

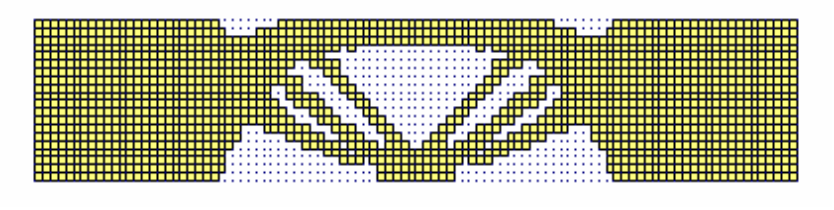

c) $w_{stiff} : w_{freq} = 0.7 : 0.3$

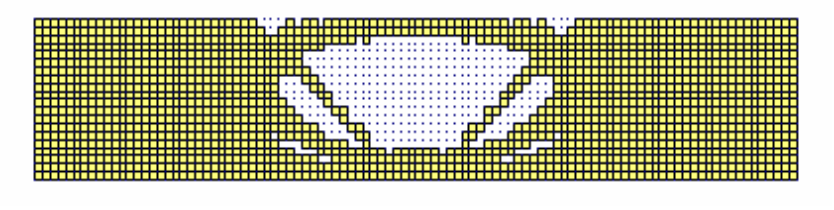

d) $w_{stiff} : w_{freq} = 0.5 : 0.5$

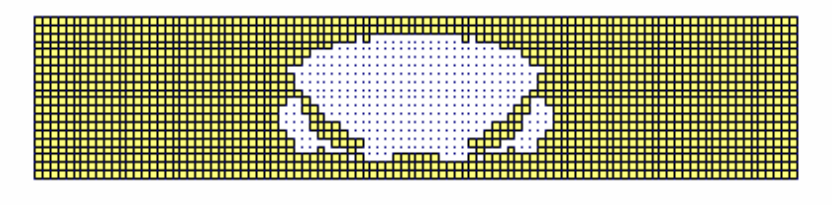

e) $w_{stiff} : w_{freq} = 0.3 : 0.7$

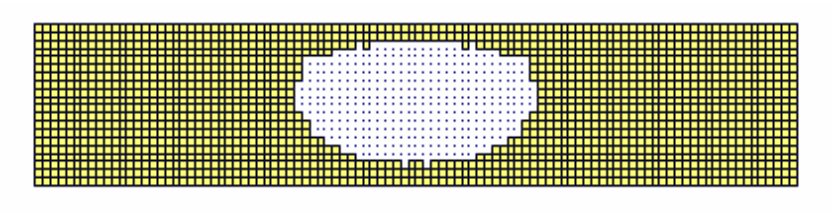

f) $w_{stiff} : w_{freq} = 0.1 : 0.9$

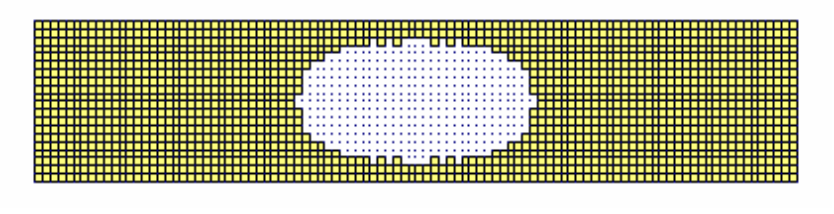

g) $w_{stiff} : w_{freq} = 0.0 : 1.0$

Figure 2.10 Optimal designs of the short beam, for different weighting criteria of stiffness and natural frequency. Material removed: 20 %.

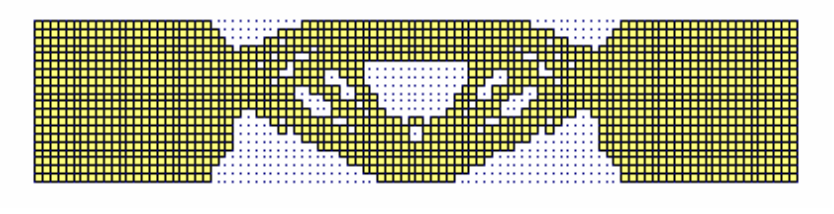

a) AND Multicriteria ESO

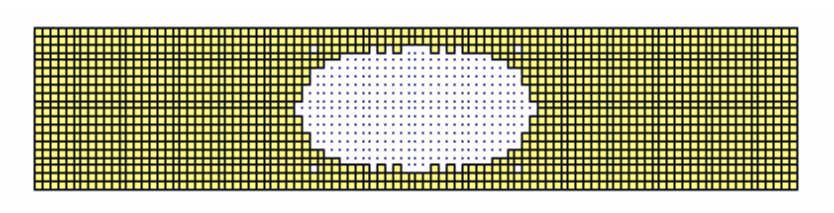

b) OR Multicriteria ESO

Figure 2.11 Optimal designs of the short beam, for the AND and OR method of multicriteria optimisation of stiffness and natural frequency. Material removed: 20 %.

2.5.3 A Rectangular Plate with Roller Supports

A structure is to be designed to support nine point loads, each of 200 N, distributed at 0.01 m intervals, under the given boundary conditions shown in Figure 2.12. The dimensions for the design domain are 0.8 m in width, 0.5 m in height and 0.01 m in thickness. Due to symmetry, only half of the design domain is analysed and is discretised into 40 × 50 four-node square elements. The material properties of the elements are Young's modulus E = 200 GPa, Poisson's ratio ν = 0.3 and density ρ = 7000 kg/m^3. In the analysis, 2-D plane stress conditions are assumed with only in-plane vibration considered.

The Pareto curves of the first mode natural frequencies and the $C \times V$ terms are presented in Figure 2.13. The product $C \times V$ is used in this example (in contrast to the compliance C being analysed in the first two examples) to enable a relative comparison to be made between the different volumes of material removed during the evolution procedure.

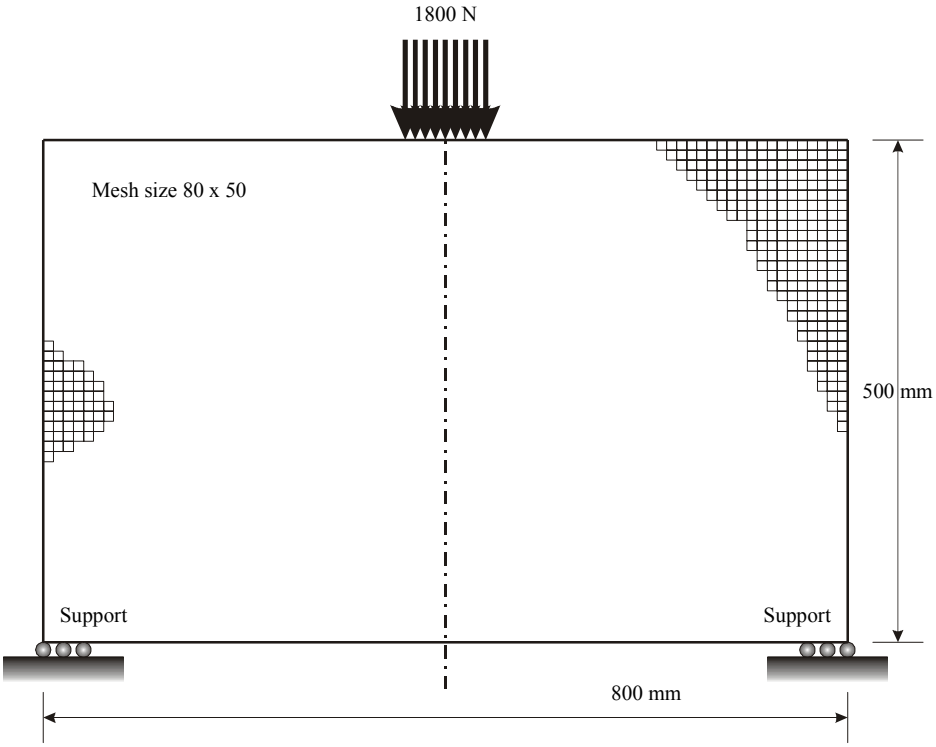

Figure 2.12 Initial design domain of a rectangular plate under loading with roller supports.

The Pareto curves are shown for 10, 20, 30, 35, and 40 % of material removed using weighted Multicriteria ESO. For each of these volume fractions, the variation in the criteria

weighting is illustrated – ranging from 100 % stiffness weighting (0 % frequency weighting) at point A, through to 0 % stiffness weighting (100 % frequency weighting) at point B. The other five points correspond to 10, 30, 50 70 and 90 % in stiffness weighting.

This however is not the case for the Pareto optimums with 35 % and 40 % of the material removed. The 35 % case does not include the criteria weighting of 0 % stiffness weighting (100 % frequency), meaning that the 90 % stiffness weighting is denoted by point B. The 40 % case excludes the criteria weighting of 10 % and 0 % stiffness weighting (90 % and 100 % frequency respectively) meaning that the 70 % stiffness weighting is denoted by point B.

The reason that such criteria weighting do not exist for the coinciding volume fractions is that elements were removed in the ESO process until the structure became unstable. In other words, elements that carried the applied loads were removed. When this occurred, the first mode of natural frequency of the design also decreased suddenly from a 'peak' ie note reduction in $C \times V$ from point 14.g) to point B of 35 % material removed. This occurred after 30 % of the material had been removed, and before it had reached 35 %.

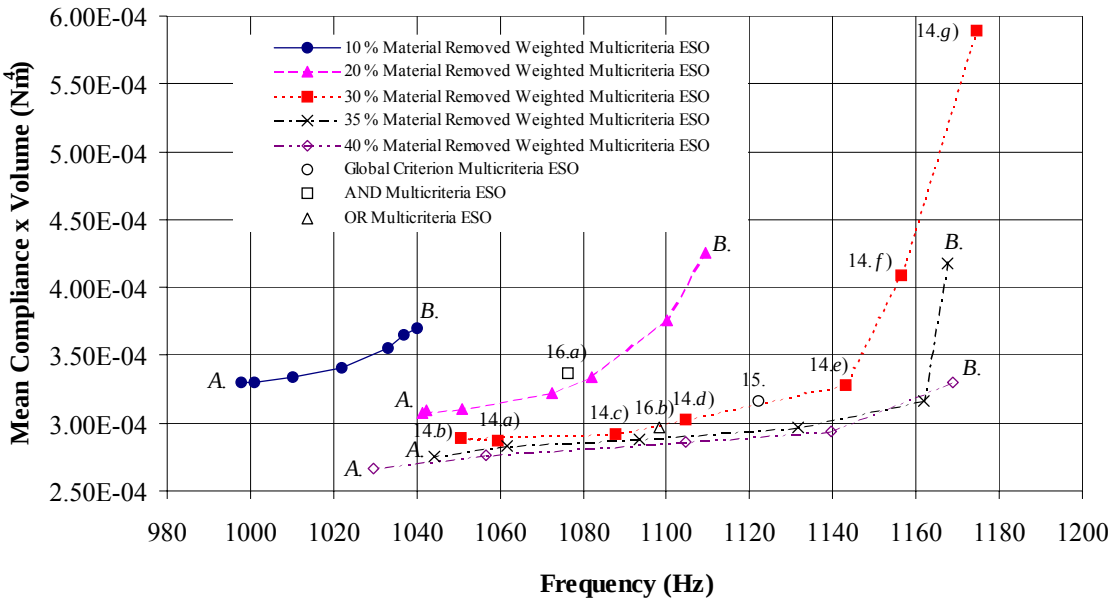

Figure 2.13 Plot of first mode natural frequency versus mean compliance × volume ($C \times V$) for a varying range in the percentage of material removed. Points marked by the letters 14.a) through to 14.g), 15. and 16.a) to 16.b) correspond to the topologies (and criteria weighting) shown in Figures 2.14, 2.15 and 2.16 respectively.

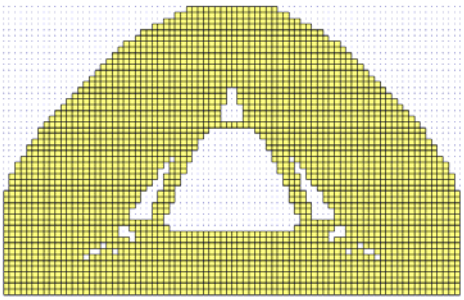

a) $w_{stiff} : w_{freq} = 1.0 : 0.0$

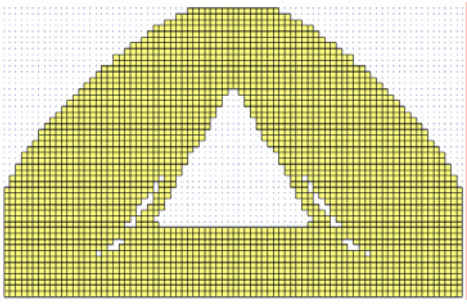

b) $w_{stiff} : w_{freq} = 0.9 : 0.1$

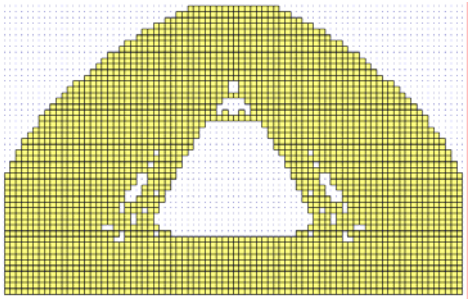

c) $w_{stiff} : w_{freq} = 0.7 : 0.3$

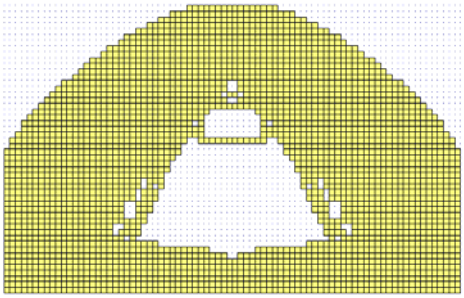

d) $w_{stiff} : w_{freq} = 0.5 : 0.5$

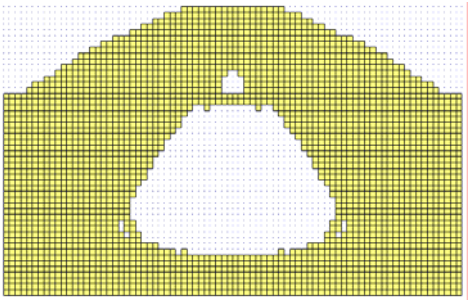

e) $w_{stiff} : w_{freq} = 0.3 : 0.7$

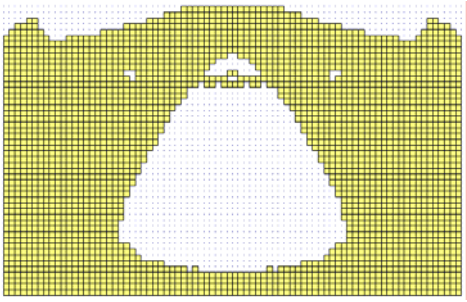

f) $w_{stiff} : w_{freq} = 0.1 : 0.9$

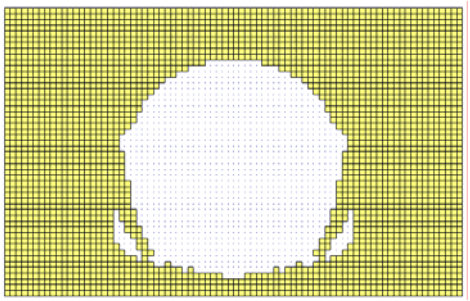

g) $w_{stiff} : w_{freq} = 0.0 : 1.0$

Figure 2.14 Optimal designs of the roller supported rectangular plate, for different weighting criteria of stiffness and natural frequency. Material removed 30 %.

Looking at all the points denoted A, including point 14.a) (which are all the points of 100 % stiffness weighting), it is clear from Figure 2.13 that as more material is removed, the $C \times V$ term decreases. This validates that the specific stiffness of the structure increases for optimisation based purely on the stiffness criteria. On the other hand, the $C \times V$ term increases for all the points denoted by B, including point 14.g), and excluding the points for the 35 and 40 % of material removed cases. This signifies that the specific stiffness decreases for optimisation based purely on the first mode of frequency.

Points 14.a) through to 14.g) in Figure 2.13 represent the natural frequencies and $C \times V$ terms for the model with 30 % of the material removed, for the given variations in criteria weighting. The matching design topologies can be seen in Figure 2.14. Although it is true for all the cases in Figure 2.13 that any improvement of one criterion requires a clear trade-off with the other, it is not so for this case. The topology based on a stiffness criteria weighting of 90 % has a lower natural frequency than the topology based on a stiffness criteria weighting of 100 % by 1.04 %. Point 14.a) still has a lower $C \times V$ term than 14.b) as expected. It is thus optimum in terms of being the stiffest possible design.

The global criterion method of Multicriteria ESO presents its frequency and $C \times V$ value as point 15. in Figure 2.13, with its topology presented in Figure 2.15. For the case of 30 % of the material removed this topology forms part of the Pareto solution. It lies in close proximity to the point formed by the weighting method, specifically, the weighting w_{stiff} : $w_{freq} = 0.5 : 0.5$. Again, implied weighting in the global criterion ESO method can be seen.

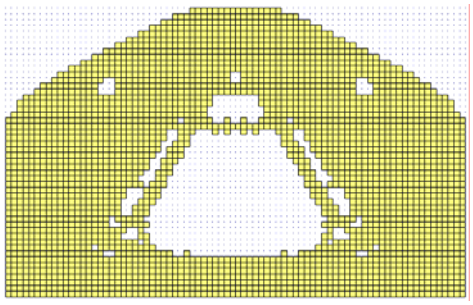

Figure 2.15 Optimum design of the roller supported rectangular plate, for the global criterion method of Multicriteria ESO of stiffness and natural frequency. Material removed: 30 %.

The frequency and $C \times V$ value for the AND Multicriteria ESO case is also presented in Figure 2.13 (point 16.a)), with the topology presented in Figure 2.16 a). Here, as can be seen, this topology does not form part of the Pareto solution for the case of 30 % of the material removed. In fact, it is quite external to the solution space. This is inconsistent with the trend of the previous examples where the AND solution has been present on the Pareto optimal curve.

To investigate this irregularity, the example was repeated again with the same result occurring. Knowing that the election of each element for removal (for the respective criterion) was based on the maximum sensitivity value that exists for that criterion $\alpha_{\max}^{crit}$ (Equation (1.5)), another variation was then used in an attempt identify this irregularity. Sometimes, instabilities occur when the maximum sensitivity number for that criterion is used. This is particularly so for the frequency criterion when elements may be attached the structure by one node only, and its sensitivity number is an order of magnitude greater than the rest. Unless the iteration deletion rate is extremely small, all of the other elements are selected to be deleted in one iteration. To overcome this instability, a modification was made to replace the $\alpha_{\max}^{crit}$ sensitivity number with the average sensitivity value that exists for that criterion $\alpha_{average}^{crit}$. Another model was therefore conducted, but again the same topology resulted.

Thus would seem that although the elements remaining in a structure are required by at least one criterion during any part of the evolution for the logical AND method, the combined effect of optimising both criteria is not always equivalent to individual effects of optimising either criterion over the different sections of the design domain.

Figure 2.16 b) below shows the topology constructed using the OR Multicriteria ESO method, with its frequency and $C \times V$ properties denoted by point 16.b) in Figure 2.13. In this case, it distinctly forms part of the Pareto solution, having a performance of frequency and $C \times V$ in between the topologies produced by the $w_{stiff} : w_{freq} = 0.7 : 0.3$ and the $w_{stiff} : w_{freq} = 0.5 : 0.5$ weighting. Its topology however is notably different in shape.

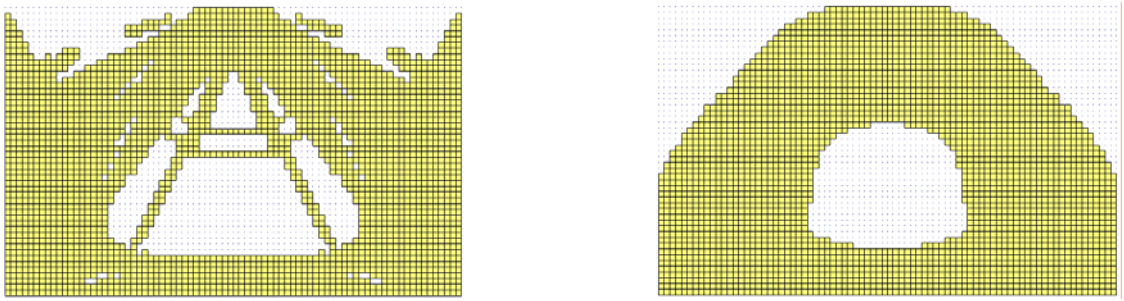

a) AND Multicriteria ESO **b)** OR Multicriteria ESO

Figure 2.16 Optimal designs the roller supported rectangular plate, for the AND and OR method of Multicriteria ESO of stiffness and natural frequency. Material removed: 30 %.

2.6 Concluding Remarks

This chapter demonstrates how the multiple criteria optimisation based on linear static analysis and natural frequency analysis (specifically stiffness and natural frequency) is incorporated successfully into ESO using the four multicriteria methods. As can be seen, the solutions produced by the Weighting method form the Pareto solution space. For the specific examples presented the Pareto solution space contains points that span the solution fairly evenly. It can be seen how each solution can be easily affected depending on the designer's preference of criteria weighting.

The rate at which elements are removed, has a direct effect on the deviation of points from the Pareto curve. Solutions converge to a Pareto exponential trend if a smaller deletion rate and a finer mesh are used. This slow removal rate is the essence for the success of the evolutionary method used. Such a result comes clearly at the expense of computational cost.

The solutions of the global criterion method also form part of the Pareto solution space. For this method, there emerges a common position on the Pareto curve that can be determined for each model. This position lies very near the 50 % stiffness: 50 % frequency point. It has been shown that the global criterion method incorporates implied equal weighting between both criteria in its mechanism.

The AND operator does not always form part of the Pareto curve. When it does, it appears not to have any notable similarity to a particular ratio of criteria weighting. These observations are inconsistent with its rationale where the removal of elements are not "conclusively" required by both criteria.

The design solutions evolved by the logical OR operator form part of the Pareto optima. However, for each model of the OR operator, there appears to be no definable position on the Pareto curve. Cases were observed where the presence of frequency sensitivity numbers with a "0" value (due to the linear frequency shift) enabled it to dominate the solution. The philosophy behind the OR operator method is that at any given iteration during the evolution, the elements remaining are conclusively required by both criteria.

Although the linear static and the natural frequency solver have been considered for Multicriteria ESO in this chapter, the procedure can be applied to other criteria including buckling and inertia properties. The next chapter introduces Evolutionary Moment of Inertia Optimisation (EMIO), and the one following it incorporates it into Multicriteria ESO.

2.7 References

Bendsøe, M., P., Kikuchi, N. (1988), "Generating Optimal Topologies in Structural Design Using a Homogenisation Method", *Computer Methods in Applied Mechanics and Engineering*, Vol. 71, pp. 197-224.

Chen, T., Y., Wu, S., C. (1998), "Multiobjective Optimal Topology Design of Structures", *Computational Mechanics*, Vol. 21, pp. 483-492.

Dems, K., Gutkowski, W. (1998), "2D Shape Optimization with Static and Dynamic Constraints", *Structural Optimization*, Vol. 15, pp. 201-207.

Grandhi, R., V., Bharatram, G., Venkayya, V. (1993), "Multiobjective Optimization of Large-Scale Structures", *AIAA Journal*, Vol. 31, No. 7, pp. 1329-1337.

Hajela, P., Shih, C., -J. (1990), "Multiobjective Optimum Design in Mixed Integer and Discrete Design Variable Problems", *AIAA Journal*, Vol. 28, No. 4, pp. 670–675.

Jensen, H., Sepulveda, A. (1998), "A Preference Aggregation Rule Approach for Structural Optimization", *Structural Optimization*, Vol. 16, pp. 246-257.

Koski, J. (1985), "Defectiveness of Weighting Method in Multicriterion Optimization of Structures", *Communications in Applied Numerical Methods*, Vol. 1, No. 6, pp. 333-337.

Koski, J. (1998), "Multicriteria Truss Optimisation", Stadler, W., (Ed.) *Multicriteria Optimization in Engineering and the Sciences*, Chapter 9, pp. 263-307, Plenum Press, New York.

Li, Q. (2000), *Evolutionary Structural Optimization for Thermal and Mechanical Problems*, Doctorate Thesis, School of Aeronautical, Mechatronic and Mechanical Engineering, University of Sydney, Australia.

Manickarajah, D., Xie, Y., M. (1997), "Optimum Design of Structures with Stress, Stiffness and Stability constraints", *15th Australasian Conference, on the Mechanics of Structures and Materials*, Melbourne, Australia, 8th-10th December.

Osyczka, A. (1981), "An Approach to Multicriterion Optimization for Structural Design", *Proceedings of the International Symposium On Optimum Structural Design*, Tucson, Arizona, 19th-22nd October.

Otswald, M. (1996), "Multicriteria Optimization of Cylindrical Sandwich Shells Under Combined Loads", *Structural Optimization*, Vol. 12, pp. 159-166.

Pietrzak, J. (1994), "Bi-criteria optimisation of structures liable to instability", *Structural and Multidisciplinary Optimization*, Vol. 7, pp. 61-65.

Pietrzak, J. (1999a), "A Systematic Search for Pareto Optimum Solutions", *Structural Optimization*, Vol. 17, pp. 79-81.

Pietrzak, J. (1999b), "Pareto Optimum Tests", *Computers and Structures*, Vol. 71, pp. 35-42.

Proos, K., A., Steven, G., P., Querin, O., M., Xie, Y., M. (1999), "Multicriteria Evolutionary Structural Optimisation", submitted to *Design Optimisation – International Journal for Product and Process Improvement*, December.

Tappeta, R., V., Renaud, J., E. (1999), "Interactive Multiobjective Optimization Procedure with Local Preferences", *Short Paper Proceedings, 3rd World Congress of Structural and Multidisciplinary Optimization*, Buffalo, New York, 17th-21st May.

Tappeta, R., Renaud, J., Messac, A., Sundararaj, G. (2000), "Interactive Physical Programming: Tradeoff Analysis and Decision Making in Multicriteria Optimisation", *AIAA Journal*, Vol. 38, pp. 917-926.

Tappeta, R., V., Renaud, J., E. (2001), "Interactive Multiobjective Optimization Design Strategy for Decision Based Design", *Journal of Mechanical Design*, Vol. 123, pp. 205-215.

Xie, Y., M., Steven, G., P. (1996), "Evolutionary Structural Optimization for Dynamic Problems", *Computers and Structures*, Vol. 58, No. 6, pp. 1067-1073.

Xie, Y., M., Steven, G., P. (1997), *Evolutionary Structural Optimisation*, Springer-Verlag, London.

Zhang, W., Domaszewski, M., Fleury C. (2001), "An Improved Weighting Method with Multibounds Formulation and Convex Programming for Multicriteria Structural Optimization", Vol. 52, pp. 889-902.

Chapter 3

Evolutionary Moment of Inertia Optimisation

3.1 Introduction

In mechatronic systems, the power transmission between the actuators and the mechanical elements is governed by the dynamic equations of motion. One way of reducing the 'fluctuations' of the required actuator forces or torques is to mechanically compensate for the gravity terms, a procedure that is referred to as static balancing (Laliberte *et al.*, 1999). This leads to a considerable reduction in the actuator forces or torques, which in-turn, allows the use of less powerful actuators. As a result, more efficient designs of mechatronic systems are obtained.

This efficiency concept is the motivation for this chapter, but is approached from a different perspective. It deals with the introduction and development of inertia optimisation. In all industrial and engineering applications (particularly robotics), one of the chief aims is to have processes that operate at a most efficient level, that is, minimum power is required. Power required to operate machinery can be minimised if forces or torques essential to drive the system to the necessary outcome are reduced. By optimising inertia – smaller forces and torques are needed. Direct consequences of inertia optimisation are that smaller engines or actuators are required (thus are lower costs for purchase and operation) and less weight is required to maintain structural stability (thus material resources are conserved).

There are many widely varying fields that incorporate both inertia and optimisation. In the field of structural and dynamic analysis and optimisation, there are numerous approaches in the use of inertial optimisation. Salajegheh (2000) in an attempt to reduce the number of structural analyses in the process of optimisation, introduced intermediate variables.

Structural forces and displacements were approximated in terms of the intermediate variables of cross-sectional areas and moments of inertia. Soykasap and Hodges (2000) applied an optimisation technique in an attempt to improve the performance of a tilt-rotor aircraft with composite blades. Having such design variables such as blade twist, box dimensions, wall thicknesses, ply angles of the laminated walls and non-structural mass, they defined different constraints, one of which was the autorotational inertia of the blades. In their shape optimisation of thin-walled beam-like structures, Vinot *et al.* (2001) used the beam characteristics of inertia and torsional rigidity to be to represented by the nodal coordinates defining the cross sectional geometry. A subset of these coordinates was then taken as the design variables for the optimisation problem.

As mentioned previously, Evolutionary Structural Optimisation has been extended to a variety of different criteria (see Section 1.3). No known work on inertia as a criterion has been implement into the ESO methodology. The research presented in this chapter examines an evolutionary method (based on ESO) applied to a criterion of inertia. Specifically, this criterion is the Moment of Inertia (MOI) in 2-D space, or the area moment of inertia of a cross-section. The method shall be identified as Evolutionary Moment of Inertia Optimisation (EMIO). The area moment of inertia is purely a geometric property of stiffness, as opposed to a material property of stiffness. Also, the analysis of the inertial criterion of an object is independent of its loads and constraints. This is what makes this process distinct from Evolutionary Structural Optimisation.

The different components of the moment of inertia that shall be examined in this chapter are the rectangular and product moments of inertia, and the polar moment of inertia. These components are directly related to the different axis of rotation (x, y) with which a beam deflects about, or the axis (z) with which a beam is rotated or accelerated about. The method is general and could be applied readily to any 2-D or 3-D object.

3.1.1 Rectangular Moments of Inertia

Any moment of inertia of an area calculated about an orthogonal axis on the plane of that area is called a rectangular moment of inertia. The rectangular moment of inertia determines a beam's resistance to bending about a particular axis, and is commonly used in the study of distributed forces and in calculating the deflections of beams (Bedford and Fowler, 1999). It is concerned with beam bending for any cross-section, whether it is circular, non-circular, symmetric or non-symmetric. This has to do with the fact that for all given cross-sections, the resulting stress from any bending moment is of a linear nature, from which the rectangular moment of inertia is based i.e. $\sigma_x = \frac{My}{I_x}$ or $\sigma_y = \frac{Mx}{I_y}$. Here, M is the applied moment, and I_x and I_y are the moment of inertia about the x and y-axis respectively.

An example that highlights the need to include the rectangular moment of inertia in EMIO can be drawn from a comparison of two beams. These beams, if being made of the same material and having the same cross-sectional area and length, will deflect differently about a defined axis depending on the shape of that cross-section. In this dissertation, EMIO will address the need of producing the optimum shape and topology in a 2-D plane that will result in beam deflections being kept to a minimum or maximum – depending on the decision makers preference.

Consider the area dA in the x-y plane as seen in Figure 3.1. The moment of inertia of dA about the x and y-axis is defined respectively as $dI_x = y^2 dA$ and $dI_y = x^2 dA$. Here, x and y correspond to the x and y distances of the element dA from the origin. Therefore, the moment of inertia of an element A about the x-axis and y-axis respectively is mathematically defined as:

$$I_x = \int_A y^2 dA \qquad\qquad I_y = \int_A x^2 dA \tag{3.1}$$

3.1.2 Product of Inertia

The product of inertia for the differential element *dA* (located at point (*x*, *y*) in Figure 3.1) is defined as $dI_{xy} = xydA$. It is used as a measure of symmetry for any given cross-sectional area. Hence for the entire area *A*, the product of inertia is:

$$I_{xy} = \int_A xy \; dA \tag{3.2}$$

3.1.3 Polar Moment of Inertia

The moment of inertia of an area about an axis that is perpendicular to the plane of the area is known as the polar moment of inertia. It cannot be used in the evaluation of torsion for geometries that are non-circular, due to the fact that the stress distribution can be non-linear. However, it is ideal for the analysis of geometries for angular or rotational acceleration. That is, the polar moment of inertia is helpful in describing the rate of change of the rate of rotation of an object. For the case of the polar moment of inertia, this chapter will also examine the EMIO algorithm in developing cross-sectional geometries, taking into account the preference to keep rotational acceleration or de-acceleration to a maximum or minimum. As the analysis is restricted to two dimensions, it shall be assumed that the shape of the cross-section in question is constant along the axis of rotation.

For the element *dA* about the pole *0* (*z*-axis), the moment of inertia is given by $dI_z = r^2 dA$. Here, *r* is the distance of the element *dA* from the origin, that is, $r^2 = x^2 + y^2$ (Figure 3.1). The polar moment of inertia of element *A* is thus mathematically defined as:

$$I_z = \int_A r^2 dA \tag{3.3}$$

Since $r^2 = x^2 + y^2$, then the polar moment of inertia is equal to the sum of the moment of inertia about the *x* and *y* axes:

$$I_z = \int_A r^2 dA = I_x + I_y \tag{3.4}$$

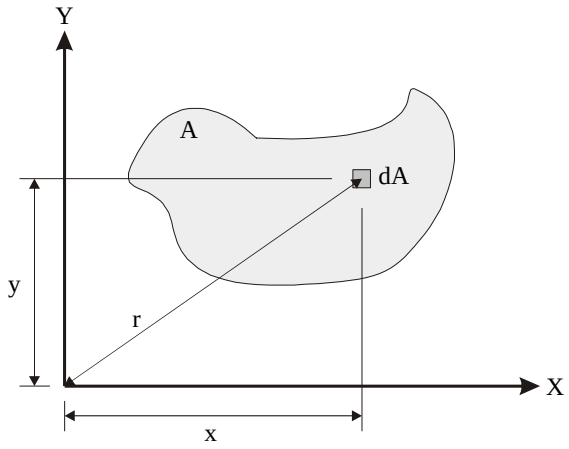

Figure 3.1 An area containing a differential elemental area *dA* in the *X*-*Y* plane.

3.2 Area Moment of Inertia of a Discretised 2-D Model

For EMIO, the cross-sectional area is discretised into *M* two-dimensional finite elements as shown in Figure 3.2. As a result, the rectangular area moment of inertia can be rewritten from Equation (3.1) as:

$$I_x = \sum_{i=1}^{M} \int_{A_i} y^2 dA \qquad I_y = \sum_{i=1}^{M} \int_{A_i} x^2 dA \tag{3.5}$$

where the local coordinate system (*x*, *y*) has its origin at the centroid as defined by: $x = X - X_c$ and $y = Y - Y_c$. Here, the centroid (X_c, Y_c) is located in the global coordinate system (*X*, *Y*), and is defined as:

$$X_c = \frac{\sum_{i=1}^{M} \int_{A_i} X dA}{\sum_{i=1}^{M} \int_{A_i} dA} \qquad Y_c = \frac{\sum_{i=1}^{M} \int_{A_i} Y dA}{\sum_{i=1}^{M} \int_{A_i} dA} \tag{3.6}$$

where *i* denotes the element number for a total of *M* elements in the given cross-section.

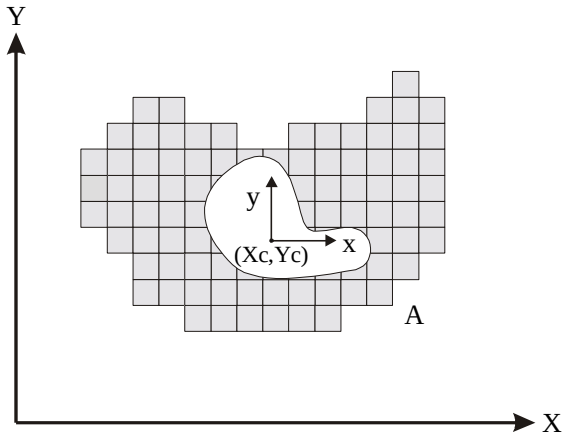

Figure 3.2 Discretised cross-sectional area *A*.

Likewise, the product and polar moment of inertia, derived from Equations (3.2) and (3.3) are respectively given as:

$$I_{xy} = \sum_{i=1}^{M} \int_{A_i} xy\,dA \qquad I_z = \sum_{i=1}^{M} \int_{A_i} (x^2 + y^2)\,dA \tag{3.7}$$

with the same definitions of the local coordinate system (*x, y*), *i* and *M* being defined above.

For material removal based on either inertia minimisation or maximisation, the moment of inertia decreases during the evolution. To know if the material is being removed in minimising or maximising way, a measure of inertia efficiency is needed. This is done by the calculation of the radius of gyration for a given cross-section. It is a measure of the distribution of the area about the axis in question, or alternatively, an indication of the MOI efficiency of a cross-section in contrast to other cross-sections. For the case of the t^{th}-axis, the inertia performance index is defined as the square root of the inertia divided by the cross-section area ie:

$$k_t = \sqrt{I_t / A} \tag{3.8}$$

where the subscript *t* represents the *x*, *y* or *z*-axis or the product moment of inertia *xy*.

Having defined the moment of inertia for a discretised FE model, the objective of EMIO is thus to minimise the moment of inertia for a certain area fraction. Strictly speaking the effect is to minimise the radius of gyration k_t ie.

$$\text{minimise } (k_t) \tag{3.9}$$

Alternatively, the radius of gyration may also be maximised, by minimising the negative of k_t.

3.3 Determination of Sensitivity Numbers for Element Removal

The procedure for optimising a cross-sectional topology based on the moment of inertia criteria first requires a calculation of the MOI of the finite element model. This was described in the preceding section. The computation of a sensitivity number for each element for the moment of inertia in question is then implemented (described in this section). These sensitivity numbers are then used by the EMIO method to determine whether their respective elements are to be removed. The EMIO method is described in greater detail in the following section.

The sensitivity number of the moment of inertia about the axis in question defines the relative contribution of each element to the overall bending or rotational performance of the cross-sectional area. Some elements have a significantly smaller contribution to the overall bending rigidity or rotational performance than others. By EMIO logic, this material is rendered ineffectual and is removed.

As a note from the programming development perspective of this approach, the sensitivity numbers for inertia can be calculated for any three-node element or four-node element (not necessarily with orthogonal sides). For a four-node element, this can be equivalent to having two three-node elements, both attached along a common edge. This subdivision of four-node to three node elements made the programming process simpler in terms of calculating the centroid and area of each element for the computation of the inertia sensitivity number.

3.3.1 Rectangular Moments of Inertia

To determine the relative contribution of each element to the overall moment of inertia about the *x*-axis and the *y*-axis, the I_x and I_y sensitivity numbers are respectively defined as:

$$\alpha_{I_x}^i = \Delta I_x^i = \int_{A_i} y^2 dA \qquad \alpha_{I_y}^i = \Delta I_y^i = \int_{A_i} x^2 dA \tag{3.10}$$

where ΔI_x^i and ΔI_y^i are the moment of inertia (about the *x*-axis and *y*-axis respectively) of each element A_i.

3.3.2 Product of Inertia

For the product of inertia, the sensitivity number can be determined:

$$\alpha_{I_{xy}}^i = \Delta I_{xy}^i = \left| \int_{A_i} xy dA \right| \tag{3.11}$$

to which the product of inertia of each element A_i is governed by ΔI_{xy}^i.

3.3.3 Polar Moment of Inertia

To estimate the relative efficiency of element usage for the polar moment of inertia, the sensitivity number can be defined as:

$$\alpha_{I_z}^i = \Delta I_z^i = \int_{A_i} (x^2 + y^2) dA \tag{3.12}$$

where ΔI_z^i is the moment of inertia (about the *z*-axis) of each element A_i.

Note that the units of all the moment of inertia analyses including the sensitivity numbers are expressed as a length dimension to the fourth power.

3.4 Evolutionary Optimisation Procedure

Having now obtained a sensitivity number for each element, the EMIO method is implemented to eliminate those elements that have been reckoned least efficient in their contribution to the moment of inertia. The process of element elimination is identical to that of Evolutionary Structural Optimisation as described in Section 1.3. Understandably, the comparison of the relative efficiency of each element to a threshold value is different:

$$\alpha_{MOI} \leq RR.(\alpha^{*}_{MOI}) \tag{3.13}$$

Here, α_{MOI} is the element sensitvity number equivalent to the moment of inertia sensitivity number being investigated, and α^{*}_{MOI} is the highest sensitivity number value over the analysis domain. For all of the examples presented in this chapter, the rejection ratio terms are $a_0 = a_2 = a_3 = 0$ and $a_1 = 0.001$, unless otherwise stated.

The methodology for evolutionary MOI optimisation is similar to that used to operate the ESO process. However, because there are variations between these methods, specifically the absence of loads and constraints in the analysis, it is necessary to document and is thus given as follows:

Step 1: Discretise the structure using a fine mesh of finite elements;

Step 2: Calculate the centroid and MOI of the structure - Equations (3.5) to (3.7);

Step 3: Calculate the MOI sensitivity number α_{MOI} – Equations (3.10) to (3.12);

Step 4: Remove a number of elements that have the lowest values of α_{MOI} i.e., that satisfy Equation (3.13);

Step 5: Repeat Steps 2 to 4 until a steady state is reached.

Step 6: Increment the steady state number using Equation (1.4).

Step 7: Repeat Steps 4 to 6 until a desired optimum is reached.

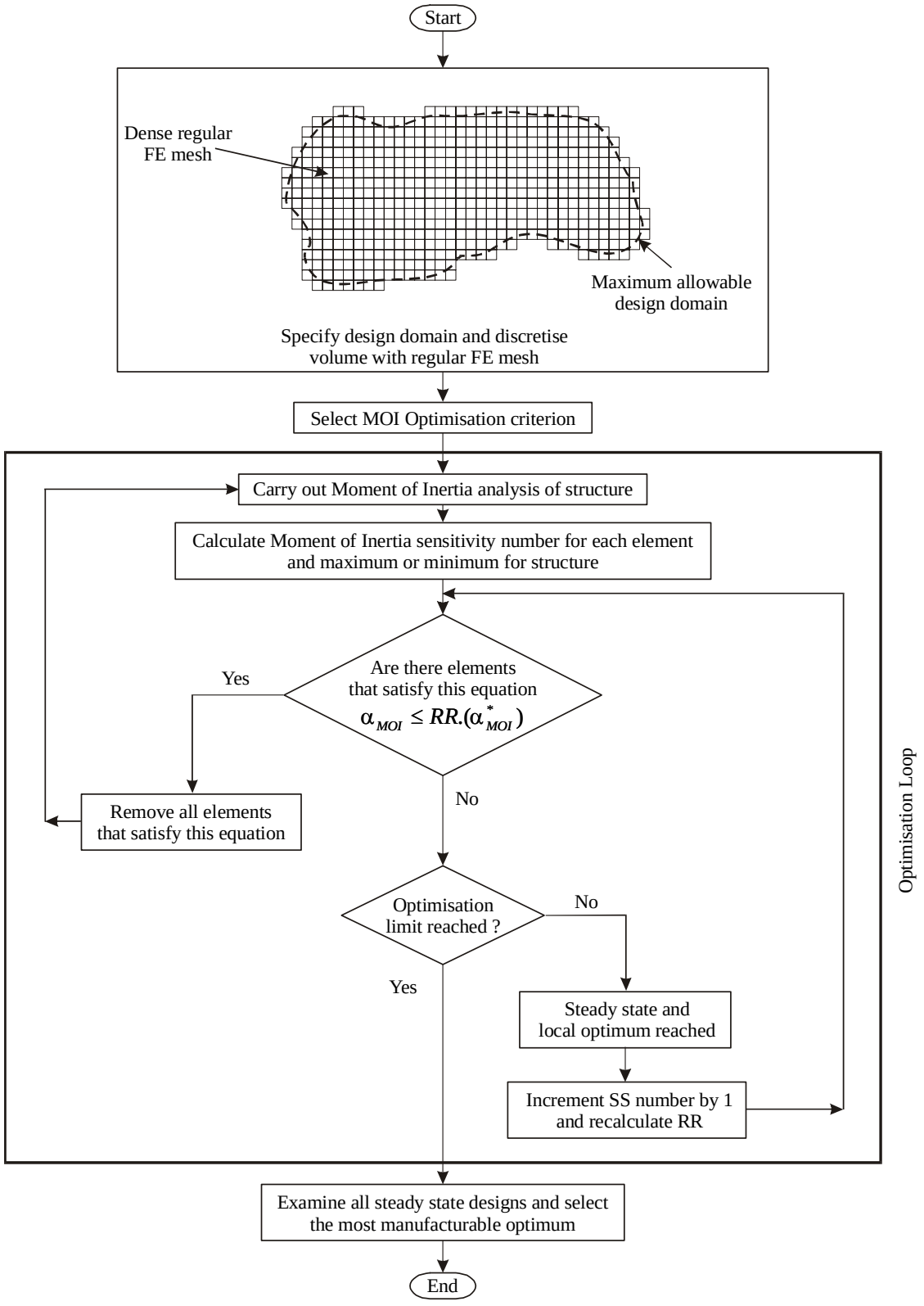

Figure 3.3 Flow-chart depicting the logical steps of the evolutionary MOI optimisation.

Figure 3.3 illustrates the set of logical steps mentioned above. As can be observed, the mesh does not take into account the surrounding environment of loads and constraints. The moment of inertia analysis is purely based on the geometrical cross section of the structure. One obvious implication of this is that the evolution time compared to that based on the linear static or frequency solver is dramatically reduced (by approximately 80 %).

It must be noted that Equation (3.13) seeks to obtain the maximum moment of inertia for a given area fraction i.e. maximisation. There is however, the objective to obtain a cross-sectional shape and topology which produces the minimum moment of inertia for a given area fraction. This is known as minimisation, and shall also be examined.

3.5 Examples and Discussion

This section, by way of five different examples illustrates the different topologies that result from using evolutionary MOI optimisation. Some of the examples correlate specifically with classical research accomplished in the past (Spunt, 1971; Chen and Atsuta, 1976; Hopkins, 1970), whereas others present new results.

The first three examples begin with the same initial design domain. They comprise of a square cross-section, consisting of 30 × 30 square elements. The dimensions of the sections are 300 mm by 300 mm. The succeeding examples have different constructs to the first three, and shall be explained specifically further on.

Also note that no nibbling constraint (Steven and Xie, 1993) has been implemented in any of these examples. The shapes and cavities have been created purely as a result of the EMIO process itself.

3.5.1 Maximisation of I_x

The first example consists of a square cross-section with dimensions defined as above. A non-design domain (where elements are not permitted to be removed) is fixed along the vertical line of symmetry of the cross-section (Figure 3.4 a)). Its width is kept at a constant of two elements and can be seen distinguished as the lighter band in Figure 3.4. It must be noted that the element constituents of the band do contribute to the cross-section's centroid and moment of inertia.

Figure 3.4 b) to Figure 3.4 d) illustrates the topologies that result from element removal for area fractions A/A_0 (of the original cross-section A_0) of 75 %, 50 % and 25 %. The iteration number that indicates where the topology fits into the evolution history is also noted.

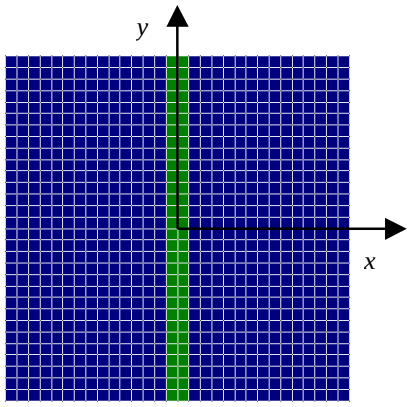

a) Initial design domain

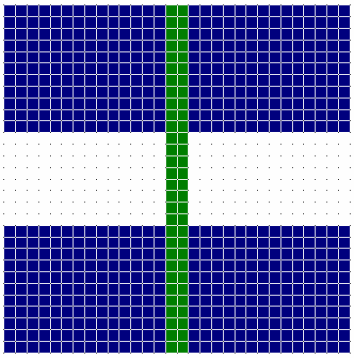

b) A/A_0 = 75 %, Iteration 4

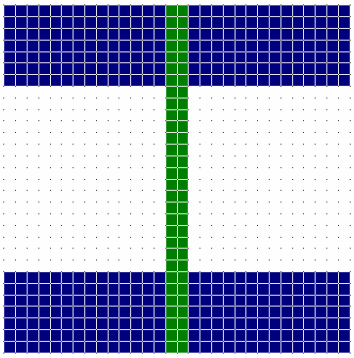

c) A/A_0 = 50 %, Iteration 8

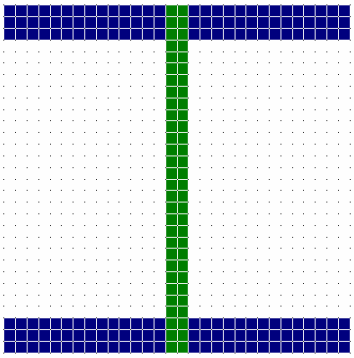

d) A/A_0 = 25 %, Iteration 12

Figure 3.4 Optimal designs subject to maximisation of I_x.

Figure 3.5 displays the evolution history of the radius of gyration about the *x*-axis (k_x) for each iteration. The other rectangular and polar radius of gyration histories (respectively k_y and k_z) are displayed in Figure 3.6.

As can be seen, evolutionary MOI optimisation removes those elements that have the least contribution to the moment of inertia about the *x*-axis. These are the elements that are closest to the *x*-axis (or alternatively, the centroidal neutral axis). As the process continues, elements are removed in the same fashion, with eventually those elements furthest away from the neutral axis being removed. They specifically have the greatest contribution, but as they are the only elements left in the process, they too are removed.

This trend is clearly seen in Figure 3.5 where the radius of gyration increases during the process. As more elements are removed, the "specific moment of inertia" (radius of gyration squared) of the cross-section increases. This measure of optimisation implies that the efficiency of the cross-section in terms of moment of inertia increases as the evolution proceeds.

It can be seen that the rate of increase of this efficiency is constant until it reaches iteration 12. A peak at this iteration suggests that there exists a design that is most efficient in comparison to the others. The corresponding topology at iteration 12 is given in Figure 3.4 d). Beyond this maximum, the radius of gyration begins to decrease (iteration 13). Iteration 13 corresponds to the topology where the remainder of the flange (or the outer rows of remaining elements) has been removed from the vertical stiffener. Further analyses were done, where the vertical stiffener was excluded from the design during the optimisation process. It was found that the radius of gyration increased at a constant rate until there was no flange remaining. These trends indicate that the vertical stiffener has a 'flattening' effect on the radius of gyration. They also highlight that the effective role of the flange in the beam's design to resist bending.

The topology of Figure 3.4 d) closely resembles that of the typical girder topology found so common in structures (Spunt, 1971; Chen and Atsuta, 1976; Hopkins, 1970) – particularly that of the civil engineering nature. Spunt (1971) in his discussion on the design of slender columns of minimum weight came to the same conclusion for maximising the flexural rigidity *EI* for a given cross-section area. He highlighted that the ideal form of a cross-

section is achieved by locating the bulk of the area a significant distance from the bending axis and providing a web shear tie (similar to the non-design domain in Figure 3.4). So this design produced by EMIO is not unlike that which has been developed over time in various industries.

An alternative design would be to split the non-design domain into two, and translate each half out to the vertical sides to form a square tube cross-section. Such a topology would inevitably increase I_y, and yet maintain the same I_x. From the viewpoint of production expense however, to produce a square tube cross-section may be more expensive than the production of an I-beam girder.

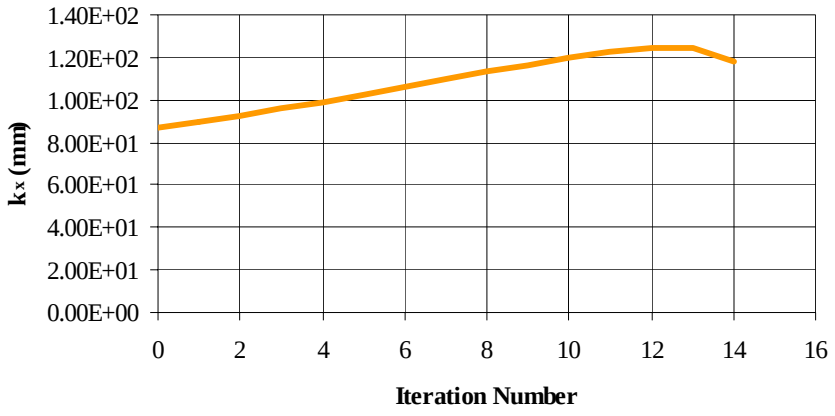

Figure 3.5 Evolution history of k_x subject to maximisation of I_x.

It is interesting to note that as a consequence of maximising I_x, the radius of gyration about the y-axis decreases at a small constant rate (Figure 3.6). This is because the elements are removed collectively parallel to the x-axis. All elements in the row contribute equally to the overall I_y (see Equation (3.5)). As the whole row is removed per iteration, the decrease in I_y per iteration is the same. The rate of decrease of the moment of inertia is greater than the rate of decrease in cross-sectional area, implying that the radius of gyration decreases i.e. $k_y = \sqrt{I_y / A}$.

The radius of gyration about the z-axis (k_z) as a result of optimising I_x changes in the same manner as k_x, though at a different scale of magnitude (Figure 3.6). As Equation (3.4)

implies, k_z is related to k_x and k_y by the relation $k_z^2 = k_x^2 + k_y^2$. This is verified by the squared summation and comparison of the values in Figures 3.5 and 3.6 for each iteration.

The product of inertia for the I-beam remains zero for each iteration. This is understandably so as there is always present an axis of symmetry about not only the *x*-axis, but also the *y*-axis as well.

It must be noted that the resulting I-beam topology produced over 12 iterations (Figure 3.4 d)) can incidentally be produced in one iteration, by increasing the rejection ratio term a_1. This is because the local centroid (on which the I_x sensitivity number is based) does not move during the maximisation of I_x. Such an example is therefore not specifically appropriate to demonstrate the evolutionary nature of the EMIO process. However, such an example where the result is self-evident, acts as a benchmark for the EMIO algorithm. This is also true for the next two examples, as it shall be seen that the centroid remains fixed during the process and the according profiles can ideally be obtained in one iteration.

In contrast to the maximisation of I_x, the minimisation of I_x for the above cross-section seeks to remove elements that act upon the aggregate I_x in the greatest manner. For each iteration therefore, the rows furthest from the centre are removed, resulting in a cruciform profile. The radius of gyration incidentally decreases. Also, if the method of maximisation and minimisation was to be applied about the *y*-axis instead of the *x*-axis, the same results would occur, but with respect to the new *y*-axis.

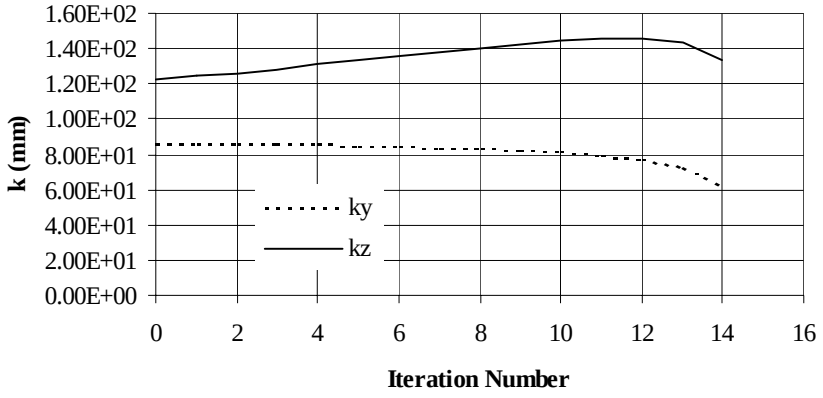

Figure 3.6 Evolution history of k_y and k_z subject to maximisation of I_x.

3.5.2 Simultaneous Maximisation of I_x and I_y

For this second example, a different non-design region is defined. Elements are located along the perimeter of the square cross-section that are not able to be removed during the evolutionary MOI optimisation process. The width of this non-design perimeter is one element wide.

Figure 3.7 exhibits this initial cross-section, along with other configurations produced for 90 %, 80 % and 60 % of the initial cross-section area. Based on removing those elements that have the lowest magnitude of I_{xy} (i.e. the smallest absolute value of I_{xy}), a small cruciform cavity develops. This cavity grows in the manner that the width of the cross-beams of the cruciform grows, as does the radius of the chamfer at the intersection of these cross-beams. The resulting topology is very much like that of a circle that is quartered, with each of these quadrants being inverted. In other words, the boundary curves are of the form $xy = constant$. Such cross-sectional topologies are not commonly evident in structures.

The tally of I_{xy} for all of the elements during the course of evolution remains zero as Figure 3.8 depicts. The symmetry of the structure is therefore conserved during the evolution. It must be noted that this evolutionary MOI optimisation process for removing elements is based purely on maximising the magnitude of the contribution of each remaining element, which is different to maximising the total aggregated contribution of each element to I_{xy}. Maximising the magnitude is removing those elements that have the smallest absolute valued sensitivity number. Maximising the total I_{xy} would be to remove those elements that have the smallest sensitivity number, including those that have a negative value.

A more apparent outcome concerns the rectangular moment of inertia. Both k_x and k_y increase at a constant rate (Figure 3.9). In effect, this form of evolutionary MOI optimisation seeks to maximise both the aggregate of I_x and I_y simultaneously, resulting in the increase of the radius of gyration about the x and y-axis. Such a point can be stated since the k_x plot in Figure 3.9 corresponds similarly to the k_x plot of Figure 3.5. Respectively for the maximisation of I_y, as implied at the end of the first example, a plot of k_y would correspond similarly to the k_y plot of Figure 3.9. However, the wide flanged beams produced as a result of independently maximising I_x and I_y are optimal when compared to I_x and I_y of the topologies displayed in Figure 3.7. This observation is identical to that for structural

topology optimisation under several load cases whereby the combined optimum is sub-optimal with respect to individual optima (Steven *et al.*, 1995).

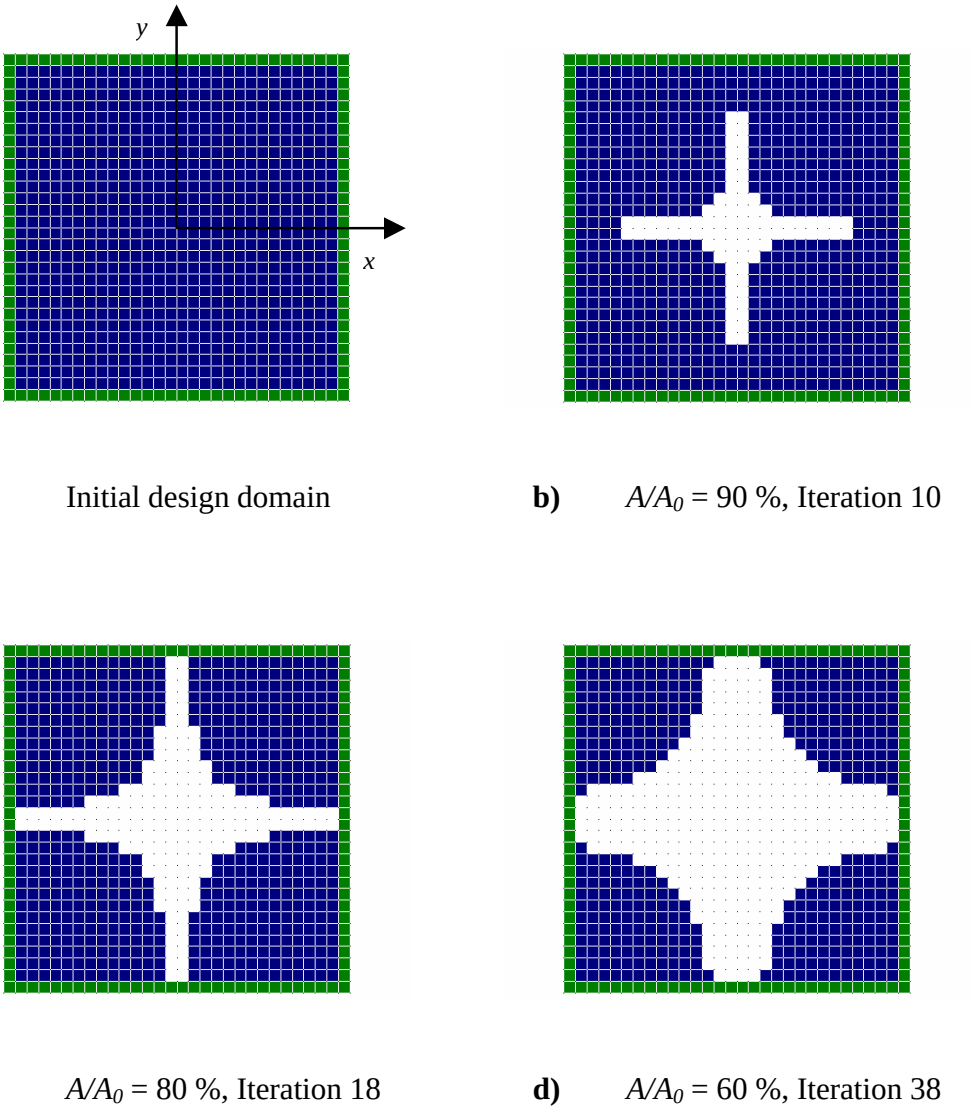

a) Initial design domain **b)** A/A_0 = 90 %, Iteration 10

c) A/A_0 = 80 %, Iteration 18 **d)** A/A_0 = 60 %, Iteration 38

Figure 3.7 Optimal designs subject to the simultaneous maximisation of I_x and I_y.

The resultant *z* radius of gyration too increases at a constant rate (see Figure 3.9 below). It evidently is related to k_x and k_y by $k_z^2 = k_x^2 + k_y^2$ as previously mentioned. Hence, there is an increase in the MOI efficiency with respect to the *z*-axis as the evolution progresses. Attention must be drawn to the reduction in the radius of gyration (for the *x*, *y* and *z*-axes). This occurs for the similar reason mentioned in the previous example. The presence of the circumferential non-design domain causes there to be 'drop' in the radius of gyration towards

the end of the evolution process. This reduction ends when all that remains is a hollow square tube. If the outer elements were alternatively declared to be part of the design domain, then the radius of gyration for all axes would increase at a constant rate until all the elements were removed.

In contrast to maximisation, the simultaneous minimisation of I_x and I_y would produce the negative region of the topologies presented in Figure 3.7, and a decrease in the radius of gyration about the *x*, *y* and *z*-axis.

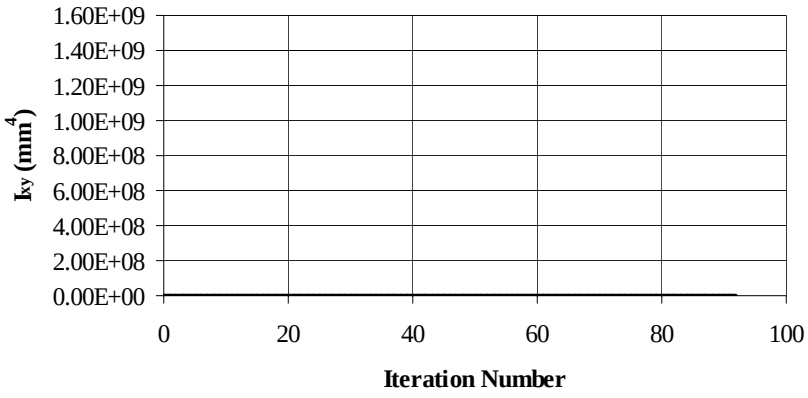

Figure 3.8 Evolution history of local I_{xy} subject to the simultaneous maximisation of I_x and I_y.

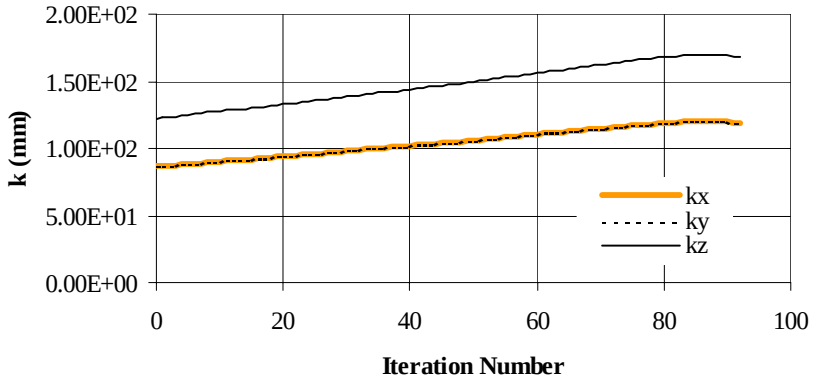

Figure 3.9 Evolution history of k_x, k_y and k_z subject to the simultaneous maximisation of I_x and I_y.

3.5.3 Maximisation of I_z

This example is of a different nature to the ones examined previously. Here, the EMIO algorithm seeks to remove material from the geometry of the structure, whilst attempting to maintain as much mass moment of inertia as possible based purely on the geometry. Figure 3.10 illustrates which elements are preferential in maintaining this inertia and which ones are not. As can be seen, a hollow circle forms in the centre of the cross-section. That is, the inner boundary follows the form $r^2 = x^2 + y^2 = constant$.

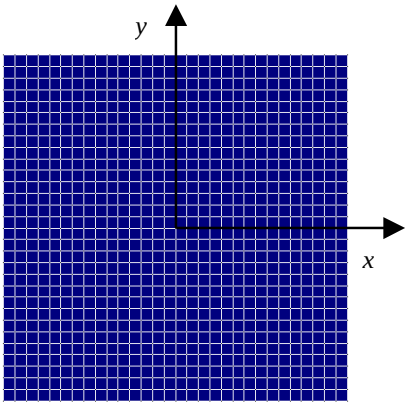

a) Initial design domain

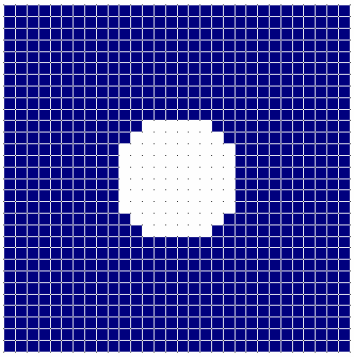

b) A/A_0 = 90 %, Iteration 12

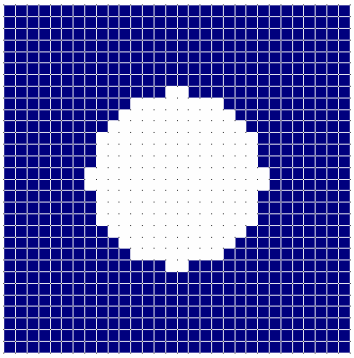

c) A/A_0 = 80 %, Iteration 22

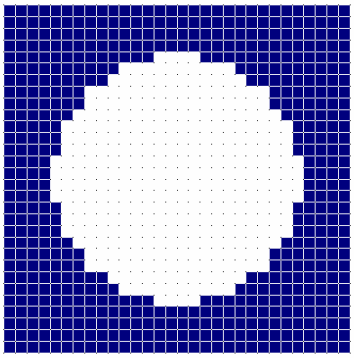

d) A/A_0 = 60 %, Iteration 39

Figure 3.10 Optimal designs subject to maximisation of I_z.

This example justifies that those elements that are closest to the axis about which the object rotates have the least influence towards the rotational inertia. As elements are removed radially from the centre per iteration, the radius of the growing circle increases. The total polar radius of gyration increases at an increasing rate (Figure 3.11), since the rate of decrease in the moment of inertia is less than the rate of decrease in the area of the section (according to Equation (3.8), if using t respect to the z-axis). In other words, more elements are removed per iteration, implying that the area of the remaining cross section is decreasing more rapidly than the decreasing inertia of the cross section. As a result, the performance index of the moment of inertia for the z-axis (k_z) increases.

The radius of gyration about the x-axis and y-axis too increases at an increased rate – see Figure 3.12. This is because the rate of change in the MOI about the z-axis, which decreases, when transposed directly to the x and y-axis, also decreases. The magnitude of k_x and k_y are identical during the design progression, due to fact that the magnitude of I_x and I_y are identical. This is because in this case, the distribution of elements is symmetric about the primary axes and the diagonal axes (external square cross-section). This duplicity in I however does not always occur because of symmetry, but ultimately on account of an even distribution of elements about both axes.

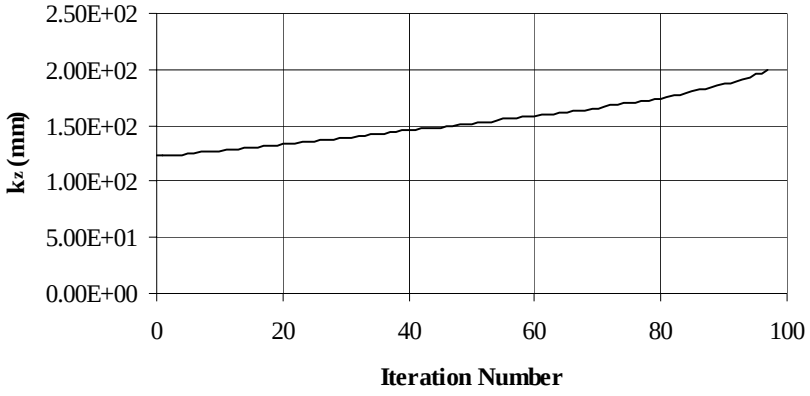

Figure 3.11 Evolution history of k_z subject to maximisation of I_z.

For reasons mentioned previously, this example, through its simplicity in shape, sets an agenda for benchmarking purposes. Taking it to a practical level, such an objective of maximising I_z for the given geometry would be effective for those tasks that would prefer as little rotational acceleration or de-acceleration as possible to take place. The desired

continuous rotation of large turbine shafts or the rolling moment of large aircraft for stability and performance purposes are instances which would benefit from I_z maximisation.

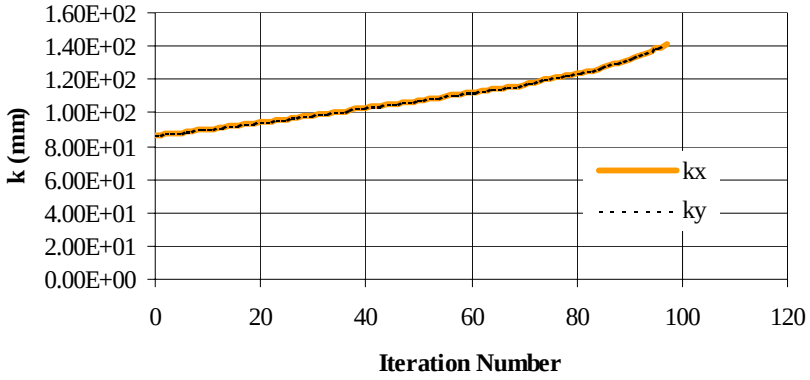

Figure 3.12 Evolution history of local k_x and k_y subject to maximisation of I_z.

In contrast to the maximisation of I_z, the minimisation of I_z produces a topology that is the inverse of this example i.e. a perfect circular profile is formed. The radius of gyration about each axis decreases. Such a motive would be useful for examples that require a greater angular acceleration or de-acceleration. That is, the preference of not having prolonged rotation in tooling after use, or the requirement in aircraft to be as maneuverable as possible by not being restricted with a large inertia. This concept can be extended further by considering other criteria in conjunction with evolutionary MOI optimisation. This is achieved through Multicriteria ESO (Proos *et al.*, 1999) and is investigated in the next chapter.

3.5.4 L-Section

Having established the framework of evolutionary MOI optimisation by focussing on individual examples and their specific objectives, this example along with next one examines two popular geometries with all the objectives of evolutionary MOI optimisation applied consecutively. This shall highlight the necessity of the evolutionary nature of MOI optimisation during the design process.

An initial design domain for this example is constructed with 700 square elements arranged in an L-shape configuration (Figure 3.13 a)). Each arm of the square L-section is 3 mm

wide, and is of a maximum length of 12 mm. The actual dimensions are not relevant in terms of the evolution process. The same shape and topology is produced for any given dimensions of the same proportion and mesh density. An exterior layer of elements defined non-design domain is assembled around the outside of the cross-section. The rejection ratio terms are set to be $a_0 = a_2 = a_3 = 0$ and $a_1 = 0.002$.

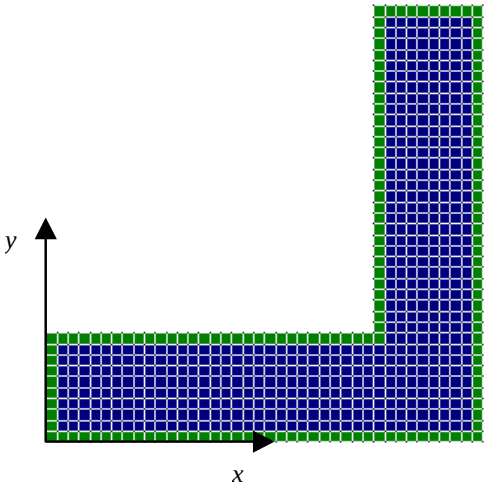

a) Initial design domain

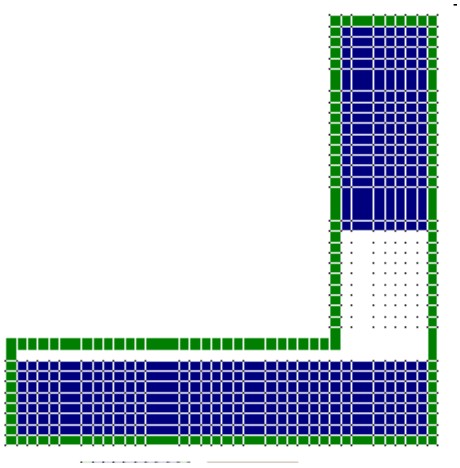

b) Maximisation of I_x, A/A_0 = 80 %, Iteration 14

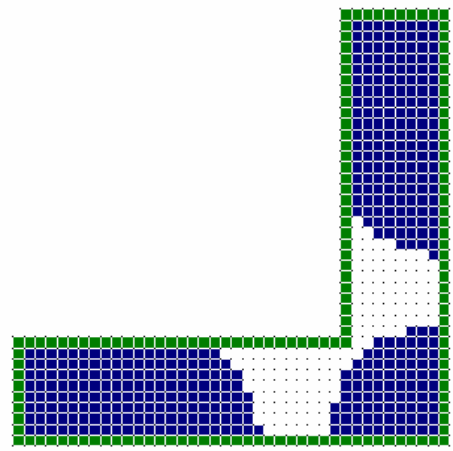

c) Maximisation of I_x & I_y, A/A_0 = 80 %, Iteration 53

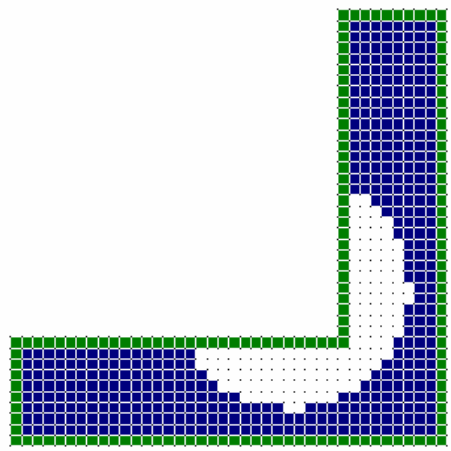

d) Maximisation of I_z, A/A_0 = 80 %, Iteration 51

Figure 3.13 Topological designs of L-section for different MOI optimisation.

Optimisation of the moment of inertia with respect to the *x*-axis and the *z*-axis, and the product of inertia can be seen in the other geometries of Figure 3.13. Each frame has been extracted from the EMIO history for an area ratio of 80 % of the initial design domain. The shape of material removed in Figure 3.13 for the maximisation of I_x, I_z and simultaneous I_x and I_y is very much similar to that established in the first series of examples (Sections 3.5.1, 3.5.2 and 3.5.3). The trends of their respective radius of gyration too are similar to the trends produced in this example. Figure 3.14 specifically confirms this for the case of the maximisation of I_z. Note the increase and the 'rounded peak' in the radius of gyration as the evolution proceeds. The peak in the evolution history exists (near iteration 170) because the perimeter of non-design elements along the boundary of the cross section is present. By not allowing elements to be removed, the non-design domain method limits the EMIO algorithm from being completely inertia efficient. But that is the beauty of the EMIO concept, it attempts to optimise whatever conditions and restrictions it is presented with. At the same time, such a non-design domain is needed to retain the integrity of the structure – particularly when cavities are evolved in topology optimisation.

Although there is a similarity in the shapes of the removed material in the previous examples, there is not an exact likeness because the configuration of the L-section is un-symmetric. During the course of the optimisation, the position of the centroid moves (evident for I_z maximisation in Figure 3.15). Having elements removed in the form $xy = constant$ about a moving centroid, evolutionary MOI optimisation by its nature produces an un-symmetric cavity in the geometry of the L-section. This confirms the necessity of the iterative nature of the evolutionary MOI optimisation during the design process.

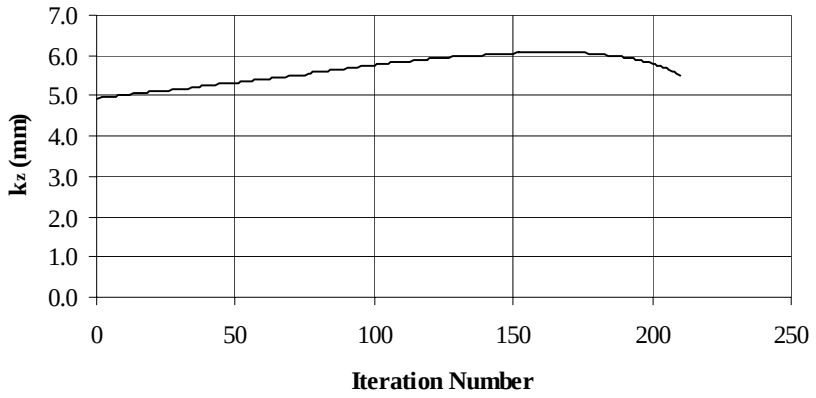

Figure 3.14 Evolution history of k_z subject to maximisation of I_z.

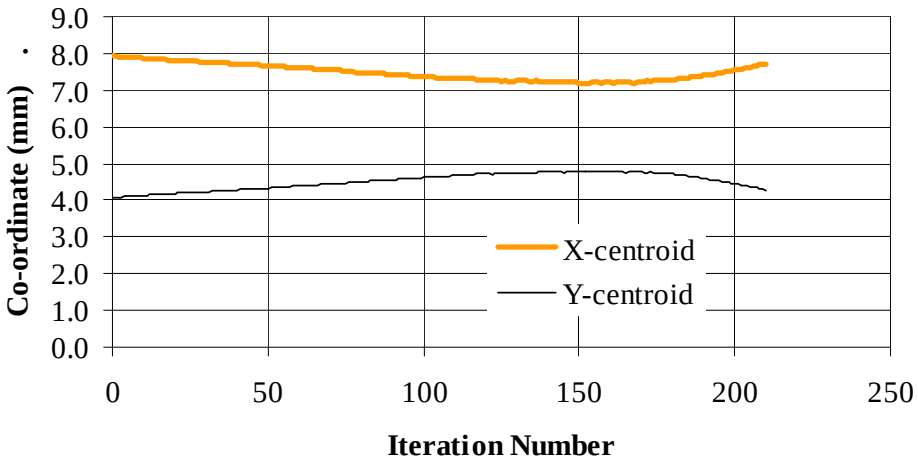

Figure 3.15 Evolution history of the *X* and *Y*-centroid subject to maximisation of I_z.

3.5.5 Circular Section with External Keyway

This final example examines the evolutionary MOI optimisation method applied to the very common example of a circular section with an external key way rotated 45 degrees to the left of the vertical. It is made up of 1560 quadrilateral elements arranged in a radial fashion. The circular section has a radius of 20 mm, and the keyway has a depth of 5 mm. A layer of elements declared non-design domain are arranged on the circumference of the section, and the rejection ratio terms are set to be $a_0 = a_2 = a_3 = 0$ and $a_1 = 0.002$. The initial design domain is pictured in Figure 3.16 a). The topologies for the maximisation of I_x, I_z and simultaneous I_x and I_y, captured at an area fraction of the initial design domain of 75 %, are given in Figure 3.16.

There is a lack of symmetry about the vertical or horizontal axes in this example that is caused by the keyway and its orientation from the vertical. The EMIO algorithm considers this factor by removing material in the most befitting way. For the maximisation of I_x, there is a bias in the material removed below the x-axis, taking into account the deficiency of cross-sectional area in the keyway above the x-axis. For the simultaneous maximisation of I_x and I_y, the bias is towards an area below the x-axis and to the left of the y-axis. For the maximisation of I_z, the bias of element removal is opposite to the side of the circle where the keyway is positioned. These are all attributable to the centroid of the cross-section occurring in the lower left quadrant of the defined origin.

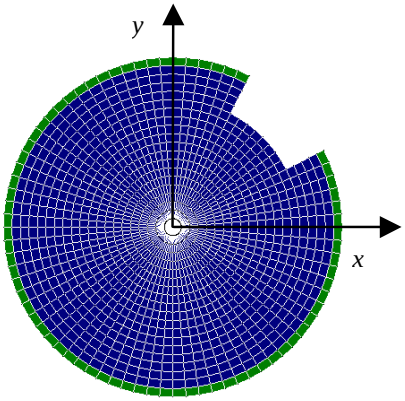

a) Initial design domain

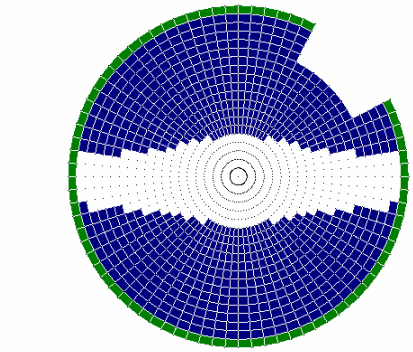

b) Maximisation of I_x, A/A_0 = 75 %, Iteration 11

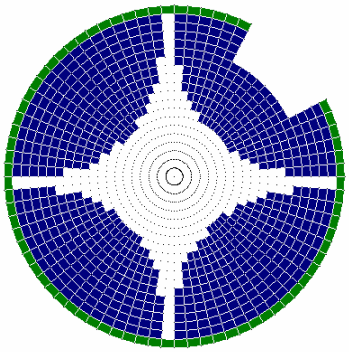

c) Simultaneous max. of I_x and I_y, A/A_0 = 75 %, Iteration 31

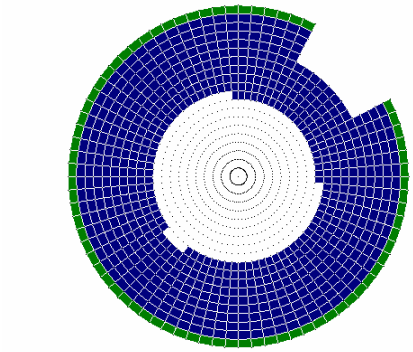

d) Maximisation of I_z, A/A_0 = 75 %, Iteration 69

Figure 3.16 Topological designs of the circular section with keyway, for different MOI optimisation.

The local product of inertia evolution history of the circular section is expressed in the graph of Figure 3.17, based on the simultaneous maximisation of I_x and I_y. A fluctuation in the product of inertia occurs for approximately 230 iterations, before increasing rapidly at the end. These fluctuations occur because of the coarse nature of the mesh where a fluctuation occurs in the centroid of the section as the design develops (see Figure 3.18). It is interesting to note that this centroid creeps away steadily from the origin of the Cartesian axes.

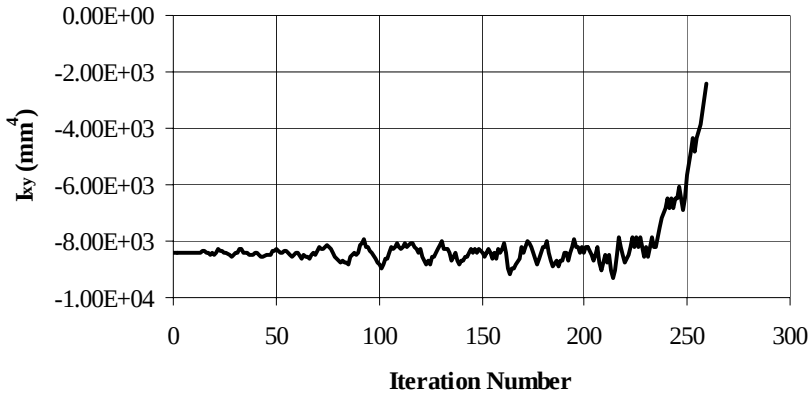

Figure 3.17 Evolution history of local I_{xy} subject to the simultaneous maximisation of I_x and I_y.

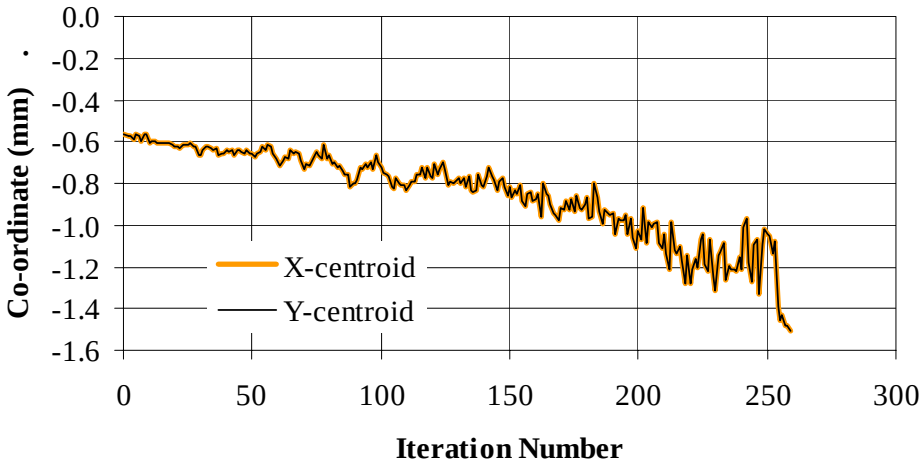

Figure 3.18 Evolution history of the *X* and *Y*-centroid subject to the simultaneous maximisation of I_x and I_y.

3.6 Concluding Remarks

This chapter has demonstrated the optimisation capability and necessity of the newly introduced EMIO algorithm based on the three components of the moment of inertia – the rectangular, product and polar moment of inertia.

All examples have illustrated that the nature of EMIO is to remove elements in a maximising or minimising way, resulting in the increase (for maximisation) or decrease (for minimisation) in the radius of gyration about a given axis. It has seen a limiting effect as influenced by a non-design domain, and the need for the iterative fashion for examples that are not axi-symmetrical. A point must also be made on this that the orientation of model would affect the rate of deletion. As seen in the first example, a large number of elements were deleted per iteration. By orientating the model, fewer elements would be removed. This of course is assuming that the deletion rate is the same for both orientations.

Related to this is the concept of EMIO based on the principal axis of inertia, rather than on the predefined axes as studied in this chapter. Such a notion is of significance, because it would allow optimisation to take place about an axis where the moment of inertia is already a minimum or maximum for that given cross-section. The resulting topology would be the same as that for a predefined axis, however, it would be displaced at an angle at which the moment of inertia was a minimum or maximum of the initial design domain.

The next logical step would be to extend this concept so that the inertia may be increased in magnitude by the adding of elements. This introduces the need for Bi-Directional Evolutionary Structural Optimisation (BESO) (Young *et al.*, 1999) where elements can be either added or removed. The other alternative would be to incorporate material shifting (adding and removing elements therefore maintaining the total amount of elements), resulting in a maintained sectional area during optimisation. Such a step is not the focus of this thesis, however, it lays the foundation for other ESO features to be combined with that which has been established in this chapter.

Further research could see an extension of evolutionary MOI optimisation to three dimensions – examining the design of objects constructed with bricks, based on the mass moments of inertia. This would be beneficial in the area of dynamics - the rotational motion of objects. Ultimately one could use EMIO (appropriate for cross-sections) together with ESO (appropriate for longitudinal stress etc) to optimise 3-D structures.

There is also a need to incorporate this evolutionary MOI optimisation solver into multicriteria optimisation (Proos *et al.*, 1999). This would see designs being created considering the MOI as studied herein, as well as other criteria from other analysis types such as linear static and natural frequency. This is examined in the following chapters for the case of inertia combined with the linear static solver (specifically – inertia and stiffness in Chapter 4) and inertia combined with the linear static and natural frequency solvers (specifically inertia, stiffness and natural frequency Multicriteria ESO - Chapter 5).

3.7 References

Bedford, A., Fowler, W. (1999), *Statics, Engineering Mechanics*, Addison Wesley Longman, Inc., USA.

Chen, W-F., Atsuta, T. (1976), *Theory of Beam-Columns, Volume 1: In-plane Behaviour and Design*, McGraw-Hill, Inc., USA.

Chu, D., N., Xie, Y., M., Hira, A., Steven, G., P. (1996), "Evolutionary Structural Optimization for Problems with Stiffness Constraints", *Finite Elements in Analysis and Design*, Vol. 21, pp. 239-251.

Hopkins, R., B. (1970), *Design Analysis of Shafts and Beams*, McGraw-Hill, Inc., USA.

Laliberte, T., Gosselin, C., Jean M. (1999). "Static Balancing of 3-DOF Planar Parallel Mechanism", *IEEE-ASME Transactions on Mechatronics*, Vol. 4, pp. 363-377.

Li, Q., Steven, G., P., Querin, O., M., Xie, Y., M. (1997), "Optimal Shape Design for Steady Heat Conduction by the Evolutionary Procedure", Dulikravich, G., S., Woodbury, K., A.,

(Eds.) *Inverse Problems in Heat Transfer and Fluid Flow, ASME Proceedings of the 32nd National Heat Transfer Conference, ASME HTD*, Vol. 340, pp. 159-164.

Li, Q., Steven, G., P., Xie, Y., M. (1999), "Evolutionary Shape Optimization - A Stress Based Sensitivity Analysis Method", *Proceedings of the Second Australian Congress on Applied Mechanics ACAM '99*, Canberra, Australia.

Manickarajah, D., Xie, Y., M., Steven, G., P. (1998), "An Evolutionary Method for Optimization of Plate Buckling Resistance", *Finite Elements in Analysis and Design*, Vol. 29, pp. 205-230.

Proos, K., A., Steven, G., P., Querin, O., M., Xie, Y., M. (1999), "Multicriteria Evolutionary Structural Optimisation", submitted to *Design Optimization - International Journal for Product and Process Improvement*.

Salajegheh, E. (2000), "Optimum Design of Frame Structures Using Two-Point Response Approximation", *Iranian Journal of Science and Technology*, Vol. 24, pp. 1-10.

Soykasap, O., Hodges, D. (2000), "Performance Enhancement of a Composite Tilt-Rotor Using Aeroelastic Tailoring", *Journal of Aircraft*, Vol. 37, pp. 850-858.

Spunt, L. (1971), *Optimum Structural Design*, Prentice-Hall, Inc., New Jersey.

Steven, G., P., Xie, Y., M. (1993), "A Simple Evolutionary Procedure For Structural Optimisation", *Computers and Structures*, Vol. 49, No. 5, pp. 885-896.

Steven, G., P., Querin, O., M., Xie, Y., M. (1995), "Multiple Constraint Environments for Evolutionary Structural Optimisation", Olhoff, N., Rozvany, G., I., N., (Eds.) *Proceedings of the First World Congress on Structural and Multidiciplinary Optimization*, Goslar, Germany, Pergamon, May 28-June 2, pp. 213-218.

Steven, G., P., Li, Q., Xie, Y., M. (2000), "Evolutionary Topology and Shape Design for Mathematical Physical Problems", in press in *Computational Mechanics*.

Vinot, P., Cogan, S., Piranda, J. (2001), "Shape Optimization of Thin-Walled Beam-Like Structures", *Thin-Walled Structures*, Vol. 39, pp. 611-630.

Young, V., Querin, O., M., Steven, G., P., Xie, Y., M. (1999), "3D and Multiple Load Case Bi-directional Evolutionary Structural Optimisation (BESO)", *Journal of Structural Optimization*, Vol. 18, pp. 183-192.

Xie, Y., M., Steven, G., P. (1997), *Evolutionary Structural Optimisation*, Springer-Verlag, London.

Zhao, C., Steven, G., P., Xie, Y., M. (1996), "Evolutionary Natural Frequency Optimization of Thin Plate Bending Vibration Problems", *Journal of Structural Optimization*, Vol. 11, pp. 244-251.

Chapter 4

Stiffness and Inertia Multicriteria ESO

4.1 Introduction

Multicriteria optimisation has been established for two different FEA conditions. The first was with the optimisation of two criteria, each with the same solver type ie linear static (stress and stiffness, Li (2000)). The second was the multicriteria optimisation of two criteria, each being analysed by a different FEA solver ie linear static and natural frequency (stiffness and natural frequency, Chapter 2). Questions now arise: does the Multicriteria ESO concept work for other solver types? Will the Pareto optimal distribution concept work for criteria of alternative FEA solver types? If such questions are satisfied, how does the distribution of Pareto points eventuate and what influences are there to this distribution? Does the relationships between the different multicriteria ESO methods established in Chapter 2 remain consistent for new different solver combinations? All these questions need to be resolved and are addressed in this chapter.

One may argue that once the multicriteria ESO method has been implemented, the use of any other criterion only serves to use the method for different applications or case studies. This is based on the assumption that knowing the name 'multicriteria optimisation' means more than one criterion, it really does not matter which criteria are used. However, this conjecture may be rebutted by the simple fact that it has not yet been shown that different unexamined criteria will consistently work with the multicriteria ESO concept. As shall be seen, there is relevance as to which criteria are used. This is particularly what this thesis seeks to contribute toward. In addition, this method cannot be seen as another application of Chapter 2, as shall be shown the development of this process specific to these solver types requires a different structure to that of Chapter 2.

This chapter develops the multicriteria ESO method for the regime of linear static and inertia analyses. More specifically, it seeks to minimise the mean compliance (ie maximise stiffness) and maximise the specific inertia (ie radius of gyration squared). The work identified in this chapter has been developed from the inertia optimisation established in the previous chapter.

The maximisation of stiffness and maximisation of specific inertia in an FEA regime is a combination that has not been studied elsewhere (to the author's knowledge). However, it appears as a desired combined objective useful to industrial and engineering applications. For example, in the field of mechatronic systems, there is the need to address the stiffness of the mechanical elements together with the inertia of the mechanical elements (affecting the operation of the actuators). For reliable operation (where accurate positioning is required), a rigid system is desired where large distortions or fluctuations are not present. Stiffness maximisation addresses this. Also, for efficient operation, lower power (required by the actuators) is desired to drive each of these mechanical elements, as is accuracy in operation where large overshoots during operation are avoided. Rotational inertia minimisation addresses these. This is just one example of many that illustrates the need for stiffness and inertia multicriteria ESO. More shall be presented in Section 4.4 in order to validate and demonstrate the method.

Because these studies have been confined to the 2-D plane (appropriate to inertia), such a method concerns the optimal topologies, shapes and sizes of cross-sectional geometries. By concentrating on the factors of cross-sectional stiffness and beam bending (or rotational dynamics), such research is vital in making ESO and structural optimisation in general, a robust and practical design tool.

4.2 Compilation and Determination of Sensitivity Numbers

As mentioned previously, it may be thought that the exploration of these two different solver types are no more than case studies of that developed in Chapter 2. From a programming perspective, this is not the case. In contrast to the method used for linear static and natural frequency multicriteria ESO, the different solver combinations of linear static and inertia analyses needed to be incorporated and arranged into the program such that the analyses of

two different sensitivity numbers could be carried out. Only when these had be incorporated, could the different multicriteria methods be used to execute the multicriteria ESO process. Such a method using this combination of analyses has never been developed or verified. It is for this reason that the following outline of the linear static and inertia multicriteria ESO method is described. The sensitivity numbers for the linear static analyses have been formulated in Section 2.2.1 and are given in Equation (2.4). Likewise, the moment of inertia sensitivity numbers have been derived in Section 3.3 and are given as Equations (3.10) to (3.12).

The same multicriteria optimisation techniques of the linear weighting method and the global criterion method will be applied to the scenario of mean compliance and inertia. The influence that these different criteria have on the multicriteria process will be examined. The formulations to combine the multi-sensitivity numbers into a new composite number using the weighting and global criterion methods have been presented in Section 2.3.

4.3 Evolutionary Optimisation Procedure

4.3.1 Weighting Method Multicriteria ESO

Having a formulation to produce an array of sensitivity numbers derived from the weighting method, the following steps illustrate how it is incorporated into multicriteria ESO:

Step 1: Discretise the structure using a fine mesh of finite elements;
Step 2: Add load/s to structure;
Step 3: Solve the linear static problem - Equation (2.1);
Step 4: Calculate the linear static sensitivity number α_i using Equation (2.4);
Step 5: Remove load/s from structure;
Step 6: Calculate the MOI of the structure - Equations (3.5) to (3.7);
Step 7: Calculate the MOI sensitivity number - Equations (3.10) to (3.12);
Step 8: Combine the two criteria sensitivity numbers using Equation (2.9) to obtain $F^i_{multicrit}$;
Step 9: Remove a number of elements that have the lowest values of $F^i_{multicrit}$;

Step 10: Repeat Steps 2 to 9 until an optimum is reached.

As can be seen, the linear static FEA solver analyses the structure with its accompanying loads and constraints. These loads are then removed from the structure (Step 5). It is in fact irrelevant whether the loads and constraints are present for the inertia analysis of the structure. However, from a programming convenience point of view, the same 'shell' from the linear static / natural frequency method was used for the linear static / inertia method. Thus the process of adding and removing the loads was repeated per iteration.

The flow-chart in Figure 4.1 clarifies the set of logical steps mentioned above. The method outlined in this chart expectantly completed the process at a faster rate than for the linear static / natural frequency multicriteria ESO. This was because of the omission of the natural frequency FE solver, which was replaced by the relatively rapid inertia solver. The process took approximately half the time of linear static / natural frequency multicriteria ESO process.

4.3.2 Global Criterion Method Multicriteria ESO

The solution procedure for achieving Multicriteria ESO using the Global Criterion Method is similar to that in Sub-section 4.3.1, with the only difference is in Steps 8 and 9 which should be replaced by these two steps:

Step 8: Combine the two criteria sensitivity numbers using Equation (2.11) to obtain $G^i_{multicrit}$;

Step 9: Remove a number of elements that have the lowest values of $G^i_{multicrit}$;

4.3.3 Logical AND and OR Multicriteria ESO

The same steps replacing the weighting method multicriteria ESO process with either the logical AND or OR multicriteria ESO process is described in Sections 2.4.3 and 2.4.4 respectively.

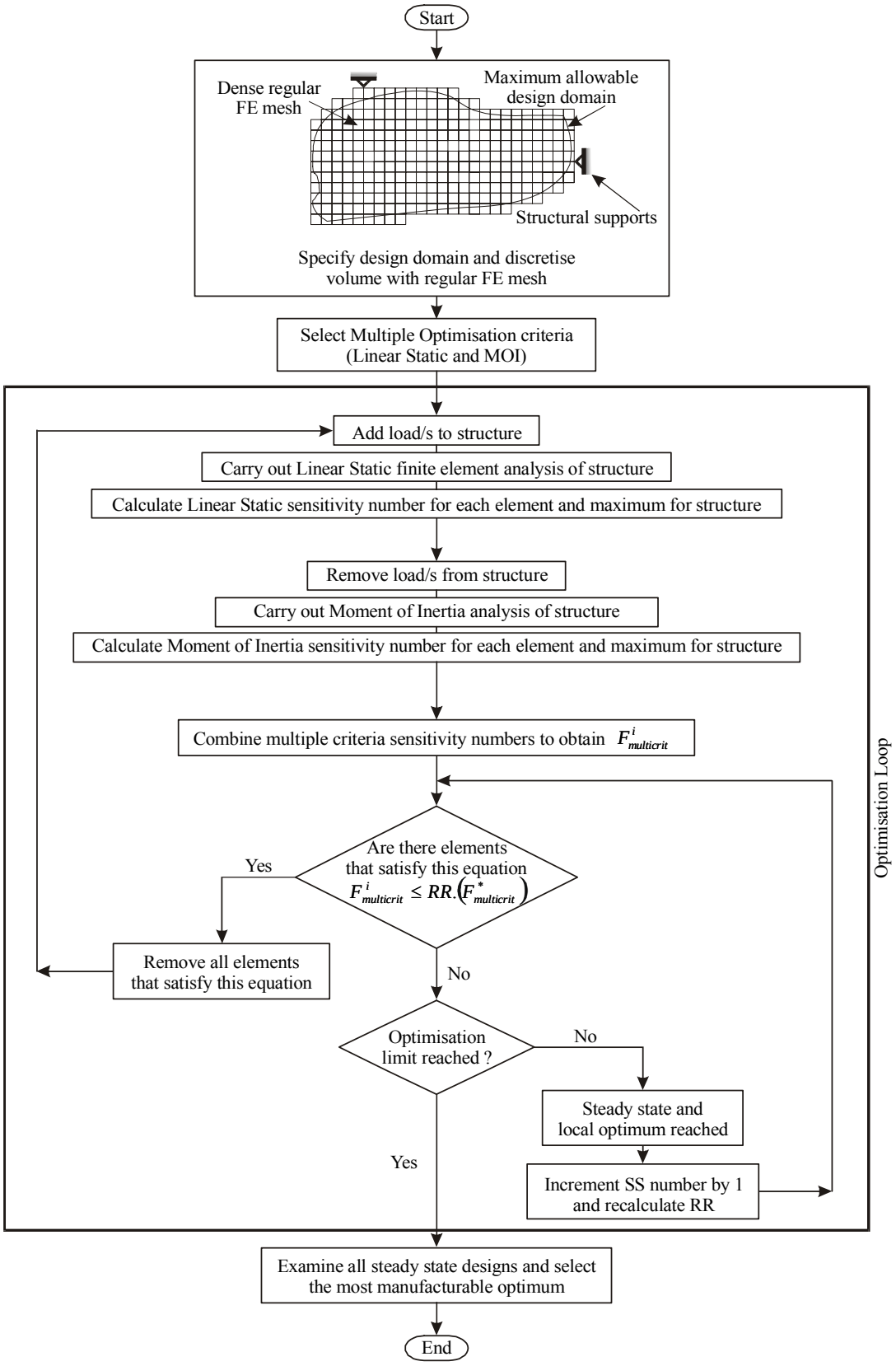

Figure 4.1 Flow chart depicting the logical steps of the weighting method Multicriteria ESO.

4.4 Examples and Discussion

The examples presented in this section are all two-dimensional plane stress problems, with only motion that is in-plane considered. All of the elements used here are of the four noded linear quadrilateral type. The two driving criteria are the maximisation of the stiffness and the maximisation of the moment of inertia.

4.4.1 A Rectangular Plate with Fixed Supports

The first example is one of a common rectangular plate that has been used in previous discrete ESO multicriteria problems (Proos *et al.*, 1999; 2000 and 2001) and in the second chapter. This rectangular plate (Figure 4.2), with the dimensions 150 mm by 100 mm, has been divided up into 45 × 30 square elements. Each element has a thickness of 1.0×10^{-3} m. The upper right corner is completely fixed, as is the lower left corner. To the other two corners, horizontal loads, each of 100 N are applied and directed away from the plate. The material properties of the plate are: Young's modulus of 70 GPa, a Poisson's ratio of 0.3, and a material density of 2700 kg/m^3. It is desired to maximise the stiffness across this loaded plate, and yet at the same time to increase the Moment of Inertia about the *z*-axis (MOIz) for a given area fraction.

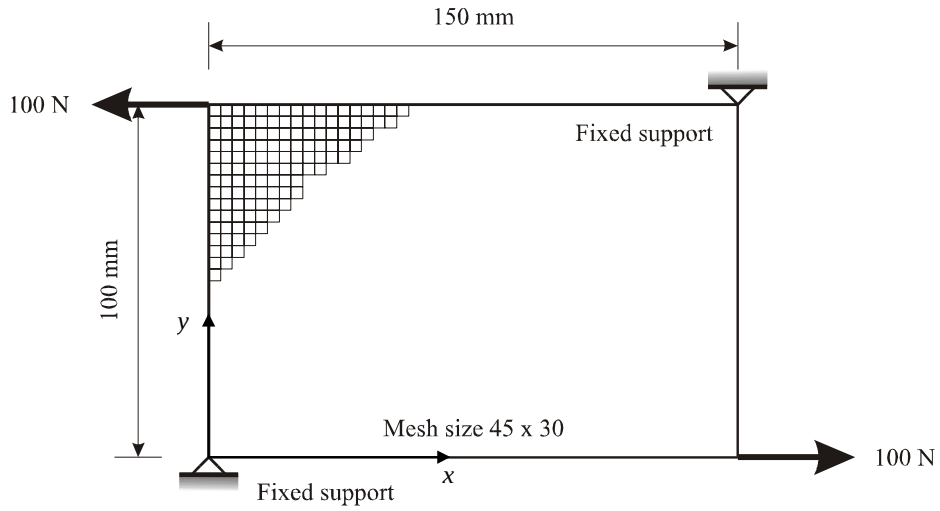

Figure 4.2 Initial design-domain of a rectangular plate under loading with fixed supports. Mean compliance × volume: 2.63×10^{-8} Nm^4, radius of gyration about *z*-axis: 5.20×10^{-2} m.

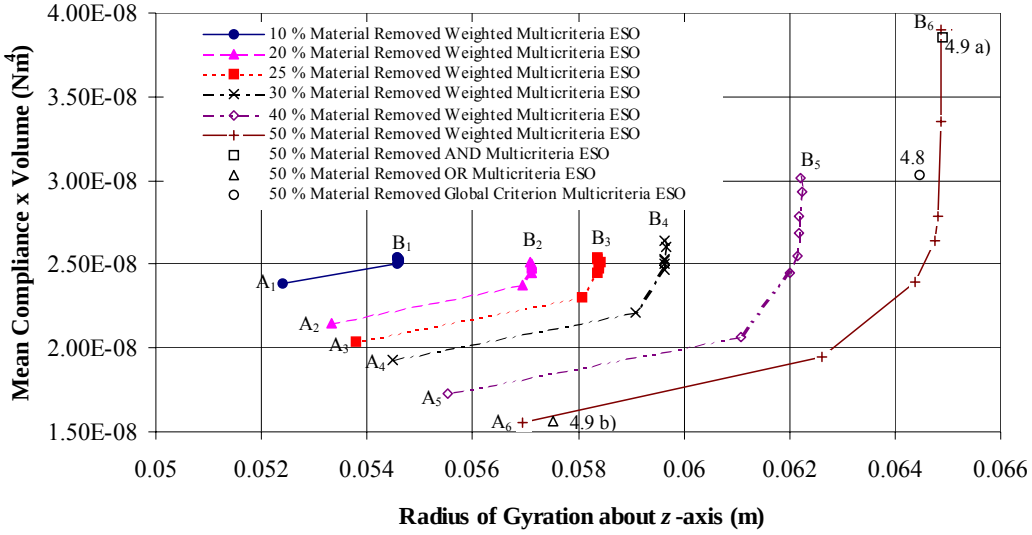

Figure 4.3 Pareto curves for radius of gyration about *z*-axis versus mean compliance × volume, for a variation of material removed.

The Pareto curves for the given various levels of material removed are displayed in the graph of Figure 4.3. Each curve is shaped such that as the weighting assigned to each criteria is varied, one criterion is bettered, but the objective of the other is compromised. The points making up each of these Pareto curves correspond to the weightings displayed in Figure 4.4. However, the topologies of Figure 4.4 are those of 50 % of the material removed during the Multicriteria ESO process.

The optimising nature of the ESO process (both for specific stiffness and the radius of gyration) is clearly evident from the arrangement of the Pareto curves. As more material is removed, the mean compliance × volume of the topology with 100 % stiffness decreases (see points A_1 to A_6). This implies that the specific stiffness increases during the evolution of the design, due to the inverse relation between the mean compliance and the structure's stiffness. The evolution of the topologies based on 100 % moment of inertia (about the *z*-axis) also follows a path towards efficiency, as indicated by the increase in the radius of gyration (see points B_1 to B_6). An additional point to note is that one of the consequential effects of the increased specific stiffness for the fully stiff topology is that the radius of gyration also increases. The converse is not the same where the specific stiffness does not increase as a result of optimising the rectangular plate based completely on moment of inertia about the *z*-axis.

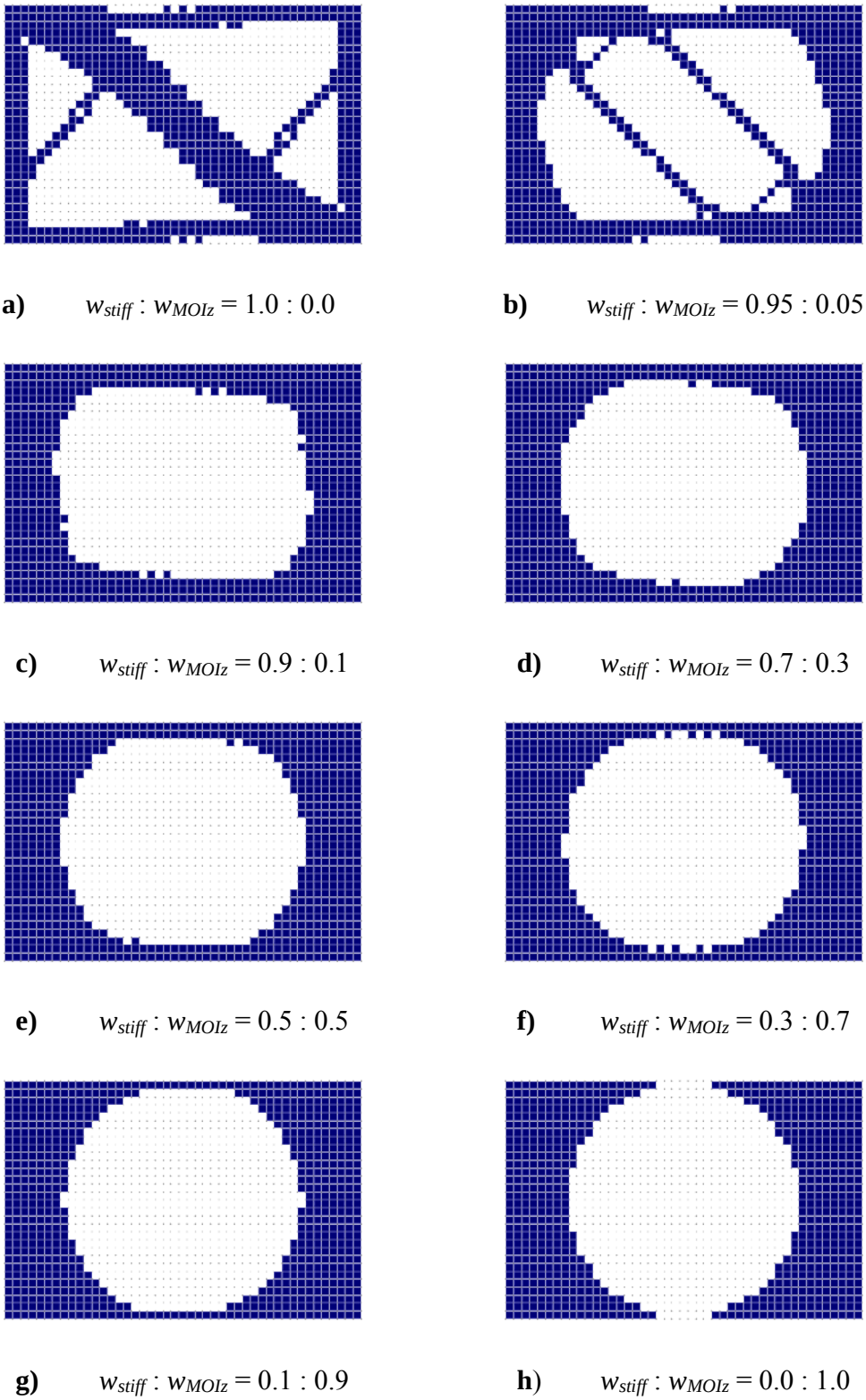

Figure 4.4 Optimal designs of the rectangular plate for different weighting criteria of stiffness and moment of inertia about the *z*-axis. Material removed: 50 %.

Figures 4.4 to 4.9 illustrate the resulting topologies for each of the four Multicriteria ESO methods for the iterations where 50 % of the material has been taken away. The dominance of the moment of inertia about the *z*-axis as seen in Figure 4.4, where the characteristic of a circle is still evident even at very low weighting of MOIz, is also portrayed in the Pareto curves of Figure 4.3. This is where most of the points making up each Pareto curve are distributed more towards the MOIz end of the curve.

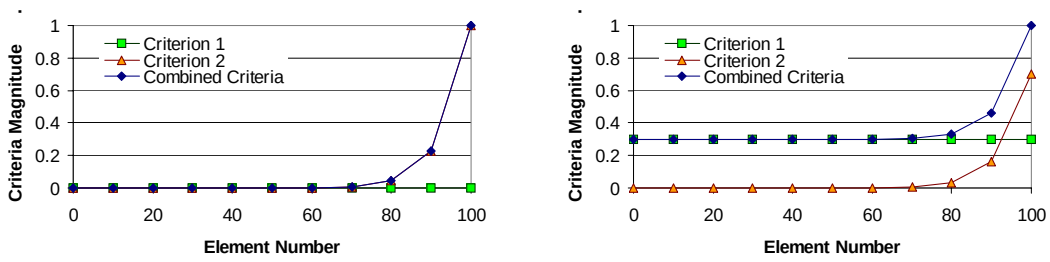

a) 0 % Criterion 1 : 100 % Criterion 2 **b)** 30 % Criterion 1 : 70 % Criterion 2

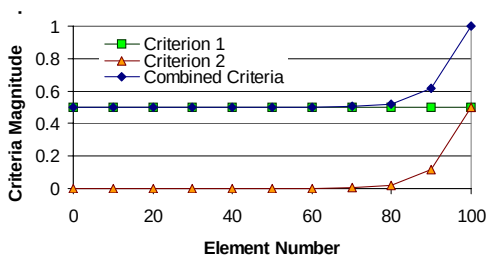

c) 50 % Criterion 1 : 50 % Criterion 2

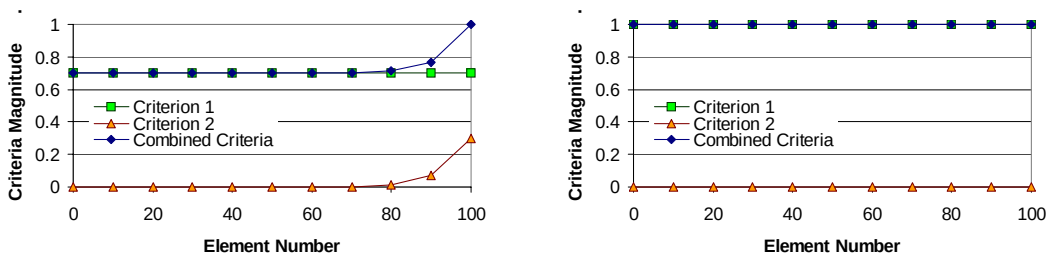

d) 70 % Criterion 1 : 30 % Criterion 2 **e)** 100 % Criterion 1 : 0 % Criterion 2

Figure 4.5 Criteria Distribution comparisons for different weighting allocations. Criterion 1: $f(x_1) = constant$, Criterion 2: $f(x_2) = (x_2)^{14}$.

The reason why this is the case is attributed to the means by which the weights are allocated to the criteria (ie linearly) as well as their relative criterion distribution to each other. For a large proportion of the weight allocations, the sensitivity number distribution of one criterion may very much dominate the combined resulting criteria numbers (as MOIz does in this case). If the distributions of the two criteria are very different, then the linear weighting method does not have as an effective role in considering each criterion. As shall be seen, it is the relative distribution of criteria to each other, combined with the weighting allocation means, that influences the final resulting combined criterion distribution.

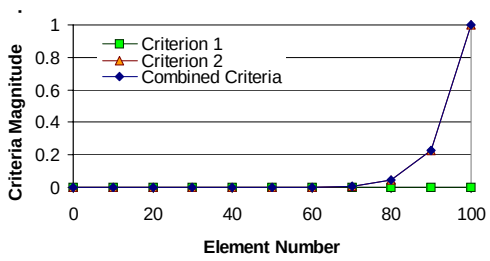

a) 0 % Criterion 1 : 100 % Criterion 2

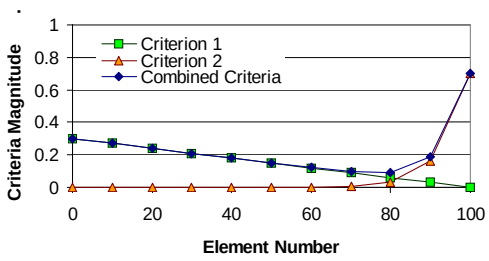

b) 30 % Criterion 1 : 70 % Criterion 2

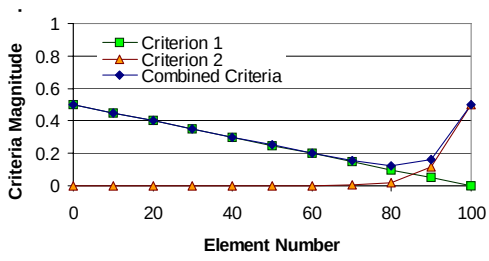

c) 50 % Criterion 1 : 50 % Criterion 2

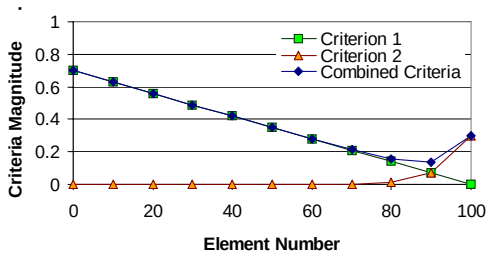

d) 70 % Criterion 1 : 30 % Criterion 2

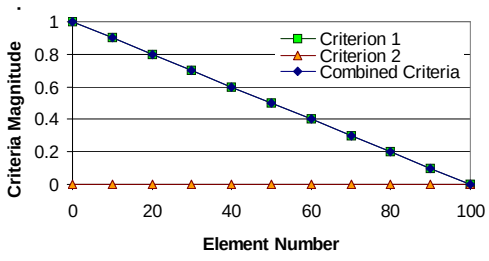

e) 100 % Criterion 1 : 0 % Criterion 2

Figure 4.6 Criteria Distribution comparisons for different weighting allocations. Criterion 1: $f(x_1) = - t\, x_1$, Criterion 2: $f(x_2) = (x_2)^{14}$.

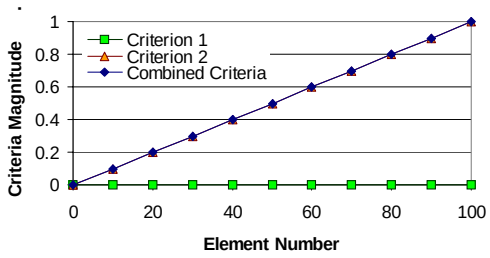

a) 0 % Criterion 1 : 100 % Criterion 2

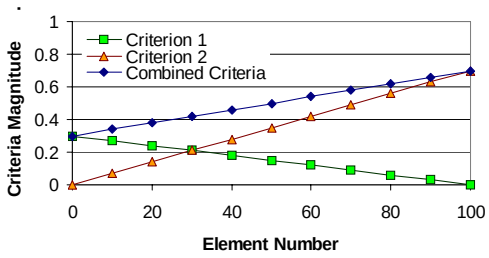

b) 30 % Criterion 1 : 70 % Criterion 2

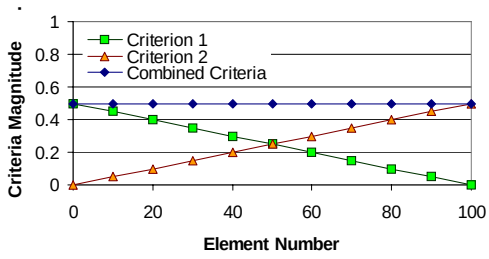

c) 50 % Criterion 1 : 50 % Criterion 2

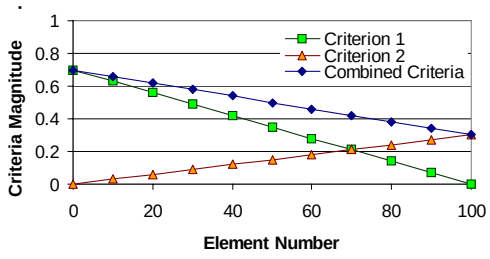

d) 70 % Criterion 1 : 30 % Criterion 2

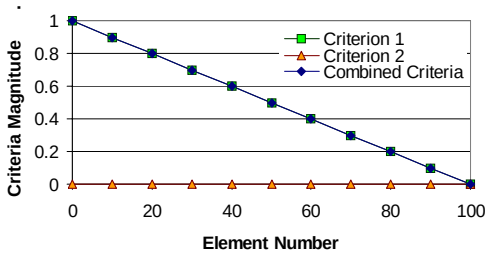

e) 100 % Criterion 1 : 0 % Criterion 2

Figure 4.7 Criteria Distribution comparisons for different weighting allocations. Criterion 1: $f(x_1) = -\,t\,x_1$, Criterion 2: $f(x_2) = t\,x_2$.

As simple example is required to demonstrate these influences. Take one criterion that has a distribution of sensitivity numbers that follows the function $f(x_1) = constant$ for 100 elements, and another criterion that has its distribution such that one or two elements have sensitivity numbers that are significantly different to the remaining elements ie follows the function $f(x_2) = (x_2)^{14}$ (fourteenth power). Note that both these criterion have been normalised and non-dimensionalised by dividing each criterion by its respective maximum value. By choosing proportions of those two criteria in a linear fashion (ie linear weighting), the graphs of Figure 4.5 result. Here, the distribution of the single criterion displayed takes into account

the weight allocation. Thus the combined criterion is a summation of these two criteria. As can be seen, for all proportions of different weighting, the combined criterion distribution holds a pattern very similar to that of the first criterion. This is because of the large spread of the first criterion sensitivity numbers compared to the non-varying second criterion.

The influence of the degree of spread can again be reinforced with the help of Figure 4.6. It shows, for different linear weighting allocations, the resulting sensitivity number distribution for the criteria that follows the functions: Criterion 1: $f(x_1) = - t\, x_1$, Criterion 2: $f(x_2) = (x_2)^{14}$. That is, the first criterion has now been changed to vary linearly. As can be seen, the distribution distinguished in criterion 2 is now not so obvious in the distribution of the combined criteria for each given weighting combination. This is because the relative spread of the first criterion is not so different from the second.

Not only is the relative spread significant, but also the pattern of the criteria's distribution. Consider two objectives, each with the same relative spread, but completely opposite distributions ie Criterion 1: $f(x_1) = - t\, x_1$ (same as previous) and Criterion 2: $f(x_2) = t\, x_2$. From Figure 4.7, the combined criterion distribution varies considerably for each different linear weight allocation. Both have the same relative spread, but completely different distributions.

Going back to the rectangular plate in the original example, the distribution of the MOIz is more spread and non-linear compared to that of the stiffness distribution, for any given combination of linear weighting and for any given iteration in the evolution. This is obvious from Equation (3.12) where the polar moment of inertia sensitivity number is a function to the power of two. Thus when it is combined with the stiffness sensitivity number, the resulting combined criterion distribution numbers ($F^{i}_{multicrit}$ - Equation (2.9)) is heavily influenced by it (that is, the combined criterion distribution is similar in spread and pattern to the MOIz distribution). As a result, the spread in Pareto optimal points for different weighting becomes 'un-even' (as seen in Figure 4.3).

In light of this, the question arises: how is the strong influence of distribution and spread between the criteria alleviated such that it does not produce 'un-even' distributions? This may be resolved by two approaches. The first is to modify the individual criterion before they are combined using the linear weighting method (Equation 2.9) such that:

$$F^{i}_{multicrit} = w_1 R_1^{\mathrm{mod}\,i} + w_2 R_2^{\mathrm{mod}\,i} + \ldots + w_N R_N^{\mathrm{mod}\,i} = \sum_{j=1}^{N} w_j R_j^{\mathrm{mod}\,i} \tag{4.1}$$

where:

w_j is still the j^{th} criteria linear weighting factor with $0.0 \leq w_j \leq 1.0$ and $j = 1,\ldots,N$;

$R_j^{\mathrm{mod}\,i} = f(\alpha_j^i, \alpha_j^*)$ is the modified function of the j^{th} criteria sensitivity number (α_j^i) for each element i and the maximum value of the j^{th} criteria sensitivity number (α_j^*).

Modifying the criterion involves more than just normalising each criterion as has been done for all examples in this thesis. It must take into account the distributions of other criteria in the multicriteria process. Caution must be adhered to in this modification, because if the relative spread of sensitivity numbers amongst elements is lost, a Pareto result is not ensured. The second option is to modify the weighting such that its allocation is not linear, but rather, dependant upon the relative distributions of criteria. That is:

$$F^{i}_{multicrit} = w_1^{\mathrm{mod}} R_1^i + w_2^{\mathrm{mod}} R_2^i + \ldots + w_N^{\mathrm{mod}} R_N^i = \sum_{j=1}^{N} w_j^{\mathrm{mod}} R_j^i \tag{4.2}$$

where:

w_j^{mod} is the j^{th} criteria weighting factor function taking into account the relative distribution between R_j^i with $0.0 \leq w_j^{\mathrm{mod}} \leq 1.0$ and $j = 1,\ldots,N$;

$R_j^i = \dfrac{\alpha_j^i}{\alpha_j^*}$ is still the ratio of the j^{th} criteria sensitivity number (α_j^i) for each element i, to the maximum value of the j^{th} criteria sensitivity number (α_j^*);

These approaches are recommendations for future research, with the continuation of the current linear weighting method to be applied here to this thesis to investigate its properties.

The Global Criterion topology of Figure 4.8 closely resembles the 50/50 weighting topology of Figure 4.4 e). The numerical evidence of this is substantiated in Figure 4.3 where the Global Criterion point 4.8 lies nearest to the displayed weighting point of 50 % stiffness / 50 % MOIz. This is also consistent with the relation between the global criterion method and the linear weighting method applied to the linear static and natural frequency solvers (Chapter 2). It reinforces that the global criterion method implicitly allocates equal weighting to the stiffness and inertia criteria.

A comparison of the logical AND topology (Figure 4.9 a)) to those of the weighting method (Figure 4.4) for this example deduces that the AND method produces topologies resembling that based on 100 % MOIz (Figure 4.4 h)). Verification of this can be made with Figure 4.3, where point 4.9 a) is positioned nearest to point B_6. However, it can been seen that by taking into account the other examples in Chapter 2, there is no distinct pattern emerging in the relation between the logical AND method and the linear weighting method.

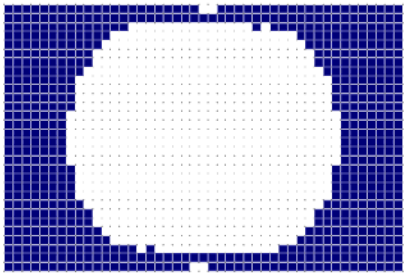

Figure 4.8 Optimum design of the rectangular plate for the Global Criterion method of Multicriteria ESO. Material removed: 50 %.

A correlation can be made between the topology of the logical OR operator (Figure 4.9 b)) and the fully stiff topology (Figure 4.4 a)) from a comparison of this topology to those of the weighting method. This correlation can be validated with the graph of Figure 4.3, where point 4.9 b) lies in the vicinity of A_6. Although not evidently useful to the designer at a practical level, this basic example is useful to highlight the proficiency of Multicriteria ESO process.

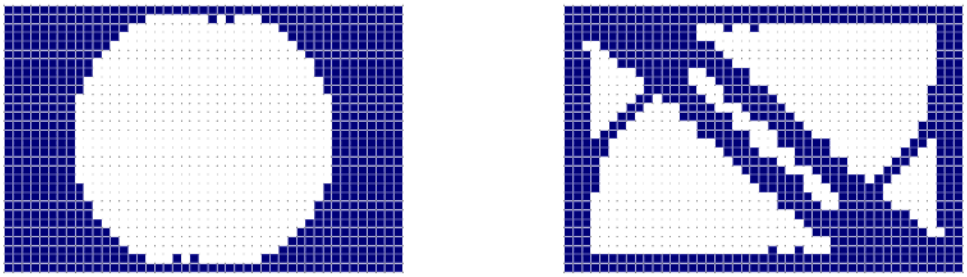

a) Logical AND operator **b)** Logical OR operator

Figure 4.9 Respective optimum designs of the rectangular plate for the logical AND and the logical OR method of Multicriteria ESO. Material removed: 50 %.

4.4.2 A Short Cantilevered Beam

The second example is based on the application of multiple objectives to a design that exists in the engineering world - in this case, aerospace. It is of a horizontal longeron of an aircraft fuselage that is attached to a skin panel enveloping the airframe (see cut-out in Figure 4.10). The cylindrical shape and stiffness is maintained with the use of vertical frames. The objectives of this example are to investigate the class of optimum topologies produced with the intention of maximising the stiffness across the cross-section of the longeron; and maximising the Moment of Inertia about the *y*-axis (MOI*y*), that is, keeping beam bending about the *y*-axis to a minimum.

The initial design-domain of the longeron's cross-section is a short cantilevered beam under loading, as illustrated in Figure 4.11. It has dimensions 160 mm × 100 mm. The beam is completely fixed along the left-hand vertical edge, and a vertical load of 100 N directed downwards is applied in the centre of the right-hand vertical edge. This simulates a series of vertical loads applied along the beam from which items of a significant weight are hung. The beam is modeled with 64 × 40 square elements, each 1.0×10^{-3} m thick. They all have a Young's modulus of 210 GPa, a Poisson's ratio of 0.3, and a material density of 7800 kg/m^3.

The resulting Pareto curves for a given variation of material removed during the Multicriteria ESO process is displayed in Figure 4.12. Although not distinctly clear, all the points are optimal in their own right – by changing from point to point for a given area fraction, one

criteria is improved, and the other is jeopardised. The corresponding topologies for 30 % of the material removed are displayed in Figure 4.13. Although not as strong as in the previous example, a distinct dominance of MOI*y* is seen in each of these topologies which corresponds to the uneven distribution of Pareto points on each optimal curve. As explained in the previous example, this is attributed to the allocation of weights linearly to two different criteria whose spread is quite different from one another. Specifically for this example, the MOI*y* criterion has a spread of a function that is squared – derived from Equation (3.10), whereas that of the linear static solver (stiffness) is not so varied in comparison.

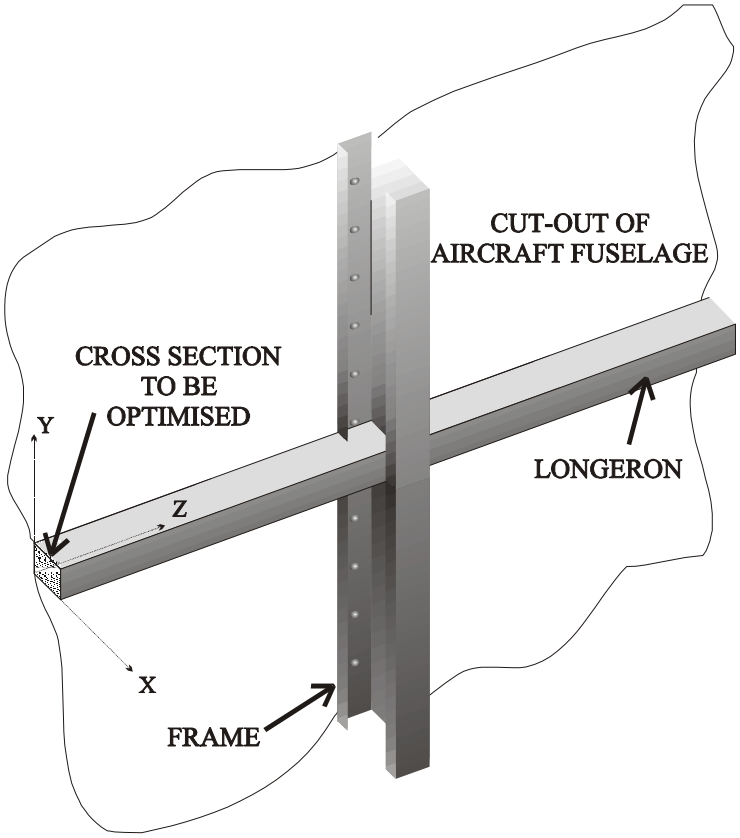

Figure 4.10 Cut-out of aircraft fuselage with longeron containing cross-section of short cantilevered beam.

The topology in Figure 4.13 a) to some might be interpreted as exhibiting checkerboarding effects. But considering that only a small amount of material has been removed, it is not clearly distinguishable. It has not been mentioned that integrated into the ESO program has been a checkerboarding suppression algorithm to eliminate the phenomenon of checkerboarding (Li, 2000). This algorithm has been activated for all the examples run in

this thesis. When integrating the checkerboarding algorithm into the multicriteria ESO process, there was the option to implement the checkerboarding algorithm after each criteria had been compiled (before they combined into one criterion using Equations 2.9 or 2.11), or after they had been combined into one. With the possibility of checkerboarding patterns arising after the criteria had been combined (if the suppression was implemented to each criterion before combining), it was decided to implement it after the criteria had been combined. This also proved a more efficient option in terms of running time ie checkerboard suppression was only run once per iteration rather than for each criterion.

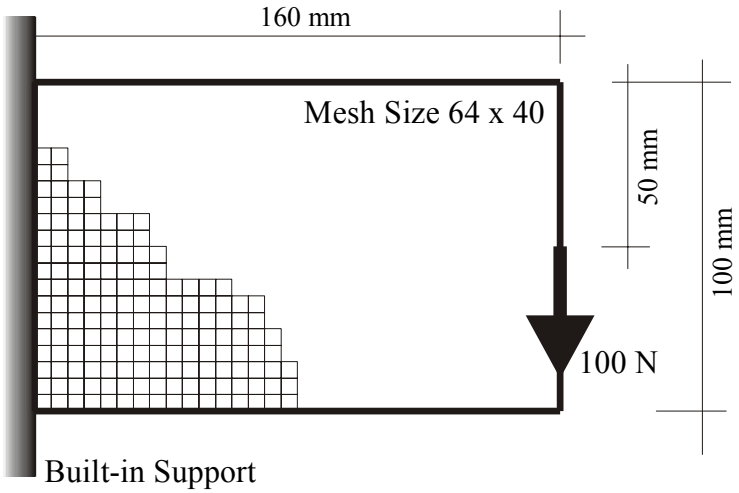

Figure 4.11 Initial design-domain of short cantilevered beam under loading. Mean compliance × volume: 8.76×10^{-9} Nm^4, radius of gyration about *y*-axis: 4.62×10^{2} m.

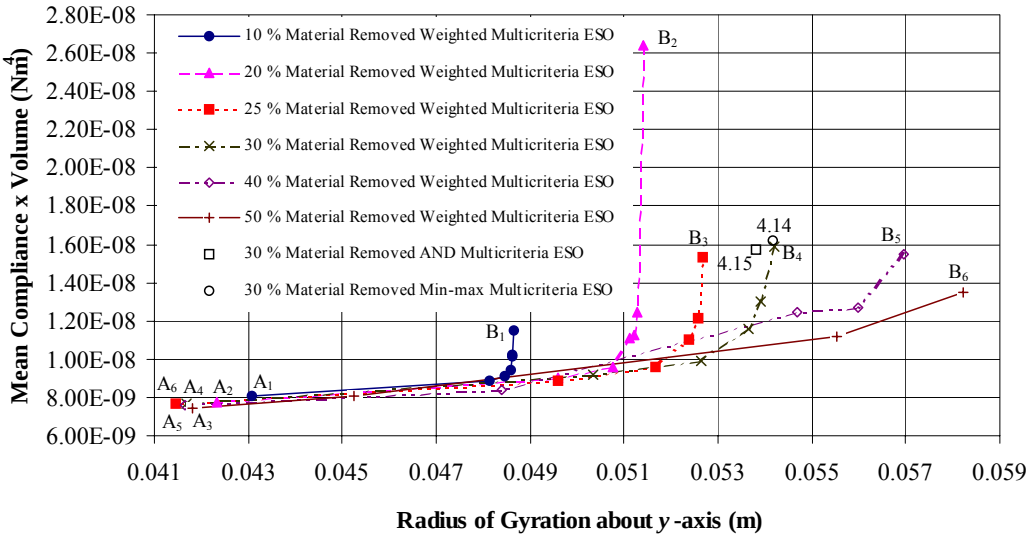

Figure 4.12 Pareto curves for radius of gyration about *y*-axis versus mean compliance × volume, for a variation of material removed.

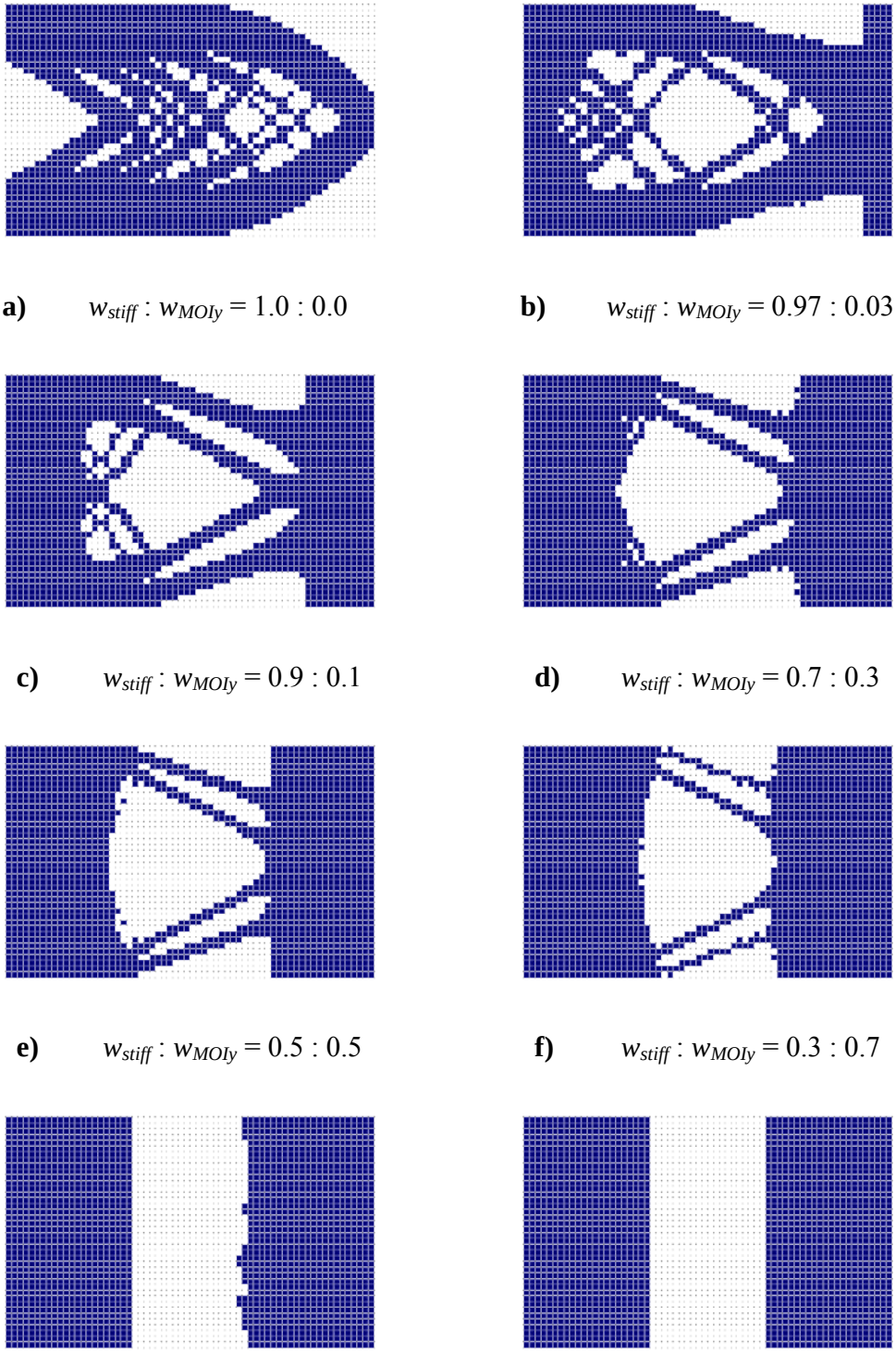

a) $w_{stiff} : w_{MOIy} = 1.0 : 0.0$ **b)** $w_{stiff} : w_{MOIy} = 0.97 : 0.03$

c) $w_{stiff} : w_{MOIy} = 0.9 : 0.1$ **d)** $w_{stiff} : w_{MOIy} = 0.7 : 0.3$

e) $w_{stiff} : w_{MOIy} = 0.5 : 0.5$ **f)** $w_{stiff} : w_{MOIy} = 0.3 : 0.7$

g) $w_{stiff} : w_{MOIy} = 0.1 : 0.9$ **h)** $w_{stiff} : w_{MOIy} = 0.0 : 1.0$

Figure 4.13 Optimum designs of the short rectangular beam, for different weightings of criteria of stiffness and moment of inertia about the *y*-axis. Material removed: 30 %.

It must be noted that for this example, not all the points could be included in the plot of Figure 4.12. This is solely due to the fact that during the optimisation process, part of the structure became detached from its support (see Figures 4.13 g) & h)), and so a mean compliance number was not able to be determined. The Pareto curves therefore do not contain the points resulting from the topologies based completely on moment of inertia about the *y*-axis. As more material is removed, this also becomes true for those topologies weighted mostly with moment of inertia and a small proportion of stiffness. For example, the topology established from the weighting 10 % stiffness and 90 % MOI*y* (Figure 4.13 g)) has become divided, and so no Pareto point can be determined. One may think that such topologies are not practical to use. However, they may indeed represent the cross-section of a lightening hole where other cross-sections are attached – as in Figures 4.13 a) to f). But this moves on from the assumption made in this chapter that the cross-section is uniform along the longeron.

From Figure 4.12, it can also be seen that during the evolution of the sole stiffness based topology (points A_1 to A_6), the specific stiffness initially increases and then decreases. This is indicated by the initial reduction of the $C \times V$ term (A_1 to A_3) followed by its growth (A_4 to A_6). The ESO process therefore displays its nature to better the specific stiffness of the structure (up to the stage where 25 % of the material is removed).

An improvement can be also seen for the radius of gyration about the *y*-axis (points B_1 to B_6). Although not based completely on the moment of inertia (for reasons explained above), there is an increase in the radius of gyration at these points, clearly indicating that the objective of ESO to optimise the structure dominated by a weighting of moment of inertia is satisfied.

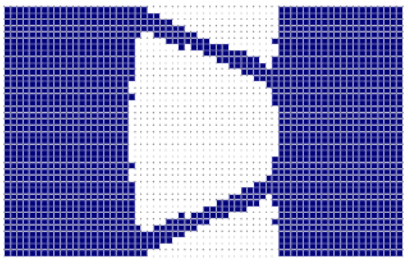

Figure 4.14 Optimal design of the short cantilevered beam for the Global Criterion method of Multicriteria ESO. Material removed: 30 %.

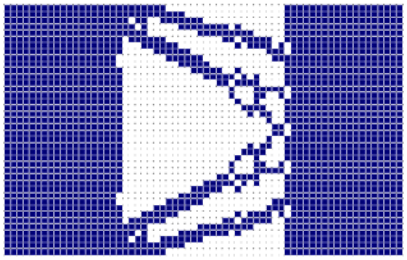

Figure 4.15 Optimum design of the rectangular plate for the logical AND method of Multicriteria ESO. Material removed: 30 %.

Figures 4.14 and 4.15 give the cross-sections that result from the Global Criterion method and the logical AND operator method. They are for 30 % of material removed. The corresponding performance values in terms of $C \times V$ and radius of gyration are noted as points 4.14 and 4.15 in Figure 4.12. The Global Criterion model is similar in shape and yet distinct in topology from any of those produced by the weighting method. The closest resemblance is the topology with the stiffness to MOI*y* weighting of 30:70 (Figure 4.13), which is confirmed by the point 4.14 lying in the vicinity of point B_4 (30 % stiffness, 70 MOI*y*) in Figure 4.12. The logical AND design is also relatively distinct in topology from those presented by the weighting method. Any hint of similarity comes from the 30 % stiffness: 70 % MOI*y* design, as also indicated by the point 4.15 appearing near the point B_4 in the graph of Figure 4.12.

The topology resulting from the OR method has been omitted from this example because it failed to produce a topology during the evolution. More specifically, during the first iteration, a vertical column of elements along the centre of the beam was removed, creating two segments. The next iteration then removed a large proportion of the remaining elements (from both segments). This was because both a load and constraint combination was not attached to each segment and thus the sensitivity numbers for the mean compliance could not be calculated.

4.4.3 A Rail Track Cross-Section

The third and final example seeks to obtain a series of multicriteria solutions of a rail track cross-section. It is derived from the intention to maximise the local specific stiffness across the section in resistance to a typical loading applied from a vehicle wheel, and the intention to simultaneously maximise the track stiffness, that is, to increase the specific MOI about the *x*-axis (MOI*x*).

To maximise the local specific stiffness expresses the intention to prevent the head of the rail from deflecting as little as possible (along the cross-sectional plane shown in Figure 4.16). Such a resistance to deflection mainly concerns those loads applied laterally from the track vehicle. Although lateral loads significantly contribute to a phenomenon known as rail over turning, where the rail actually turns over on its side (if the rail is not restrained properly by rail fasteners) (Zarembski, 1993), they do contribute to the deflection of the rail head. It is this deflection which is one of the objectives to minimise.

The other is to maximise the track stiffness. It is a component that seeks to keep the depression of the track per unit length of rail to a minimum. This high track stiffness is beneficial because it results in a decreased track deflection under wheel loading, which in turn reduces track deterioration (Zarembski, 1993). The maximisation of the specific moment of inertia about the *x*-axis directly addresses the need to maximise this track stiffness. This latter inertia quantity is often referred to as the square of the Radius of Gyration (RoG) i.e. $(\text{MOI}x)/A = (I_x)/A = (\text{RoG}x)^2$.

This rail cross-section is divided into three sections, each of which can be seen in Figure 4.16. To the top section - the rail head (made up of 742 square elements, all of which are declared non-design elements) a load of 120 N is applied at an angle of 65 degrees to the horizontal. Such a load angle (derived from the ratio of the lateral to the vertical force) lies in the critical range for potential instability for rail rotation (Zarembski, 1993). This is of course primarily dependent on the magnitude of this load. The ESO process in seeking an optimum design however is unaffected by the magnitude of a single load case. This case is not true for multiple loading. The shape of the head and its relative position to the base is declared non-design in order to maintain consistency to allow compatibility between this new track design and the vehicles that use the conventional design.

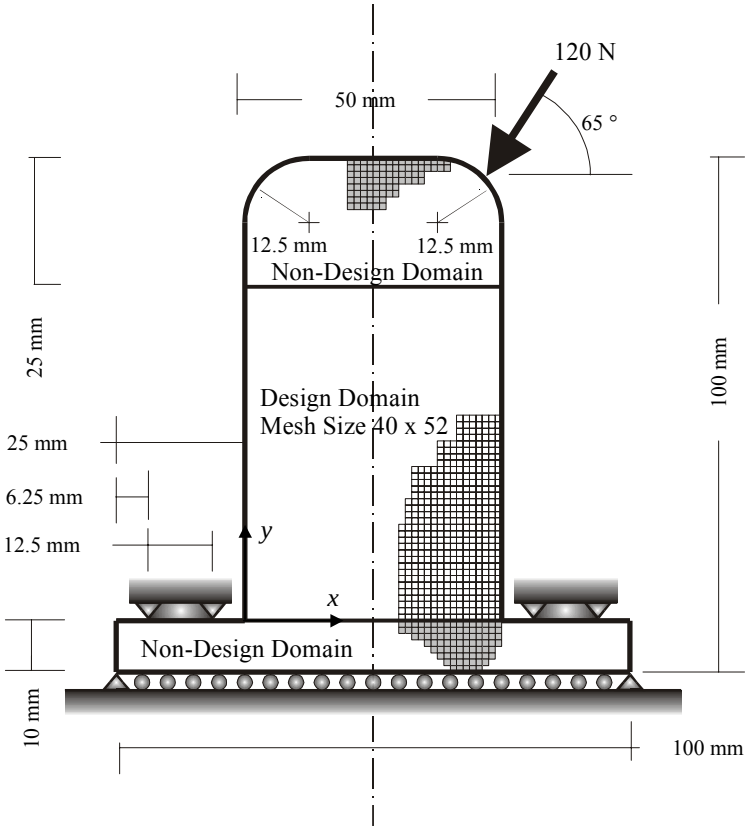

Figure 4.16 Initial design-domain of a railway section under loading. Mean compliance × volume: 1.49×10^{-9} Nm^4, radius of gyration about *x*-axis: 2.99×10^{-2} m.

The bottom section – the base of the cross-section, is modeled with 640 square non-design elements. Here, the support conditions are applied – modelling the tie down of the track. The bottom corners are completely fixed, as are two segments (each 12.5 mm long) on top of the base section. The bottom of the base plate is placed on roller supports. Again, this is defined non-design to maintain compatibility with conventional track tie down methods.

The mid-section of the cross-section is the domain where the optimisation method is applied. It consists of 40 by 52 square elements, all of which are design-domain elements. To this mid-section a nibbling constraint has been applied meaning that the creation of cavities is prevented. Such cavities (if numerous and complex in shape) are difficult to manufacture at a cost effective price. It must be noted that all of the elements used in this example have dimensions 1.25 mm × 1.25 mm. The dimensions of the track cross-section can be seen in Figure 4.16.

Figure 4.17 presents the resulting Pareto curves for the various multicriteria methods applied to the railway track problem. They are for different proportions of material removed, from 10 % through to 50 %. Obvious from a first glance is that the nature of each curve is Pareto. They are also distinctly positioned where, as more material is removed the radius of gyration generally increases and the specific stiffness decreases. There is an approximate even distribution of points along each curve. This is not portrayed so effectively in Figure 4.17 because of the scaling of the ROG*x* axis of the figure. If each Pareto curve was plotted on a separate curve and scaled accordingly, it would become clearer that the Pareto are quite evenly distributed. This even distribution means that taking into account the nibbling constraint, the two criteria distributions amongst the elements are fairly similar.

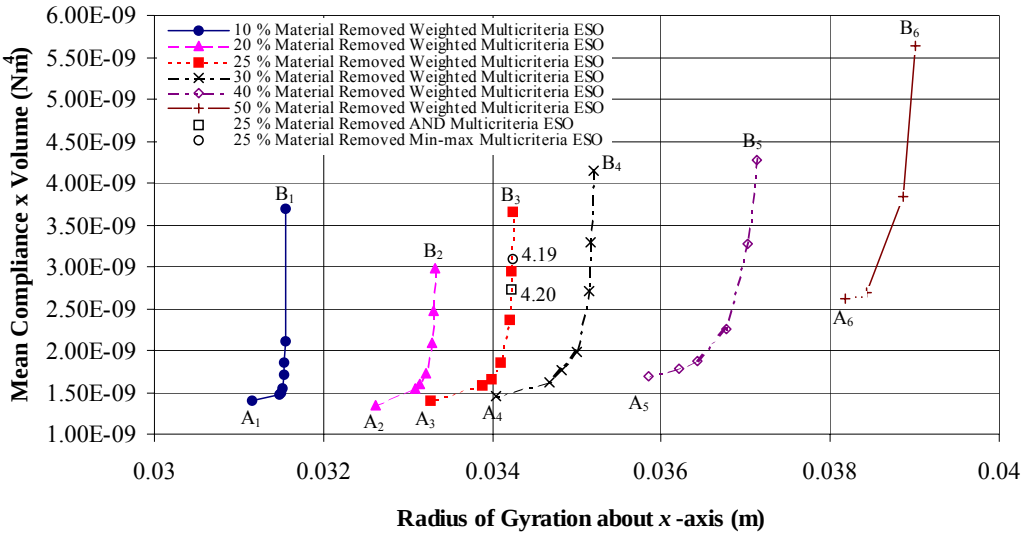

Figure 4.17 Pareto curves for radius of gyration about *x*-axis versus mean compliance × volume, for a variation of material removed.

Concentrating on the lower end points of each curve (points A_1 to A_6, representing the points for the completely stiff topology), it can be observed that the mean compliance multiplied by the volume term initially decreases and then increases. This would appear to indicate that there exists a moment during the evolution where the method fails to recognize any elements that has a maximising effect on the specific local stiffness. No doubt, this occurrence is example dependent and could possibly be caused by the use of the nibbling constraints or the existence of non-design regions. With nibbling, some of the theoretical concepts do not always work. The ESO objective to minimise the $C \times V$ term is achieved for the first proportion of material removed – up to around the 20 % mark (point A_2).

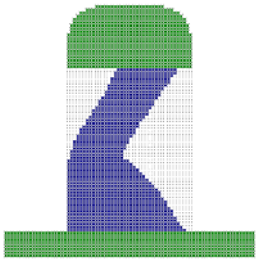

a) $w_{stiff} : w_{MOIx} = 1.0 : 0.0$

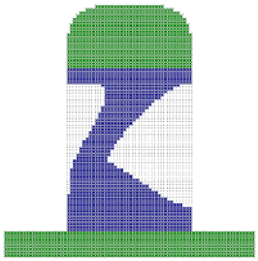

b) $w_{stiff} : w_{MOIx} = 0.97 : 0.03$

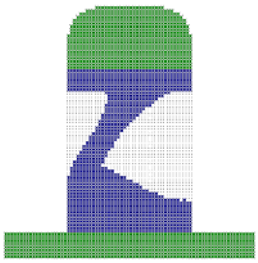

c) $w_{stiff} : w_{MOIx} = 0.95 : 0.05$

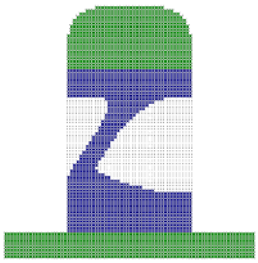

d) $w_{stiff} : w_{MOIx} = 0.9 : 0.1$

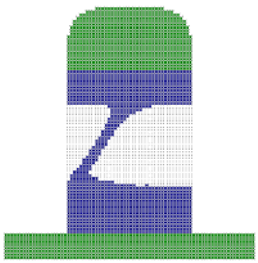

e) $w_{stiff} : w_{MOIx} = 0.7 : 0.3$

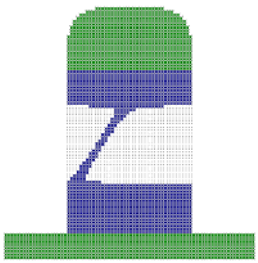

f) $w_{stiff} : w_{MOIx} = 0.5 : 0.5$

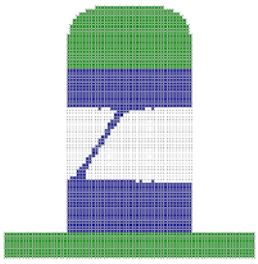

g) $w_{stiff} : w_{MOIx} = 0.3 : 0.7$

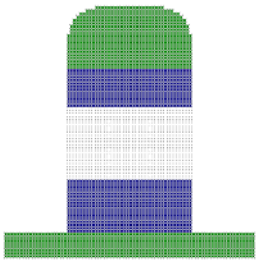

h) $w_{stiff} : w_{MOIx} = 0.0 : 1.0$

Figure 4.18 Optimal designs of the railway track cross-section, for different weighting criteria of stiffness and moment of inertia about the *x*-axis. Material removed: 25 %.

The optimising objective of maximising the radius of gyration about the *x*-axis is highlighted with the terms B_1 to B_6 (where each point has a greater magnitude of RoG*x* than the last). It should be noted that in this example, each point corresponds to the 30 % stiffness / 70 % MOI*x* weighting topology during the evolution process. This excludes points B_5 and B_6, where they respectively represent the points of the 50 % stiffness / 50 % MOI*x*. This is because the mean compliance values cannot be evaluated for the cross-sections with greater proportions of MOI*x* than those presented in points B_1 to B_6. This is evident in Figure 4.18 h) (for the case of 25 % material removed) where the head of the rail has become detached from the rail base – meaning the applied load is detached from its support.

Figures 4.19 and 4.20 a) portray the optimum rail track shapes for 25 % material removed using the global criterion method and the logical AND method. Their relative markers on the Pareto curve are respectively presented as points 4.19 and 4.20 in Figure 4.17. The AND marker lies closest to the 50 % stiffness / 50 % MOI*x* weighting as does the global criterion markers. This is confirmed with the similarity of the shapes of Figures 4.19 and 4.20 to the 50 % stiffness / 50 % MOI*x* weighting shape of Figure 4.18 f). This similarity was identified in Chapter 2, where the global criterion method produced topologies similar to the 50/50 linear weighting. The topology for the logical OR operator is shown in Figure 4.20 b). Seen in this topology is the combined effect of inertia and stiffness optimisation. However, because of the thin portion at the centre of the cross section connecting the head to the base of the rail, a very large $C \times V$ term resulted. This was not inside the defined limits of the graph of Figure 4.17 and so is excluded.

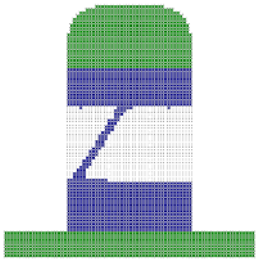

Figure 4.19 Optimum design of the railway track, for the Global Criterion method of Multicriteria ESO of stiffness and moment of inertia about the *x*-axis. Material removed: 25 %.

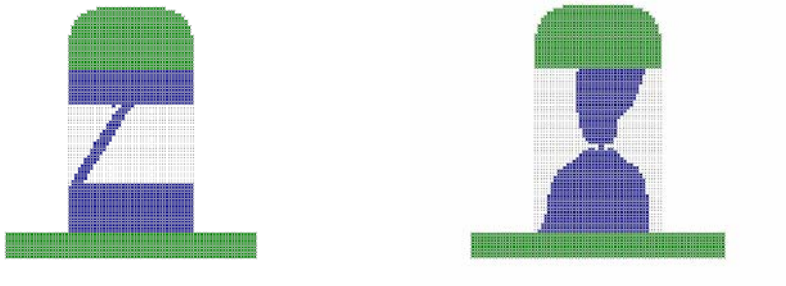

a) Logical AND operator **b)** Logical OR operator

Figure 4.20 Optimum design of the railway track cross-section, for logical AND and OR operation of stiffness and moment of inertia about the *x*-axis. Material removed: 25 %.

This example has addressed the optimisation of two criteria relevant to the betterment of performance of a rail track cross-section. It has also brought attention to the need to include other criteria as well. In relation to safety considerations, one such criteria of direct relevance would be the optimisation of torsional stiffness (Zarembski, 1993) (preventing rail over turning). Other criteria such as frequency (concerning passenger comfort) could also be addressed in the future as analysed by Markine *et al.* (2000).

4.5 Concluding Remarks

This chapter has successfully endeavored to present a range of multicriteria optimisation methods applied to the discrete ESO technique for the linear static and inertia solvers. It has done this in reference to the maximisation of stiffness simultaneously with the maximisation of the specific moment of inertia. This has been achieved using a simple example for the verification of the method's capability, and a combination of practical examples highlighting its usefulness to the designer.

From this chapter, it can be concluded that the ESO weighting method is proficient in presenting the designer with range of options taking into account multicriteria. However, it was found that the relative spread and pattern of the elemental sensitivity number distribution for each criterion influenced the way the weighting points were distributed about the Pareto curves. Suggestions were made to take into account these different elemental sensitivity distributions for each criteria.

It was also verified (as has been done in Chapter 2) that the Global Criterion method has the tendency to produce shapes and topologies that resemble that of the weighted 50 % : 50 % method. Because of the difference in elemental sensitivity number distribution for each criterion, the distance between the global criterion solution and the utopia point is not minimum (as defined in Section 1.4.2.1). Again this can be obtained by applying a weighting scheme that is not necessarily linear or modifying the sensitivity values such that the linear weighting scheme could be applied (see Equations 4.1 and 4.2).

No general analogy can be confirmed with a comparison between the logical AND method to the weighting method. In these presented examples, the AND always formed part of the Pareto curve. This was not the conclusion made in the second chapter for the linear static and frequency criteria examined. Likewise, with respect to the OR operator method, topologies were not produced that were part of the Pareto curve produced by the linear weighting method. Such a conclusion was not made in the second chapter where the OR operator method always formed part of the Pareto optima.

This research has paved the way for the inclusion of other combinations of criteria such as torsional stiffness and specific moment of inertia, and the investigation of the simultaneous optimisation of three or four criteria. The next chapter will present such research embracing the multicriteria optimisation of three criteria – using three different FE solvers.

4.6 References

Adali, S. (1983), "Pareto Optimal Design of Beams Subjected to Support Motions", *Computers and Structures*, Vol. 16, pp. 297-303.

Carmichael, D., G. (1980), "Computation of Pareto Optima in Structural Design", *International Journal for Numerical Methods in Engineering*, Vol. 15, pp. 925-952.

Chu, D., N., Xie, Y., M., Hira, A., Steven, G., P. (1996), "Evolutionary Structural Optimization for Problems with Stiffness Constraints", *Finite Elements in Analysis and Design*, Vol. 21, pp. 239-251.

Das, I., Dennis, J., E. (1997), "A Closer Look at Drawbacks of Minimizing Weighted Sums of Objectives for Pareto Set Generation on Multicriteria Optimization Problems", *Structural Optimization*, Vol. 14, pp. 63-69.

Das, I. (2000), "Applicability of Existing Continuous Methods in Determining the Pareto Set for Nonlinear, Mixed-Integer Multicriteria Optimization Problems", *AIAA/NASA/USAF/ISSMO Symposium on MDO*, Long Beach, California, 6-8th September.

Grandhi, R., V., Bharatram, G., Venkayya, V. (1993), "Multiobjective Optimization of Large-Scale Structures", *AIAA Journal*, Vol. 31, No. 7, July.

Hajela, P., Shih, C., -J. (1990), "Multiobjective Optimum Design in Mixed Integer and Discrete Design Variable Problems", *AIAA Journal*, Vol. 28, No. 4, pp. 670–675.

Koski, J. (1994), "Multicriterion Structural Optimisation", Adeli, H., (Ed.) *Advances in Design Optimisation*, Chapter 6, pp. 194-224, Chapman and Hall, Great Britain.

Li, Q., Steven, G., P., Querin, O., M., Xie, Y., M. (1997), "Optimal Shape Design for Steady Heat Conduction by the Evolutionary Procedure", Dulikravich, G., S., Woodbury, K., A., (Eds.) *Inverse Problems in Heat Transfer and Fluid Flow, ASME Proceedings of the 32nd National Heat Transfer Conference*, ASME HTD, Vol. 340, pp.159-164.

Li, Q., Steven, G., P., Xie, Y., M. (1999), "Evolutionary Shape Optimization A Stress Based Sensitivity Analysis Method", *Proceedings of the Second Australian Congress on Applied Mechanics ACAM '99*, Canberra, 9th-12th February.

Li, Q., Steven, G., P., Querin, O., M. (2000), "Stress Based Optimisation of Torsional Shafts Using an Evolutionary Procedure", submitted to *International Journal of Solids and Structures*, January.

Manickarajah, D., Xie, Y., M., Steven, G., P. (1998), "An Evolutionary Method for Optimization of Plate Buckling Resistance", *Finite Elements in Analysis and Design*, Vol. 29, pp. 205-230.

Markine, V., L., Toropov, V., V., Esveld, C. (2000), "Optimisation of Ballastless Railway Track using Multipoint Approximations: Issue of Domain-Dependant Calculability", *AIAA/NASA/USAF/ISSMO Symposium on MDO*, Long Beach, California, 6-8th September.

Pietrzak, J. (1999), "Pareto Optimum Tests", *Computers and Structures*, Vol. 71, pp. 35-42.

Proos, K., Steven, G., P., Querin, O., M., Xie, Y., M. (1999), "Multicriteria Evolutionary Structural Optimisation", submitted to *Design Optimization - International Journal for Product and Process Improvement*, December.

Proos, K., Steven, G., P., Querin, O., M., Xie, Y., M. (2000), "Multicriteria Evolutionary Structural Optimisation using the Weighting and the Global Criterion Methods", *AIAA/NASA/USAF/ISSMO Symposium on MDO*, Long Beach, California, 6-8th September.

Proos, K., A., Steven, G., P., Querin, O., M., Xie, Y., M. (2001), "Multicriterion Evolutionary Structural Optimisation Using the Weighting and the Global Criterion Methods", *AIAA Journal*, Vol. 39, No. 10, pp. 2006-2012.

Xie, Y., M., Steven, G., P. (1997), *Evolutionary Structural Optimisation*, Springer-Verlag, London.

Zarembski, A., M. (1993), *Tracking Research & Development*, Simmons-Boardman Books, Inc., United States of America, March.

Zhao, C., Steven, G., P., Xie, Y., M. (1996), "Evolutionary Natural Frequency Optimization of Thin Plate Bending Vibration Problems", *Structural and Multidisciplinary Optimization*, Vol. 11, pp. 244-251.

Chapter 5

Stiffness, Frequency and Inertia Multicriteria ESO

5.1 Introduction

The previous chapters have seen the multicriteria ESO methods developed for the linear static/frequency solvers and the linear static/inertia solvers. The question still remains; will the trends found for combining these different solvers differ if more than two criteria are used? That is, does the relationship between the different methods established for bi-criteria optimisation crumble if tri-criteria optimisation is introduced?

This chapter seeks to develop multicriteria based on three types of FE solvers: linear static, natural frequency and inertia. It is not just an another application of multicriteria optimisation, but rather, the development of a platform to accommodate the multicriteria optimisation of these three solver types. Such a platform has never been established.

More specifically, the platform developed in this chapter shall demonstrate the optimisation of structures simultaneously taking into account the objectives to maximise the stiffness, maximise the first mode of natural frequency and to maximise the radius of gyration. It does so using the four multicriteria ESO methods used previously. Referring back to the previous robotic example (Section 4.1), these three criteria are entirely appropriate to be included in the design of many mechanical systems. The need to maintain low inertia (for operational efficiency), high stiffness (for rigidity during operation) would be added to the preference to maximise the frequency of the system (for precision and accuracy of operation) or to avoid stimulating vibration induced by some ambient frequencies. Here, no ‘shake’ would be desired (associated with damping) as would the need to avoid the resonant natural frequencies of the various engines or actuators.

Many publications have dealt with tri-criteria optimisation. However, none have dealt with discrete finite element optimisation methods. For example, Adali (1983) determines the optimal design of a clamped-hinged beam with the objectives to minimise the maximum deflection, minimise the maximum normal and shearing stresses and maximise the fundamental eigenfrequency. The design variable was the area function of the beam, which was approximated by linear splines in order to convert the continuous problem into a finite dimensional one. Rao (1984) used various multicriteria methods (including the global criterion and utility methods) to optimise the specific example of a cantilever beam with a tip mass subjected to a stochastic base excitation. Here the objectives were the minimisation of the structural mass, the maximisation of the natural frequency of vibration and the minimisation of the fatigue damage of the beam.

Tseng and Lu (1990), optimised large-scale structural systems with the objective to minimise the weight of the structure, the maximum member stress and the maximum nodal displacement whilst maximising the fundamental natural frequency. Saravanos and Chamis (1992) sought to simultaneously minimise the natural frequency, minimise the structural weight and minimise the material cost of various composite structures (plate and beam) using the global criterion method. They found that the proposed multiobjective formulation, as opposed to single objective functions, simultaneously improved the objectives.

In 1993, Osyczka and Montusiewicz (1993) used a random search method to produce a set of Pareto optimal solutions using discrete decision variables. They applied this technique to the real life problem of a gear set design that included three objective functions. Ohkubo and Taniwaki (1995) used a two-stage optimisation technique involving both continuous shape and sizing variables and discrete material for truss structures. This was done subject to stress, displacement and fundamental natural frequency constraints. The minimisation of the material volume and the combined displacements and the maximisation of the natural frequency of a specific simple three-bar truss example were dealt with by Turkkila and Koski (1999). They were able to represent the minimal surface of the three criteria optimisation problem as projection figures and contour curves.

The following sections shall outline the approach to simultaneously optimise Finite Element structures incorporating the three developed solvers mentioned above.

5.2 Evolutionary Optimisation Procedure

The determination of the sensitivity numbers for the three criteria in question have been previously formulated in Sections 2.2 and 3.3. The same methods for combining these into a single formulated criterion using the linear weighting and the global criterion methods have also been presented. It was decided that even though three criteria were used, the constant $p = 2$ term associated with the global criterion method was to be maintained. This was to analyse each criterion relative to the others by the root mean square.

Because the multicriteria optimisation involving the three FE solvers is different from that already established (for the different combinations using two FE solvers), it is necessary to outline the steps and the flow chart to implement it. These steps and flow chart follow. The operation time experienced to complete the three different analyses of the structure and to search for elements to be removed per iteration was approximately a fragment longer than the multicriteria method for linear static and natural frequency. However, it was not much longer as the time to solve the inertia properties was very short.

5.2.1 Weighting and Global Criterion Method Multicriteria ESO

The evolutionary procedure for weighted or global criterion Multicriteria optimisation based on ESO for three criteria is a bit more extensive in comparison to two criteria. For the combined optimisation of stiffness, fundamental frequency and moment of inertia, the procedure is given as follows, with the flow chart outlined in Figure 5.1:

Step 1: Discretise the structure using a fine mesh of finite elements;

Step 2: Add load/s to structure;

Step 3: Solve the linear static problem - Equation (2.1);

Step 4: Calculate the linear static sensitivity number α_i using Equation (2.4);

Step 5: Remove load/s from structure;

Step 6: Solve the eigenvalue problem - Equation (2.5);

Step 7: Calculate the natural frequency and the corrected natural frequency sensitivity number α_i using Equations (2.7) and (2.8);

Step 8: Calculate the centroid and MOI of the structure - Equations (3.5) to (3.7);

Step 9: Calculate the MOI sensitivity number - Equations (3.10) to (3.12);

Step 10: Combine the three criteria sensitivity numbers using Equation (2.9 or 2.11) to obtain $F^i_{multicrit}$ or $G^i_{multicrit}$;

Step 11: Remove a number of elements that have the lowest values of $F^i_{multicrit}$ or $G^i_{multicrit}$;

Step 12: Repeat Steps 2 to 11 until an optimum is reached.

The FE solvers were compiled in this order for programming convenience. The inertia solver was inserted into that already developed program platform for the linear static and the natural frequency solver. It really did not matter where it was placed, as it did not require knowledge of the inclusion of the loads and constraints.

5.2.2 Logical AND Multicriteria ESO

The procedure for Multicriteria ESO using the AND logical operator can be identified by modifying Steps 10, 11 and 12 of the linear weighting method:

Step 10: Remove a number of elements that simultaneously satisfy the deletion criteria of the stiffness sensitivity number AND the deletion criteria of the frequency sensitivity number AND the deletion criteria of the inertia sensitivity number;

Step 11: Repeat Steps 2 to 10 until an optimum is reached.

5.2.3 Logical OR Multicriteria ESO

Like wise, the method for accomplishing Multicriteria ESO using the OR logical operator also uses the linear weighting procedure with the following steps modified:

Step 10: Remove a number of elements that satisfy either the deletion criteria of the stiffness sensitivity number OR the deletion criteria of the frequency sensitivity number OR deletion criteria of the inertia sensitivity number;

Step 11: Repeat Steps 2 to 10 until an optimum is reached.

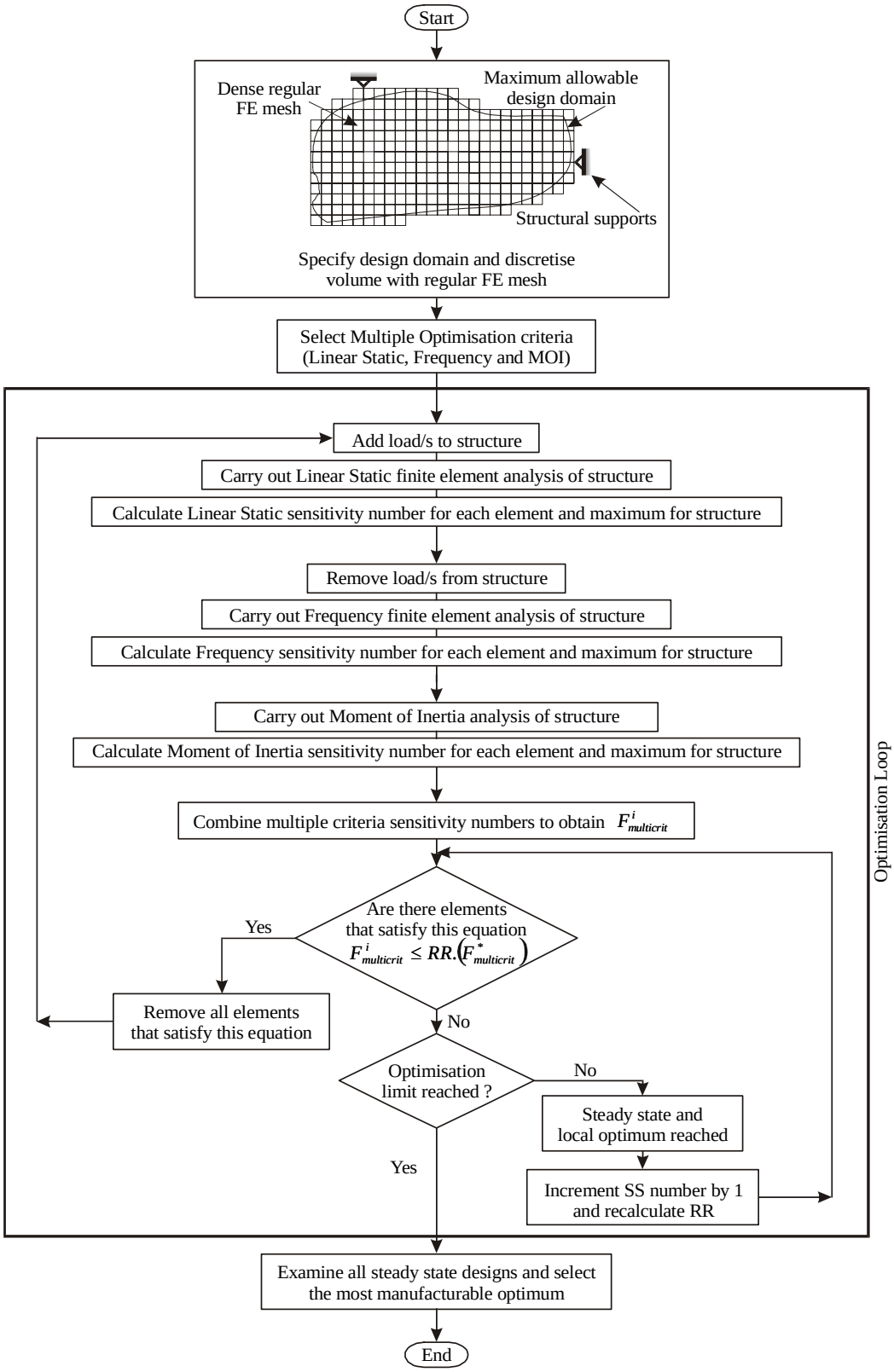

Figure 5.1 Flow chart depicting the logical steps of the Weighting method Multicriteria ESO.

5.3 Examples and Discussion

Two examples are presented in this section - one for the purpose of validating the multicriteria method for the three objective criteria, and the other for illustrating its usefulness in application. Both examples use four noded linear quadrilateral elements, with each being 1 mm thick. They are both two-dimensional plane stress problems where only motion along the 2-D plane is considered. The material used in both examples have the following properties: Young's modulus E = 70 GPa, Poisson's ratio ν = 0.3 and density ρ = 2700 kg/m^3.

5.3.1 A Rectangular Plate with Fixed Supports

The first example is that which has been used in previous chapters. Its purpose is to showing the legitimacy of Multicriteria ESO applied to three criteria. It is of a simple rectangular plate (Figure 5.2) that has its upper right and lower left corner completely fixed. To the other two corners, horizontal loads, each of 100 N are applied, directed away from the plate. The particular objectives of optimisation are the maximisation of stiffness, the maximisation of the first mode of natural frequency and the maximisation of the radius of gyration about the x-axis. Such objectives have previously been applied to this problem, but have been limited to a two criteria combination of these objectives, in Chapters 2 and 4 of this thesis.

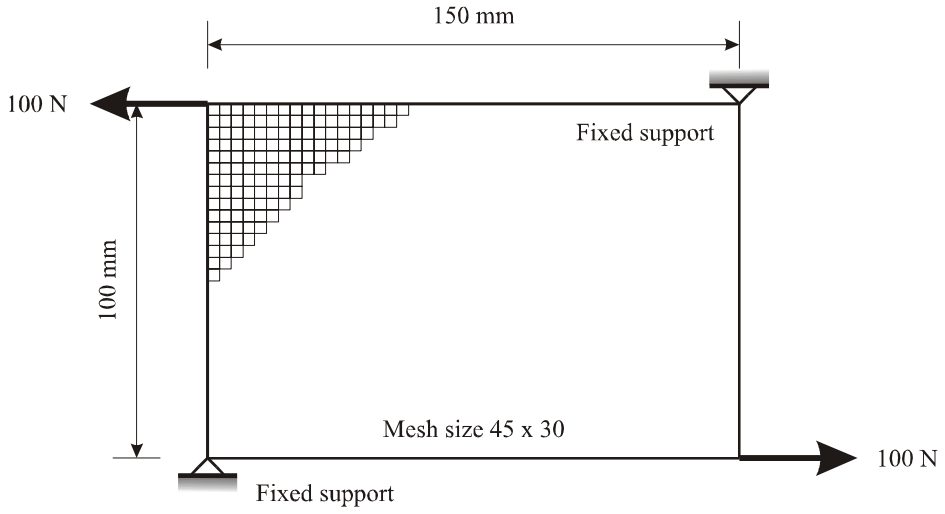

Figure 5.2 Initial design-domain of a rectangular plate under loading with fixed supports. Mean compliance × volume: 2.63 × 10^{-8} Nm^4, frequency: 2498.9 Hz, radius of gyration about x-axis: 0.02885 m.

A difficulty now arises in the attempt to capture how all three criteria vary for different proportions of weight. If all criteria are to be portrayed in a two-dimensional figure, then a three-dimensional Pareto plot or surface would needed to be constructed. An attempt to do this was carried out using various spreadsheets and programs with the result of a finite number of points distributed around a three dimensional plot. The dilemma in this method of display was that there was no simple curve fitting function that would connect the points together (based on the points being closest to each other) to form a smooth surface. The alternative was to display each criterion as affected by the respective proportion of weight allocated to it. This is what follows.

Figures 5.3, 5.4 and 5.5 display the resulting criteria values of the topologies (captured at 25 % of the material removed) for the various multicriteria methods. Figure 5.3 shows how the product of the compliance and volume of the structure varies for the given diversity of weighting assigned to the stiffness criteria. Also included are the specific compliance ($C \times V$) terms for the logical AND and OR method, the Min-max method, as well as a linear curve fit applied to the data of the weighting method.

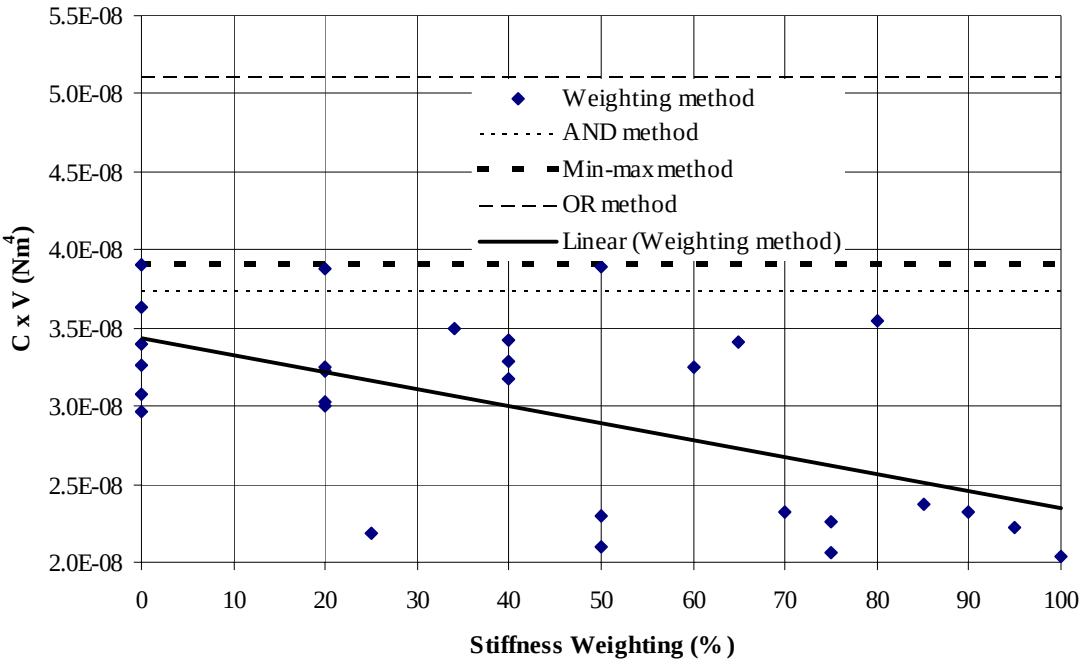

Figure 5.3 Plot of mean compliance × volume versus assigned weighting to stiffness criterion for the four methods. Also displayed is the linear best-fit function to the Weighting method data. Material removed: 25 %.

The trend of the *CV* terms in the Weighting method data as influenced by the stiffness criteria assigned to the removal of elements is generally that of a decrease. This is affirmed by the linear curve fit, and by the observation that the topology based completely on 100 % stiffness has the lowest *CV* term. The general decrease in *CV*, means that the specific stiffness is greater for those topologies that have an increased weighting assigned to stiffness (because of the inverse relation between the *CV* term and the specific stiffness). This shows the optimising nature of Multicriteria ESO for the case of stiffness.

The spread in the weighting data for various stiffness weighting comes as a consequence of using more than two criteria. By holding the stiffness weighting criteria constant, and varying the other two proportions of criteria, the consequent change in topologies affects the *CV* term, as can be seen by this spread. The lack of opportunity to capture each topology at exactly 25 % of the material removed also contributes to the spread of the data. This occurs because of the relatively large rejection rate used to remove elements. Such a drawback could be altered by using a smaller rejection rate in the element removal process, but would be done so at the expense of computational time.

Looking at the other three methods of Multicriteria ESO, they appear to have no significant improvement compared to the Weighting method. Although, the AND method and the Min-max method do have some resemblance to the data produced from the Weighting method with low proportions of stiffness criteria.

Figure 5.4 shows the corresponding fundamental frequency for the given variations of weighting assigned to frequency. It can be observed from the linear trend line of the data points from the Weighting method that the fundamental frequency of the rectangular plate increases for a given increase in the weighting assigned to frequency. It can also be clearly seen that the topology based completely on 100 % natural frequency has the highest frequency for 25 % of the material removed. This trend in data although scattered, again portrays how the Multicriteria ESO process is successful in satisfying its second objective.

A distinct spread occurs amongst the Weighting method data points, which can again be attributed to the presence of the other two criteria and the slight variation in the volume of each analysed model.

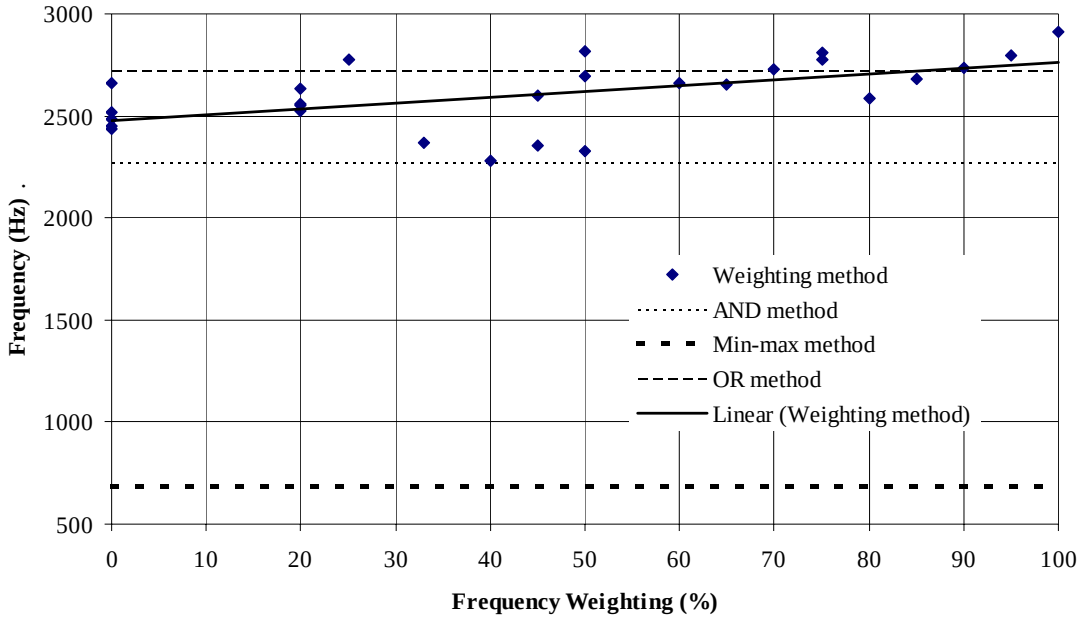

Figure 5.4 Plot of first mode natural frequency versus assigned weighting to frequency criterion for the four methods. Also displayed is the linear best-fit function to the Weighting method data. Material removed: 25 %.

The other three methods again seem to have no relation to the Weighting method. However, the AND and the OR methods do have comparable frequencies when contrasted with those of the Weighting method. The Min-max method appears to fall short considerably in terms of natural frequency.

The radius of gyration about the *x*-axis for a variation in the weighting assigned to the MOI criteria can be seen in Figure 5.5. There appears to be a distinct tendency of the Weighting method data to converge together as the MOI weighting is increased. This is also coupled with the effect of an increasing radius of gyration as indicated by the linear trend plot. Note that the RoG about the *x*-axis for different weighting converges rapidly towards maximum, even at small MOI weighting. This suggests that the MOI criterion is influential in the multicriteria optimisation process. This is because as discussed in Chapter 4, the distribution of the inertia criteria amongst the elements is greatly different from that of the stiffness and frequency criteria. And so, the resulting combined criterion takes on a form similar to that of the inertia distribution at every iteration. To create a more 'equalising' effect on the criteria, the sensitivity numbers would need to be modified or a more sophisticated algorithm would need to be applied to the weighting allocations (see Equations (4.1) and (4.2)).

The multicriteria method is successful in also satisfying the third objective to maximise the radius of gyration. Merged with the other criteria, it becomes obvious that the complete Multicriteria ESO process fulfils all objectives. This is clear having observed the patches of points produced for each criteria in the Multicriteria ESO process. Any inclination of producing a 3-D Pareto surface would require a significant amount of solutions to be created. The larger the amount of solutions, the more distinct the Pareto surface would emerge. It would also require the development of a function to create a surface from these finite points.

The three alternative Multicriteria ESO methods are also displayed in terms of their RoG about the *x*-axis. The AND method and the Min-max method compare considerably well with the Weighting method data. In fact, both methods have the equivalent RoG about the *x*-axis to that of the structure based completely on 100 % MOI about the *x*-axis. This may not be said of the logical OR method, which has a distinctly lower RoG. It still remains inside the limits of the RoG defined by the topologies produced for the 0 % MOI weighting (see the five points on the left hand of Figure 5.5).

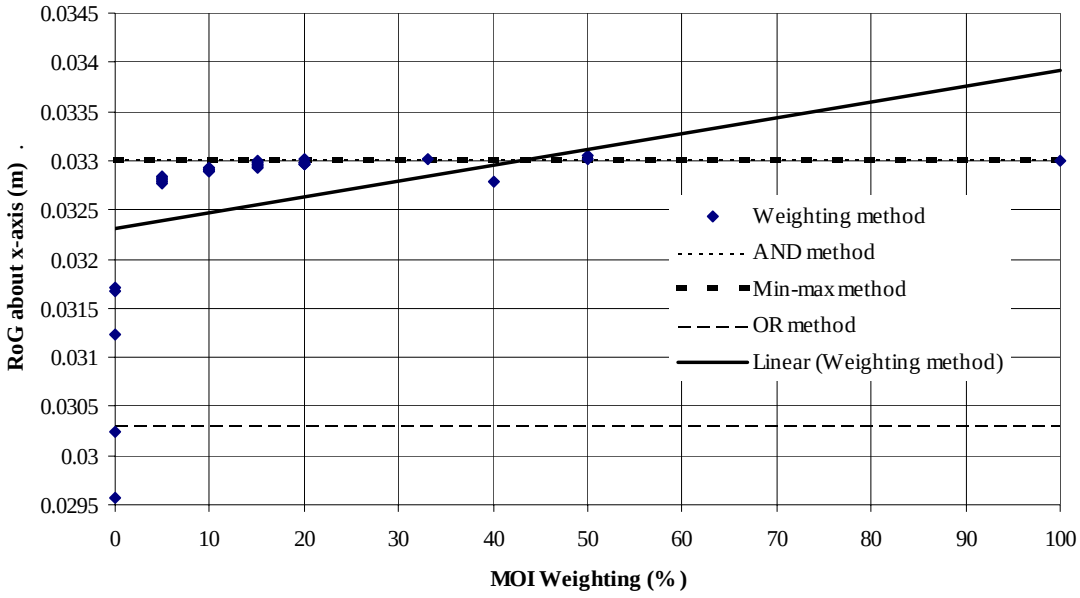

Figure 5.5 Plot of radius of gyration about the *x*-axis versus assigned weighting to MOI criterion for the four methods. Also displayed is the linear best-fit function to the Weighting method data. Material removed: 25 %.

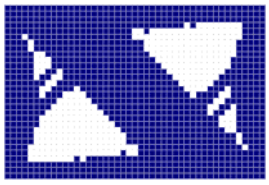

a) 1.0 : 0.0 : 0.0

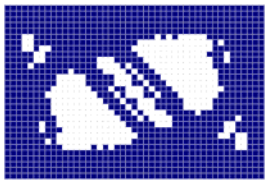

b) 0.5 : 0.5 : 0.0

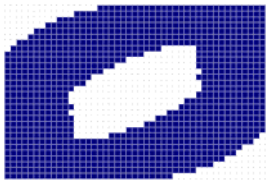

c) 0.0 : 1.0 : 0.0

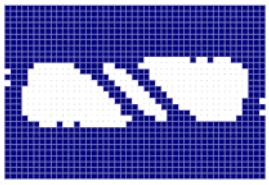

d) 0.95 : 0.0 : 0.05

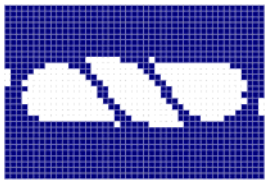

e) 0.5 : 0.45 : 0.05

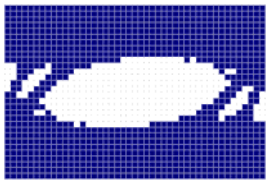

f) 0.0 : 0.95 : 0.05

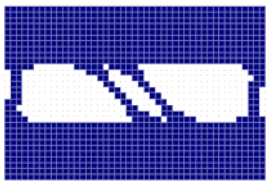

g) 0.9 : 0.0 : 0.1

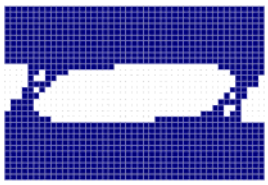

h) 0.4 : 0.5 : 0.1

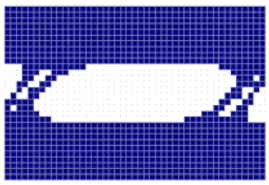

i) 0.0 : 0.9 : 0.1

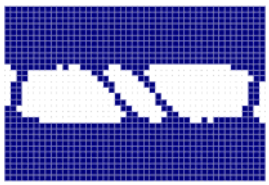

j) 0.85 : 0.0 : 0.15

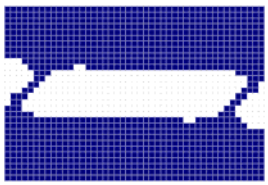

k) 0.4 : 0.45 : 0.15

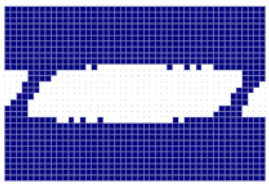

l) 0.0 : 0.85 : 0.15

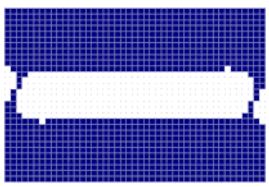

m) 0.8 : 0.0 : 0.2

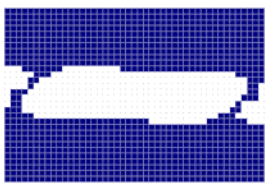

n) 0.4 : 0.4 : 0.2

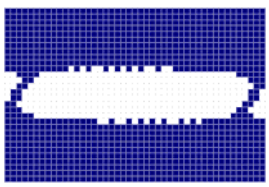

o) 0.0 : 0.8 : 0.2

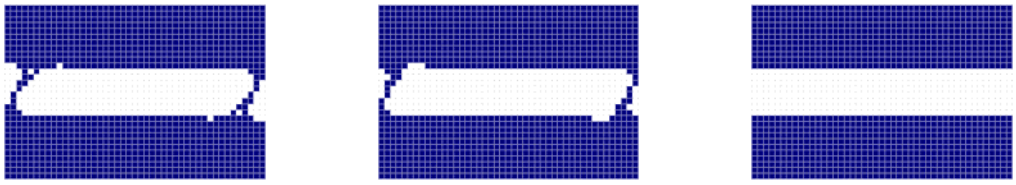

p) 0.34 : 0.33 : 0.33 **q)** 0.0 : 0.5 : 0.5 **r)** 0.0 : 0.0 : 1.0

Figure 5.6 Optimal designs of the rectangular plate for different weighting criteria, in order of stiffness, natural frequency and moment of inertia about the *x*-axis. Material removed: 25 %.

A sample of the topologies produced from the different methods is displayed in Figures 5.6 and 5.7. Figure 5.6 shows those for the Weighting method and Figure 5.7 for the Global Criterion method, the logical AND operator method and the logical OR operator method. They are all for 25 % of the material removed. The gradual transformation in the topologies and shapes of the Weighting method designs can be seen as affected by the different proportions of criteria used. It must be reiterated how dominant the designs are affected by the MOI weighting. That is, there is little change in the shape and topology of the designs that are based on 20 % MOI (Figure 5.6 m)), and that based on 50 % MOI (Figure 5.6 q)) or even 100 % MOI (Figure 5.6 r)).

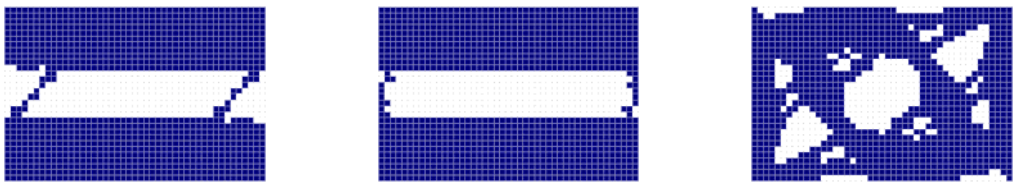

a) Min-max **b)** AND **c)** OR

Figure 5.7 Optimal designs of the rectangular plate for the Min-max method, the logical AND method, and the logical OR operator method of Multicriteria ESO. Material removed: 25 %.

The Min-max method and the logical AND method also appear closely linked to the Weighting method designated with a large portion of MOI. This claim is confirmed by the relatively consistent RoG for the latter portion of MOI weighting in Figure 5.5. In fact, by

keeping in mind that global criterion means implied weighting, it becomes obvious from this example that this is true. The min-max topology of Figure 5.7 a) closely resembles the equal weighting one of Figure 5.6 p). Additionally, the equal weighting point of Figure 5.5 dissects the min-max line for the inertia criterion. The topology for the logical OR operator method is radical in that it bears no comparison in shape or topology compared to any of the other topologies produced by the other methods. This is verified by the graphs of Figures 5.3, 5.4 and 5.5 where the magnitude of the OR method in terms of the three criteria is quite distinct from the other methods.

5.3.2 A Circular Plate

The second example is one that is used to highlight the proficiency of the Multicriteria ESO method within a practical setting. It is of a wheel that has the objective to be as stiff or rigid as possible when experiencing a torque load, the objective to have a fundamental frequency as high as possible and to have a rotational moment of inertia as high as possible.

For the case of stiffness, this objective is apparent where the desire is to have as little deflection from the original shape as possible under loading. The maximisation of the fundamental frequency is characterized by the wish to increase it so as to avoid its resonance at low frequencies. Such a phenomenon may result in undesired deflections and may ultimately lead to catastrophic fatigue type failure, depending on the interaction of these deflections and the applied loads. To have the rotational moment of inertia maximised is to increase the propensity of the object to continue rotating whilst and after the torque is applied. Such an objective is useful in many different fields such as the rotation of turbines – particularly in marine and aeronautical applications, and the rotation of spindles or flywheels – in the areas of tooling or the manufacture of fabrics etc.

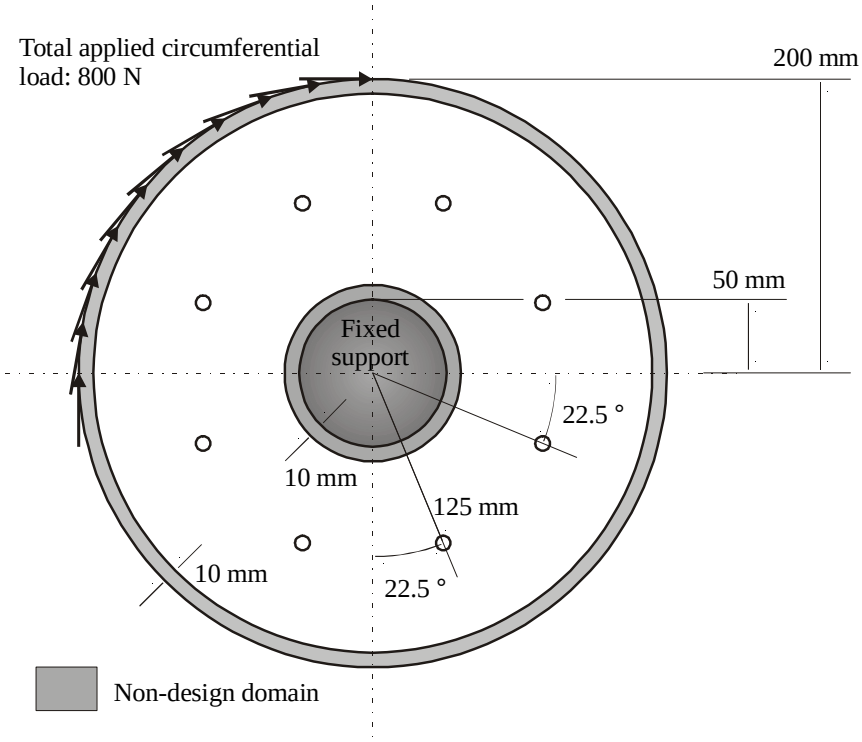

Figure 5.8 Initial design domain of circular plate with circular fixed support. Load applied tangentially at each node on the outer circumference of plate. Mean compliance × volume: 1.55×10^{-6} Nm^4, frequency: 382.41 Hz, radius of gyration about *z*-axis: 0.1458 m.

The wheel in this example (Figure 5.8) is simulated by having the centre completely fixed and the outer nodes each having point loads of magnitude 5 N applied tangentially all the way around the outer circumference. The result is a total applied load of 800 N. The outer diameter of the wheel is 400 mm and the inner is 100 mm. The initial design domain consists of 2384 elements. Of this, 320 are defined as non-design domain. This takes the form of two concentric rings of elements – one on the outer circumference, and one on the inner. Eight initial cavities equally spaced are positioned 125 mm from the centre of the wheel. The use of symmetry in modelling is prevented from being used because of the need for the moment of inertia analysis to include the geography, relative size and shape of each element present. A nibbling constraint is applied to the design process.

Applying the four multicriteria methods of ESO to this design, the resulting measures of the three criteria in question are displayed in Figures 5.9, 5.10 and 5.11. They are for the evolution history captured when 20 % of the material is removed. Figure 5.9 shows how the *CV* product varies for the different portions of weighting assigned to stiffness. The linear

trend line applied to the Weighting method data indicates that as more weighting is assigned to stiffness, the *CV* product decreases. This highlights an increase in the specific stiffness (*K/V*) for those shapes with a higher allocated portion of stiffness. This is inherent in the Multicriteria ESO technique. The shape based on 100 % stiffness is also optimal in terms of stiffness as indicated by the point on the right hand side of Figure 5.9.

As experienced in the first example, the Weighting method data has a considerable spread that converges as a greater amount of bias is allocated towards stiffness. This occurs because for any given percentage of stiffness weighting, the weighting of the other two criteria are adjusted. An irregularity occurs in this spread as well, which can be attributed to the use of more than two criteria in the design process and having the mismatch of volumes for the comparison of different designs. The use of a smaller deletion rate, a finer mesh and a more comprehensive amount of designs produced would alleviate this irregularity.

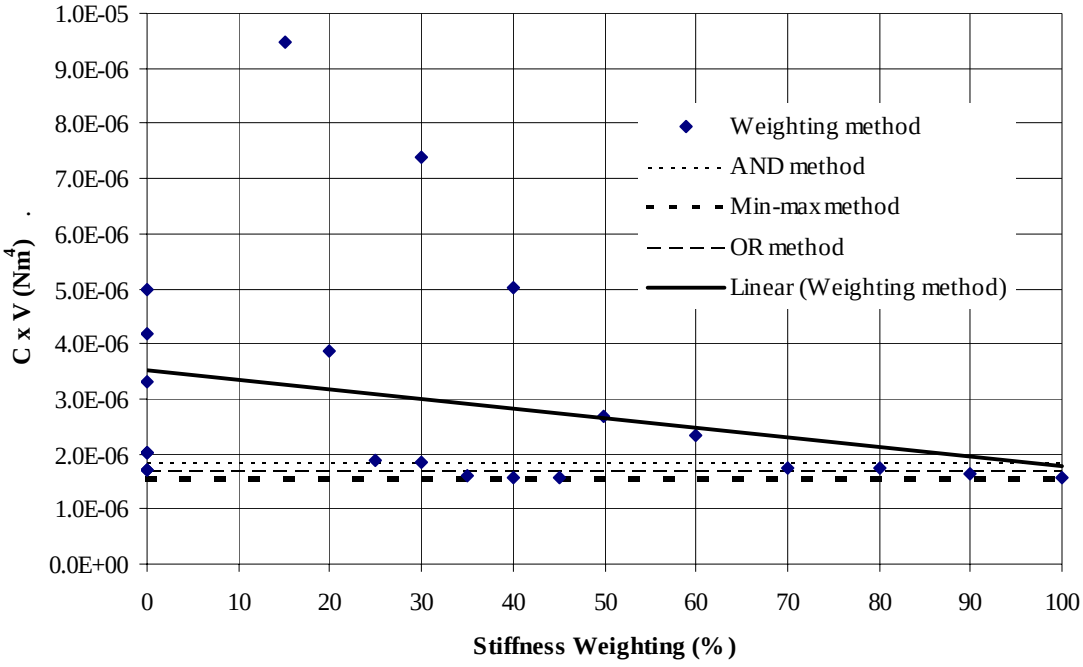

Figure 5.9 Plot of mean compliance × volume versus assigned weighting to stiffness criterion for the four methods. Also displayed is the linear best-fit function to the Weighting method data. Material removed: 20 %.

The other three methods compare extremely well with the Weighting method in terms of the *CV* product. They all have *CV* values that are comparatively similar to that of the 100 % stiffness design.

Figure 5.10 portrays how the first mode of natural frequency varies for the weighting assigned to the frequency criteria. Although not so clear from the data points, the linear trend line clearly indicates a rise in natural frequency as more weighting is assigned towards it. Again this is an intrinsic aspect of Multicriteria ESO.

It is interesting to note that the 100 % frequency design (which alternatively contains no weighting of stiffness and inertia) has a fundamental frequency which is lower compared to those in its vicinity ie for designs based on frequency weighting of 70, 80 and 90 %. This may be caused by the frequency component of ESO becoming unstable from a point onwards where the method is unable to remove further elements so as to have an effect where the frequency is increased (the limiting case is to have no elements with zero frequency). This dilemma too may be exaggerated by the nibbling restriction on the model, or upon the mismatch of volume compared to the other volumes.

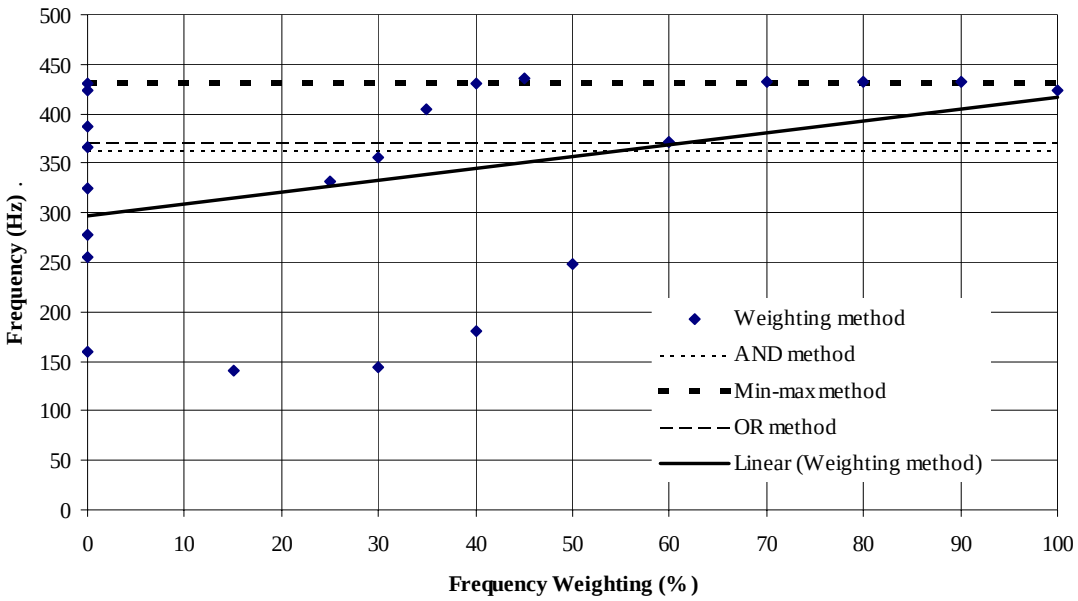

Figure 5.10 Plot of first mode natural frequency versus assigned weighting to frequency criterion for the four methods. Also displayed is the linear best-fit function to the Weighting method data. Material removed: 20 %.

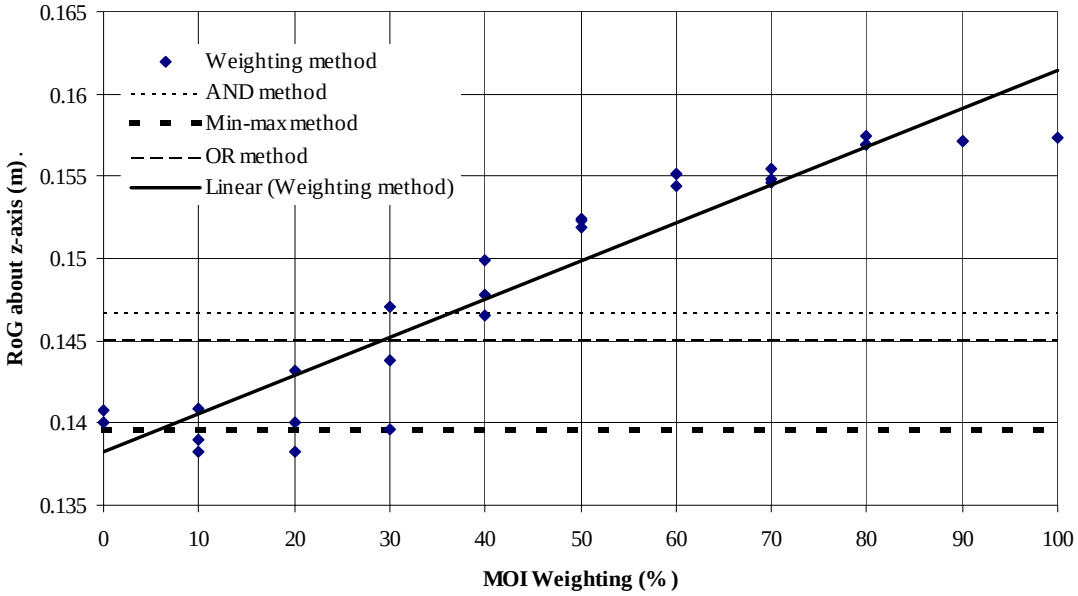

Figure 5.11 Plot of radius of gyration about the *z*-axis versus assigned weighting to MOI criterion for the four methods. Also displayed is the linear best-fit function to the Weighting method data. Material removed: 20 %.

The Global Criterion method, together with the logical AND and OR operator method produce frequencies that are considerably high when compared to the Weighting method. Of significance is the Global Criterion method, which produces a frequency that is similar to the highest of that created by the Weighting method.

The radius of gyration about the *z*-axis is displayed in Figure 5.11 for the four multicriteria methods. The Weighting method with its variation in weight allocated to the moment of inertia about the *z*-axis is also given. In this, a distinguishable trend is observed, where the radius of gyration about the *z*-axis increases at a decreasing rate, for a given increase in weighting of MOI in the process. This upward trend is confirmed by the increase in the radius of gyration for the linear best-fit function. As expected, the greatest radius of gyration occurs for the arrangement based on 100 % MOI.

Once again, the Multicriteria ESO technique has achieved its third particular objective of maximising the RoG. This corroborates the conclusion of the previous example whereby all three criteria were complied with in terms of there being topologies that would indeed increase simultaneously the required physical characteristics. It is evident that again a patch

of optimum solutions has been produced. Any digression from a recognisable trend is caused by the mismatch in the volume of each analysed model, the presence of the nibbling constraint and the finite amount of models with different weighting analysed (in contrast to an infinite amount).

Of particular interest in this example in contrast to the previous one, is the rate at which the radius of gyration increases. The convergence towards the maximum is not so sudden, meaning that only the shapes created from a large portion of MOI criteria have a radius of gyration in the vicinity of the maximum. This is so for 80 and 90 % MOI weighting. This also establishes that the influence of the MOI criterion is not so strong or dominant for this example. For each iteration, the distribution of MOI element sensitivity numbers would be not that different to those of the other two criteria. And so it can be seen (from this case particularly) that the use of a linear weighting scheme is sometimes appropriate, and that modifications to the weighting scheme or sensitivity numbers are not always necessary. There exists in the Weighting method data a slight deviation in the points from that of a orderly trend. Generally too there is a convergence of points, but any digression from this trend, as well the slight deviation may be caused by the factors mentioned above and in the previous example.

The radius of gyration for the alternate three methods does not appear to be associated with the maximum produced by the 100 % MOI design. The methods do, however, exist in the range of data put together by the Weighting method – especially for the lower quotas of weighting. One significant point may be made for this example in relation to the alternate three methods. Each method produced *CV* products, fundamental frequencies and RoG's that were relatively equivalent in magnitude to each other and to the Weighting method. This was not the case for the first example, where the results were quite diverse.

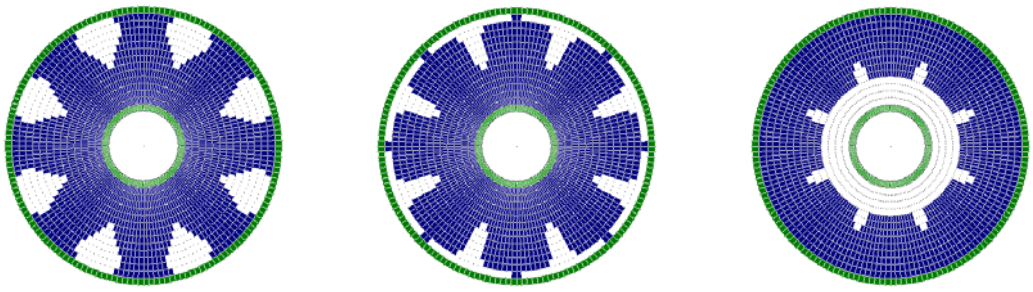

a) 1.0 : 0.0 : 0.0 **b)** 0.0 : 1.0 : 0.0 **c)** 0.0 : 0.0 : 1.0

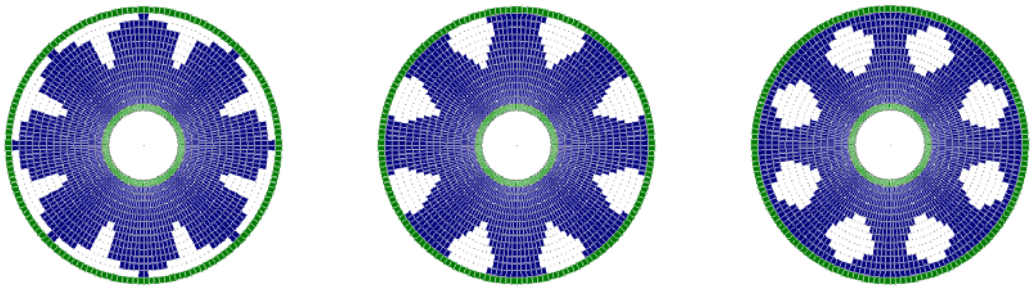

d) 0.0 : 0.8 : 0.2 **e)** 0.4 : 0.4 : 0.2 **f)** 0.8 : 0.0 : 0.2

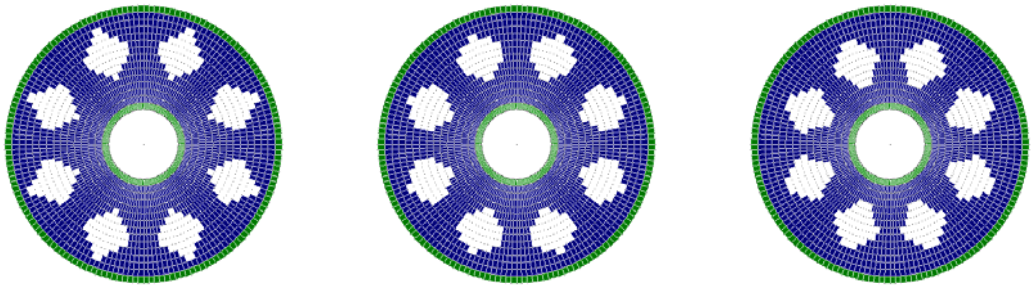

g) 0.0 : 0.6 : 0.4 **h)** 0.3 : 0.3 : 0.4 **i)** 0.6 : 0.0 : 0.4

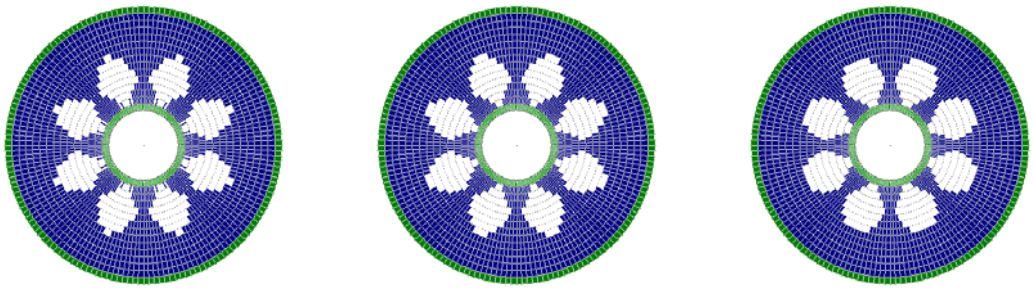

j) 0.0 : 0.4 : 0.6 **k)** 0.2 : 0.2 : 0.6 **l)** 0.4 : 0.0 : 0.6

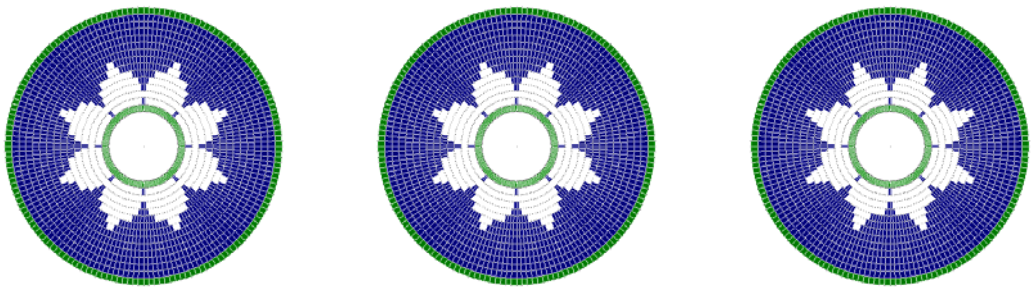

m) 0.0 : 0.2 : 0.8 **n)** 0.1 : 0.1 : 0.8 **o)** 0.2 : 0.0 : 0.8

Figure 5.12 Optimal designs of the circular plate for different weighting criteria, in order of stiffness, natural frequency and moment of inertia about the *z*-axis. Material removed: 20 %.

Figure 5.12 displays a sample of the various shapes produced from the Weighting method, that correspond directly to the results of the previous three graphs. As the weighting of the moment of inertia about the *z*-axis is increased, more material is distributed as far away as possible from its centre. This can be seen by the drift of the cavity towards the centre as the weighting are appropriately altered. The significant variations in each design for a given alteration in the allocated weights shows that each criterion is influential in the multicriteria process and that the linear weighting scheme is appropriate for this example.

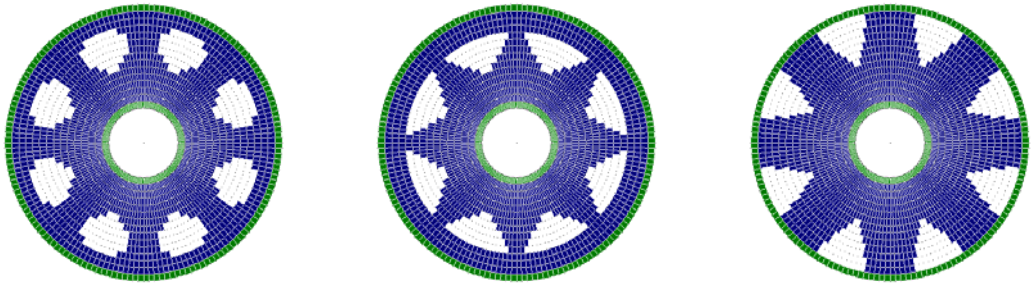

a) Min-max **b)** AND **c)** OR

Figure 5.13 Optimal designs of the circular plate for the Min-max method, the logical AND method, and the logical OR operator method of Multicriteria ESO. Material removed: 20 %.

Note that the topology based entirely on the moment of inertia (Figure 5.12 c)) shows a detachment of the rim to the axle. This is impractical in terms of application, and possesses no certain quantities of mean compliance and frequency. This detachment also exists for those topologies which have a MOI weighting greater than or equal to 80 % (see Figures 5.12 m) to 5.12 o)).

Figure 5.13 shows the various topologies produced by the Min-max, the logical AND operator and the logical OR operator method caught at 20 % of the material removed. Each is unique in its shape, and is not unlike many of the industrial designs that exist today. This may also be said for the majority of the shapes produced by the Weighting method. The topology of the min-max method (Figure 5.13 a)) when aligned with the approximate equivalent allocation of criteria for the weighting method (Figure 5.12 h)) can be seen to resemble it. Here, there is equal weighting, which as has been iterated for other FEA solver combinations, is also true for three criteria optimisation.

5.4 Concluding Remarks

It may be concluded from this chapter that the Weighting method, the Global Criterion method, the logical AND operator method and the logical OR operator method used in the Multicriteria ESO technique are successful in producing optimum solutions for the three criteria in question. However, this is not always the case for the logical OR operator method. It only sometimes produces solutions equivalent to the weighting method. The Weighting method does well to produce a patch or series of points, each point distinctly optimum in its own right. Each criterion is bettered as the weighting assigned to that criterion is increased. The linear allocation of priority was seen appropriate for one example but not the other.

It was found that generally the global criterion and the AND multicriteria methods produced solutions that coincided with that of the Weighting method. No distinct relationship between them was recognised, except for the global criterion method. It corresponded with the equal allocation of criteria in the linear weighting method.

Any deviation from the above observations were attributed to a number of factors. These were the use of a coarse mesh in comparison to a fine mesh, the use of a relatively large rejection ratio in comparison to a smaller one, the use of a small number of models analysed in comparison to a large amount (restricted by computational time) and the use of the nibbling constraint.

Although all the objectives in this chapter were to maximise all three criteria, there is present in the algorithm the option to also minimise these criteria. Such could have been done to minimise the fundamental frequency or alternately, minimise the radius of gyration (for the case of high acceleration and de-acceleration of wheels). Any assortment of minimisation and maximisation would be feasible. This chapter also paves the way for the multicriteria optimisation of alternative combinations of three criteria or the incorporation of four or more criteria. Those criteria that could be included in this combination are those which have been employed in the single criterion optimisation of ESO. The same multicriteria principles used in this research could also be extended to other developments used in ESO such as multiple load case analyses (Xie and Steven, 1994), analyses using brick, 3-D shell and axis-symmetric elements as well as bi-directional ESO (Young *et al.*, 1999).

The need for the development of a more effective technique to display all three criteria in one plot has been indicated. This includes an algorithm to surface fit a set of finite points in the three dimensional realm.

5.5 References

Adali, S. (1983), "Pareto Optimal Design of Beams Subjected to Support Motions", *Computers and Structures*, Vol. 16, pp. 297-303.

Ohkubo, S., Taniwaki, K., "Total Optimal Synthesis Method for Truss Structures Subject to Static and Frequency Constraints", *Microcomputers in Civil Engineering*, Vol. 10, pp. 39-50.

Osyczka, A., Montusiewicz, J. (1993), "A Random-Search Approach to Multicriterion Discrete Optimization", Gutkowski, W., Bauer, J. (Eds.) *Discrete Structural Optimization, IUTAM Symposium Zakapane*, Poland, 31st August – 3rd September.

Rao, S. (1984), "Multiobjective Optimization in Structural Design with Uncertain Parameters and Stochastic Processes", *AIAA Journal*, Vol. 22, pp. 1670-1678.

Saravanos, D., Chamis, C. (1992), "Multiobjective Shape and Material Optimization of Composite Structures Including Damping", *AIAA Journal*, Vol. 30, pp. 805-813.

Turkkila, T., Koski, J. (1999), "Graphical Representation of Minimal Points in Three Criterion Optimization Problems", *Short Paper Proceedings of the 3rd World Congress of Structural and Multidisciplinary Optimization*, Buffalo New York, 17th – 21st May, pp. 419-421.

Tseng, C., H., Lu, T., W. (1990), "Minimax Multiobjective Optimisation in Structural Design", *International Journal for Numerical Methods in Engineering*, Vol. 30, pp. 1213-1228.

Xie, Y., M., Steven, G., P. (1994), "Optimal Design of Multiple Load Case Structures using an Evolutionary Procedure", *Engineering Computations – International Journal for Computer-Aided Engineering and Software*, Vol. 11, pp. 295-302.

Young, V., Querin, O., M., Steve, G., P., Xie, Y., M. (1999), "3D and Multiple Load Case Bi-Directional Evolutionary Structural Optimization (BESO)", *Structural and Multidisciplinary Optimization*, Vol. 18, pp. 183-192.

Chapter 6

Constant Width Layer ESO

6.1 Introduction

Structural optimisation development is at the stage where the focus is no longer on the optimisation method itself, but rather, on the features of the method that enables it to model real structures. Most structures, (if not all) in reality are not isotropic as assumed by many structural optimisation methods. In fact, many structures (especially biological ones) are composed of different materials or the same material with continually varying properties. The trunks of trees, biological teeth, bone structure, ceramics and cast iron metals are a few examples.

The most basic form of structural optimisation incorporating varying material properties is Homogenisation (Bendsøe, 1988, Bendsøe and Kikuchi, 1992). Although the material itself is isotropic, a material property of density is chosen as the design variable. Each element is allocated a micro-void where its geometry and size are varied, in effect controlling the element density. Thus the optimised design can be described by a domain of elements, each with a density of material that can take on all of the values between zero and one, and for which intermediate values make physical sense.

Jog *et al.* (1993) and Olhoff *et al.* (1993) have developed this further by constructing as their material variable an element composed of a rank-2 layering. First, a rank-1 composite is constructed of alternating layers of a stiffer and the more flexible materials. The rank-2 composite is then constructed of alternating layers of the stiff material and the rank-1 composite. The rank-1 one layering direction is perpendicular to the rank-2 direction. Again

although the composite consists of a stiffer and a more flexible isotropic material, the effect is an optimised design made of a varying material structure.

A slight variation to this comes in the form of having the material elastic modulus as the design variable. This is an option that is incorporated in Morphing Evolutionary Structural Optimisation (Querin, 1997). In this, a set of elastic modulus is predefined to which each element can vary amongst. An initial design domain of elements is defined and is analysed in order to examine their appropriateness to be altered. If found appropriate, the element's discrete value (that is allowed to morph) is exchanged to the next discrete elastic modulus in the set. Rispler (1998) also modified the ESO method to shape optimise metallic inserts in a composite material. In the original ESO method, unstressed material of a loaded structure is discarded in an incremental stepwise fashion. The modified approach by Rispler consists of changing the finite element's property (from composite to metal) of highly stressed elements around a loaded hole in a stepwise fashion, allowing the formation of an insert. The creation of this secondary material zone reduces the stress concentration on the composite material, providing stress relief.

The work developed in this chapter also uses two materials in the ESO shape optimisation process. It has arisen out of the need to maintain a layer of constant width material (of a property distinct to the remainder of the structure) during the optimisation process, and to investigate whether this changed material layer has an effect on the optimum result.

Many conditions (situations) exist in the real world where structures consist of a material core that is surrounded by a thin layer of an alternative material. Shot peening results in a hardened material layer on the surface of the object. This hardened layer may have different material properties compared to the inner remaining material such as the Young’s modulus and the Poisson’s ratio. In some cases this outer layer may have a higher or a lower elastic modulus. Other examples with distinguished layers are case hardening, cold forming, sandwich composites or objects coated with a different material such as a coat of paint or corrosive layer or dental restored crowns. By using the ‘nibbling’ option of ESO (Xie and Steven, 1997) and adding a newly formulated Constant Width Layer (CWL) algorithm, the Constant Width Layer ESO (CWL ESO) method is established in this chapter. It identifies this procedure and establishes it with some simple examples. Chapter 7 then goes on to use this particular algorithm in the area of dental crown restorations.

6.2 Constant Width Layer Algorithm

The CWL algorithm is based on a 'ripple' effect - where if one discrete element is removed, all elements in the region surrounding that element are affected. Those elements affected in turn affect others. The user defines the degree of influence on the surrounding elements. The algorithm consists of two parts. The first notes which elements in the model is to be removed (determined by the ESO method) and the second is the material morphing of elements, surrounding the removed elements. The amount of elements to be morphed depends on the number of elements defined to maintain the surrounding width layer. The user defines this.

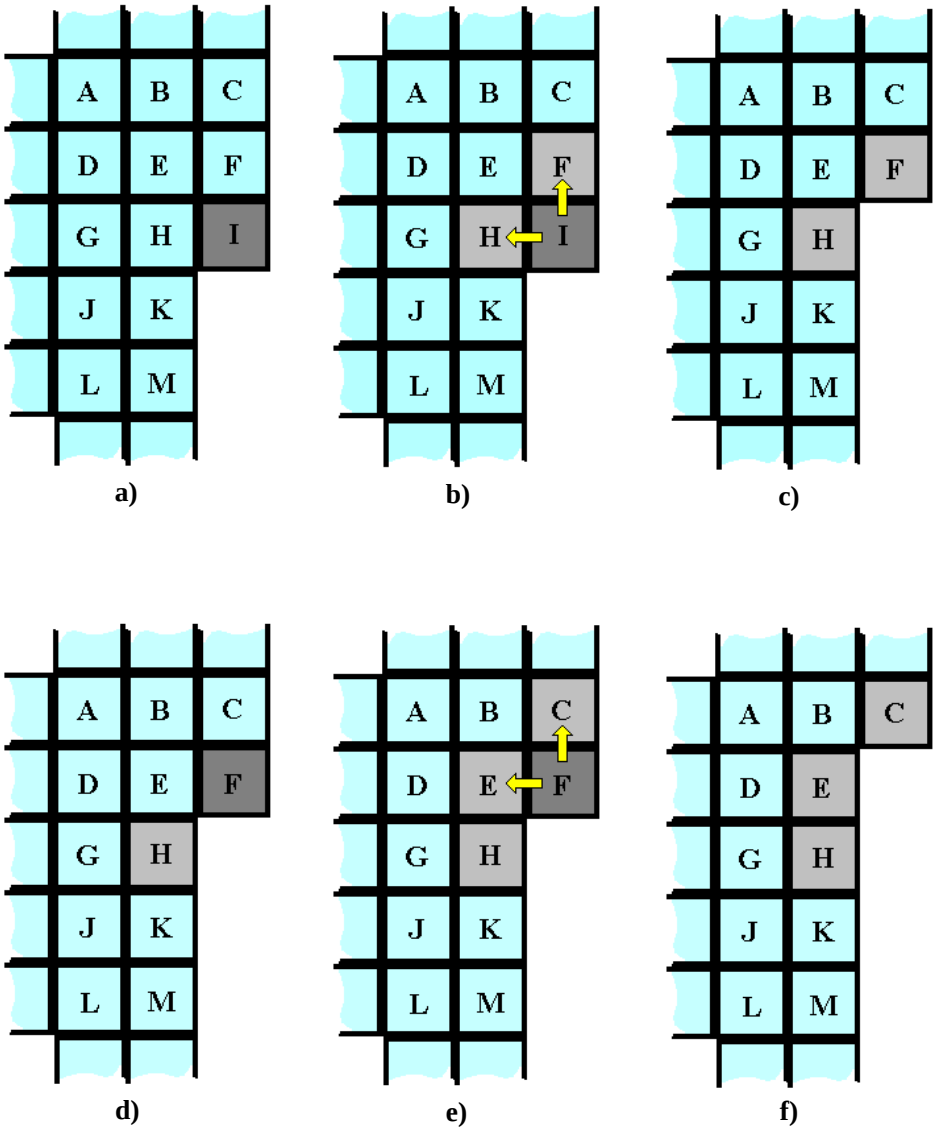

Figure 6.1 Section of model with CWL algorithm defined for one element width.

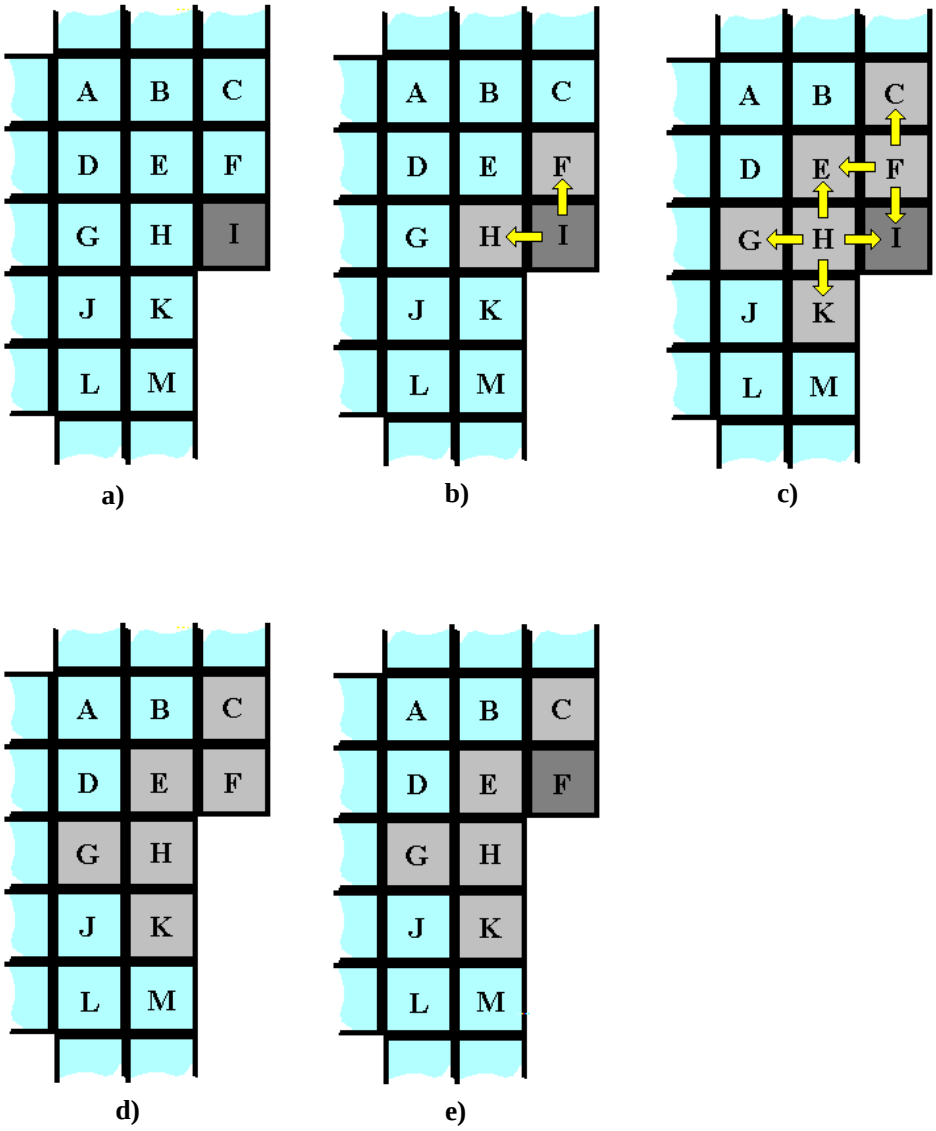

Figure 6.2 Section of model with CWL algorithm defined for two-element width.

As an example, take a portion of a model, identified by elements A to M (Figure 6.1 a)). Presume that the layer of elements with a different property width to the remainder of the structure is defined to be one. If element I is selected by the ESO algorithm to be removed (Figure 6.1 a)), the CWL algorithm searches for its adjacent elements. Note that it only selects elements that are orthogonal - in this case, elements H and F. Having identified these adjacent elements, the CWL algorithm changes their property to another property type pre-defined by the user (Figure 6.1 b)). The ESO method then resumes its normal process, deleting the identified element I (Figure 6.1c)) and continues on to the next iteration. If it selects another element to be deleted – say element F (Figure 6.1 d)), then the CWL

algorithm identifies and changes the property type of the adjacent orthogonal elements (Figure 6.1 e)). Having done this, ESO deletes element F (Figure f)). This process repeats itself iteratively.

The same process can be used, however, with a different pre-defined width to be morphed along the boundary. Take the previous example, but with a definition of a layer of two elements to be maintained along the boundary. Figures 6.2 a) to e) illustrate the process. If element I is identified to be removed (Figure 6.2 a)), then the CWL algorithm firstly selects the orthogonal elements H and F (Figure 6.2 b)) to be morphed. Knowing that the layer width has been defined as two, it then secondly selects the elements orthogonal to those already selected ie elements C, E, G, I, and K (Figure 6.2 c)) and morphs them. Because element I has already been selected to be removed, it is omitted from the list of elements to be morphed. The ESO algorithm then deletes the chosen element I (Figure 6.2 d)), and repeats its process again of selecting new elements to be removed (Figure 6.2 e)) and selecting new elements to be morphed as bound by the CWL algorithm.

6.3 Constant Width Layer ESO Procedure

The CWL ESO algorithm is incorporated into the ESO process. It uses the morphing function of ESO (Nha *et al.*, 1998; Querin, 1997) to change the plate properties. The steps that defined the CWL ESO method are as follows:

Step 1: Discretise the structure using a fine mesh of finite elements;
Step 2: Define loads, constraints and CWL element width;
Step 3: Carry out linear static FEA of structure - Equation (2.1);
Step 4: Morph elements using CWL algorithm;
Step 5: Remove elements that satisfy Equation (1.3);
Step 6: Repeat steps 3 to 5 until a steady state is reached;
Step 7: Increment steady state number and update *RR* using Equation (1.4);
Step 8: Repeat Steps 3 to 7 until a desired optimum is reached.

6.4 Examples

Because CWL ESO uses the morphing of elements in terms of properties only (in contrast to plate thickness morphing), the potential variation of applications is vast. For example, plain strain, plane stress, shells, axisymmetric and 3-D brick elements can all be used. The examples illustrated in this subsection use two types of these elements. They are the plain strain and plane stress elements. The objective in these examples was to create a uniform stress along the boundary of the structure by removing those elements with the smallest von Mises stress. For both examples, the rejection ratio equation terms (introduced in Equation (1.4)) were set as $a_0 = a_2 = a_3 = 0$ and $a_1 = 0.05$.

6.4.1 Short Cantilever Beam

Plane strain elements have been used for this first example. It is the cross section of a beam that has the left-hand side totally fixed and that has a load of 100 N applied vertically downward on the right-hand side (Figure 6.3). The dimensions of the cross-section are 200 mm × 100 mm. At the core of the beam are elements with Young's modulus E = 50 GPa. Around the perimeter of the cross section is a layer of elements that surround this core. The amount of elements making up the layer is pre-defined to be 10 mm wide. These elements have a Young's elastic modulus E = 210 GPa. Both element types have a Poisson's ratio of ν = 0.33. Three different conditions are examined in the example. Each condition has a different mesh density for the same dimensions: 10 × 20 elements, 20 × 40 elements and 30 × 60 elements. The effect of this coarseness shall be examined. For all conditions, an ESO optimised result (not using the CWL algorithm) shall be produced as a comparison.

Figures 6.4 to 6.6 show the different CWL topologies for the different mesh 'intensities' compared to the standard ESO topologies. They are for different proportions of material removed. The CWL layer of elements is a lighter shade in contrast to the darker core elements. It is obvious that at different stages during the process, the CWL method produces different topologies in contrast to the standard ESO method. A significant proportion of the outer stiff material is lost in the standard ESO method (but is retained during the CWL method) and so the topology for that given material is different.

By reducing the elemental size (thereby increasing the mesh fineness), it can also be observed from these figures that the width of the outer layer of elements, particularly around bends or curves is maintained. In the coarse mesh (Figure 6.4), because of the selection of CWL elements orthogonally, the result is a jagged outer layer of material. In contrast, a less jagged and more consistent width outer layer is produced (Figures 6.5 and 6.6). This is because as more layers of elements are created and used in the outer layer, these elements are selected to maintain that consistent width from the principle of orthogonal selection.

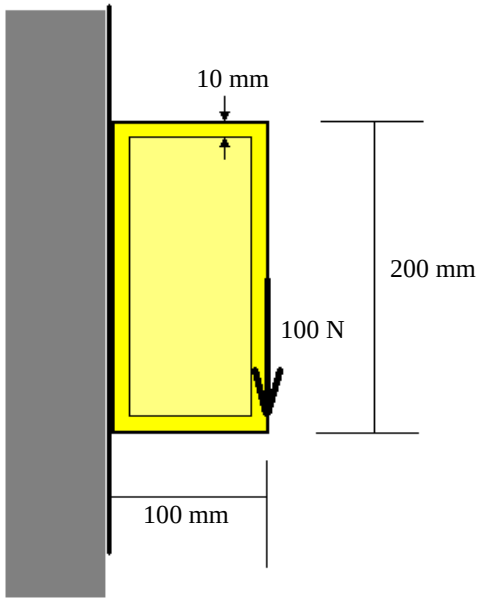

Figure 6.3 Initial Design domain of short cantilever beam.

A measure of the structure's efficiency in terms of the von Mises stress is to observe how close the mean stress of the structure (σ_{mean}) is to the maximum stress of the structure (σ_{max}). The ultimate preference is to have the ratio approaching unity during the evolution. A measure of this efficiency is given in Figure 6.7 for the different mesh densities. During the evolution, all conditions approach the ideal condition of stress unity, but never reach it. In all conditions, the ratios remain higher than the standard ESO ratios, indicating that there is a difference in the efficiencies between these methods. This is because the CWL process retains a uniform width layer of the same stiffer material compared to the standard ESO method that only removes the stiffer elements.

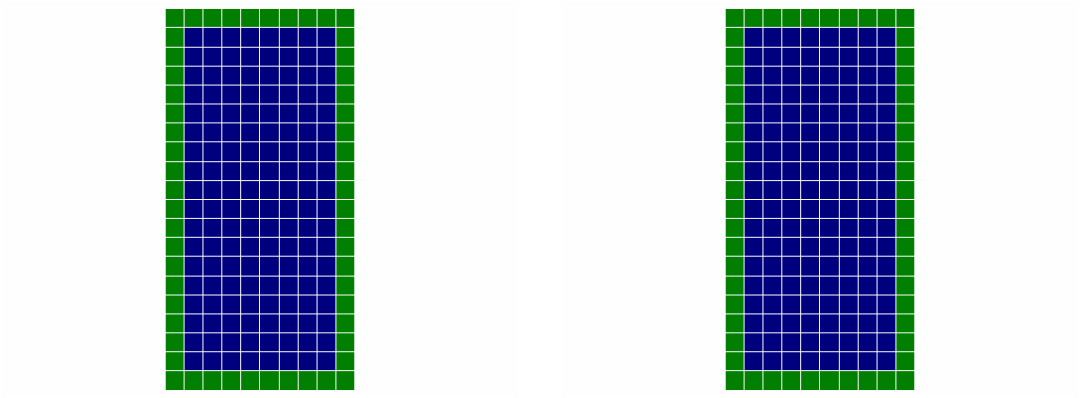

a) CWL ESO. Area removed: 0 mm^2 **b)** ESO. Area removed: 0 mm^2

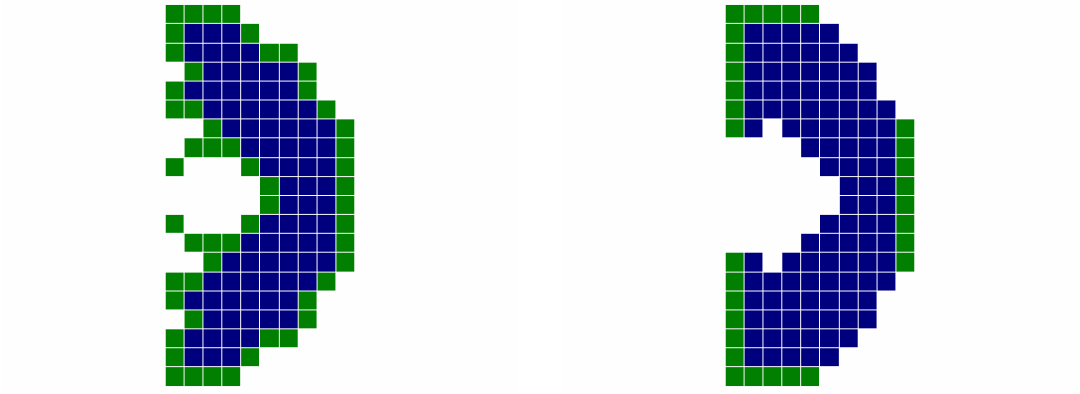

c) CWL ESO. Area removed: 6000 mm^2 **d)** ESO. Area removed: 6000 mm^2

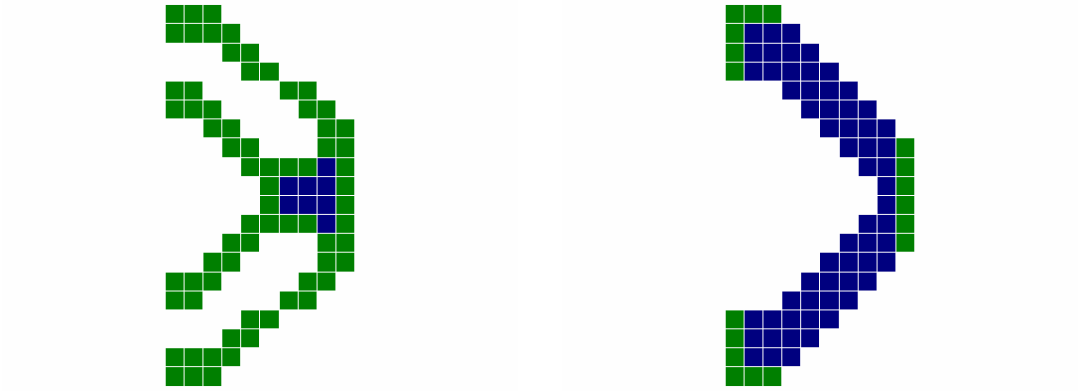

e) CWL ESO. Area removed: 12000 mm^2 **f)** ESO. Area removed: 12000 mm^2

Figure 6.4 Various CWL ESO and standard ESO topologies of short cantilevered beam during evolution. Mesh size: 10 × 20.

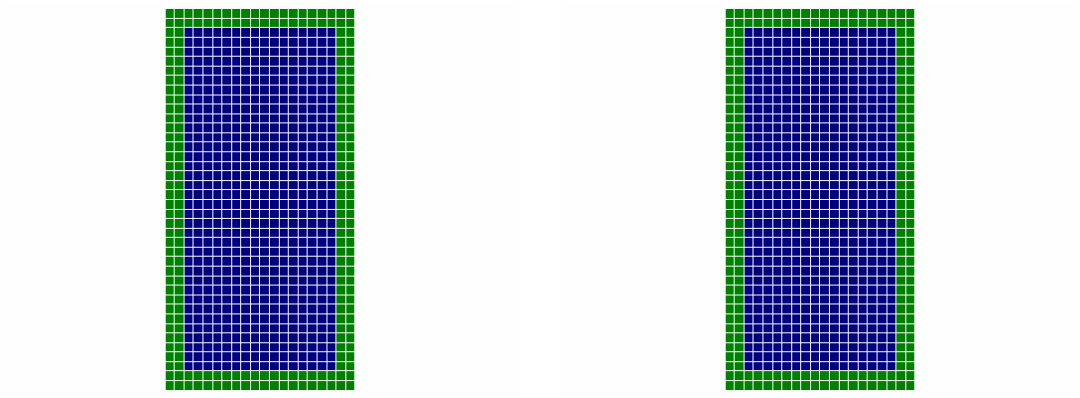

a) CWL ESO. Area removed: 0 mm^2 **b)** ESO. Area removed: 0 mm^2

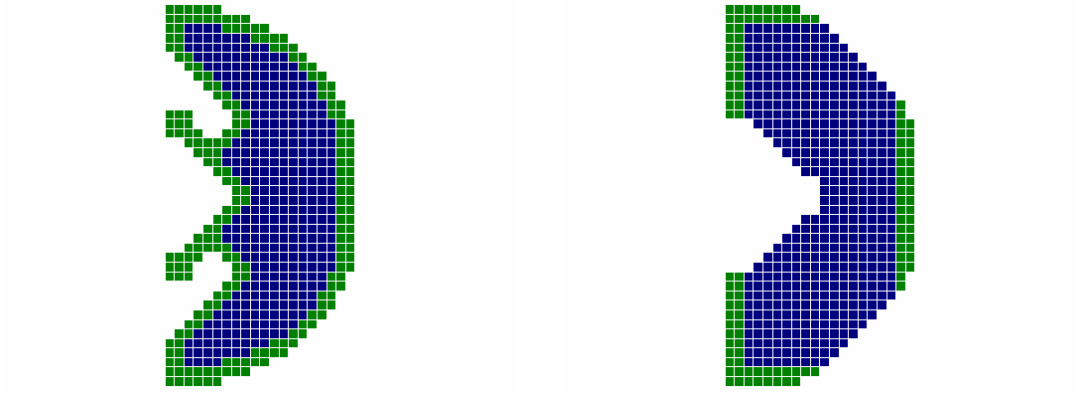

c) CWL ESO. Area removed: 6000 mm^2 **d)** ESO. Area removed: 6000 mm^2

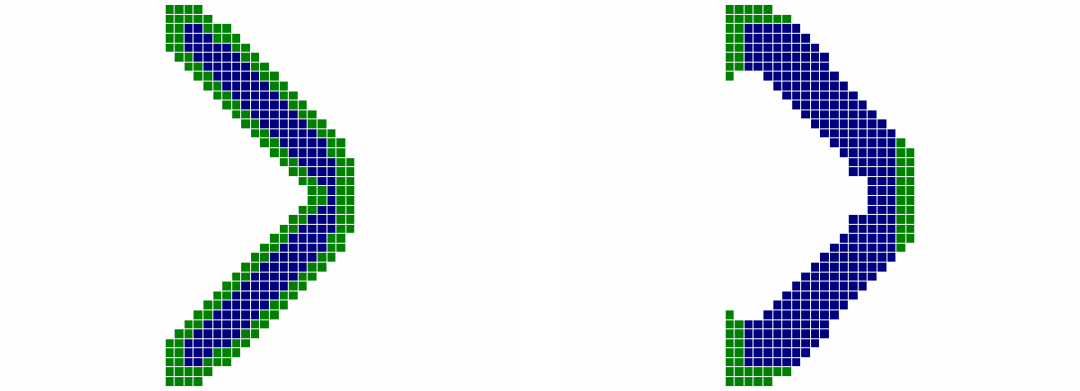

e) CWL ESO. Area removed: 12000 mm^2 **f)** ESO. Area removed: 12000 mm^2

Figure 6.5 Various CWL ESO and standard ESO topologies of short cantilevered beam during evolution. Mesh size: 20 × 40.

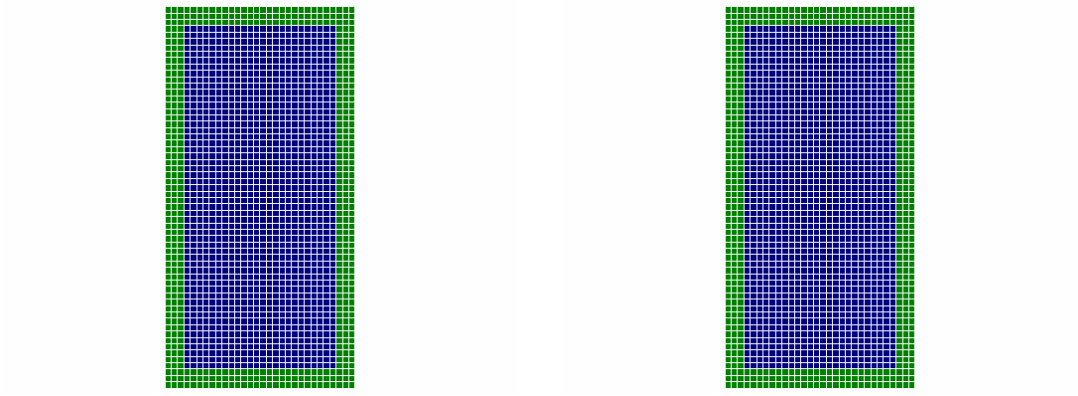

a) CWL ESO. Area removed: 0 mm^2 **b)** ESO. Area removed: 0 mm^2

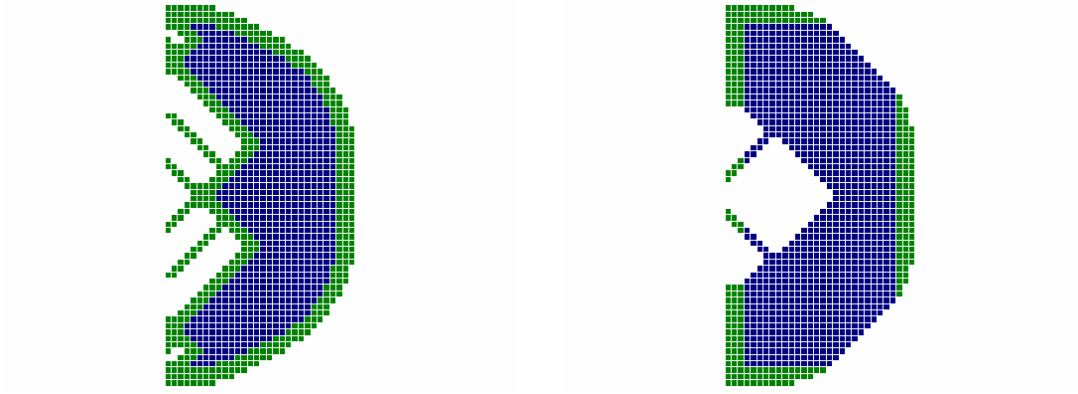

c) CWL ESO. Area removed: 6000 mm^2 **d)** ESO. Area removed: 6000 mm^2

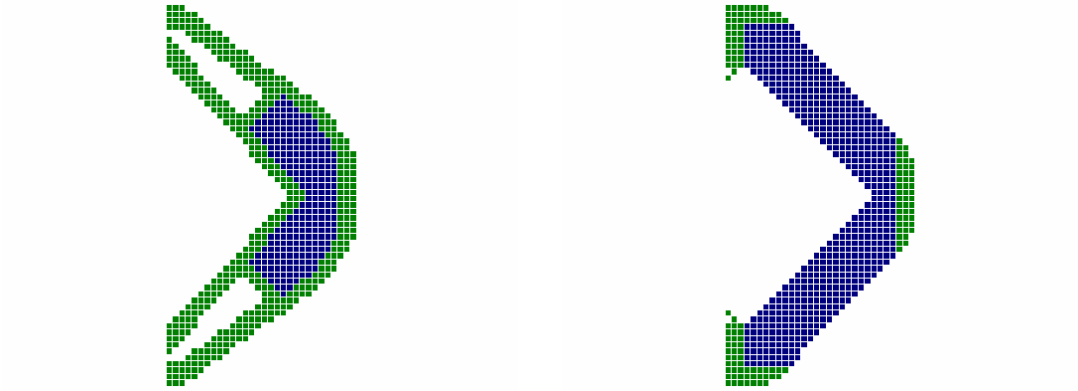

e) CWL ESO. Area removed: 12000 mm^2 **f)** ESO. Area removed: 12000 mm^2

Figure 6.6 Various CWL ESO and standard ESO topologies of short cantilevered beam during evolution. Mesh size: 30 × 60.

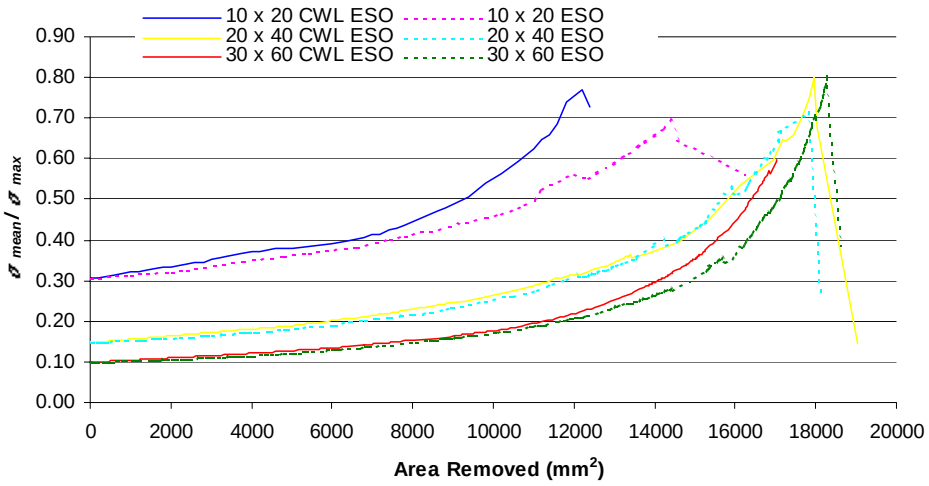

Figure 6.7 Ratio of Mean Von Mises stress to Maximum Von Mises stress of cantilever beam during evolution.

6.4.2 Rectangular Plate with Hole

The second example showing the workings of the CWL algorithm is that of a rectangular plate with a square hole. The plate has dimensions 200 mm × 300 mm, with the small hole of size 5 × 5 mm at its centre. Distributed along the horizontal edges of the plate is a uniform vertical load of 100 N/mm and along the vertical edges is a horizontal uniform load of 50 N/mm. The centre point along the bottom edge is completely fixed and the centre point on the top edge is allowed to translate vertically.

All elements have a Young's modulus of E = 70 GPa and Poisson's ratio of ν = 0.33. This is with the exclusion of elements at the centre of the plate surrounding the hole. They have a Young's modulus of E = 210 GPa and a Poisson's ratio of ν = 0.33. The pre-defined layer width to be morphed using the CWL algorithm is 10 mm. The outer string of elements along the perimeter of the plate is defined as a non-design domain. A nibbling constraint is applied to the small hole in the centre of the plate. The size of each element is 10 × 10 mm, however in the centre region of the plate (surrounding the hole) are smaller elements of size 2.5 × 2.5 mm. All elements have a thickness of 1 mm. The anatomy of the initial design domain is shown in Figure 6.8.

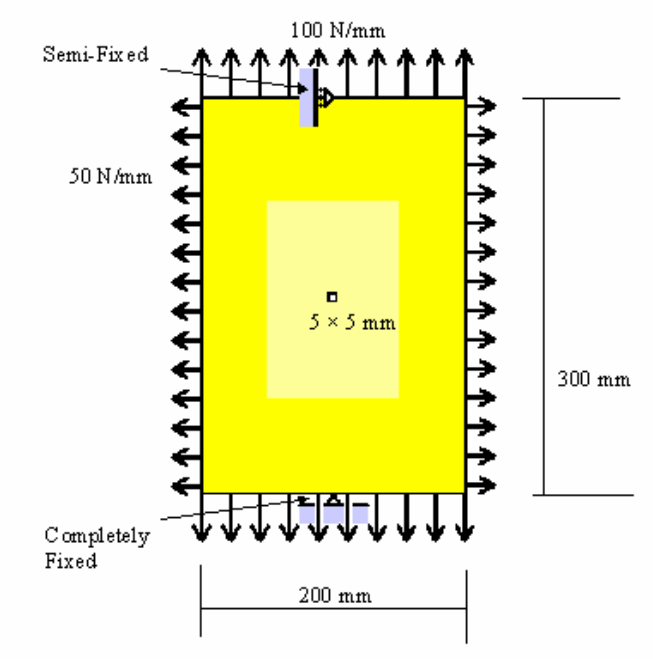

Figure 6.8 Initial Design domain of rectangular plate with hole.

Magnified sections of the different topological stages of element removal for both the CWL and standard ESO are given in Figure 6.9. As can be seen, during the process, the thickness of the second material layer surrounding the hole remains consistent, as was intended at the conception of the CWL ESO technique. Around the narrower ends of the forming ellipse, the width of the layer is thinner than around the broader sides. Using a finer mesh with a greater number of elements across the layer may change this. Alternatively, the algorithm can be modified to include diagonal elements that are triggered in the selection of elements in the morphing process (in contrast to the selection of orthogonal elements).

Note that the volumes of the shown topologies between both models are not exactly equivalent. This is because a higher evolution rate of a_1 = 0.05 was used and thus for a specific defined volume, the amount of elements removed did not necessarily correspond to the desired volume. Taking this into account it can be seen that for this example, the actual shape and size of the hole for the CWL ESO method is identical to that of the standard ESO method. This is because the stress distribution around the edges of the hole (where the nibbling constraint confines element removal to) are similar, but are of different magnitude for each example. They are of course different throughout the remainder of the structure (particularly across the stiff collar maintained by the CWL ESO method), but because of the nibbling constraint, are made irrelevant during element removal.

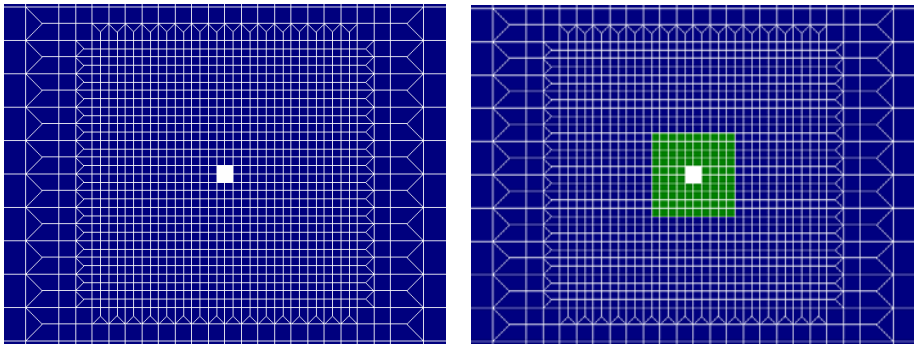

a) ESO. Area removed: 0 mm^2 **b)** CWL ESO. Area removed: 0 mm^2

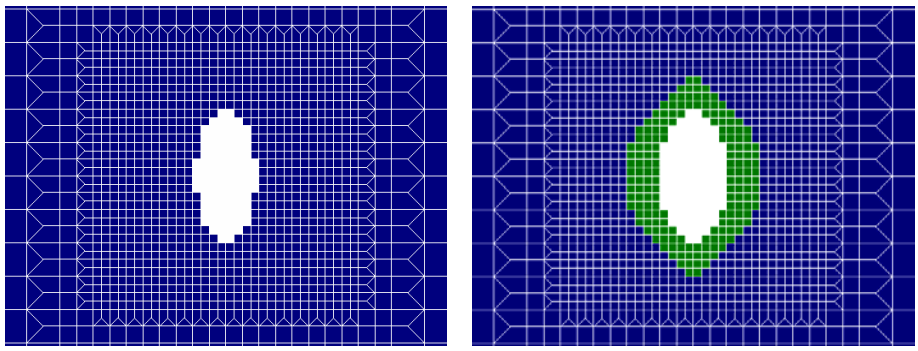

c) ESO. Area removed: 500 mm^2 **d)** CWL ESO. Area removed: 500 mm^2

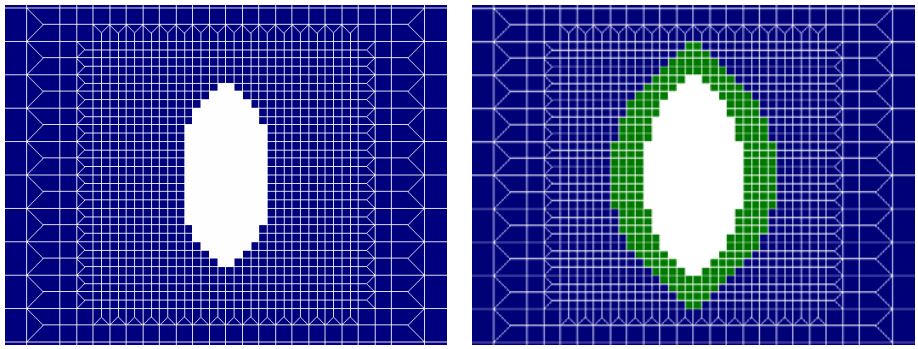

e) ESO. Area removed: 1000 mm^2 **f)** CWL ESO. Area removed: 1000 mm^2

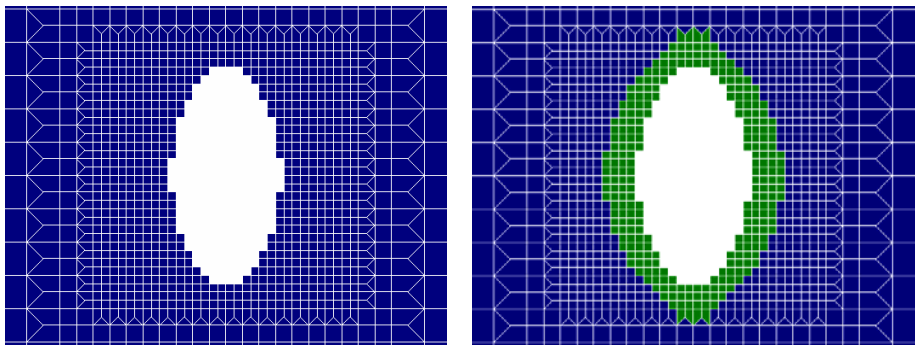

g) ESO. Area removed: 1500 mm^2 **h)** CWL ESO. Area removed: 1500 mm^2

Figure 6.9 Various CWL ESO and standard ESO topologies of plate during evolution.

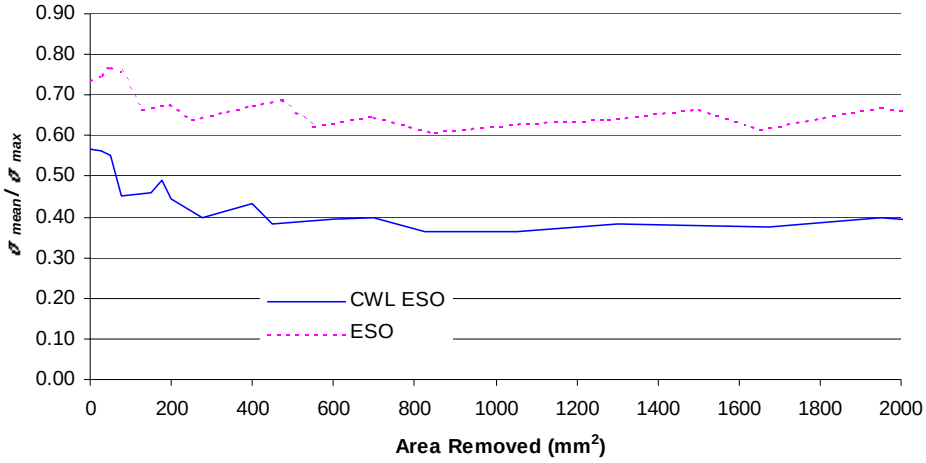

Figure 6.10 Ratio of Mean Von Mises stress to Maximum Von Mises stress of plate during evolution.

Figure 6.10 gives a measure of the efficiency of the CWL process in contrast to the standard ESO process. Both ratios of mean von Mises stress to maximum von Mises stress fluctuate together during the evolution. However, the CWL ESO model manages to maintain a lower ratio. This is because the presence of a stiff collar around the hole initially creates a higher maximum stress in contrast to the maximum stress of the standard ESO model.

6.5 Concluding Remarks

This chapter has managed to introduce and demonstrate a new algorithm that maintains a defined layer of alternative material during the ESO process. It can be seen that with this new algorithm, the level of optimisation effectiveness is maintained or even bettered. It has also been seen that a finer mesh produces a more uniform width during the process. This is of course at the cost of computational time.

The development of this algorithm has left open other options to develop ESO further such that models can be optimised more appropriate to the real life structures that exist. This method can be extended to include many layers of different material to be maintained rather than just two discrete material types. The result would be many interfaces across the structure where it becomes a section of material of consistently varying properties. The finer

the mesh and the more property types that are morphed, the more continuous the change in properties becomes and thus the more realistic is the modelling. This would model materials that have varying properties through the structure as a result of a manufacturing process ie conduction surface hardening, cooling processes where smaller crystals form along the boundary and are larger toward the centre (the pore sizes, shapes etc also change the further away from the external surface). Having established the CWL ESO technique, it is now appropriate to use it for a more realistic example - that of a dental bridge, which is examined in the next chapter.

6.6 References

Bendsøe, M. (1988), "Composite Material as a Basis for Generating Optimal Topologies in Shape Design", *Structural Optimization*, pp. 31-37.

Bendsøe, M., Kikuchi, N. (1992), "Topology and Layout Optimization of Discrete and Continuum Structures", Kamat, M., (Ed.), *Structural Optimization: Status and Promise*, AIAA Inc., Washington, United States of America, pp. 517-547.

Jog, C., Haber, R., Bendsøe, M. (1993), "Topology Design using a Material with Self-Optimizing Microstructure", Pederson, P., (Ed.), *Optimal Design with Advanced Materials*, Elsevier Science, New York, United States of America, pp. 7-23.

Nha, C., Xie, Y., Steven, G. (1998), "An Evolutionary Structural Optimization Method for Sizing Problems with Discrete Design Variables", *Computers and Structures*, Vol. 68, pp. 419-431.

Olhoff, N., Thomsen, J., Rasmussen, J. (1993), "Topology Optimization of Bi-Material Structures", Pederson, P., (Ed.), *Optimal Design with Advanced Materials*, Elsevier Science, New York, United States of America, pp. 191-206.

Querin, O. (1997), *Evolutionary Structural Optimisation: Stress Based Formulation and Implementation*, Doctorate Thesis, School of Aeronautical, Mechatronic and Mechanical Engineering, University of Sydney, Australia.

Rispler, A. (1998), *Analysis and Optimisation of Highly Loaded Joints*, Doctorate Thesis, School of Aeronautical, Mechatronic and Mechanical Engineering, University of Sydney, Australia.

Xie, Y., M., Steven, G., P. (1997), *Evolutionary Structural Optimisation*, Springer-Verlag, London, UK.

Chapter 7

Optimisation of an Anterior Ceramic Dental Bridge

7.1 Introduction

The dental technology industry today faces the ongoing challenge of producing superior dental bridge designs based on mechanical reliability whilst retaining excellent aesthetic, biological and functionality qualities (El-Ebrashi *et al.*, 1970; Kappert and Knode, 1993).

Seeking to satisfy the aesthetic criteria, demand has recently increased towards the use of all-ceramic bridge systems. This alternate option to traditional metal-ceramic systems allows better translucency and simulation of a natural tooth appearance (Castellani *et al.*, 1994). It offers better refraction of light and produces better reflections in the mouth of the patient. Grey and shadowed zones resulting from metal reinforced bridges are avoided (Kappert and Knode, 1993).

The mechanical reliability of ceramic bridge structures greatly depends upon stress magnitudes and variations. Dental ceramics are inherently fragile in tension (Fahmy, 1996). Many attempts have been made to examine the stresses developed in ceramic bridges (Craig, 1987; Hood *et al.* 1975). Craig *et al.* (1987) have used photo-elastic modelling to quantify these stresses. They were able to identify how notches and the direction of loading influenced the magnitudes of the stresses developed. Kelly *et al.* (1995) analysed fixed partial dentures using the finite element technique to examine the principal stress distribution throughout the structure. They also undertook a comparison of laboratory failed and clinically failed ceramic bridges. Extensive studies have too been completed to examine the forces required to break various bridge designs (Kappert and Knode, 1993; Qualtrough, 1997).

The objective of this chapter is to analyse the mechanical behavior of an anterior (front of mouth) bridge tooth geometry, made of a new dental ceramic material called In-Ceram (Vita Zahnfabrik H. Rauter GmbH & Co. KG, 1998; Kappert and Knode, 1993; Qualtrough, 1997). Then an optimised profile will be obtained and compared using the CWL ESO technique developed in the previous chapter. This algorithm was used in the context of von Mises stress. For this chapter - particularly for the case of ceramics, principal stresses are used.

It must be mentioned that the multicriteria methods developed in previous chapters (particularly stiffness, natural frequency and inertia) are not adopted into the optimisation of teeth. This is because the major emphasis of teeth optimisation is the desire to reduce tensile stresses in order to reduce the likelihood of fracture. In this chapter, the CWL ESO method shall be used to solely search out the best possible shape whereby the principal stress along the bridge surface are made uniform, whilst maintaining a constant width of material for aesthetic purposes.

7.2 Modelling Procedure

A number of 2-D finite element models, based on the external shape of a horizontal cross-sectional slice taken from a pre-existing anterior 3-unit ceramic dental bridge (Figure 7.1), have been constructed. These models are used to mimic the behaviour of the ceramic bridge loaded horizontally. Whilst real numerical values were not achievable, substantive qualitative conclusions can be made from the analysis.

Although not the case in reality, each 2-D bridge is modelled to be symmetric about the mid pontic unit of the bridge (Figure 7.2). This allows only half of the model to be analysed thus saving computational time during the analysis. Symmetry is modelled with the use of boundary constraints. A central node on the dentin tooth core is allowed to translate horizontally only.

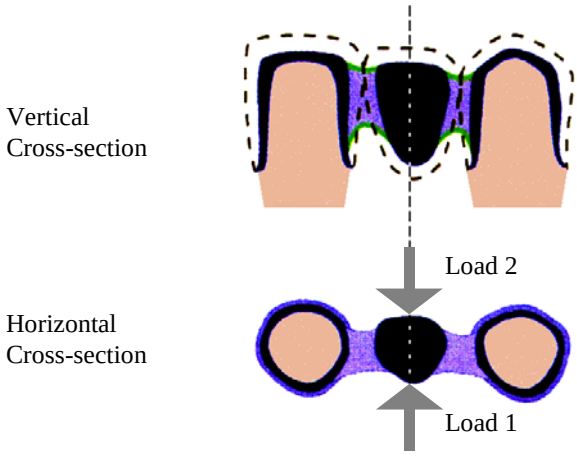

Figure 7.1 Vertical and horizontal cross-section of an all-ceramic 3-unit anterior bridge structure (Vita Zahnfabrik H. Rauter GmbH & Co. KG, 1998).

For each of these models, the exterior shape of the bridge is maintained, but a variation in the proportion of materials is examined. A different proportion in the thickness of the outside porcelain veneer to the In-Ceram is allocated to each model. The range in thickness of the veneer ceramic varies from 0 mm to 1.6 mm by increments of 0.20 mm. Note that the veneer ceramic is only placed on the front of the pontic tooth.

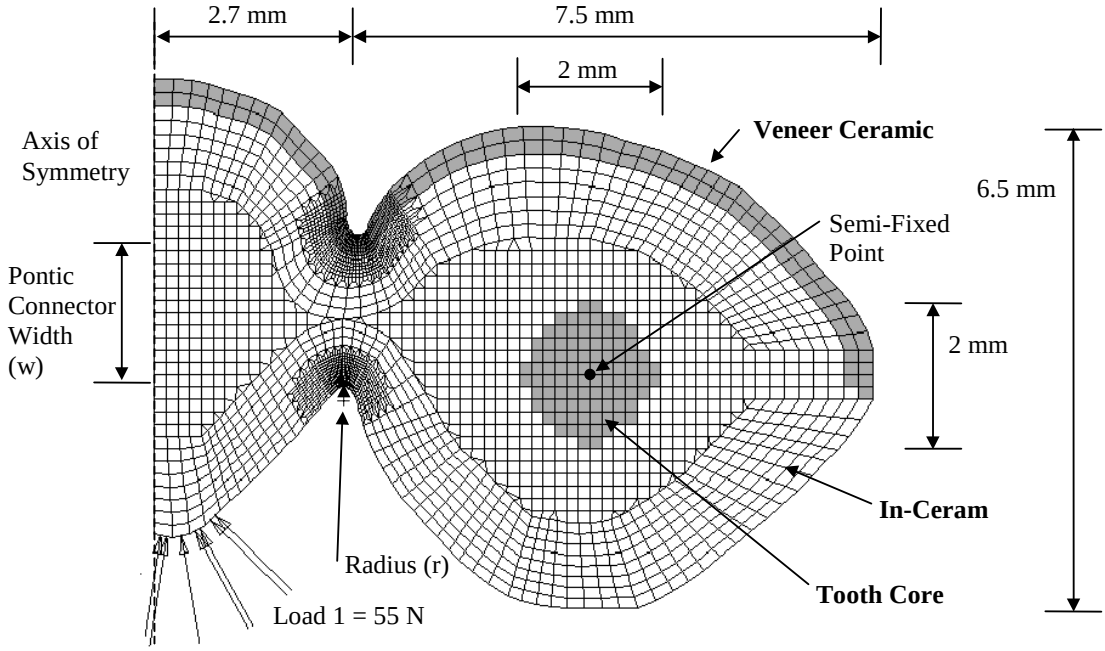

Figure 7.2 Anterior bridge model. Veneer thickness: 0.4 mm. Loading from the 'back of mouth'.

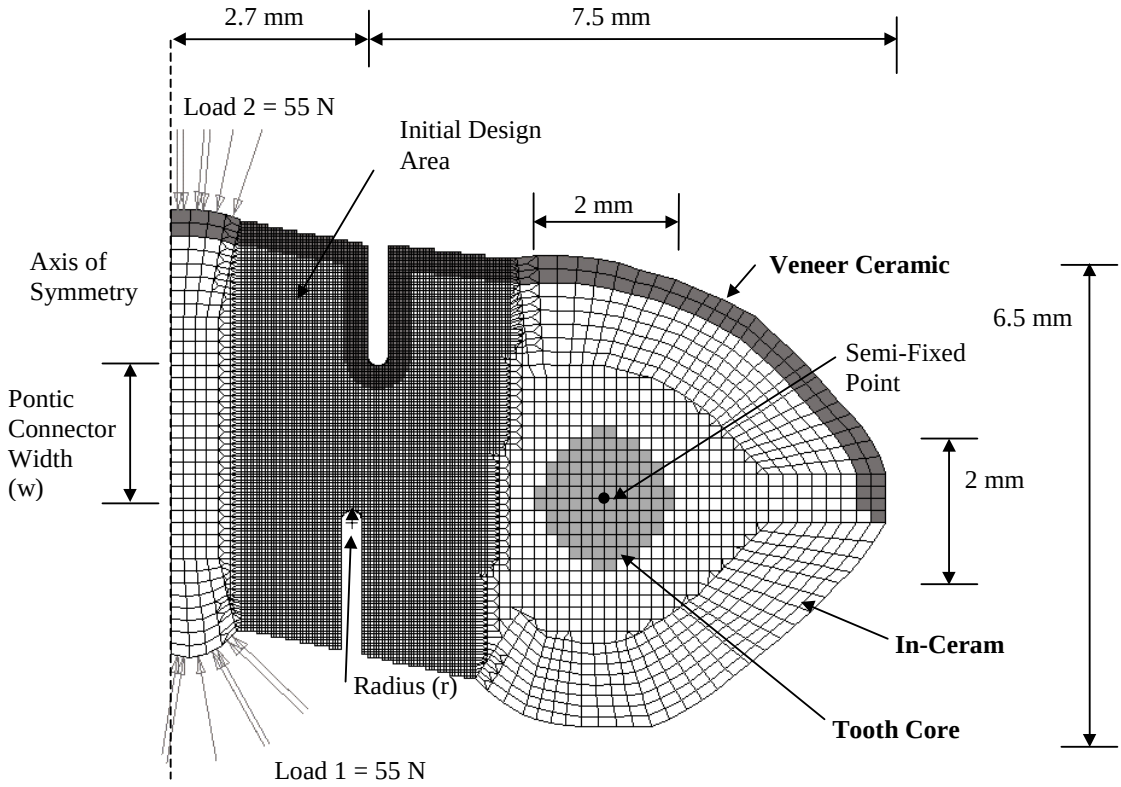

Figure 7.3 Initial ESO Design domain for anterior bridge. Veneer thickness: 0.4 mm.

Two loading cases will be analysed for each anterior tooth model. The first shall be from the 'front of the mouth' (Figure 7.2) and the second from the 'back of the mouth'. For the front loading case, a stress is applied on the plane strain model that results in a horizontal force of 55 N per unit thickness. For a loaded region of 4 mm vertical height, this implies that the total applied load is 220 N. For the loading case from the 'back of the mouth', the stress applied to the model also results in a horizontal force of 55 N per unit thickness. For a loaded region of 4 mm vertical height, there is also a total applied load of 220 N. These extreme loading cases are based on the knowledge that an average maximum bite force of nearly 200 N occurs in the anterior tooth area (Kappert and Knode, 1993).

All of the anterior bridge models consist of a total of 2929 elements: 2838 quadrilateral elements and 91 triangular elements. The triangular elements are not placed in stress-critical areas. Each model contains elements of three property types (or two property types for those models without a veneer coating ie 0 mm thick veneer layer). The first property type is the In-Ceram material, which has a Young's elastic modulus of 250 GPa. The second is dentin - the ceramic of the tooth core, to which the bridge is attached. It has a Young's elastic

modulus of 20 GPa. The third property type is the veneer coating which covers the front and the outer sides of the bridge. It has a Young's modulus of 70 GPa. All material has a Poisson's ratio of 0.3. The elements used are of the 2-D plane strain type to model the effect of surrounding material.

Having created the anterior bridge under horizontal loading, another model is developed (Figure 7.3) and optimised using the CWL ESO method. This CWL ESO model is based on the original anterior bridge model, the difference being an initial design domain replacing the notched areas. The ratio between the width of the pontic connector (w) to the radius of the notch (r) is identical to that of the original anterior model (Figures 7.2 and 7.3). The initial design of the ESO bridge model consists of 12896 quadrilateral and triangular plate elements. This model shall then be analysed and compared with the models of the pre-existing bridge.

7.3 Evolutionary Structural Optimisation Process

The model developed by the ESO algorithm had as its main driving factor the aim to be as uniformly stressed over the surface of the bridge as possible, without detracting from the other factors such as aesthetics, appearance and functionality. Such a combination of contradicting objectives have been taken into account through careful modelling of the initial design (by specifying a fixed depth and radius of each notch), and the character of the ESO process itself to imitate nature.

During the evolution of the CWL ESO model, different quadrants of the notch were 'frozen' by declaring them non-design domains. This was in order to maintain a continuous curve between the tooth, the notch and the pontic tooth. This happened at different times for the four quadrants (divided by the notch line and a midline dividing the front and back of the bridge) during the evolution, and so each was frozen when that continuity was reached. The tooth, tooth core and pontic regions not existing near the notched regions were also declared non-design domains. This was to maintain the natural shape of the teeth.

7.4 Results and Discussion

The principal stress distribution as a result of the FEA for the anterior bridge model is illustrated in Figure 7.4. This model had a loading applied from the 'back of the mouth', and a porcelain thickness of 0.40 mm. A region of tensile stress occurred at the edge of the tooth notch with maximum tensile stress value of 116.1 MPa.

Another region of peak stress was a band of tensile stress that occurred at the interface of the veneer ceramic and the In-Ceram material near the front notch. This high tensile band specifically existed in the In-Ceram material. The FEA results show that the difference in elastic modulus across the veneer/In-Ceram interface caused the peak stresses to occur in the In-Ceram (Hood *et al.*, 1975).

It is found that this phenomenon was very similar to results obtained by Kelly *et al.* (1995). Their investigation showed that for approximately 70 to 78 % of all their test samples (in vitro and in vivo), crack initiation occurred at the core-veneer interface. This indicated that the interface was both a location of high tensile stress and an important source of structural flaws.

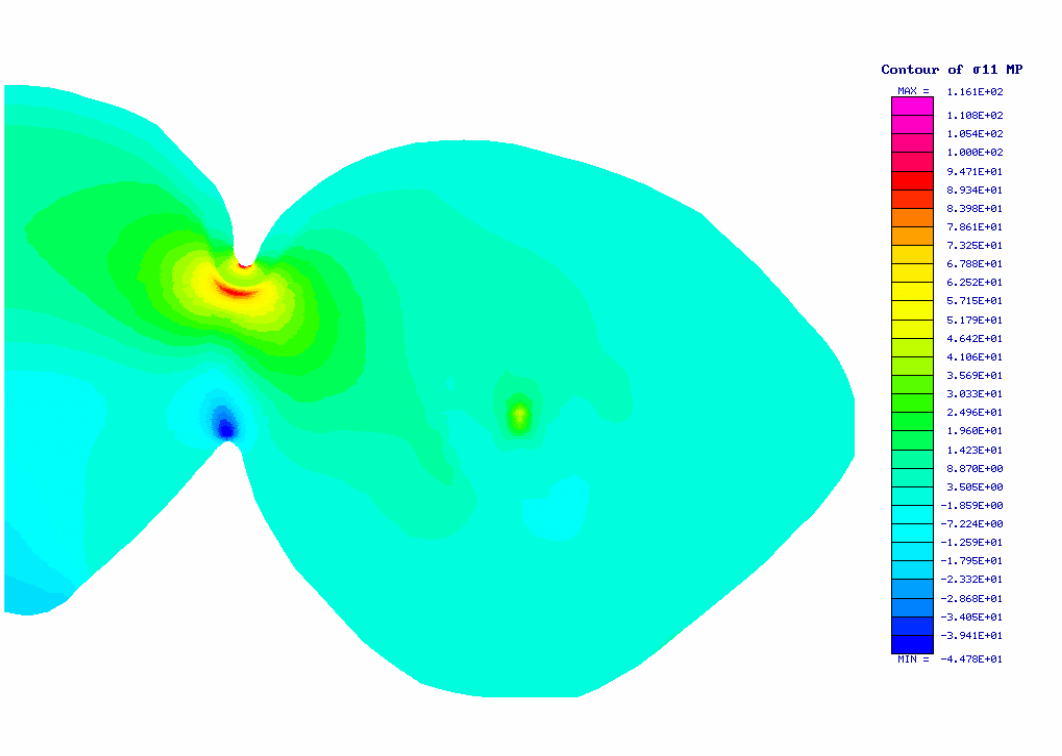

Figure 7.4 Stress distribution for anterior bridge model with loading from 'back of mouth'. Model area: 49.8 mm^2.

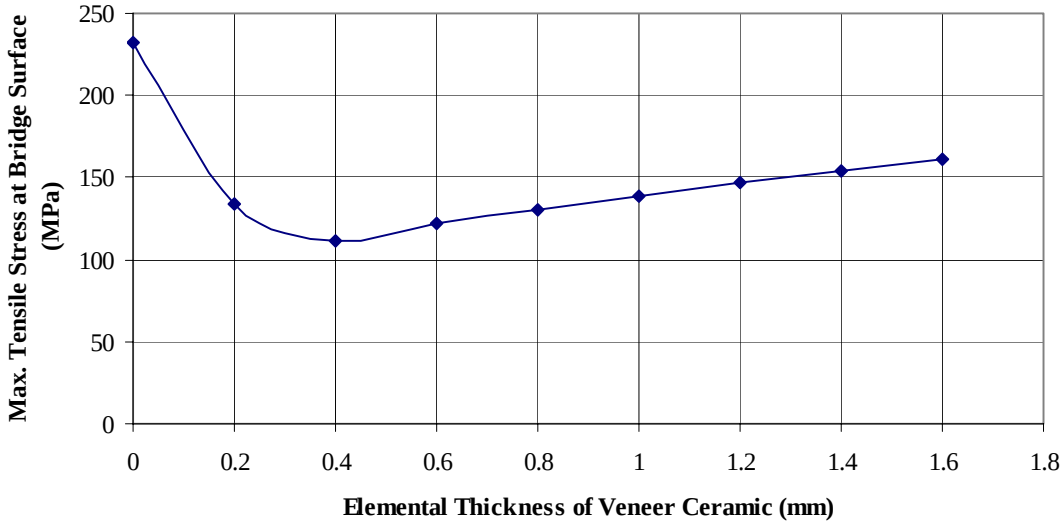

Figure 7.5 Plot of maximum tensile stress (principal) at bridge surface versus elemental thickness of veneer ceramic. Loading from 'back of the mouth'.

Figure 7.5 graphically shows how the maximum tensile principal stress varied for each model coated with a different thickness of porcelain and loaded from the 'back of the mouth'. This was measured at the bridge surface. For all models, the maximum tensile stress existed on the surface of the front notch. There was a thickness in the veneer coating that resulted in the lowest maximum tensile stress. It occurred for a veneer thickness of 0.4 mm. The maximum tensile stress was greater than the yield stress of the porcelain for those bridges with a porcelain thickness greater than 1 mm or less than 0.2 mm. To decrease the probability of structural failure, the bridge design may need to be modified. Altering the geometry of the notch (El-Ebrashi *et al.*, 1970) may do this. In effect, the width of the bridge could be increased, thereby decreasing the maximum stress in the bridge to a value below the failure stress. Alternately, the notch radius could be adjusted (Kappert and Knode, 1993).

From Figure 7.5, it may be concluded that in bridge design there exists an optimum proportion of porcelain coating to In-Ceram material that will allow the lowest maximum tensile stress to exist. This needs to be compared to the desired thickness restrained by the aesthetic factor.

An indication of how the maximum principal tensile stress varied for different thickness veneer ceramic models, measured at the interface between the In-Ceram material and the veneer ceramic is presented in Figure 7.6. The maximum always occurred in the In-Ceram

region. As can be seen, the value decreased at a decreasing rate for an increase in the thickness of the veneer. All tensile stress values lay below the yield stress value of the In-Ceram.

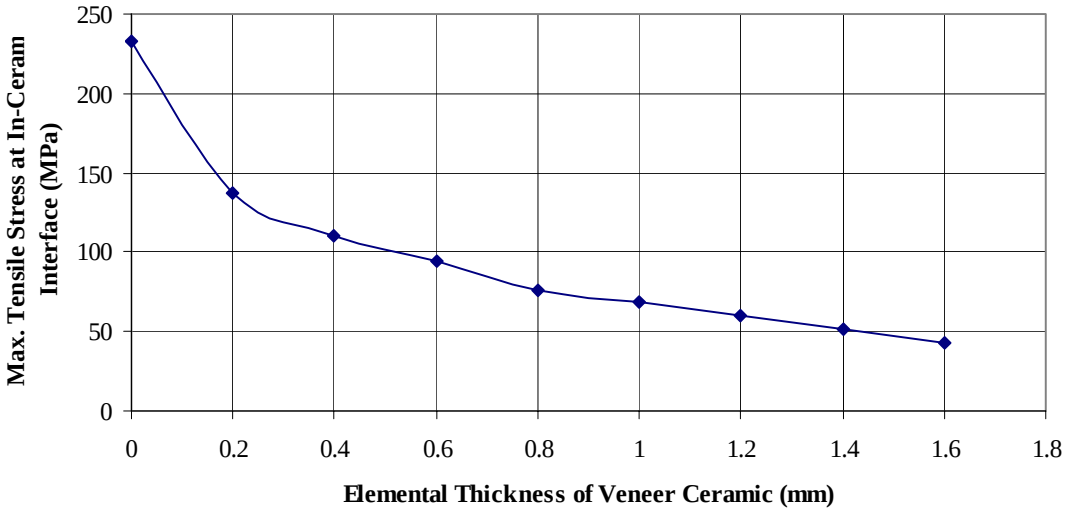

Figure 7.6 Plot of maximum tensile stress (principal) at In-Ceram/Veneer interface versus elemental thickness of veneer ceramic. Loading from 'back of mouth'.

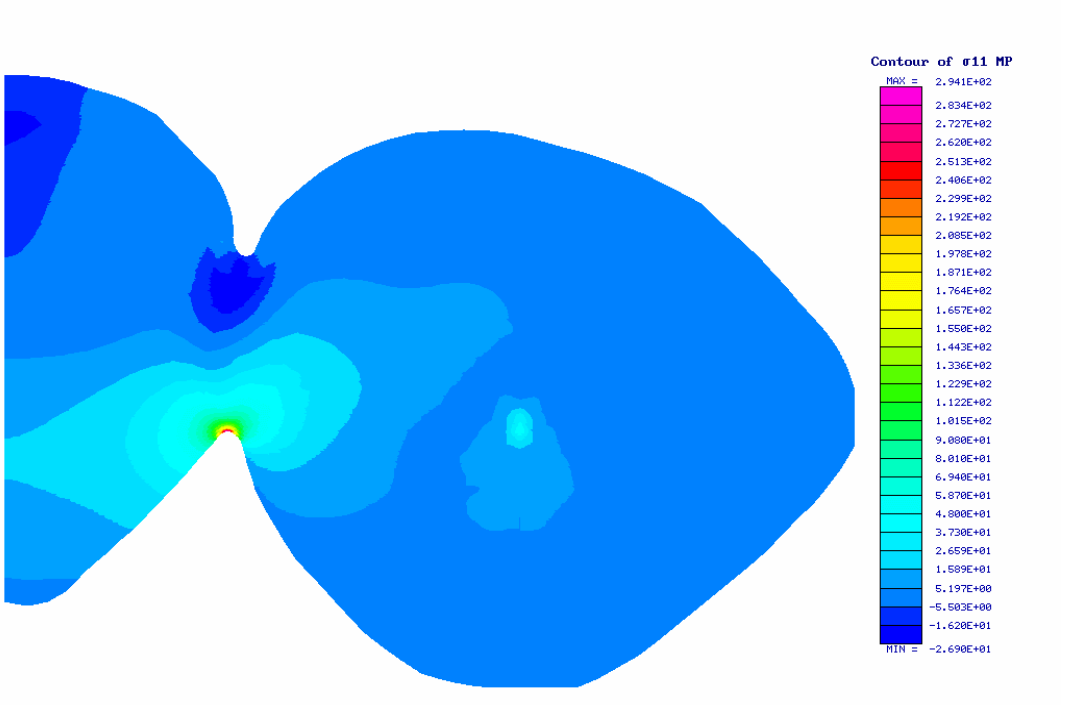

Figure 7.7 Stress distribution for pre-existing anterior bridge model with loading from 'front of the mouth'. Model area: 49.8 mm^2.

The stress distribution in the anterior bridge with a loading from the 'front of the mouth' is shown in Figure 7.7. Here, as expected, the point of maximum tensile principal stress existed in the notch at the back of the bridge. Its value was 294.1 MPa. This highlights a technical advantage of the In-Ceram material, which has an exceptionally high yield stress of approximately 500 MPa.

Figure 7.8 demonstrates that the maximum tensile stress in the model, for the 'front of the mouth' loading case, was affected by a variation in the porcelain thickness. This stress increased at a decreasing rate for an increase in the veneer porcelain thickness up to 1.6 mm.

Each model loaded from the 'front of the mouth' had the location of maximum stress occur in the rear notch as observed in Figure 7.7. All maximum tensile stresses existed below the fracture strength of In-Ceram.

An appropriate change in the geometry of the dental bridge would also lower this level of maximum stress for any given porcelain thickness. By decreasing the depth of the notch seen in Figures 7.5 and 7.8, the width of the pontic connector would effectively be increased. This increase in width would result in a stress decrease throughout the structure (due to the increase in the bridges' cross sectional area).

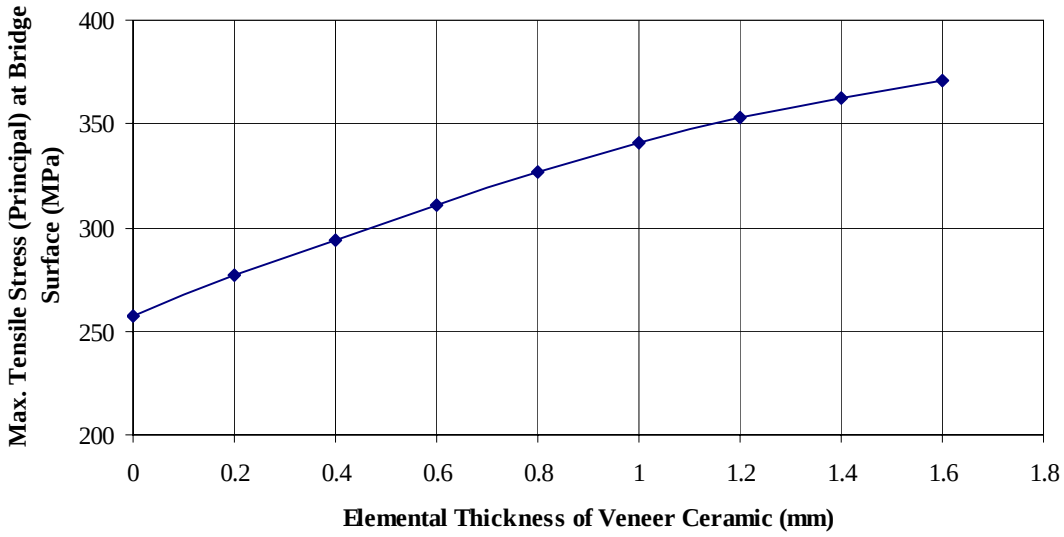

Figure 7.8 Plot of maximum tensile stress (principal) at In-Ceram interface versus elemental thickness of veneer ceramic. Loading from 'front of the mouth'.

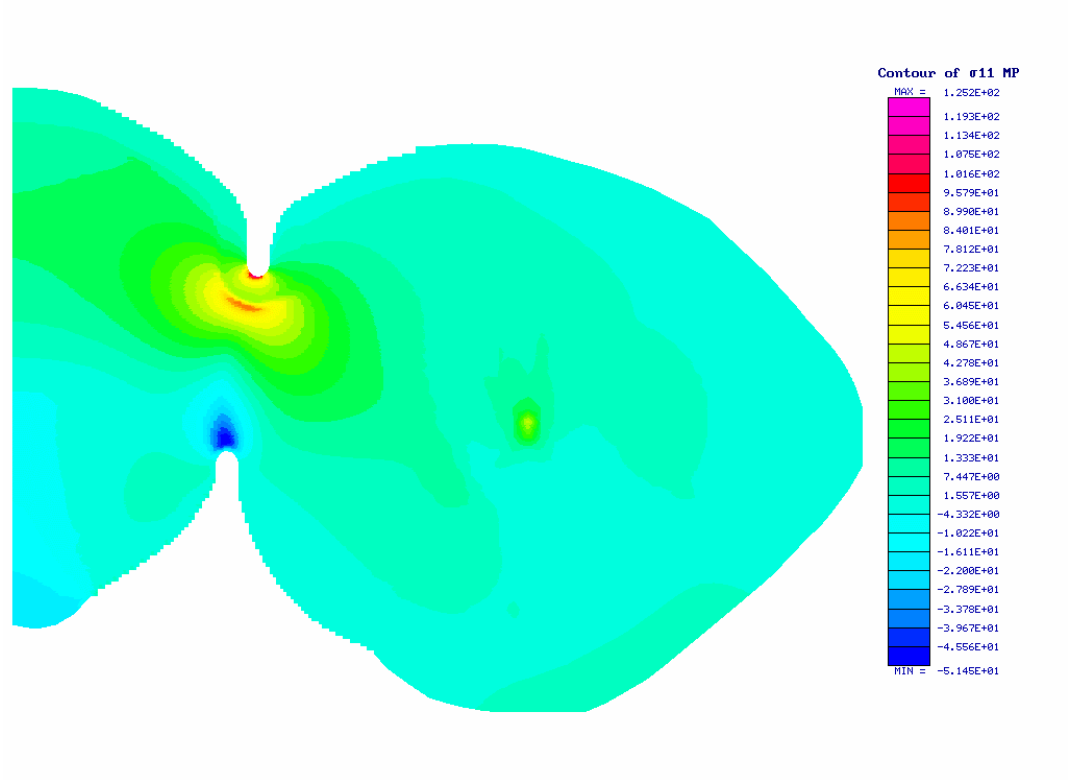

Figure 7.9 Stress distribution of optimised anterior bridge model with loading from the 'back of mouth'. Model area: 50.6 mm^2.

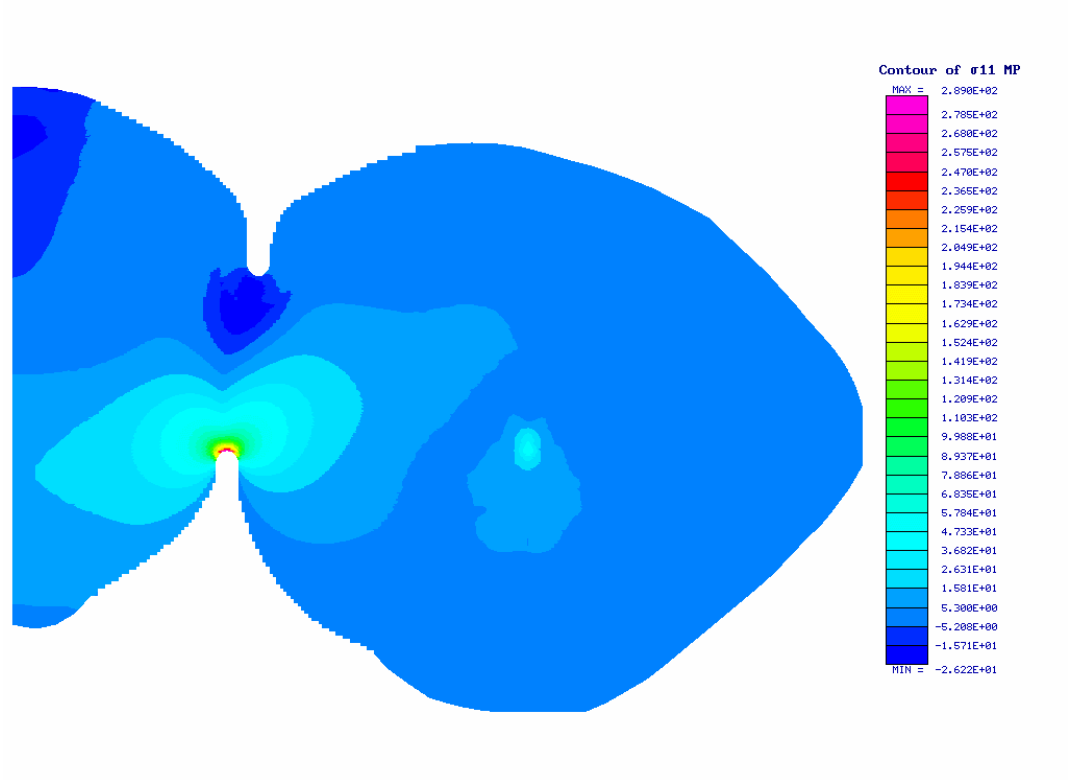

Figure 7.10 Stress distribution of optimised anterior bridge model with loading from the 'front of mouth'. Model area: 50.6 mm^2.

Figures 7.10 and 7.11 show the principal stress contours of the optimised design for both load cases. For the first load case condition (loading from the 'back of mouth' – Figure 7.9), the magnitude of stress along the majority of the model's surface was almost constant. Such was the intention of the ESO process. This is different to the distribution of stress along the pre-existing model, which varied considerably along the majority of its edge (Figure 7.4). The maximum tensile stress at the notch and the peak stress at the In-Ceram – porcelain interface of the ESO bridge were also comparable to those of the pre-existing bridge.

Such an outcome can also be observed for the optimised model under the second loading case (loading from the 'front of mouth' – Figure 7.10). A uniform stress pattern existed along most of the bridge boundary, and stress magnitudes were comparable to the 2-D model based on the original bridge (Figure 7.7).

In light of these comparisons, it may be concluded that the ESO method works well to produce bridge designs which are based purely on structural reliability, whilst taking into account the aesthetic factor set through initial modelling. It is interesting to note that such an ESO design replicates that which has been already produced by the dental technician.

7.5 Concluding Remarks

In this chapter, the results indicate that In-Ceram is an adequate and appropriate material to be used in the make-up of dental bridges. The design and construction of the bridges is mainly restricted by the properties of the porcelain veneer. There exists an ideal specific thickness of veneer that will minimise the maximum tensile principal stress. FEA also revealed that a maximum principal tensile stress existed on the notch surface, with a band of high stress occurring on the In-Ceram/Porcelain interface.

The design of the current anterior bridge is notch size and shape dependent. The recommendation is to decrease the maximum tensile principal stress, which existed on the front notch for a loading from the 'back of the mouth', and existed in the rear notch for a loading from the 'front of the mouth'.

The ESO method incorporating the CWL algorithm demonstrated it capability to produce an optimised bridge, resulting in a more uniform stress along the boundary whilst producing a design that very much imitates those produced by technicians today.

In this chapter, the author has endeavored to use dimensions and loads that closely resembled actual values and thus feels that some realistic quantitative conclusions can be drawn from the present studies. Future research direction anticipates complete 3-D modelling of the scenarios studied here in.

7.6 References

Castellani, D., Baccetti, T., Giovannoni, A., Bernardini, U., D. (1994), "Resistance to Fracture of Metal Ceramic and All-Ceramic Crowns", *The International Journal of Prosthedontics,* Vol. 7, No. 2, pp. 149-154.

Craig, R., G. (1987), *Dental Mechanics In H. Kardestuncer Finite element handbook*, McGraw Hill, New York, pp. 1424.

EL-Ebrashi, M., K., Craig, R., G., Peyton, F., A. (1970), "Experimental Stress Analysis of Dental Restorations. Part VII. Structural Design and Stress Analysis of Fixed Partial Dentures", *Journal of Prosthetic Dentistry*, Vol. 23, No. 2, pp. 177-186.

Fahmy, N. (1996), *Novel Designs in Abutment Preparation for Posterior All Ceramic Bridges*, Doctorate Thesis, Faculty of Oral and Dental Medicine, Cairo University.

Hood, J., A., A., Farah, J., W., Craig, R., G. (1975), "Stress and Deflection in Three Different Pontic Designs", *Journal of Prosthetic Dentistry*, Vol. 33, pp. 54.

Kappert, H., F., Knode, H. (1993), "In-Ceram: Testing a New Ceramic Material", *Quintessence Dental Technology*, No. 16, pp. 87-97.

Kelly, J., R., Tesk, J., A., Sorenson, J., A. (1995), "Failure of All ceramic Fixed Partial Dentures In Vitro and In Vivo: Analysis and Modeling", *The Journal of Dental Research*, Vol. 74, pp. 1253-1258.

Qualtrough, A., J., E., Piddock, V. (1997), "Ceramics Update", *Journal of Dentistry*, Vol. 25, pp. 91-95.

Vita Zahnfabrik H. Rauter GmbH & Co. KG (1998), *Vita Full Ceramics, Vita In-Ceram® Alumina, Brochure B/IC-AL*.

Chapter 8

Optimisation of a Posterior Ceramic Dental Bridge

8.1 Introduction

All-ceramic bridges are currently being created by dental technicians, although the potential of such systems has yet to be fully exploited (Qualtrough and Piddock, 1997). Ceramic bridges are not yet financially economical in comparison to bridges made of high-gold alloys. The primary reason for this is the requirement of specialised equipment to fashion such bridges. The development of such bridges is not yet a fully proven technology (Kappert and Knode, 1993).

As mentioned previously, the analysis of stress (magnitude and distribution) is useful for indicating the physical response of the system such as the most likely place for fracture to occur, though it does not aim to indicate specifically at what magnitude of applied load that fracture will occur. Such a study, amongst others, needs to include the probability of fracture, ie Weibull modulus (Kelly, 1995; Tesk and Anusavice, 1988; Hornberger, 1995). However, a comparison of the fracture strength of each material with the tensile stresses that exist in each corresponding material will indicate which system is most likely to fail. Many methods have been used to evaluate the stress distribution of various all-ceramic bridges. A selection of these includes the method of photoelastic analysis (El-Ebrashi *et al.*, 1970; Hood *et al.*, 1975) and Finite Element Analysis (FEA) (Kelly *et al.*, 1995; Pospiech *et al.*, 1996; Kamposiora *et al.*, 1996).

Issues have been raised in the past two decades in addressing the modelling methods and types of dental restorations and are summarised by Korioth and Versluis (1997). Tesk and

Anusavice (1988) have highlighted the role of FEA in dental prostheses and the future direction required to effectively encompass the complexity of the prosthesis.

The ability of FEA to provide an accurate method to approximate a dental prosthesis is closely coupled with the manner in which the Finite Element (FE) model is constructed. This includes caution with the type of FEs used (2-D plane-stress, 2-D plane-strain or axisymmetric, 3-D brick elements), the particular way that the mesh is constructed and the way that the system is modelled in terms of constraints and loads (Ridlon, 1987; Tesk and Anusavice, 1988; Korioth and Versluis, 1997).

The relative merits of using the different types of FEs available are discussed by Korioth and Versluis (1997). The method of mesh construction can substantially affect the accuracy of the FEA solution. Generally, the finer the mesh (meaning more elements for a given model), the more accurate the solution of the FEA. As the FE mesh is refined, results converge towards the exact solution. In particular, the construction of a fine mesh of elements in regions exhibiting steepest stress slopes (where stresses are rapidly changing), or stress concentrations, is vital. Such regions are likely to include rapidly changing boundaries (ie notches, sharp curves etc) or interfaces between different properties. The generation of transitions from coarse to fine meshes is an important aspect of FEA mesh construction (Cook, 1974; Ridlon, 1987; G+D Computing, 1999).

FEs also perform best when their aspect ratio, the ratio of the longest edge to the shortest edge, is one. Thus, for four noded 2-D elements the preference is to create elements which depict a square, and for three noded 2-D elements, equilateral triangles. The model can be improved by choosing higher order elements. The preference thus exists for the use of four noded elements in contrast to three noded elements. Accuracy in modelling uniformly distributed loads along an element comes about with an FEA program that equates this load to the nodes of the element in a ‘consistent’ rather than ‘lumped’ fashion. This is where the conversion takes into account bending in each element that results from the uniformly distributed load (Cook, 1974; Ridlon, 1987; G+D Computing, 1999).

Paying particular attention to these details, it is obvious that the method of mesh construction plays a key role in obtaining accurate and therefore useful results in the analyses of dental prostheses. In areas of high tensile stress, the probability of fracture is greatest. Therefore it

is vital to analyse those areas of high tensile stresses and investigate the influences on these peak tensile stresses.

In the current chapter, an investigation is carried out whereby In-Ceram is modelled in various Posterior (back of the mouth) dental tooth bridges. The functionality of In-Ceram shall be observed for four proposed single bridge profiles. Three of these shall be compared with optimised profiles obtained from the ESO algorithm. Note that because the design area of concern does not involve a constant thickness layer of material, the CWL ESO method is not used. Nevertheless, this chapter is a useful extension from the analysis and optimisation of the dental bridge of the previous chapter. Such optimisation work has not been done previously.

8.2 Modelling Procedure

Various two-dimensional finite element bridge models (taken from a 2-D vertical cross-section of a posterior bridge) are analysed. Such a vertical cross-section is used to mimic the full behaviour of a tooth loaded vertically. These models are the Bullet Pontic (Figure 8.1), Ridge Lap Pontic (Figure 8.2) and the Sanitary Pontic bridges (Figure 8.3). A fourth model (Figure 8.4) is also developed using the ESO being developed. This model is also analysed and compared with the existing models. In this chapter, the posterior bridge models are all non-symmetric.

All of the models are analysed with the FEA software STRAND6, running on a Pentium 166 processor-based computer. The models are made of Linear Quadrilateral, 2-D plane strain type elements to model the effect of surrounding material. Assume that all materials in the models have a Poisson's ratio of 0.3.

Three property types are included in all the posterior models. A constant thickness veneer ceramic (Young's elastic modulus 70 GPa) is modelled on top of the bridge and is kept constant at a thickness of 0.5 mm for each model. The second material type is the In-Ceram of modulus 250 GPa, and the third is the machined tooth with which the In-Ceram material is attached. It has a modulus of 20 GPa.

As these are only initial models, a conservative approach is taken in the constraints of the models. The models are fixed along an inner section of their base (see Figures 8.1, 8.2 and 8.3), with no rotation allowed.

A stress is applied to all the vertical bridge models. This results in a vertical force of 55 N per unit thickness directed downwards. Assuming that the plane strain models are $1/6^{th}$ of the total width of the bridge, this simulates a bridge structure experiencing a total applied load of 330 N.

The Bullet Pontic bridge consists of 15272 quadrilateral plate elements. The Ridge Lap Pontic bridge is made of 15819 quadrilateral plate elements and the Sanitary Pontic bridge consists of 13431 quadrilateral plate elements. The initial design domain of the bridge structure to be evolved consists of 18086 quadrilateral plate elements. The removal of these elements and thus the final optimised design was based on a criterion that the maximum principal stress distribution becomes more uniform over the boundary.

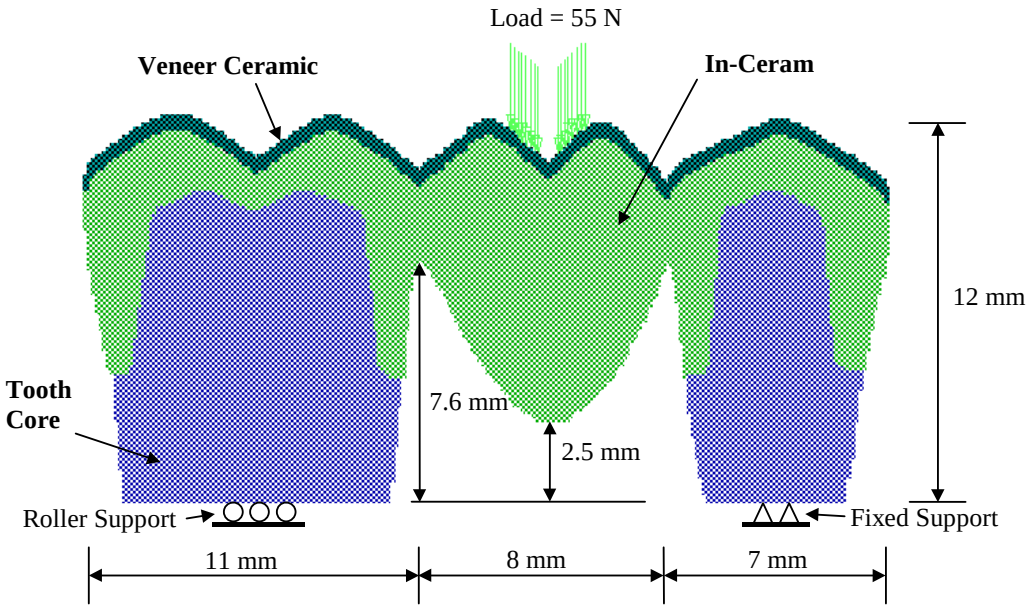

Figure 8.1 Bullet Pontic bridge model: loading and constraints.

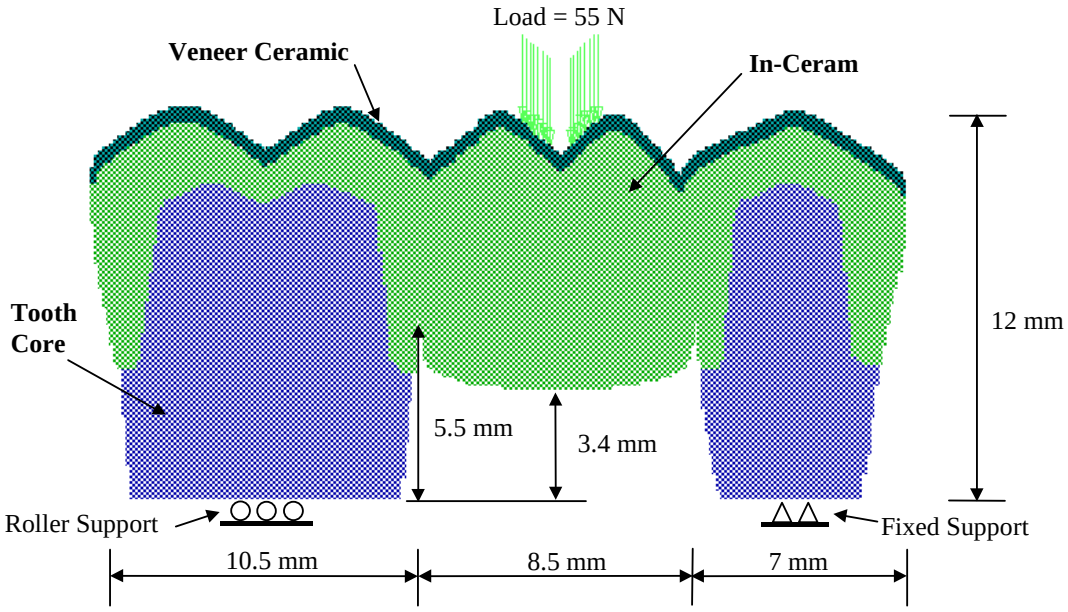

Figure 8.2 Ridge Lap Pontic bridge model: loading and constraints.

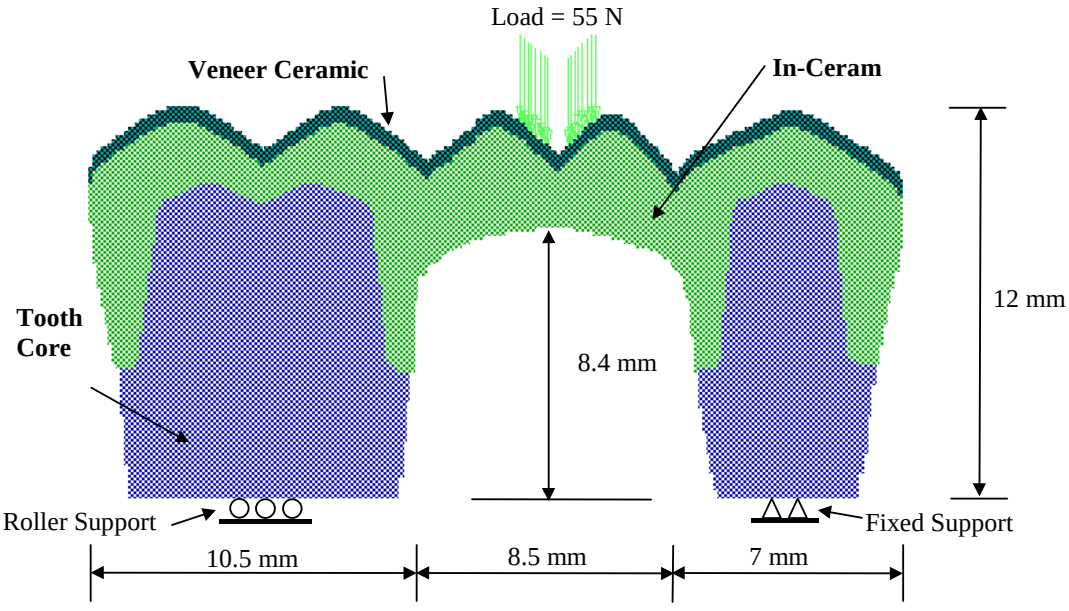

Figure 8.3 Sanitary Pontic bridge model: loading and constraints.

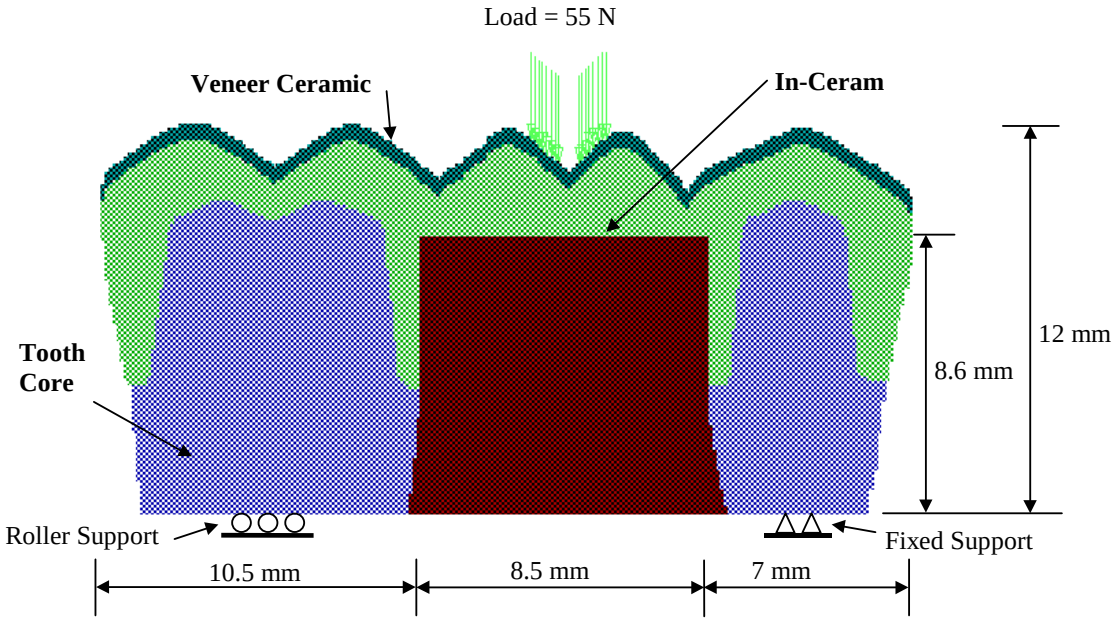

Figure 8.4 Initial ESO Design domain for posterior bridge.

8.3 Results and Discussion

Figure 8.5 illustrates how the stress is distributed over the Bullet Pontic bridge as a result of the downward vertical loading (as viewed in Figure 8.1). This loading causes two highly stressed (tensile) regions on either side of the Pontic. These stresses peak at 83.29 MPa.

In Figure 8.6, the distribution of stress in the Ridge Lap Pontic as a result of the vertical loading (as defined in Figure 8.2) can be seen. Again as for the Bullet Pontic bridge, two regions of high tensile stress occur where the crowns are joined to the Ridge Lap Pontic. The maximum is 51.5 MPa – 61.8 percent of the maximum stress that occurred for the Bullet Pontic bridge. The decrease in stress is attributed to a larger material thickness connecting the Pontic to the adjoining crowns.

One point to note is that the elements making up the models in Figures 8.6 through to Figure 8.12 are square elements. This means that the boundary of the models are jagged and caused a non-smooth distribution of stress on the boundary. However, this irregularity in the stress distribution is considered insignificant because a very fine mesh is used.

The stress distribution as a result of a vertical load (as shown in Figure 8.3) on the Sanitary Pontic bridge is illustrated in Figure 8.8. Here, the region of maximum tensile stress has shifted to the bottom centre of the Pontic tooth. Its magnitude is 109.7 MPa – a 31.7 percent increase from the maximum stress in the Bullet Pontic bridge. This region of maximum stress is not as concentrated as that in the above two bridges.

Figure 8.8 through to Figure 8.12 show the evolution process of the bridge over a range of 400 iterations.

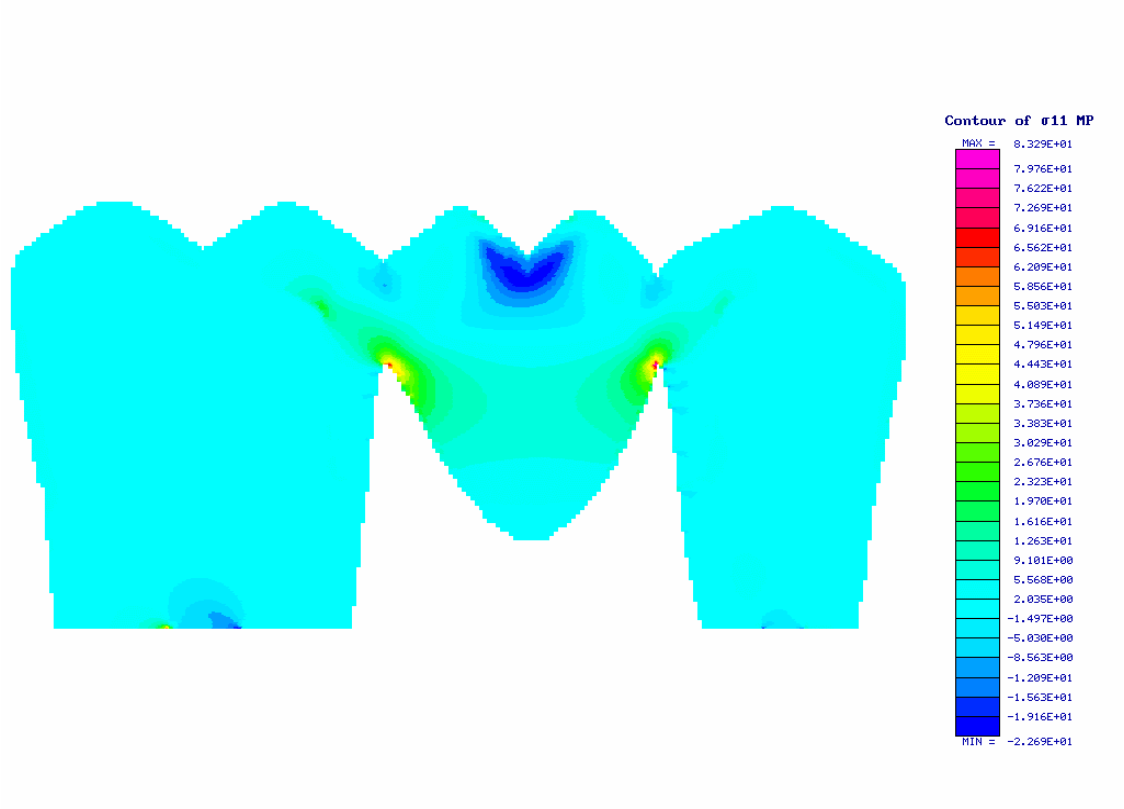

Figure 8.5 Stress distribution for Bullet Pontic Bridge.

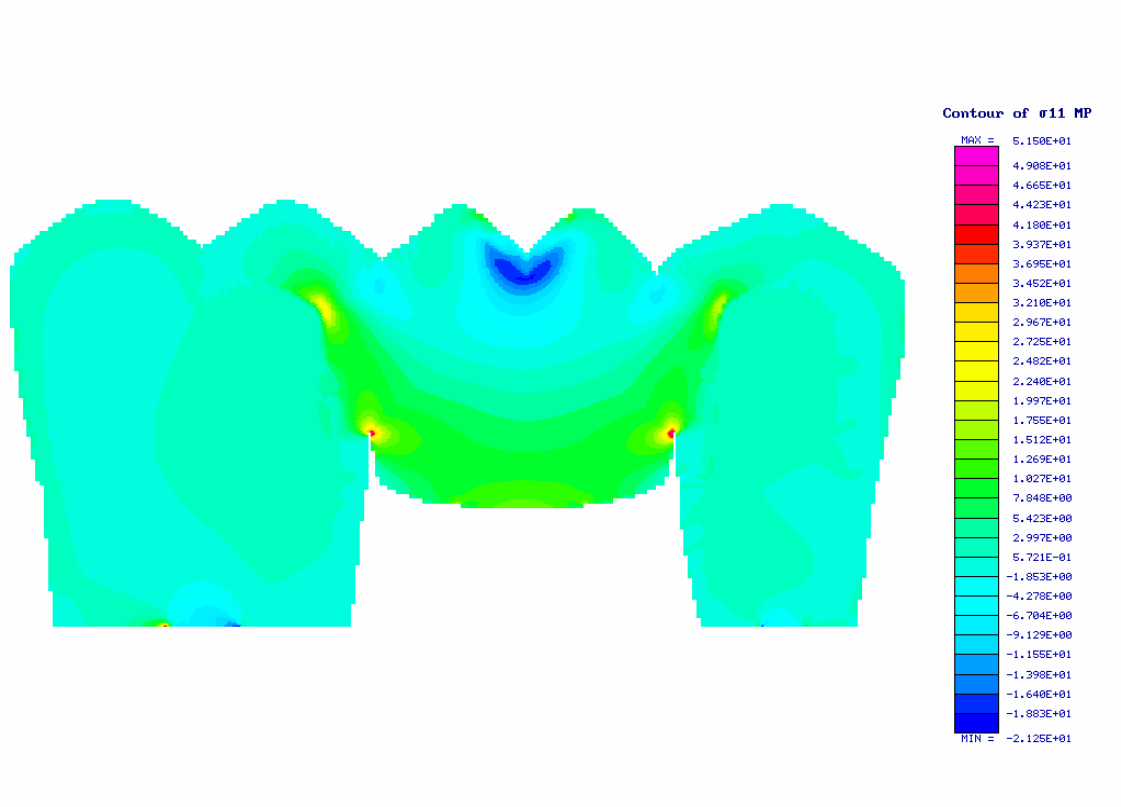

Figure 8.6 Stress distribution for Ridge Lap Pontic Bridge.

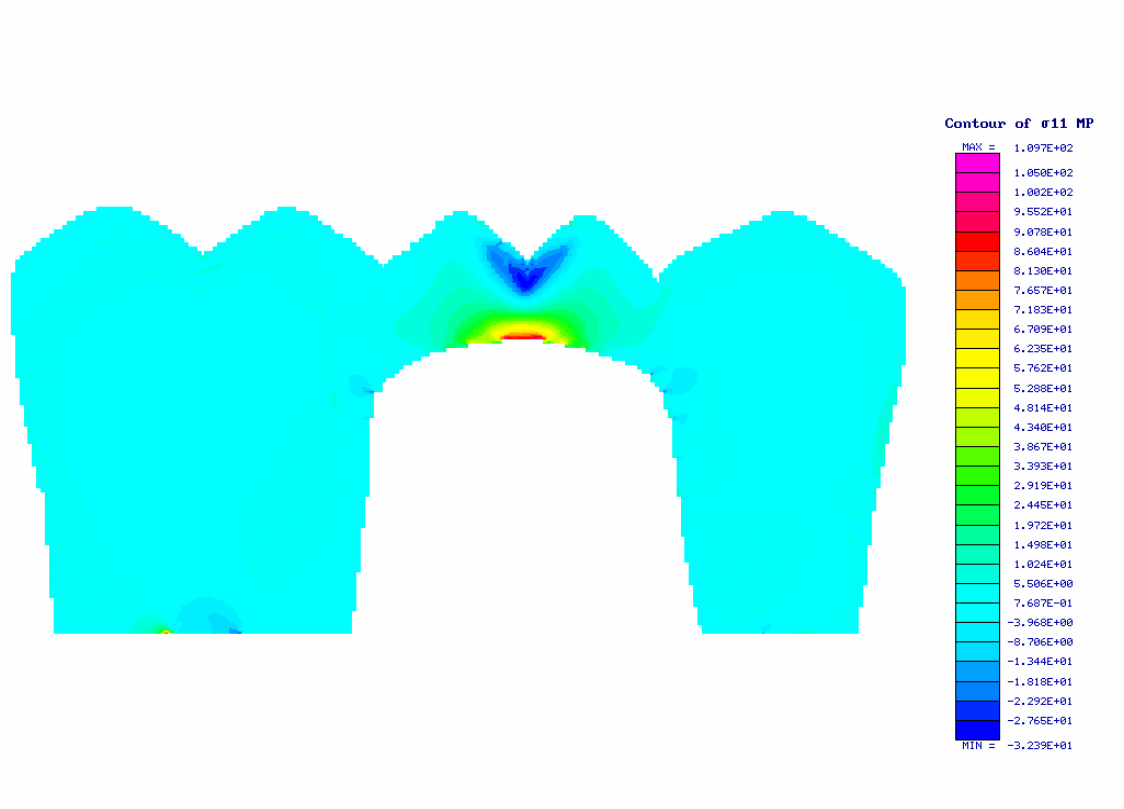

Figure 8.7 Stress distribution for Sanitary Pontic Bridge.

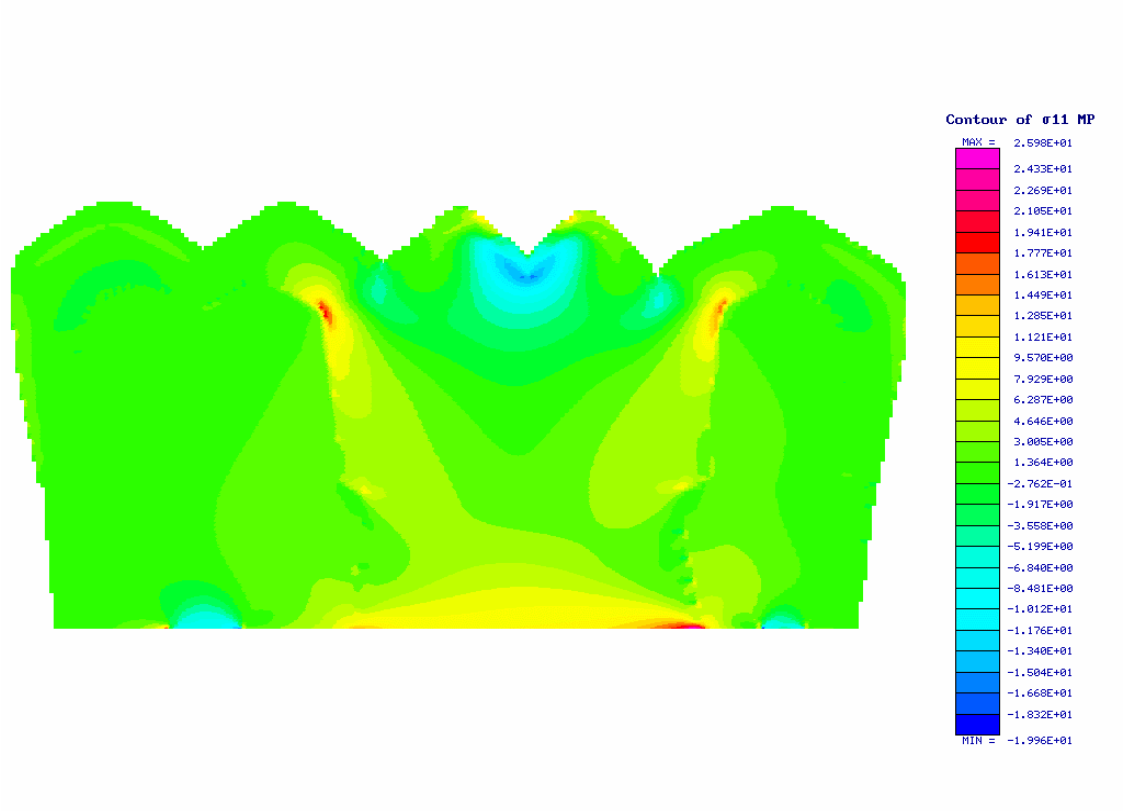

Figure 8.8 Principal stress distribution for ESO Initial design domain posterior bridge.

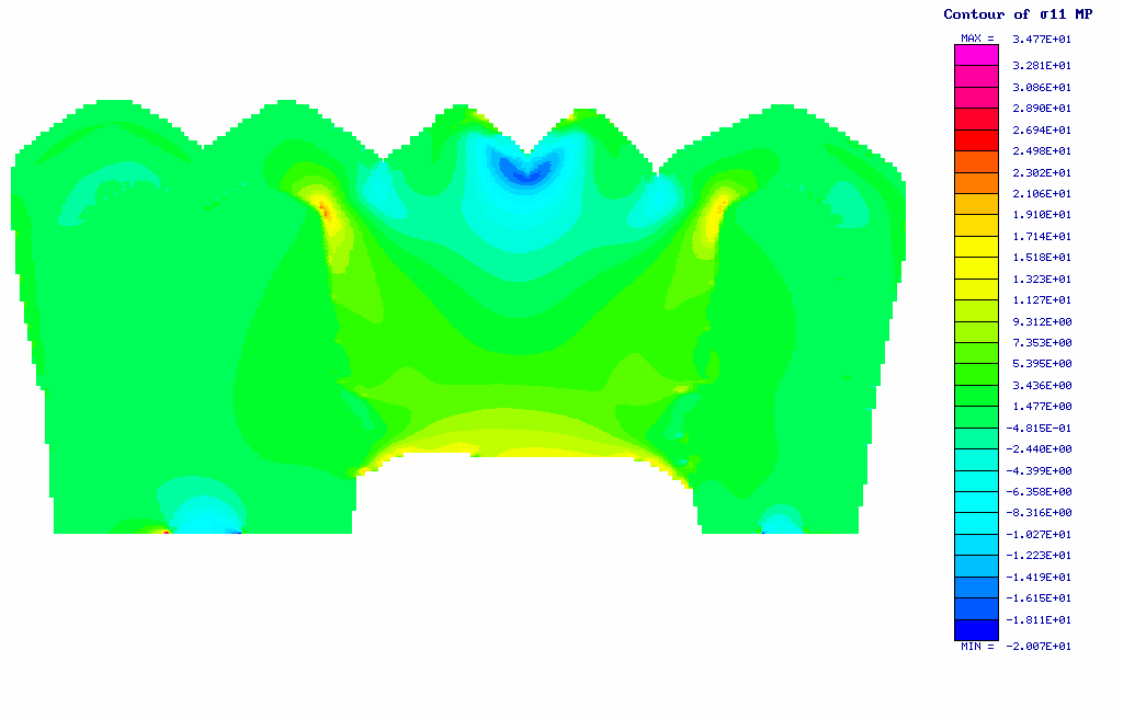

Figure 8.9 Principal stress distribution for ESO posterior bridge - Iteration 175.

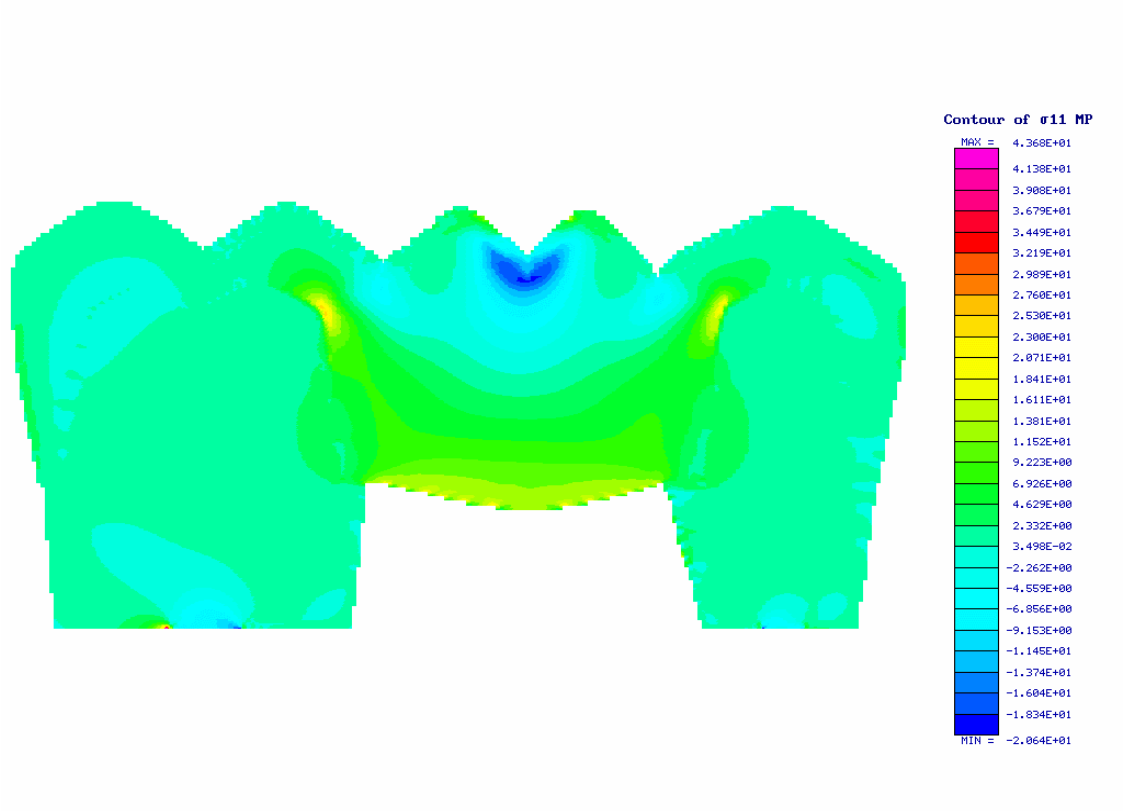

Figure 8.10 Principal stress distribution for ESO posterior bridge - Iteration 200.

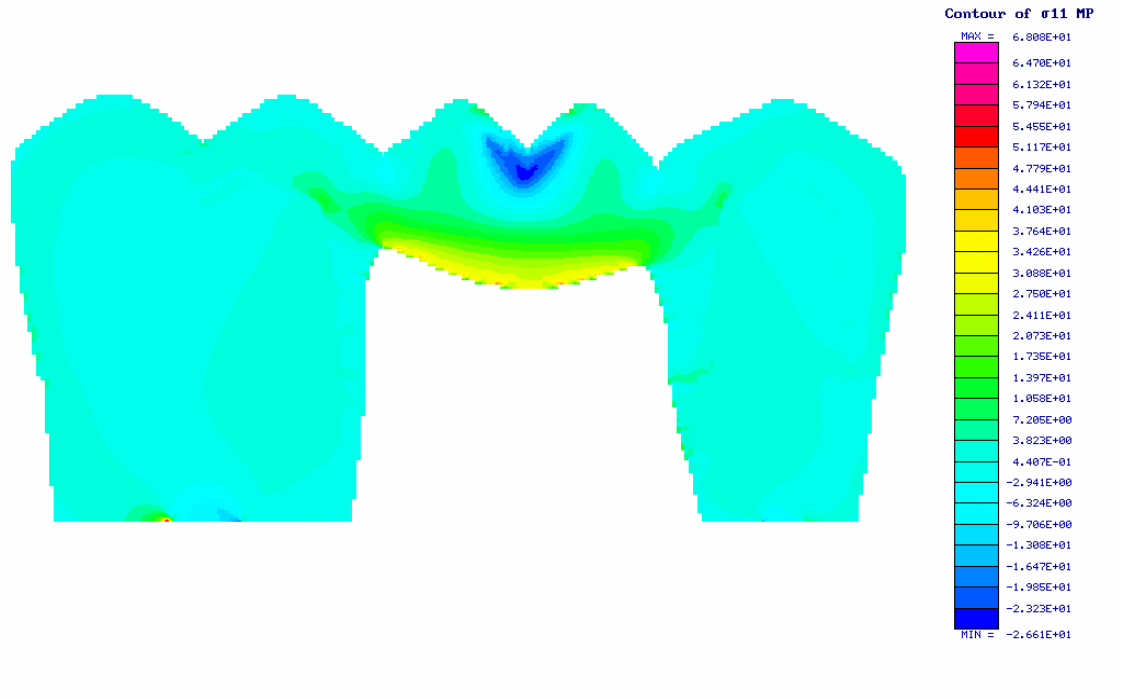

Figure 8.11 Principal stress distribution for ESO posterior bridge - Iteration 300.

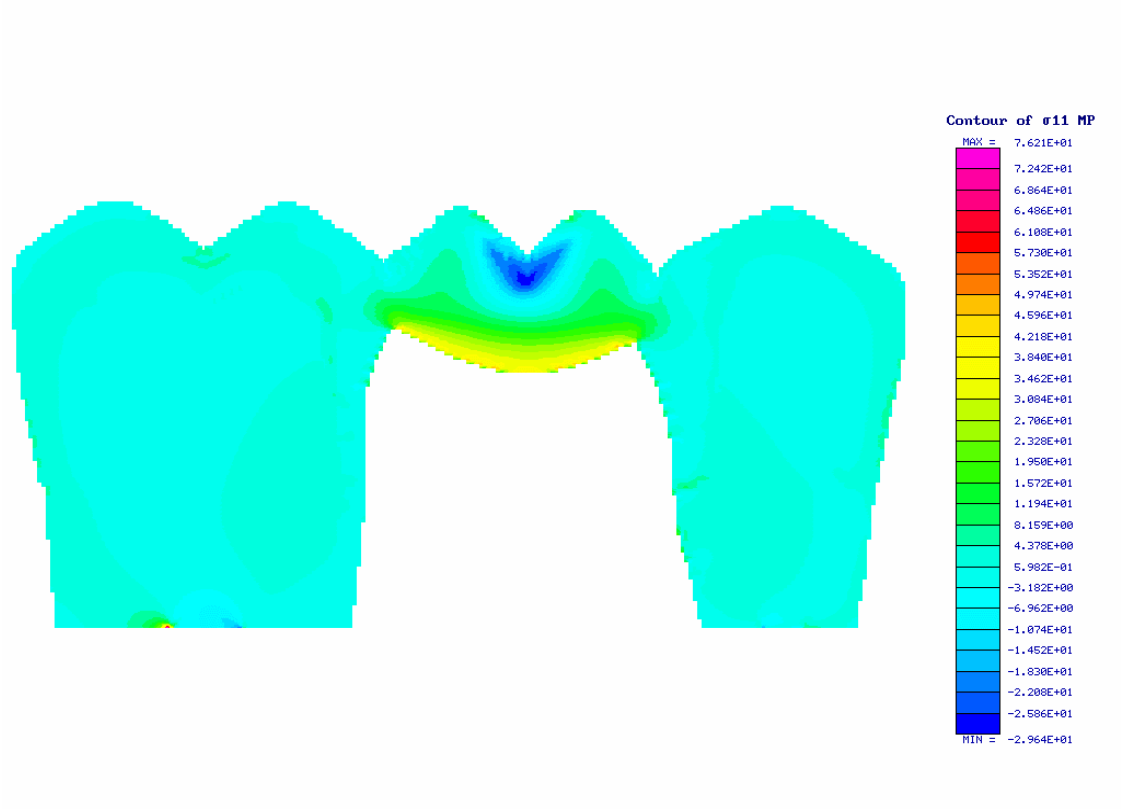

Figure 8.12 Principal stress distribution for ESO posterior bridge - Iteration 400.

Comparing the volumes and stresses of these optimised designs (Figures 8.9 to 8.13) to those pre-existing designs shown in Figures 8.6 to 8.8, the optimised designs are all more efficient in their performance. For example, by examining the optimised design at ESO iteration 300, the volume from the initial design domain decreases by 22.8 %. This results in a maximum principal stress of 68.08 MPa. Comparing this to the Bullet Pontic bridge (whose volume decrease is 15.6 % compared to the ESO initial design domain), its maximum stress is 82.29 MPa. Hence for comparable volumes, the non-optimised Bullet Pontic bridge shape generates a 23 % higher maximum surface stress.

As the ESO algorithm proceeds to iteration 400, the volume of the optimised bridge decreases by 24.9 % compared to the ESO initial design domain with a resulting value of the maximum principal stress of 76.21 MPa. In comparison, the Sanitary Pontic bridge has its volume reduced 25.7 % from the initial ESO volume with an maximum principal stress of 109.7 MPa. Thus for almost the same volume of material the non-optimised Sanitary Pontic has greater stress by 44 %.

Note that these volume comparisons are for the whole bridge domain and not just the central portion.

Table 8.1 also makes the comparison between the maximum tensile principal stress that occurs in the Pontic part of the bridge to the maximum compressive principal stress that occurs just below the point of application of the vertical load. This comparison is for the ESO and pre-existing models. For a beam type structure, this ratio of maximum tensile to maximum compressive stress would be unity showing that the tensile bending stress equals the compressive bending stress. For other structural forms it is considered that the closer the design is to unity (one), the better. For all the ESO bridge shapes the value is closer to one than for their corresponding predefined shapes.

Hence it can be seen from all these comparisons, the optimised designs has lower maximum stresses compared to those existing models with similar volumes. This highlights the fact that the stresses in the bridge are shape and size dependant – variables that the Evolutionary Structural Optimisation method can effectively determine.

Table 8.1 Comparison of the maximum tensile and compressive principal stresses.

Bridge Type	$\lvert\sigma_{11_{max\ tens}}\rvert$ **(MPa)**	$\lvert\sigma_{11_{max\ com}}\rvert$ **(MPa)**	$\lvert\sigma_{11_{max\ ten}}\rvert/\lvert\sigma_{11_{max\ com}}\rvert$
Bullet Pontic	83.29	22.69	3.67
Ridge Lap	51.50	21.25	2.42
Sanitary Pontic	109.7	32.39	3.39
ESO Iteration 0	25.98	19.96	1.30
ESO Iteration 175	34.77	20.07	1.73
ESO Iteration 200	43.68	20.64	2.12
ESO Iteration 300	68.08	26.61	2.56
ESO Iteration 400	76.21	29.64	2.57

8.4 Concluding Remarks

These results indicate that In-Ceram is an adequate and appropriate material to be used in the make-up of dental bridges. The design and construction of the bridges is mainly restricted by the properties of the porcelain veneer. There exists an ideal specific thickness of veneer that will minimise the maximum tensile principal stress.

Table 8.2 Comparison of Volumes and Stresses for each bridge design.

Bridge Type	**% Volume decrease from Initial ESO Design Domain**	**Max Tensile Principal Stress(MPa)**	**% stress increase for non-ESO shapes**
ESO Iteration 200	12.31	43.6	**18%**
Ridge Lap Pontic	*12.53*	*51.5*	
ESO Iteration 300	22.84	68.08	**23%**
Bullet Pontic	*15.56*	*82.29*	
ESO Iteration 400	24.91	76.21	**44%**
Sanitary Pontic	*25.74*	*109.7*	

The designs of the existing posterior tooth bridges are adequate in carrying the loads defined in this chapter. The ESO program has gone one step further in producing designs with similar volumes, and yet lower maximum principal stresses (summarized in Table 8.2). The shape of the bottom of the Pontic tooth is crucial in reducing the magnitude of the maximum principal tensile stress. The ESO process for shape optimisation has, in this chapter, demonstrated that its effect is to make the surface of the design space uniformly stressed.

8.5 References

Cook, R. (1974), *Concepts and Applications of Finite Element Analysis*, John Wiley, New York, pp. 311-353.

El-Elbrashi, M., Graig, R., Peyton, F. (1970), "Experimental Stress Analysis of Dental Restorations. Part VII. Structural Design and Stress Analysis of Fixed Partial Dentures", *Journal of Prosthetic Dentistry*, Vol. 23, pp. 177-186.

G+D Computing Pty. Ltd. (1999), *Using Strand7*, G+D Computing Pty. Ltd., Sydney, Australia.

Hood, J., Farah, J., Craig, R. (1975), "Stress and Deflection of Three Different Pontic Designs", *Journal of Prosthetic Dentistry*, Vol. 33, pp. 54-59.

Hornberger, H. (1995), *Strength Microstructure Relationships in a Dental Alumina Glass Composite*, Doctorate Thesis, The University of Birmingham, Birmingham, United Kingdom.

Kamposiora, P., Papavasilious, G., Bayne, S., Felton, A. (1996), 'Stress Concentration in All-Ceramic Posterior Fixed Partial Dentures', *Quintessence International*, Vol. 27, pp.701-706.

Kappert, H., F., Knode, H. (1993), "In-Ceram: Testing a new ceramic material", *Quintessence Dental Technology*, Vol. 16, pp. 87-97.

Kelly, J. (1995). "Perspectives on Strength", *Dental Materials*, Vol. 11, pp. 103-110.

Kelly, J., R., Tesk, J., A., Sorenson, J., A. (1995), "Failure of All ceramic Fixed Partial Dentures In Vitro and In Vivo: Analysis and Modelling", *The Journal of Dental Research*, Vol. 74, pp. 1253-1258.

Korioth, T., Versluis, A. (1997), "Modelling the Mechanical Behaviour of the Jaws and their Related Structures by Finite Element (FE) Analysis", *Critical Review on Oral Biological Medicine*, Vol. 8, pp. 90-104.

Pospiech, P., Rammelsberg, P., Goldhofer, G., Gernet, W. (1996), "All-Ceramic Resin-Bonded Bridges, A 3-Dimensional Finite-Element Analysis Study", *European Journal of Oral Science*, Vol. 104, pp. 390-395.

Qualtrough, A., J., E., Piddock, V. (1997), "Ceramics Update", *Journal of Dentistry*, Vol. 25, pp. 91-95.

Ridlon, S. (1987), "Modelling Guidelines", Meyer, C. (Ed.), *Finite Element Idealization – for Linear Elastic Static and Dynamic Analysis of Structures in Engineering Practice*, American Society of Civil Engineers, New York, pp. 212-271.

Tesk, J., Anusavice, K. (1988), "Summary of Conference on Design of Dental Prostheses", *Dental Materials*, Vol. 4, pp. 49-50.

Chapter 9

Conclusions

9.1 Achievements

Evolutionary Structural Optimisation is establishing itself to be a simple and efficient structural optimisation method. As has been outlined in this thesis, to date, much work has been done on ESO to enable it to reach this status. The work developed herein has endeavoured to add more features to the ESO process. The significance of this is that it takes ESO to a level where the additional features are beneficial to engineering practice. Industry, in its search to model the environment that exists around it as accurately as possible, needs such features to operate at an optimum condition. The more numerous and complex the factors that are taken into account in the design process, the more accurate and appropriate the modelling and the design proposed for the given environment will be. With this significance in mind, a summary of the work presented in this thesis is as follows:

1. Developed, incorporated and investigated four multicriteria ESO methods (for 2-D plate elements) for the FE solver combinations of:
   a) linear static FEA and natural frequency FEA (bi-criteria optimisation);
   b) linear static FEA and inertia FE solver (bi-criteria optimisation) and;
   c) linear static FEA, natural frequency FEA and inertia FE solver (tri-criteria optimisation).

   The four multicriteria methods were:
   i) The Linear Weighting method;
   ii) The Global criterion method;
   iii) The Logical AND operator method and;
   iv) The Logical OR operator method.

2. Proposed and developed a new evolutionary procedure that optimises structures with the objective to maximise or minimise any component of moment of inertia. These components were:
   a) rectangular moments of inertia I_x and I_y;
   b) polar moment of inertia I_z and;
   c) product moment of inertia I_{xy}.

3. Proposed, developed and incorporated a constant width layer algorithm into the ESO method (CWL ESO) that morphs the material properties of a layer of elements - the width of which can be selected by the user.

4. Utilised the CWL ESO method to optimise the shape of an all-ceramic, 3-unit anterior dental bridge. Also optimised an all-ceramic, 3-unit posterior dental bridge.

During this research, the algorithms were developed and incorporated into the EVOLVE program (Querin, 1997; Xie and Steven, 1997) using Fortran90 code (Hahn, 1994). For the multicriteria ESO algorithms, approximately 2000 lines of new code were added. In addition, the inertia solver consisted of 800 lines of code. 200 lines of Fortran90 code was added to the EVOLVE code to incorporate the CWL algorithm.

As a result of these studies, a total of 12 articles have been published in various international journals or conferences (see List of Publications at beginning of thesis).

9.2 Research Outcomes

9.2.1 Multicriteria ESO

- The linear weighting method always produced solutions with Pareto nature - where if one criterion was bettered, it was at the expense of the other/s.

- The distribution of points along the Pareto solution space was not always even. This was attributed to the relation between the sensitivity number distributions of each criterion and to the linear allocation of weight (or priority) to them.

- The element removal rate and the mesh fineness had a direct effect on the deviation of points from this Pareto nature. The smaller the removal rate or the finer the mesh, then the smaller the deviation of points from the Pareto curve. This occurred at the expense of computational cost.

- The amount of solutions created also had an effect on the formation of the Pareto curve. As more solutions were made, more points defining the curve were produced, and a more accurate Pareto curve was obtained.

- The solutions of the global criterion always formed part of the Pareto curve. Its solution was considerably similar to the equal weighting condition for the linear weighting method. This was because the global criterion method in its formulation implied an equal weight.

- The logical AND and the OR operator ESO methods did not always form part of the Pareto curve. When they did, no recurring relationship was found between them and the linear weighting method. This was dependant on the relative sensitivity number distributions amongst the criteria.

9.2.2 Evolutionary Moment of Inertia Optimisation

- An efficiency measure of the EMIO algorithm (radius of gyration) indicated that the evolving structures were optimised in terms of their inertia properties.

- The presence of a non-design domain 'dampened' the radius of gyration, causing the value to 'drop off' toward the end of the evolution.

- EMIO is useful and indeed necessary for the efficient optimisation of non-symmetrical FE cross-sections. If the structure is symmetric about the *x* or *y*-axis, it may be evolved in one iteration.

9.2.3 Constant Width Layer ESO

- The CWL ESO method has managed to maintain a constant layer of fixed width along the boundary during shape optimisation.

- A finer mesh produces a more uniform width during the evolution. This comes at the expense of computational cost.

9.2.4 Optimisation Ceramic Dental Bridges

- The mechanical responses of an anterior all-ceramic dental bridge is notch size and shape dependent.

- The mechanical performance of an all-ceramic 3-unit anterior bridge is greatly restricted by the material properties of the porcelain veneer.

- The CWL ESO method was able to imitate the anterior bridge design, resulting in a more uniform stress along the boundary.

- For posterior all-ceramic dental bridges, the shape of the Pontic tooth is crucial in reducing the magnitude of maximum principal tensile stress.

- The ESO algorithm modified the shape of this Pontic, creating uniform stresses along the surface of the structure and in some instances, significantly reducing some of the maximum stresses that existed in the models.

9.3 Future Directions

From this research, many research possibilities have been created, which no doubt, would continue to aid in the quest for making ESO as flexible and robust as possible in the optimisation of any given structure. Some of these are:

1. Investigate the appropriateness of, and incorporate other multicriteria methods into ESO not yet investigated;

2. Expand the criteria available to be simultaneously used in ESO to other FEA solver types such as linear buckling and non-linear static. This would also include other ESO criterion already established ie buckling (Manickarajah *et al.*, 1998), torsional stiffness (Li *et al.*, 1999a), electrostatic (Li, 2000) and magnetostatic (Li, 2000) problems;

3. Expand the number of criteria to be optimised beyond that of three;

4. Investigate and apply the same multicriteria methods to other features of ESO such as morphing, BESO, Group ESO (Lencus *et al.*, 1999) and to that of that of multiple load cases (Querin, 1997) or multiple constraint conditions (Xie and Steven, 1997). For example, allocate weightings to various loads applied to the structure;

5. Investigate the effects of alternative values of the constant term p for the global criterion case;

6. Modify and investigate the weighting multicriteria ESO method to allocate weight to each criterion not in a linear fashion as has been done in this dissertation;

7. Investigate the effect of modifying the sensitivity numbers of each criterion for the linear weighting method;

7. Integrate Bi-directional Evolutionary Structural Optimisation (BESO) (Young *et al.*, 1999) and material shifting (Li *et al.*, 1999a) into the Evolutionary Moment of Inertia Optimisation method;

9. Convert the Evolutionary Moment of Inertia Optimisation method to include the optimisation of inertia based on the principal axes of inertia rather than the x and y-axis, and the optimisation of a cross-section where the X and Y-centroid is kept fixed during the evolution;

10. Extend the Evolutionary Moment of Inertia Optimisation method to that of 3-D elements including plates and bricks (Querin, 1997), and connected to this, morphing (Chu *et al.*, 1998) and BESO (Young *et al.*, 1999).

11. Incorporate consecutive multiple layers to be used in CWL ESO. This may include differing widths as defined by the decision maker.

Although the above wish list of potential research continues to grow, it has been demonstrated that this thesis has contributed significantly in the enhancement of ESO being used as an appropriate design tool in research, commercial and industrial applications.

9.4 References

Chu, D., N., Xie, Y., M., Steven, G., P. (1998), "An Evolutionary Method for Optimal Design of Plates with Discrete Variable Thickness Subject to Constant Weight", *Structural Optimization*, Vol. 17, pp. 55-64.

Hahn, D. (1994), *Fortran 90 for Scientists and Engineers*, Edward Arnold, United Kingdom.

Lencus, A., Querin, O., M., Steven, G., P., Xie, Y., M. (1999), "Modifications to the Evolutionary Structural Optimisation (ESO) Method to Support Configurational Optimisation", *CD-Rom Proceedings of the 3rd World Congress of Structural and Multidisciplinary Optimization*, New York, USA.

Li, Q., Steven, G., P., Querin, O., M., Xie, Y., M. (1997), "Optimal Shape Design for Steady Heat Conduction by the Evolutionary Procedure, Inverse Problems in Heat Transfer and Fluid Flow", Dulikravich, G., S., Woodbury, K., A., (Eds.) *ASME Proceedings of the 32nd National Heat Transfer Conference*, ASME HTD, Vol. 340, pp.159-164.

Li, Q., Steven, G., P., Querin, O., M., Xie, Y., M. (1999a), "Evolutionary Optimization for Cross Sectional Shape of Torsional Shafts", *Proceedings of the 3rd World Congress on Structural and Multidisciplinary Optimization (WCSMO-3)*, CD Volume, New York, USA.

Li, Q., Steven, G., P., Xie, Y., M. (1999b), "Evolutionary Shape Optimization A Stress Based Sensitivity Analysis Method", *Proceedings of the Second Australian Congress on Applied Mechanics ACAM '99*, Canberra, Australia, 9th-12th February.

Li, Q. (2000), *Evolutionary Structural Optimization for Thermal and Mechanical Problems*, Doctorate Thesis, School of Aeronautical, Mechatronic and Mechanical Engineering, University of Sydney, Australia.

Manickarajah, D., Xie, Y., M., Steven, G., P. (1998), "An Evolutionary Method for Optimization of Plate Buckling Resistance", *Finite Elements in Analysis and Design*, Vol. 29, pp. 205-230.

Querin, O., M. (1997), *Evolutionary Structural Optimisation: Stress Based Formulation and Implementation*, Doctorate Thesis, School of Aeronautical, Mechatronic and Mechanical Engineering, University of Sydney, Australia.

Xie, Y., M., Steven, G., P. (1997), *Evolutionary Structural Optimisation*, Springer-Verlag, London, UK.

Young, V., Querin, O., M., Steven, G., P., Xie, Y., M. (1999), "3D and Multiple Load Case Bi-directional Evolutionary Structural Optimisation (BESO)", *Journal of Structural Optimization*, Vol. 18, pp. 183-192.